Republic of Iraq
Ministry of Higher Education and Scientific Research
University of Babylon
College of Engineering
Civil Engineering Department

Behavior of Reinforced Concrete Horizontally Curved Box Girders with Openings Under Monotonic and Repeated Loads

A Dissertation

Submitted to the College of Engineering in the University of Babylon in Partial Fulfillment of the Requirements for the Degree of Doctor of Philosophy in Engineering / Civil Engineering / Structures

By

Ameer Mohsin Hashim

(B.Sc. Civil Engineering 2003)

(M.Sc. Structural Engineering 2014)

Supervised by

Prof. Dr. Ammar Yasser Ali

2022 A.D. 1443 A.H.

بِسْمِ اللَّهِ الرَّحْمَنِ الرَّحِيمِ

﴿يَرْفَعِ اللَّهُ الَّذِينَ آمَنُوا مِنْكُمْ وَالَّذِينَ أُوتُوا الْعِلْمَ دَرَجَاتٍ وَاللَّهُ بِمَا تَعْمَلُونَ خَبِيرٌ﴾

صدق الله العلي العظيم

(سورة المجادلة\ الآية11)

CERTIFICATION

I certify that the preparation of the thesis entitled ***" Behavior of Reinforced Concrete Horizontally Curved Box Girders with Openings Under Monotonic and Repeated Loads"***, was prepared by ***"Ameer Mohsin Hashim"***, under my supervision at University of Babylon, Department of Civil Engineering in the partial fulfillment of the requirements for the degree of Doctor of Philosophy in Civil Engineering (Structural Engineering).

Signature:

Name: ***Prof. Dr. Ammar Yaser Ali***

Date: / / 2022

EXAMINING COMMITTEE CERTIFICATION

We certify as an Examining Committee that have read this dissertation entitled ***"Behavior of Reinforced Concrete Horizontally Curved Box Girders with Openings Under Monotonic and Repeated Loads "***, which is submitted by ***"Ameer Mohsin Hashim"*** and examined the student in its content and what related to it, and found it meets the standard of a dissertation for the degree of Doctor of Philosophy in Civil Engineering (Structure Engineering).

Signature:
Name: ***Prof. Dr. Ammar Y. Ali***
(Member and Supervisor)
Date: / / 2022

Signature:
Name: ***Asst. Prof. Dr. Najla'a H. Alshareef***
(Member)
Date: / / 2022

Signature:
Name: ***Asst. Prof. Dr. Sadjad A. Hemzah***
(Member)
Date: / / 2022

Signature:
Name: ***Prof. Dr. Qasim M. Shakir***
(Member)
Date: / / 2022

Signature:
Name: ***Prof. Dr. Muyasser M. Jomaa'h***
(Member)
Date: / / 2022

Signature:
Name: ***Prof. Dr. Nameer A. Alwash***
(Chairman)
Date: / / 2022

Approved by the Head of the Civil Engineering Department

Signature:
Name: ***Prof. Dr. Thair J. Mizhir***
(The Head of the Civil Engineering Department)
Date: / / 2022

Approved by the Dean of the College of Engineering

Signature:
Name: ***Prof. Dr. Hatem H. Obeid***
(The Dean of the College of Engineering)
Date: / / 2022

ACKNOWLEDGEMENT

In the name of ALLAH, the most compassionate the most merciful.

First, great thanks are to **Almighty Allah**, for enabling me to complete this work.

I would like to express my sincere gratitude to my supervisor; **Prof. Dr. Ammar Y. Ali** for his remarkable suggestions, encouragement and guidance through the research; I will never forget his support as long as I live, I am really indebted to him.

Appreciation is also extended to the head and members of my thesis examining committee for their time and efforts.

Great thanks to the dean of the College of Engineering, head and staff of the Civil Engineering Department at the University of Babylon for their appreciable support.

Thanks are also extended to the dean of the College of Engineering, head of the Civil Engineering Department, and special thanks to Dr. Sadjad A. Hemzah, Dr. Bahaa H. Abbas and staff of Laboratories at University of Karbala for their assistance in using the various facilities during the experimental program.

A special thanks and gratitude to my family for their care, patience and encouragement throughout the research period.

I do not know how can I express my profound respect and thanks to my friends who helped in my work.

Ameer M. H. Al. Janabi

2022

Abstract

This study looks at the behavior and performance of reinforced concrete horizontally curved box beams with vertical or transverse openings unstrengthen and strengthened by hybrid concrete or external strengthened by EBR- CFRP laminates around openings under monotonic or cyclic loading. In addition to a pilot beam, the experimental investigation included the manufacture and testing of fifteen reinforced concrete curved box beams categorized into three groups. The first group included six specimens (one without opening and five with vertical openings) under monotonic loads, the second group consisted of five specimens with transverse openings under monotonic loads, while the third group included four specimens (one without opening and three with transverse openings) under repeated load. The experimental program considers a set of independent variables: direction of axis of openings, place of opening along span of beam, carrying out a strengthened technique utilizing hybrid concrete technique (reactive powder concrete RPC around openings) or external strengthened by EBR- CFRP laminates around opening. All continuous box beams with two spans have been tested under effect of concentrated loads at top face of each midspan.

The experimental results indicated that the existence of openings at region of maximum torsion (at angle 60°) and shear force led to some reduction in ultimate load by approximately 11.5% for beam with vertical openings, however a considerable reduction 46.4% for beam with transverse openings compared with beam without opening. The use of hybrid concrete (reactive powder concrete RPC) enhanced the ultimate load capacity of the beam with opening at angle 60° by a ratio of 4.8% and 25.9% for vertical and transverse opening, respectively. Utilizing of EBR- CFRP laminates around opening as external strengthening achieved an increasing the ultimate load for beam with vertical openings, while that of beam with transverse opening still less than the control beam with a ratio

25.9%. The deformation response of unstrengthened and strengthened curved box beams under repeated load was similar to that subjected to monotonic load with a slight reduction due to effect of fatigue for both types of strengthening around opening hybrid concrete (reactive powder concrete RPC around openings) or external strengthened by EBR- CFRP laminates.

The numerical work included a model of three-dimensional finite element, utilizing a model of concrete damaged plasticity and material properties obtained from laboratory tests was conducted to simulate all fifteen specimens of experiment, in addition to parametric study to consider the effects of some variables that have not been studied throughout the experimental program within a software package ABAQUS/standard 2017. The parametric study included the effects of some parameters on response of horizontally curved reinforced concrete box beams; shape of openings, radius of curvature and strength of RPC. Finite element results were compared with that obtained from experiment in terms of load-midspan deflection and cracking-propagation behavior with an average of variance of roughly 5%, 8% and 20% for cracking load, ultimate load and service deflection, respectively. As a result of parametric study, the presence of a circular or rectangular openings in vertical direction led to an approximately same ultimate load by FEM for beam with a square opening at angle 60°, while in the transverse direction the ultimate load was increased slightly for circular opening and a slight decrease for rectangular opening, when compared to the ultimate load of beam with a square opening. The ultimate load of the curved beam without openings exhibits an increase by decrease the curvature (1/R) for the identical length by approximately (10.5% and 19.41%) for curvature (0.67 and 0.0) if compared to that with (1/R) = 0.87 of experimental work, for curved beam with openings increased by about (14.7% and 59.4%) for curvature (0.67 and 0.0). A slight increase in ultimate load of the curved beam with opening at angle 60°, 6.4% and 3.8% for vertical and transverse openings, respectively when using

RPC with 200 MPa compared to that using RPC with 120 MPa. Using finite element analysis were able to accurately anticipate the behavior of horizontally curved box beams with openings, as well as the response of the beams with different parameters.

List of Contents

Contents	Page No.
List of Contents	I
List of Figures	VII
List of Plates	XI
List of Tables	XIII
Notation	XV
Abbreviation	XVII
Chapter One: Introduction	**1-24**
1.1 General	1
1.2 Reinforced concrete horizontally curved beams	1
1.3 Box or Hollow Beam	3
1.4 Opening	4
1.4.1 Transverse Openings	5
1.4.2 General Guidelines for Selection the Size and Location of Web Openings	7
1.4.3 Vertical Opening	8
1.4.4 General Guidelines for Selection the Size and Location of vertical Openings	9
1.5 Analysis for Ultimate Strength Under Combined Torsion, Bending and Shear	10
1.6 Failure Modes for Beam with Small Opening Under Combined Torsion, Bending, and Shear	12
1.7 Design for Torsion	13
1.7.1 Design for Beam Type Failure	13
1.7.2 Design for Frame Type Failure	14
1.8 Cyclic Loading	15
1.9 Self-Compacting Concrete (SCC)	16

Contents	Page No.
1.10 Concept of Hybrid Sections	17
1.11 Reactive Powder Concrete (RPC)	17
1.12 Fiber Reinforced Polymer (FRP)	19
1.12.1 Configuration of Fiber Reinforced Polymer (FRP)	21
1.12.2 Advantages and Disadvantages of (FRP)	22
1.12.3 Applications of (FRP) Laminates	23
1.13 Objective of the Current Study	23
1.14 Layout of Thesis	24
Chapter Two: Literature Review	**25-60**
2.1 Introduction	25
2.2 Experimental and Analytical Studies on Reinforced Concrete curved Beams	25
2.3 Experimental and Analytical Studies on Reinforced Concrete Box Beams	32
2.4 Experimental and Analytical Studies on Beams (Girders) with Openings	45
2.4.1Transverse Openings	45
2.4.2 Vertical Openings	53
2.5 Summary on Concluding Remarks	58
Chapter Three: Experimental Work	**61-102**
3.1 General	61
3.2 Experimental Program	61
3.2.1 General Description	61
3.2.2 Description of Tested Circular Beams	65
3.2.2.1 Circular Curved Box Beams without Opening	65
3.2.2.2 Circular Curved Beams with Vertical Openings (Group I)	67
3.2.2.3 Circular Curved Beams with Transverse Openings (Group II)	67

Contents	Page No.
3.2.2.4 Circular Curved Box Beams Under Repeated Load (Group III)	70
3.2.3 Strengthening Techniques	70
3.2.3.1 Strengthening by Concrete Hybridization	70
3.2.3.2 Strengthening by EBR-CFRP Laminates	71
3.3 Material Properties of Tested Specimens	75
3.3.1 Self-compacting concrete	75
3.3.1.1 Cement	75
3.3.1.2 Coarse Aggregate (Gravel)	76
3.3.1.3 Fine Aggregate (Sand)	76
3.3.1.4 Superplasticizer	77
3.3.1.5 Limestone powder (LSP)	78
3.3.1.6 Water	78
3.3.2 Reactive Powder Concrete (RPC)	78
3.3.2.1 Cement	78
3.3.2.2 Fine Aggregate (Sand)	79
3.3.2.3 Silica Fume	79
3.3.2.4 Steel Fibers	80
3.3.2.5 Superplasticizer	81
3.3.2.6 Water	81
3.3.3 External Bond Reinforcement (EBR) Scheme	81
3.3.3.1 Carbon Fiber Reinforced Polymer (CFRP) Laminate	81
3.3.3.2 Epoxy Sikadur-330	82
3.3.4 Steel Reinforcement	83
3.4 Concrete Mix Design	84

Contents	Page No.
3.4.1 Self-compacting concrete (SCC)	84
3.4.1.1 Mix Proportion of Self-compacting concrete	84
3.4.1.2 Mixing Procedure of Self-compacting concrete	86
3.4.2 Reactive Powder Concrete (RPC)	87
3.4.2.1 Mix Proportion of Reactive Powder Concrete	87
3.4.2.2 Mixing Procedure of Reactive Powder Concrete	87
3.5 Reinforcement Steel Framwork Preparation	88
3.6 White Polystyrene Preparation	89
3.7 Formwork Preparation	89
3.8 Casting and Curing of Tested CB Specimens	90
3.9 Control Samples	94
3.10 Installation of CFRP Laminates	96
3.11 Instruments and Testing Procedure	97
3.11.1 Testing Machine	97
3.11.2 Supporting and Loading Conditions	98
3.11.3 Test Instruments	100
3.11.4 Loading History	101
3.11.5 Testing Procedure	102
Chapter Four: Experimental Results and Discussion	**103-170**
4.1 General	103
4.2 Mechanical Properties of Control Samples	103
4.3 Structural Response of Tested Specimens	105
4.3.1 General Behavior	105
4.3.2 Pilot Specimen	106

Contents	Page No.
4.3.3 Control Specimens	106
Specimen $CB_1.L_1$	106
Specimen $CB_{12}.L_2$	109
4.3.4 First Test Group (CBs with Vertical Openings)	112
Specimen $CB_2.V37.L_1$	113
Specimen $CB_3.V60.L_1$	115
Specimen $CB_4.V82.L_1$	118
4.3.4.2 Strengthened specimens	121
Specimen $CB_8.V60.S_1.L_1$	121
Specimen $CB_{10}.V60.S_2.L_1$	124
4.3.5 Second Test Group (CBs with Transverse Openings)	127
4.3.5.1 Unstrengthened specimens	127
Specimen $CB_5.T37.L_1$	127
Specimen $CB_6.T60.L_1$	130
Specimen $CB_7.T82.L_1$	133
4.3.5.2 Strengthened specimens	136
Specimen $CB_9.T60.S_1.L_1$	136
Specimen $CB_{11}.T60.S_2.L_1$	139
4.3.6 Third Test Group (CBs with Transverse Openings Under Cyclic Loading)	142
Specimen $CB_{13}.T60.L_2$	142
Specimen $CB_{14}.T60.S_1.L_2$	145
Specimen $CB_{15}.T60.S_2.L_2$	148
4.4 Effect of Considered Variables on Structural Response	151

4.4.1 Cracking Load and Cracking Pattern	151
4.4.2 Ultimate Strength and Failure Modes	154
4.4.3 Deformation Response	155
4.4.4 Ductility	159
4.4.5 Energy Absorption	161
4.4.6 Stiffness Criteria	164
4.4.6 Width of Cracks	167
Chapter Five: Finite Element Analysis	**171-200**
5.1 General	171
5.2 Main Meshing Elements	171
5.2.1 3D Solid Element	172
5.2.2 Truss Element	173
5.2.3 Shell Element	173
5.3 Model Geometry and Boundary Conditions	174
5.4 Load	176
5.5 Convergence Investigation	176
5.5.1 Effect of Mesh Size	176
5.6 Finite Element Analysis Results and Discussion	178
5.6.1 Deformation Response	178
5.6.2 First Cracking and Ultimate Loads	187
5.6.3 Deflection at Service Load and Ductility Index	188
5.6.4 Crack Pattern and Modes of Failure	189
5.7 Parametric Study	191
5.7.1 Effect of Opening Shape	192
5.7.2 Effect of Curvature	195
5.7.3 Effect of RPC Strength	198
Chapter Six : Conclusions and Recommendations	**201-206**
6.1 General	201
6.2 Conclusions	201
6.2.1 Experimental Work Conclusions	201
6.2.2 Finite Element Analysis Conclusions	205
6.3 Recommendations for Further Works	206
References	**205-215**
Appendix A	**A1-A6**
Appendix B	**B1-B11**
Appendix C	**C1-C22**

List of Figures

Figure No.	Title	Page No.
1.1	Horizontally Curved Beam Loading and Forces	3
1.2	Typical Layout of Pipes for High Rise Building	5
1.3	Collapses Mechanism at Large Opening	6
1.4	Guidelines for Location of Web Opening for straight beam	8
1.5	Location of conduits and pipes passing vertically through girders, beams, and joists	10
1.6	Failure surfaces for a solid beam in Modes 1, 2, and 3	12
1.7	Frame-type failure of a beam with a small opening under torsion	13
1.8	Idealized free-body diagram at opening of a beam under loading	14
1.9	Typical composition of FRP materials	20
1.10	Stress-Strain Relationship of Fibers and Steel	21
1.11	Some Types of FRP Laminates fiber alignment	22
2.1	yield surfaces for combined bending and torsion, at a section where a plastic hinge was formed	26
2.2	Geometry of Test Specimens (Badawy,1977)	30
2.3	Stress distribution on typical plates (Arendts, 1969)	33
2.4	Elastically clamped plate (Luo et al, 2003)	35
2.5	Decompositions of elastically clamped plate under local distributed load for top slab	35
2.6	Cases study and test (Kurian & Menon, 2007)	37
2.7	Loading cases of the five tested girders (Galal & Yang, 2009)	38
2.8	(a) Rectangular, (b) Trapezoidal and (c) Circular cross-section of box girder bridge	40
2.9	Geometry and Dimensions of Reinforced Concrete Beam (Jabbar et al., 2016)	41
2.10	Modeled Beams (a) S, (b) H, (c) H100 (d) H200 (e) H300(Jabbar et al., 2016)	42
2.11	Typical Shear Failure of a Beam with Small Openings Containing no Shear Reinforcement ((Hanson, 1969), (Somes & Corley, 1974)	46

2.12	Modes of Failure for Small Opening, (M A Mansur, 1998)	51
2.13	(a)Strengthening Schemes of T- Beams with Openings (b) Openings Location (Dawood & Al-Jazaeri, 2014)	54
3.1	Circular Box Beam Specimen Identification	64
3.2	Tested Circular Curved Box Beams Flow Chart	64
3.3	Details of Specimens (all units in millimeters): (a) Geometry, Supports and Loading (b) Cross Section and Reinforcement	66
3.4	Vertical Openings (Group I) (all units in millimeters): (a) Specimen with Openings at angle 37° (b) Specimen with Openings at angle 60° (c) Specimen with Openings at angle 82° (d)Section A-A through Opening	68
3.5	Transverse Openings (Group II) (all units in millimeters): (a) Specimen with Openings at angle 37° (b) Specimen with Openings at angle 60° (c) Specimen with Openings at angle 82° (d)Section A-A through Opening	69
3.6	Details of Strengthening Schemes by using RPC (all units in millimeters) for Specimen $CB_8.V60.S_1.L_1$	71
3.7	Details of Strengthening Schemes by using RPC (all units in millimeters) for Specimens $CB_9.T60.S_1.L_1$ and $CB_{14}.T60.S_1.L_2$	72
3.8	Strength Restoring Schemes (all units in millimeters) for Specimen $CB_{10}.V60.S_2.L_1$	73
3.9	Strength Restoring Schemes (all units in millimeters) for Specimens $CB_{11}.T60.S_2.L_1$ and $CB_{15}.T60.S_2.L_2$	74
3.10	Test Setup Layout (a)Side View Schematic Drawing (b) Top View Schematic Drawing	99
3.11	Typical Loading History of Repeated Loaded Specimens	101
4.1	Load-Midspan Deflection Curve for Specimen $CB_1.L_1$	107
4.2	Torsional moment-Midspan Twisting Angle Curve for Specimen $CB_1.L_1$	107
4.3	Load-Midspan Deflection Curve for Specimen $CB_{12}.L_2$	109
4.4	Torsional moment-Midspan Twisting Angle Curve for Specimen CB12.L2	110
4.5	Load-Midspan Deflection Curve for Specimens (CB1.L1and CB2.V37.L1)	113
4.6	Torsional moment-Midspan Twisting Angle Curve for Specimens ($CB_1.L_1$and $CB_2.V37.L_1$)	113
4.7	Load-Midspan Deflection Curve for Specimens (CB1.L1and CB3.V60.L1)	115
4.8	Torsional moment-Midspan Twisting Angle Curve for Specimens (CB1.L1and CB3.V60.L1)	116

4.9	Load-Midspan Deflection Curve for Specimens (CB1.L1and CB4.V82.L1)	119
4.10	Torsional moment-Midspan Twisting Angle Curve for Specimens (CB1.L1and CB4.V82.L1)	119
4.11	Load-Midspan Deflection Curve for Specimens ($CB_1.L_1$, CB_3.V60.$L_1$and CB_8.V60.S_1.L_1)	122
4.12	Torsional moment-Midspan Twisting Angle Curve for Specimens ($CB_1.L_1$, CB_3.V60.$L_1$and CB_8.V60.S_1.L_1)	122
4.13	Load-Midspan Deflection Curve for Specimens ($CB_1.L_1$, CB_3.V60.$L_1$and CB_{10}.V60.S_2.L_1)	125
4.14	Torsional moment-Midspan Twisting Angle Curve for Specimens ($CB_1.L_1$, CB_3.V60.$L_1$and CB_{10}.V60.S_2.L_1)	125
4.15	Load-Midspan Deflection Curve for Specimens ($CB_1.L_1$and CB_5.T37.L_1)	128
4.16	Torsional moment-Midspan Twisting Angle Curve for Specimens ($CB_1.L_1$and CB_5.T37.L_1)	128
4.17	Load-Midspan Deflection Curve for Specimens ($CB_1.L_1$and CB_6.T60.L_1)	130
4.18	Torsional moment-Midspan Twisting Angle Curve for Specimens ($CB_1.L_1$and CB_6.T60.L_1)	131
4.19	Load-Midspan Deflection Curve for Specimens ($CB_1.L_1$and CB_7.T82.L_1)	134
4.20	Torsional moment-Midspan Twisting Angle Curve for Specimens ($CB_1.L_1$and CB_7.T82.L_1)	134
4.21	Load-Midspan Deflection Curve for Specimens ($CB_1.L_1$, CB_6.T60.L_1 and CB_9.T60.S_1.L_1)	137
4.22	Torsional moment-Midspan Twisting Angle Curve for Specimens ($CB_1.L_1$, CB_6.T60.L_1 and CB_9.T60.S_1.L_1)	137
4.23	Load-Midspan Deflection Curve for Specimens ($CB_1.L_1$, CB_6.T60.$L_1$and CB_{11}.T60.S_2.L_1)	140
4.24	Torsional moment-Midspan Twisting Angle Curve for Specimens ($CB_1.L_1$, CB_6.T60.L_1 and CB_{11}.T60.S_2.L_1)	140
4.25	Load-Midspan Deflection Curve for Specimens ($CB_{12}.L_2$ and CB_{13}.T60.L_2)	143
4.26	Torsional moment-Midspan Twisting Angle Curve for Specimens (CB12.L2 and CB13.T60.L2)	143
4.27	Load-Midspan Deflection Curve for Specimens ($CB_{12}.L_2$, CB_{13}.T60.L_2 and CB_{14}.T60.S_1.L_2)	146
4.28	Torsional moment-Midspan Twisting Angle Curve for Specimens ($CB_{12}.L_2$, CB_{13}.T60.L_2 and CB_{14}.T60.S_1.L_2)	146
4.29	Load-Midspan Deflection Curve for Specimens ($CB_{12}.L_2$, CB_{13}.T60.L_2 and CB_{15}.T60.S_2.L_2)	149
4.30	Torsional moment-Midspan Twisting Angle Curve for Specimens ($CB_{12}.L_2$, CB_{13}.T60.L_2 and CB_{15}.T60.S_2.L_2)	149

4.31	Load-Midspan Deflection Response for CBs of Group I	155
4.32	Torsional moment-Midspan Twisting Angle Response for CBs of Group I	156
4.33	Load-Midspan Deflection Response for CBs of Group II	157
4.34	Torsional moment-Midspan Twisting Angle Response for CBs of Group II	157
4.35	Variation of Cumulative Ductility Factor of Specimens of Group III	161
4.36	Variation of Cumulative Energy Absorption of Specimens of Group III	162
4.37	Comparison of Cumulative Energy Absorption of Specimens of Group III	163
4.38	Width of Major Cracks up to Service Load for CBs in Group (I)	168
4.39	Width of Major Cracks up to Service Load for CBs in Group (II)	169
4.40	Width of Major Cracks up to Service Load of Final Cycle for CBs in Group (III)	170
5.1	C3D8R Element type used in FE simulation (Wu, 2015) of concrete and steel plates	172
5.2	Truss element(T3D2) (Metwally, 2014)	173
5.3	Three Dimensions View of Curved Beams FE model	174
5.4	Typical Boundary Conditions and Applied Load of Modelled Curved Beams	175
5.5	Mesh Density of the Control Curved Box Beams (CB1.L1 specimen)	177
5.6	Results of Convergence Study	178
5.7	Experimental and Numerical Load-Midspan Deflection Curves of (Group I) Under Monotonic Load	180
5.8	Experimental and Numerical Load-Midspan Deflection Curves of (Group II) Under Monotonic Load	181
5.9	Experimental and Numerical Torsional moment-Midspan Twisting Angle Curves of (Group I)	183
5.10	Experimental and Numerical Torsional moment-Midspan Twisting Angle Curves of (Group II)	184
5.11	Experimental and Numerical Load-Midspan Deflection Curves of (Group III) Under Cyclic Load	186

5.12	Cracking Patterns of Finite Element Model for Specimens (a)$CB_1.L_1$, (b)$CB_3.V60.L_1$and (c)$CB_6.T60.L_1$	190
5.13	Load–Midspan Deflection Curves of FEM for Beams with Various Shapes of Vertical Openings at Angle 60°	192
5.14	Torsional moment-Midspan Twisting Angle Curves of FEM for Beams with Various Shapes of Vertical Openings at Angle 60°	193
5.15	Load–Midspan Deflection Curves of FEM for Beams with Various Shapes of Transverse Openings at Angle 60°	193
5.16	Torsional moment-Midspan Twisting Angle Curves of FEM for Beams with Various Shapes of Transverse Openings at Angle 60°	194
5.17	Load–Midspan Deflection Curves of FEM for Beams without Openings	196
5.18	Load–Midspan Deflection Curves of FEM for Beams with Transverse Openings at Angle 60°	197
5.19	Load–Midspan Deflection Curves of FEM for Strengthened Beams with Vertical Openings at angle 60°	199
5.20	Load–Midspan Deflection Curves of FEM for Strengthened Beams with Transverse Openings at angle 60°	199

List of Plates

Plate No.	Title	Page No.
1.1	Horizontally Curved Beam in Building and Girder Bridges	2
1.2	Horizontally curved box girder (Alhamaidah, 2017)	4
1.3	Vertical Opening (a) Horizontally Curved Girders (Baghdad-Iraq) (b) Concrete Frame Building (Babile-Iraq)	9
1.4	Applications of Reactive Powder Concrete (Russell et al., 2013)	19
1.5	Formats of FRP Items (ISIS, 2007)	20
3.1	Steel Fibers Used in this Study	80
3.2	Testing Machine of Steel Reinforcing Bars	84
3.3	Slump flow, V-Funnel and L Box tests	85
3.4	Preparation of Cage of Steel Reinforcement	88

3.5	White Cork Operation	89
3.6	Semicircular Molds and Tools	90
3.7	Preparation and Casting Operation of Test Specimens	91
3.8	Test of Control Samples	95
3.9	Application of CFRP Laminates on Concrete Element	96
3.10	Loading Machine Used in the Tests	98
3.11	Test Setup	99
3.12	Instruments used in Testing	101
3.13	Test Program of Specimens	102
4.1	Specimen $CB_1.L_1$	108
4.2	Mode of Failure and Cracks Pattern for Specimen $CB_1.L_1$	108
4.3	Specimen $CB_{12}.L_2$	110
4.4	Mode of Failure and Cracks Pattern for Specimen $CB_{12}.L_2$	111
4.5	Specimen $CB_2.V37.L_1$	114
4.6	Mode of Failure and Cracks Pattern for Specimen $CB_2.V37.L_1$	114
4.7	Specimen CB3.V60.L1	116
4.8	Mode of Failure and Cracks Pattern for Specimen $CB_3.V60.L_1$	117
4.9	Specimen $CB_4.V82.L_1$	120
4.10	Mode of Failure and Cracks Pattern for Specimen $CB_4.V82.L_1$	120
4.11	Specimen $CB_8.V60.S_1.L_1$	123
4.12	Mode of Failure and Cracks Pattern for Specimen $CB_8.V60.S_1.L_1$	123
4.13	Specimen CB10.V60.S2.L1	126
4.14	Mode of Failure and Cracks Pattern for Specimen CB10.V60.S2.L1	126
4.15	Specimen $CB_5.T37.L_1$	129
4.16	Mode of Failure and Cracks Pattern for Specimen $CB_5.T37.L_1$	129
4.17	Specimen $CB_6.T60.L_1$	131

4.18	Mode of Failure and Cracks Pattern for Specimen $CB_6.T60.L_1$	132
4.19	Specimen $CB_7.T82.L_1$	135
4.20	Mode of Failure and Cracks Pattern for Specimen $CB_7.T82.L_1$	135
4.21	Specimen $CB_9.T60.S_1.L_1$	138
4.22	Mode of Failure and Cracks Pattern for Specimen $CB_9.T60.S_1.L_1$	138
4.23	Specimen $CB_{11}.T60.S_2.L_1$	141
4.24	Mode of Failure and Cracks Pattern for Specimen $CB_{11}.T60.S_2.L_1$	141
4.25	Specimen $CB_{13}.T60.L_2$	144
4.26	Mode of Failure and Cracks Pattern for Specimen $CB_{13}.T60.L_2$	144
4.27	Specimen $CB_{14}.T60.S_1.L_2$	147
4.28	Mode of Failure and Cracks Pattern for Specimen $CB_{14}.T60.S_1.L_2$	147
4.29	Specimen $CB_{15}.T60.S_2.L_2$	150
4.30	Mode of Failure and Cracks Pattern for Specimen $CB_{15}.T60.S_2.L_2$	150

List of Tables

Table No.	Title	Page No.
1.1	Main Steps for Producing Reactive Powder Concrete (Maroliya, 2012)	18
1.2	Advantages and Disadvantages of FRP (ACI-440,2006)	22
3.1	Designation and Details of Tested Circular Beam Specimens	63
3.2	Chemical and Physical Properties of Cement	75
3.3	Gravel Properties	76
3.4	Sand Properties	77
3.5	Technical Description of Sika ViscoCrete -5930-L	77
3.6	Chemical test of (LSP)	78

3.7	Cement Chemical and Physical Test Results	79
3.8	Typical properties of silica fume	80
3.9	Properties of Steel Fibers	81
3.10	Typical properties of MasterGlenium	81
3.11	Technical Properties of (CFRP) Laminates	82
3.12	Technical Properties of Epoxy Resin Materials	82
3.13	Properties of Reinforcing Steel Bars	83
3.14	Fresh concrete test results	85
3.15	Mix Proportion of Self-Compacting Concrete	86
3.16	Trail Mixes Proportion of RPC	87
4.1	Mechanical Properties of Control Samples	104
4.2	Cracking Load, Ultimate Load and Failure Modes of the of Tested CB Beams	152
4.3	Service Deformations of Tested CBs	158
4.4	Ductility Factor of Tested CBs Subjected to Monotonic Loading	160
4.5	Stiffness Criteria of Tested CBs Subjected to Monotonic Loading	164
4.6	Stiffness Degradation for CBs Subjected to Repeated Loading	165
4.7	Type and Width of Major Crack of Tested CBs Subjected to Monotonic Loading.	167
4.8	Type and Width of Major Crack of Tested CBs Subjected to Repeated Loading	169
5.1	Experimental and FEM Cracking and Ultimate Loads of CBs.	187
5.2	Experimental and FEM Results (Service Deflections and Ductility Factors)	188
5.3	Comparison of Effect of Shapes of Vertical Openings at Angle 60° by the FE Model	194
5.4	Comparison of Effect of Shapes of Transverse Openings at Angle 60° by the FE Model	195

5.5	Comparison of Effect of Curvature for Beams without Openings by the FE Model	197
5.6	Comparison of Effect of Curvature for Beams with Transverse Openings at Angle 60° by the FE Model	198
5.7	Comparison of Effect of RPC Version for Beams with Vertical Openings by the FE Model	200
5.8	Comparison of Effect of RPC Version for Beams with Transverse Openings by the FE Model	200

Notation

The major symbols used in the text are listed below; others are defined as they first appear.

Symbol	Description
As	Area of main reinforcement (mm^2)
Av	Area of web reinforcement (mm^2)
b_w	Web width (mm)
d	Effective depth (mm)
D_f , d_f	Nominal diameter of steel fiber (mm)
E_c	Concrete modulus of elasticity (MPa)
E_f	Steel fiber modulus of elasticity (MPa)
E_m	Plain concrete modulus of elasticity (MPa)
E_s	Steel modulus of elasticity (MPa)
f	Stress at any strain (ε) (MPa)
f'_c	Cylinder compressive strength of concrete (MPa)
f_{cb}	Ultimate biaxial compressive strength of concrete (MPa)
f_{cu}	Cubic compressive strength of concrete (MPa)
f_t	Concrete tensile strength of splitting test(MPa)
f_u	Ultimate strength of steel (MPa)
f_y	Yield strength of steel (MPa)
k	Stiffness criteria (kN/mm)
L_f , l_f	Length of steel fiber (mm)
Mn	Nominal moment capacity (kN.m)
Mu	Ultimate moment capacity (kN.m)
P_{cr}	Cracking load (kN)
$P_{cr(EXP.)}$	Cracking load obtained from experimental tests (kN)
$P_{cr(FEM)}$	Cracking load obtained from finite element analysis (kN)
P_n	Nominal load capacity (kN)
$P_{ser.}$	Service load (kN)

P_u	Ultimate load(kN)
$(P_u)_{EXP.}$	Ultimate load obtained from experimental tests (kN)
$(P_u)_{FEM}$	Ultimate load obtained from finite element analysis (kN)
s	Spacing of transverse reinforcement, center to center(mm)
V_c	Shear resistance of concrete (kN)
V_f	Volume fraction of steel fibers (percent)
Vs	Shear strength of web reinforcement (kN)
V_u	Ultimate shear force (kN)
X, Y, Z	Global coordinate system (denoting Cartesian coordinate)
$(\Delta u)_{EXP.}$	Experimental mid span deflection at ultimate load (mm)
$(\Delta u)_{FEM}$	Numerical mid span deflection at ultimate load (mm)
$(\Delta s)_{EXP.}$	Experimental mid span deflection at service load (mm)
$(\Delta s)_{FEM}$	Numerical mid span deflection at service load (mm)
ε	Concrete compressive strain
ε_{cu}	Ultimate compressive strain of concrete
ρ	Longitudinal tensile reinforcement ratio
ρ_f	Steel fibers ratio
σ_h^a	Ambient hydrostatic stress
υ_s	Poisson's ratio of steel reinforcement
$\emptyset$	Diameter of reinforcement bar (mm)
μ	Ductility ratio
υ	Poisson's ratio of concrete

Abbreviations

Abbreviation	Description
ACI	American Concrete Institute
ASCE	American Society of Civil Engineers
ASTM	American Society for Testing and Material
AASHTO	American Association of State Highway and Transportation Officials
CB	Circular Beam
BS	British Standards
CFRP	Carbon Fiber Reinforced Polymer
EBR- CFRP	External Bond Reinforcement- Carbon Fiber Reinforced Polymer
EXP.	Experimental
EFNARC	European federation of national trade associations representing producers and applicators of specialist building products
FE	Finite Element
FEM	Finite Element Method
FRP	Fiber Reinforced Polymer
GPa	Giga Pascal (kN/mm^2)
HC	Hybrid Concrete
HSC	High Strength Concrete
HRWRA	high range water reduction admixtures
IQS	Iraqi Specifications
IS	Indian Standards
ISIS	Intelligent Sensing for Innovative Structures
LSP	Limestone powder
LVDT	linear variable differential-transformer
MPa	Mega Pascal (N/mm^2)
No.	Number (issue)
NSC	Normal Strength Concrete
NSM	Near Surface Mounted
RC	Reinforced Concrete
RPC	Reactive Powder Concrete
Rebar	Reinforcing bar
Ref.	Reference
SCC	Self compact concrete
Vol.	Volume

CHAPTER ONE

Introduction

1.1 General

Box girders, have gained wide acceptance in freeway and bridge systems, as well as large space building, because of their structural adequacy, improved stability, maintainability, cost-effectiveness, and pleasant aesthetics **(Gupta et al., 2010)**.On the other hand, utilizing of straight part construction has reduced when compared to curved girders since, in cities when multi-level constructions and elevated roadways are required, geometric constraints are frequently used to contemporary highway bridges. As a result, a curved alignment must be developed. Despite the fact that the expense of constructing a curved girder superstructure is greater, because the number of intermediate supports, expansion joints, and bearing details has been eliminated, the total cost of the curved girder system has decreased dramatically. A more visually beautiful construction is provided by the continuous curved girder. Despite the benefits mentioned above, horizontally curved girders are more difficult to construct than straight girders. Because of the girder curvature, curved girders are exposed to vertical bending as well as torsion. In the 1960s, researchers began to pay attention to the intricacies of curved girders and developed theories **(Alhamaidah, 2017)**. Curved box beams have been more common and have been an intriguing subject of research because to the needs of stricter route and high torsional stiffness, as well as a desire for a higher sense of aesthetics.

1.2 Reinforced Concrete Horizontally Curved Beams

Reinforced concrete horizontally curved beams are widely employed in a variety of applications, including modernized highway intersections,

elevated highways, rounded building corners, and circular balconies, domes ring beam, etc. plate 1.1 **(Subramani et al., 2014)**. It is getting increasingly common to utilize horizontally curved girders for highway bridges or urban interchanges, so it is necessary to construct structures with a curved layout. The geometry of a beam curved in plan can be circular, elliptical, or parabolic, and it is generally fabricated of circular arcs with variable radii or centers.

Plate (1.1) Horizontally Curved Beam in Building and Girder Bridges

There is a major difference between the behavior of straight and curved beams. For straight beams, the in plane behavior and the out of plane buckling are considered independent in the theory of small displacement. The primary loading for horizontally curved beams is perpendicular to the plane of curvature of the beam, as shown in Figure 1.1. The vertical or out of plane displacement begins as soon as the load is applied. The vertical displacement of the beam is combined with horizontal displacement and twisting, resulting in nonlinear behavior of the beam with respect to the applied load. As a result, while evaluating displacement and stresses in horizontally curved beams, vertical displacement, horizontal displacement, and twisting of the beam should all be taken into account at the same time **(Yen et al., 2006)**. In another meaning, the significance of including

torsional effects in the analysis and design of such beams is an unique feature of their analysis and design.

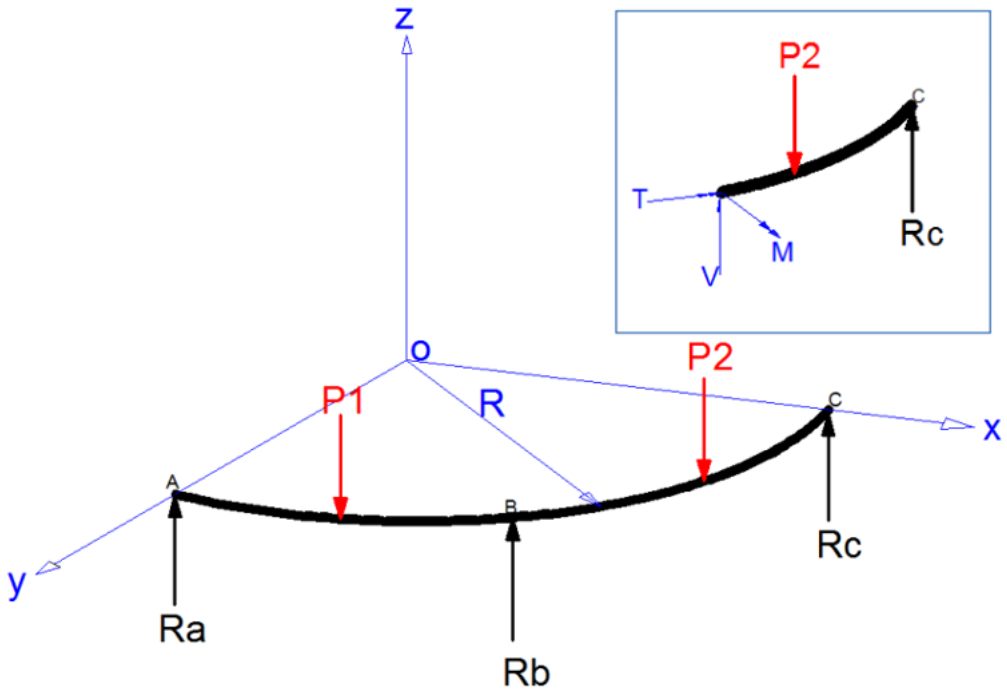

Figure (1.1) Loading and Forces of Horizontally Curved Beams

1.3 Box or Hollow Beam

Hollow structural sections are becoming more popular and used to pass electrical and mechanical utilities while also minimizing the height of the building and the cost of materials and construction. Furthermore, the utilization of hollow beams allows other beams to cross each other without requiring the pipes to be relocated.

The assessment and layout of curved box-girders are very intricate due to its behavior which consisting of torsion, shear and bending, see plate 1.2.

Plate (1.2) Horizontally Curved Box Girder **(Alhamaidah, 2017)**

1.4 Opening

Box girder (hollow beams) which carry a number of electrical cables and ducts for several services like water supply, sewage, air-conditioning, electricity, telephone, and computer network, sometimes needs to include an opening in webs and flanges to reach and sustain those cables and ducts. The presence of openings in reinforced concrete beam may lead to a reduction in its cross-section dimensions and lead to reduce flexural and torsional rigidity. Therefore, many problems in its behavior will occur such as strength reduction, excessive cracking, increase in deflection at service load, and reduce the beam's stiffness **(M A Mansur & Tan, 1999)**.

The influence of opening on the structural response of the beam depends upon the location and size of openings. Although, small openings in an undesirable location can result in a significant reduction in the strength of beam, therefore it is vital to choose the suitable size and location for the openings. It is desirable to include a reinforced concrete beam with openings having the same strength, stiffness, and cross-section dimensions of the solid beam, by providing special reinforcement in sufficient quantity with proper detailing **(Vedenoja, 2017)**.

There are two common directions of openings in reinforced concrete beams (girders), either vertical opening (the beams are crossed in the direction of their full depth) or transverse opening (the beams are crossed in the direction of their full width).

1.4.1 Transverse Openings

Usually, pipes and ducts results in aesthetic loss, so it is placed under the beam and covered by a suspended ceiling, thus creating a "dead space" alternatively, these ducts might be passed through transverse openings in the floor beams. This arrangement of building services, as illustrated in Figure 1.2, results in a substantial decrease in headroom and a more compact design. In the case of small structures, the savings may not be considerable when compared to the whole cost. However, for multistory buildings, any reduction in story height will result in a significant reduction in total height, Air-conditioning and electrical duct lengths, plumbing risers, walls and partition surfaces, and overall foundation load **(M A Mansur, 2006)**.

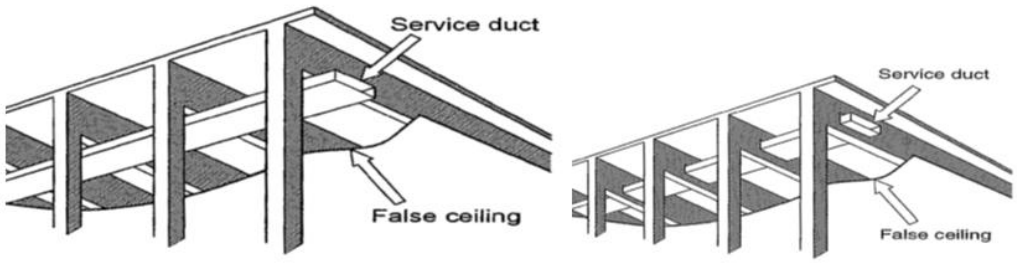

(a) (b)

Figure (1.2) Typical Layout of Pipes for High Rise Building **(M Abdul Mansur & Hasnat, 1979)**.
a-Typical layout of service ducts.
b- Alternative arrangement of service ducts

With regard to the size of openings in web of beams, many authors utilized the phrases small or large with no identifying them or establishing a clear limit between them. **(M Abdul Mansur & Hasnat, 1979)** describes a circular, square, or have a roughly square dimension openings as small, in contrast to **(Somes & Corley, 1974)**, when the diameter of a circular opening exceeds 0.25 times the depth of the beam web, it is regarded large. However, the researchers consider the concept of categorizing an opening as small or large depending on the response of beam. When the size of openings is kept under a certain range to maintain the behavior beam, or when the normal beam theory applicable, the opening can be labeled as a small. When the provision of openings eliminates beam-type behavior, the opening is described as a large opening **(M A Mansur et al., 1999)**.

As a result, failure modes of small openings are identified by two different modes of failures. These failures are known as "beam-type" and "frame-type" failures, and require independent consideration for the entire layout. With regards to openings with large dimensions, however, the beam-type behavior converts into a Vierendeel mode (Figure 1.3) as the dimension of opening is expanded. The following is a summary of the effects of creating a web opening on the overall response of a beam **(M Abdul Mansur & Hasnat, 1979).**

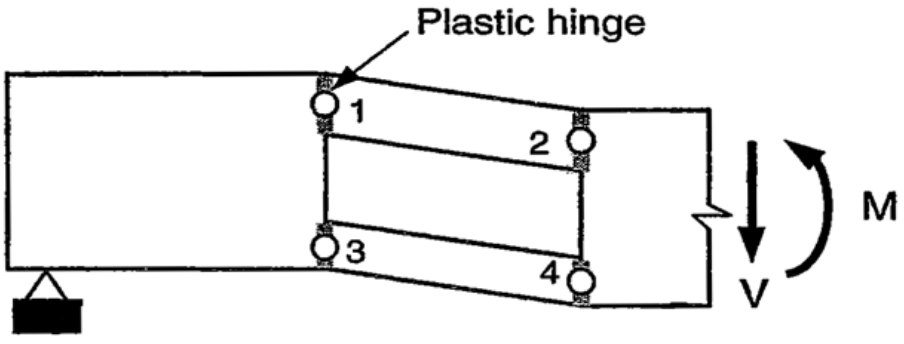

Figure (1.3) Collapses Mechanism at Large Opening
(M Abdul Mansur & Hasnat, 1979)

1- Including of an opening in the beam web causes a prematurely inclined crack, and first crack loading reduces as the length or depth of the opening increases.

2- The opening corners are subjected to wider cracking unless further reinforcement is included to minimize the propagation of cracks.

3- Increases of opening dimensions (length or depth), reduce the strength and stiffness of the beam when the same reinforcing amount and scheme are still used. The eccentricity of the opening, on the other hand, consists of only a slight influence on stiffness and strength.

4- Above and below the opening chord members behave similarly to the Vierendeel panel, with contraflexure points roughly in the middle of the span of chord. As illustrated in Figure 1.3, failure is caused due to development of four plastic hinges at all corners of the opening.

1.4.2 General Guidelines for Selection the Size and Location of Web Openings.

Figure 1.4 illustrate the following recommendations were offered to assist in the selection of the size and location of the web opening:

1. For efficiency of construction, openings in T-beams should typically be flush with the flange. Openings in rectangular beams are often located near the middle of the section, as well as they can be located eccentrically through the depth. It is necessary to be careful to ensure that the parts of the chord above and below are reinforced and adequately covered with concrete. In addition, the compression chord must have enough concrete area to create the ultimate compression block in flexure, as well as sufficient depth to provide efficient shear reinforcement.

2. To avoid the crucial zone for failure due to shear and reinforcing congestion, the space between the supports and the openings need not be

less than half depth of the beam. Similarly, any opening that is less than half depth of the beam distant from a point load should not be used.

3. The height of openings must be kept under half depth of the beam.

4. The stability of the parts of chord, particularly the chord under compression, and the serviceability limits of deflection are the parameters that restrict the length of an opening. As the opening expands, it is desirable to use several openings supplying the same path rather than utilizing a one opening.

5. To ensure that each opening works independently when utilizing multi openings, the gap between two openings next to each other should not be less than half depth of the beam.

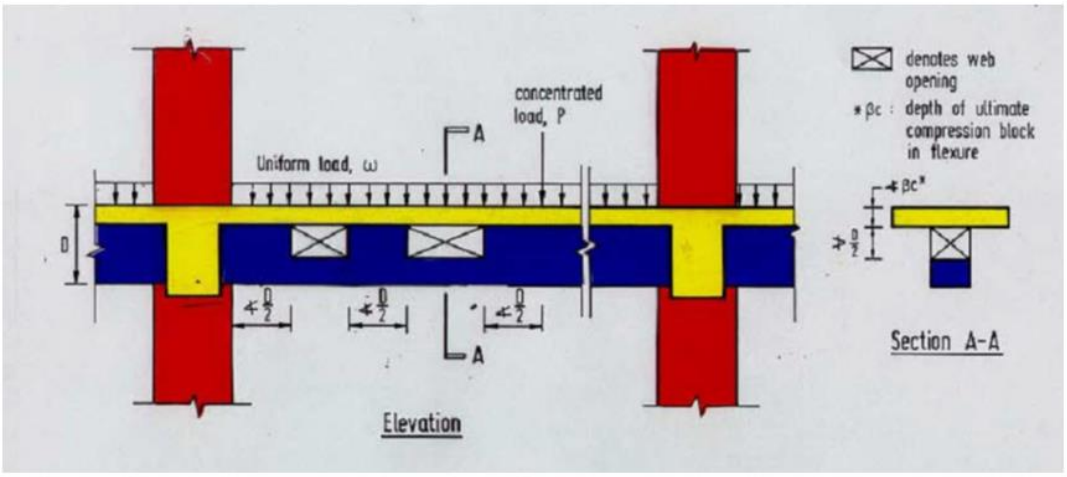

Figure (1.4) Recommendations for Location of Opening in Web of straight beam **(Tan et al., 1996)**

1.4.3 Vertical Opening

The vertical opening used to insert the services between the floors vertically through the beams of building and girders of bridge as shown in Plate 1.3. The horizontal opening, on the other hand, may be appropriately positioned without crossing the compression zone of the beam and therefore has no effect on the ultimate moment capacity. **(M A Mansur & Tan, 1999)**, Vertical openings always cause damage separate from them, reducing the

amount of concrete required to generate the whole compressive stress block.

Plate (1.3) Vertical Opening
(a) Horizontally Curved Girders (Baghdad-Iraq)
(b) Concrete Frame Building (Babile-Iraq)

Due to the reduced concrete area may result in a decrease in the maximum flexural and shear strength of beam, and because the presence of a vertical opening may interrupt the longitudinal or transverse reinforcement, the design of such a beam requires specific attention, which must be approved by a licensed design professional. **(ACI Committee 314, 2016)**.

1.4.4 General Guidelines for Selection the Size and Location of Vertical Openings.

The American Concrete Institute (ACI) suggests inserting the opening vertically through a beam, girder, or joist using the enforcing procedures in their guide of design for reinforced concrete structures, ACI 314R-16:

a. The diameter of the opening should not be greater than one third of the beams width.

b. The location of the vertical opening must be in plan no closer to the support face than one-quarter of the span length ($l_s/4$), or farther away than one-third of the span length (($l_s/3$).

c. The vertical opening should be located in the middle third of the member width and it should be spaced horizontally at least three diameters center-to- center.

d. Reinforcing bars should not be allowed to be cut due to opening penetration at any location.

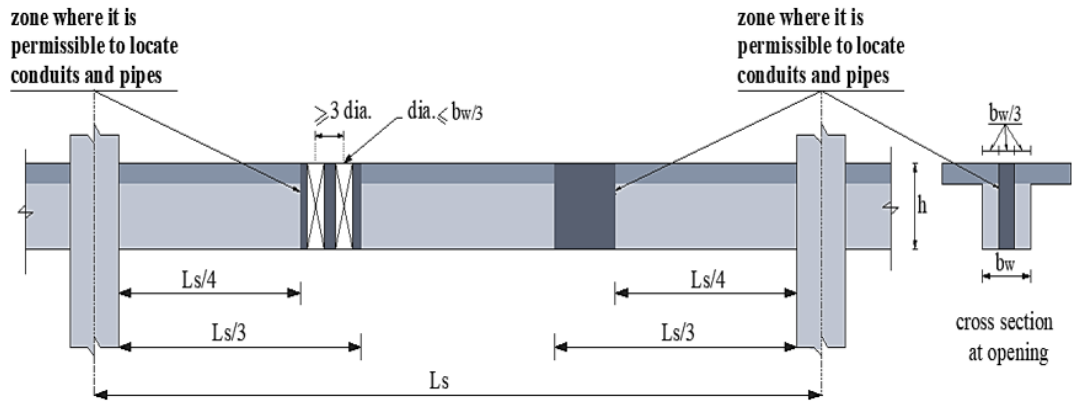

Figure (1.5) Location of conduits and pipes passing vertically through girders, beams, and joists **(ACI 314-16)**.

1.5 Ultimate Strength Analysis Under Combined Torsion, Bending and Shear

Any solid beam subjected to shear, bending and torsional moments simultaneously can be analyzed based on the well-known skew-bending theory for torsion in concrete beams. In the case of a solid beam, the theory deems three basic failure modes classified as Mode 1, Mode 2, and Mode 3, according to the location of concrete compression zone near the top, side, and bottom of the beam, respectively, as shown in Figure 1.6. Aspect ratio of the beam section, relative proportion of top and bottom longitudinal steel,

and the ratio of applied torque to bending moment with or without a combination with transverse shear generally govern the failure modes. When a relatively small transverse opening is introduced through the beam web, and the beam is subjected to predominant torsion, one would expect no changes in the mode of failure. This has been confirmed experimentally by several investigators **(Hasnat & Akhtanizzamam, 1987); (M Abdul Mansur & Hasnat, 1979); (Mohammad A Mansur et al., 1983) ; (M A Mansur & Paramasivam, 1984)**. As a result, for beams with a small opening, an examination identical to that of a solid beam can be used. With this argument, the evaluation depending on number of failure mechanisms categorized as mode 1, mode 2, and mode 3. The surface of failure is expected to pass through the opening center since that represents a possible origin of weakness in a beam. Each collapse mode is evaluated independently while creating strength equations for such beams, and the following guideline are used to minimize the difficulties **(M A Mansur & Tan, 1999)**:

1- The pattern of reinforcement in the vicinity of the opening consists of longitudinal bars above and below the opening, full-depth stirrups close to either side of the opening, and closed stirrups at the throat section (above and below the opening), in addition to the normal top and bottom reinforcement in the solid section.

2- Stirrup spacing is consistent over the length of the beam, both at the solid region and at the cords.

3- Failure occurs on a warped plane. The boundaries of the warped plane are defined on the three sides of the beam by a spiral crack and on the fourth side by a compression zone that joins the ends of the spiral crack.

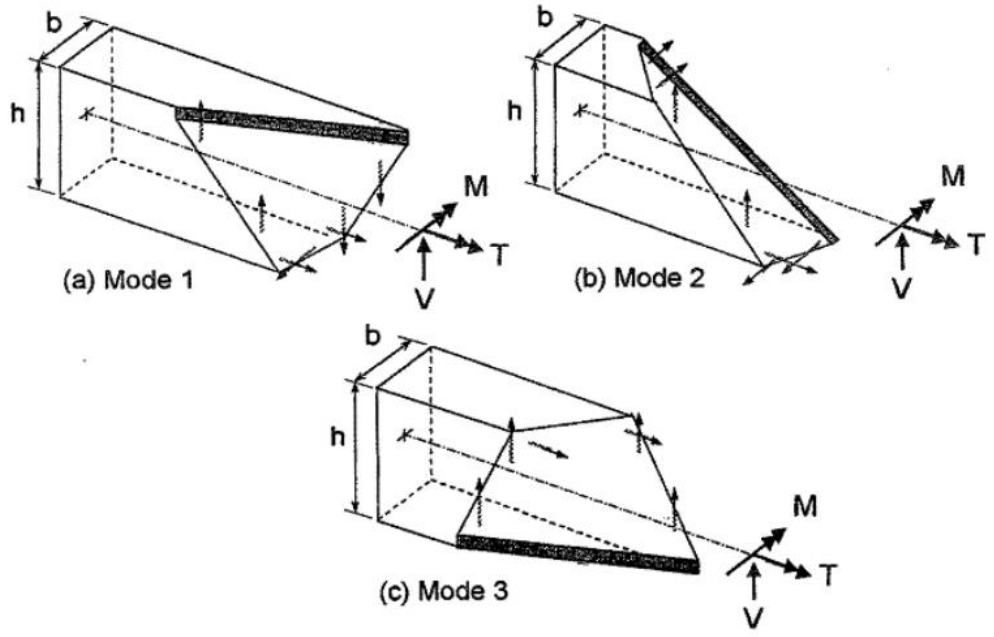

Figure (1.6) Failure surfaces for a solid beam in Modes 1, 2, and 3.
(M A Mansur & Tan, 1999)

4- The three lines wrapping round in the beam with a steady inclined angle define the plane of failure on three sides of the beam.

5- Outside compression region, the concrete has no tension as it cracked.

6- Outside the compression region, all reinforcement that crosses the failure plane yields with failure.

7- Reinforcing steel in the compression zone, as well as the reinforcement of dowel action, are neglected.

1.6 Failure Modes for Beam with Small Opening Under Combined Torsion, Bending, and Shear

A structural part is susceptible to torsion, bending, shear, and axial forces in general, although the influence of axial load is frequently neglected when analyzing and designing a beam. As a result, simultaneous bending, shear and torsion may be regarded the popular loading situation for beams, also

this load scenario is dealt with three separate of mode failure as illustrated in Appendix A.

.

1.7 Design for Torsion

The failure surface has already been assumed to pass through the opening center as well as encroaching on the solid part of the beam in the theory of skew-bending for beams with a small opening under torsion as in the above description. Many torsion tests have revealed this **(Hasnat & Akhtanizzamam, 1987); (M Abdul Mansur & Hasnat, 1979); (M A Mansur & Paramasivam, 1984)**, These failure patterns are substantially the same as beam without an opening, and so are referred to as "beam-type" failure. Only the reinforcing bars in the solid portion out of the opening region contributes in resisting the subjected load, according to the equations developed. When enough rebars are utilized to avoid failure in these modes, a probability that the failure may happened in the cords upper and lower the opening. Figure 1.7 displays this kind of failure. It is described as "frame-type" failure as it comparable to "frame-type" shear failure of a beam has openings with small dimension. The members framing the opening resist the whole applied actions, independent of the solid section of the beam, in this kind of failure, and then require a different consideration in design.

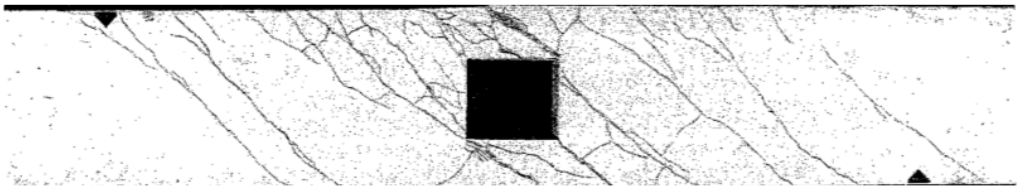

Figure (1.7) Frame-type failure of a beam with a small opening under torsion **(Hasnat & Akhtanizzamam, 1987)**

1.7.1 Design for Beam Type Failure

Australian Code, AS 1480 (1974), provides torsional design based on failure mechanisms described in skew-bending theory, which All of them

are classified beam-type failures. When a small opening is included, the strength equations for different types of failure are essentially the same, and they are proven correspond quite well with obtained test results **(Hasnat & Akhtanizzamam, 1987); (M Abdul Mansur & Hasnat, 1979); (M A Mansur & Paramasivam, 1984)**, the same technique may be utilized with slight adjustments for the presence of openings for designing such beams. Appendix A contains the design equations for the many probable types of failure under dominant torsion.

1.7.2 Design for Frame Type Failure

When the cords above and below the opening are not appropriately strengthened for carrying load being transferred through them, this variety of failure occurs. The subjected shear can be supposed to be carried by the chord parts in percentage to their areas of cross-sectional under this situation of combined bending and shear. Similarly, the torque applied to the chord parts, which causes lateral shear stresses, perhaps considered to be withstand by the couple created as a result of these stresses, as illustrated in Figure 1.8.

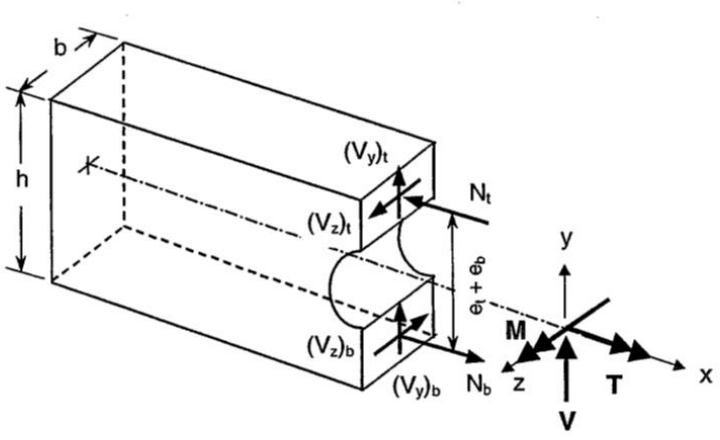

Figure (1.8) Idealized free-body diagram at opening of a beam under loading **(Mohammad A Mansur et al., 1983)**

The above study may be acceptable from the investigation of **(Mohammad A Mansur et al., 1983)**. It was proposed that the applied torque in a beam with an opening is prevented due to torsion by each part and by the couple created by the transverse shear, also demonstrated that when the length of the opening diminishes, the torsional component reduces, as the opening lowers to a square (or circular) in size, it becomes insignificant as compared to the latter segment (couple generated by lateral shear). Using Figure 1.8 as an example, the transverse shear, Vz, possibly supposed to be presented by

$$(V_z)t = (V_z)b = \frac{Tu}{\theta t+\theta b} \qquad 1.1$$

The difficulty of combining torsion, bending, and shear for frame-type failure is therefore reduced to design each chord element for shear in transverse and vertical direction, using the typical mechanism for applied bending moment.

1.8 Cyclic Loading

A cyclic loading is a series of (loads or displacements) that occurs in the pattern of repeated cycles with constant or varying intensity. There are two major forms of cyclic loading that are widely used. **(Al-Shimmari, 2006)**:

a- **Repeated loading,** the term "repeated load" refers to a series of loading cycles that range from zero to peak load in one direction, with all cycles moving in the same direction (positive or negative).

b- **Reversed cyclic loading,** implies a series of loading cycles that change from one-way peak load to reverse peak load around a midpoint, with both positive and negative half-cycles in each cycle.

During their service lives, many concrete buildings are subjected to cyclic loads. These cyclic loads can come from a variety of sources, including

earthquake ground motion, wind pressure, wave action, explosions, traffic, and other types of recurring loads **(Al-Shimmari,2006)**. One of the most dangerous cyclical loads is earthquakes because they occur abruptly, intensely and without previous warning **(A. Y. Ali, 1990)**.

1.9 Self-Compacting Concrete (SCC)

Self-Compacting Concrete reveals the important developments in concrete technology. It is a different kind of high performance concrete, which can flow under its own weight **(Hwang et al., 2006)**. It can be used to fill restricted parts, such as those in the joint zone between columns and beams, and to repair certain structural parts **(Paultre et al., 2005)**. SCC is a fluid mix, which is suitable for casting such difficult sections, especially in high-density reinforcement. To achieve that, a self-consolidating or self-compacting concrete must have a fluidity that permits to complete consolidation without any vibration, therefore three properties characterize a concrete mixture as a self-compacting **(Goodier, 2003)**:

-Flow ability: the capability to entirely fill the regions and corners of the formwork wherever it is placed.

-Passing ability: the capability to move through the congested reinforcement without blockage or separation of components.

-Segregation resistance: the ability to preserve the coarse components of blend as a homogenous substance

The viscosity of such concrete should be reasonable to prevent bleeding and segregation, a relatively value of low yield to supply high flow ability, and should sustain its homogeneity through curing, transporting, and installing to confirm acceptable structural behavior and long-term durability. SCC should be developed in such a way that it achieves a suitable balance of stability and deformability **(Parashar et al., 2020)**.

1.10 Concept of Hybrid Sections

Engineers' ongoing efforts to mix two or more materials in a structural element to take use of their beneficial properties gave rise to the concept of hybrid structural elements. Firstly, to improve the load carrying requirements in steel sections, the hybrid section is utilized. The concept of hybrid section idea including two or more type of concrete in one section. Hybrid reinforced concrete is spread extensively today **(Barbuta et al., 2009)**. The term "Hybrid reinforced concrete" is usually referred to one of the following concepts: **-**

1-Utilizing hybrid reinforcing bars.

2-Using (FRP and steel) rebars.

3- Different types of concrete.

In this study, the third concept is utilized in the vicinity of the opening in attempt to restore and enhance the overall performance of reinforced concrete beams. When the hybrid concept is expanded to composite concrete members and because of the progress in concrete technology, it is relatively easy to produce composite sections that have high compressive strength, high ductility, high energy absorption and high tensile strength at the same time. These properties can be accomplished by placing at least two distinct types of concrete together, so that each type is utilized to its best advantage and as a result, a concrete member becomes a "hybrid" **(Bernard et al., 1998)**.

1.11 Reactive Powder Concrete (RPC)

Reactive powder concrete (RPC) is a type of ultra-high strength fiber concrete (UHPC) that has a high strength, ductility, and durability due to a unique mixture of constituent materials. The composition of reactive

powder concrete includes cement (ordinary Portland cement), very fine sand (0.15-0.6) mm, silica fume, micro steel fibers. This type of concrete has a low water-binder ratio (less than 0.2) and requires a superplasticizer to achieve high flow ability, the maximum particle size of mixture is (0.6) mm to avoid weaknesses of the microstructure **(Bonneau et al., 1997)**. The mechanical properties that can be achieved include the compressive strength of the range between 200 and 800 MPa **(Richard & Cheyrezy, 1995)**. The main steps for producing reactive powder concrete can be listed in Table 1.1.

Reactive powder concrete used for many important applications, such as larger spaces, seismic zones, construction of power plants, railway bridges, and buildings that require light and narrow parts, such as stadium roofs, long bridges, and explosion-proof structures are all examples of current repairs that improve the performance of damaged parts of structures **(Lahlou et al., 1992)**. RPC can even replace steel in pressure members when durability is a concern due of its excellent durability (for example in the case of marine as marine installations) **(O'Neil et al., 1997)**. Apart from the attractive structures designed for architectural objectives, like the bus shelters in USA and Martel tree in France **(Sadrekarimi, 2004)**. Plate 1.4 depicts several examples of reactive powder concrete applications from throughout the world.

Table (1.1) Main Steps for Producing Reactive Powder Concrete (**Maroliya, 2012**)

steps	reason
Eliminating of coarse aggregate	Improve the homogeneity
Optimization of the granular mixture	Getting very dense matrix by improving the packing

Table (1.1) continue

Optimization of the pozzolanic material (Silica fume)	Lowering the anhydrate cement
Using superplasticizer	Reduce W/C ratio and improve the workability
Heat treatment after hardened	Improve the microstructure
Optional steps	
Adding small size of steel fibers	Improve the ductility
Applying pressure before and during setting	More improving of compaction

Seoul footbridge, South Korea Sherbrook footbridge, Canada

Plate (1.4) Applications of Reactive Powder Concrete **(Russell et al., 2013)**

1.12 Fiber Reinforced Polymer (FRP)

One of the significant advancements in concrete constructions is fiber reinforced polymer. Because of the benefits offered, FRP is being used in the building and repair of structures, for example, high proportion of (strength to weight and stiffness to weight) and magnificent characteristics for (fatigue, non-magnetic, resistance of corrosion and chemicals) **(A. A. el**

Ali, 2011). FRP compounds consist of fiber and matrix (resin) as shown in Figure 1.9. The matrix covers and transfers stress between fibers while the fibers offer strength and stiffness **(Rathod & Vora, 2015)**.

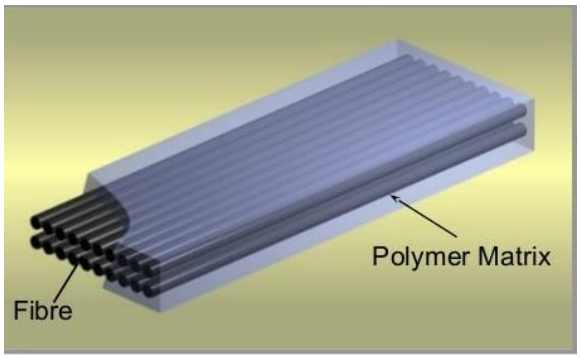

Figure (1.9) Typical composition of FRP materials **(Mazzolani, 2001)**

Many FRP materials have been developed with different types of fibers, which include glass, aramid and carbon fibers. Several forms of FRP are produced such as, strips, bars, 2D grid, 3D grid or standard structural forms, as shown in Plate 1.5 **(ISIS, 2007)**. High tensile quality of FRP bars make them an effective alternative to steel bars, but at a similar time no plastic behavior (yield) appears before failure when exposed to tensile.

Figure 1.10 shows how uniaxially loaded fiber materials and steel respond in various manners.

Plate (1.5) Formats of FRP Items **(ISIS, 2007)**.

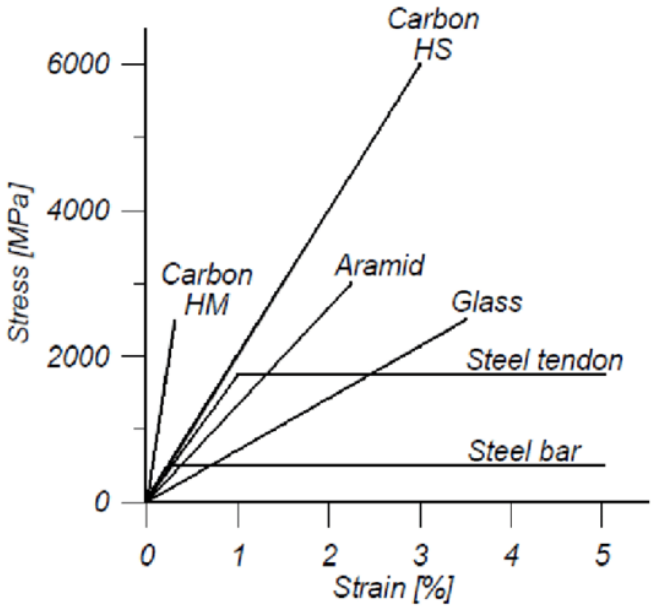

Figure (1.10) Stress-Strain Relationship of Fibers and Steel **(Carolin, 2003)**

1.12.1 Configuration of Fiber Reinforced Polymer (FRP)

FRP materials have been manufactured as laminates for using in reinforced concrete members in terms of external reinforcement technique, it is installed to the outer surface of concrete. The mechanical characteristics of FRP laminates rely upon the sort of resin and fibers additionally their volume fraction. Nevertheless, FRP laminates have high tensile strength, low Young's modulus and brittle response of linear-elastic to failure **(Mohsen, et al., 2011)**.

FRP laminates have two or more distinctive fiber alignment such as: unidirectional (majority of fibers in one direction) and multi- directional fabrics (fibers in more than one direction) see Figure 1.11.

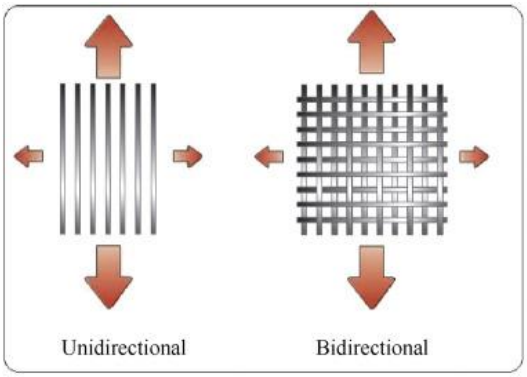

Figure (1.11) Some Types of FRP Laminates fiber alignment (Karataş & Gökkaya, 2018)

1.12.2 Advantages and Disadvantages of (FRP)

Late years have seen a quick development for applying progressed FRP composite in a large parts of the world because of its preferences and the nature of the materials utilized in the production. **(ACI-440,2006**) displays some of the advantages and disadvantages of FRP reinforcement, as shown in Table 1.2.

Table (1.2) Advantages and Disadvantages of FRP **(ACI-440,2006)**.

Advantages of FRP	Disadvantages of FRP
High longitudinal tensile strength	No yielding before brittle rupture
Corrosion resistance	Low transverse strength
Nonmagnetic	Low modulus of elasticity
High fatigue endurance	Susceptibility of damage to polymeric resins and fibers under ultra violet radiation exposure
Light weight (about 1/5 to1/4 the density of steel)	High coefficient of thermal expansion perpendicular to the fibers, relative to concrete
Low thermal and electric conductivity	May be sensitive to fire depending on matrix type and concrete cover thickness
	Difficult to bend it to make stirrups or anchorage hooks
	Little bond with concrete

1.12.3 Applications of (FRP) Laminates

Many applications in the field of structural engineering have FRP laminates. FRP laminates are used as a group of strengthening materials that can fulfil most of the needs for strengthening or refurbishing of structural building. Reasons for the application can be a change of use and/or loading, modification of the structural system as well as prevention or repair of structures in seismically endangered zones. The enthusiasm for the use of FRP laminates is due to the simplicity and speed of installation.

1.13 Objective of the Current Study

This study is intended to investigate experimentally and numerically the structural behavior of circular box beam specimens, made with vertical and transverse opening. The main objectives include: -

1- Executing experimental program to explore the structural behavior of horizontally curved (circular) box beam with and without openings, under effect of monotonic and cyclic loads.

2- A comparison of the performance of horizontally curved box beam in terms of the following main variables:

- Direction of opening axis, (vertical through flange) and (transverse through web).
- Location of opening through span of curved beams near (end support, internal support and mid span).

3- Examining the effectiveness of the techniques to restoring strength and serviceability properties of curved beam included openings by using hybridization

of concrete (NC and RPC) and external bond reinforcing EBR-CFRP laminates around openings.

4- A nonlinear finite element method technique be utilized in this study by using ABAQUS program for analysis of horizontally curved box beam with opening. The numerical results compared with the corresponding experimental data.
5- As well as, investigating the parametric study of several important variables which are not considered in the experimental program, such as: radius of curvature, other shapes of openings and RPC with other compressive strength.

1.14 Layout of Thesis

Six chapters constitute up the present research. The current chapter (chapter one) provides an overview of applications of box girder, horizontally curved beam, consequences of openings in reinforced concrete beams and their effects on performance of reinforced concrete curved box beams, failure modes of beam with opening, cyclic loading, Self-Compacting Concrete (SCC), reactive powder concrete (RPC), fiber reinforced polymer (FRP), and concept of hybrid sections. The main objectives of the current research are additionally incorporated into this section. Most previous studies related to the current study were presented in chapter two. The third chapter offers the latest studies relevant to experimental program, specimen details, material characteristics and method of testing. The fourth chapter presented discussion and evaluation of the results of present work. The modeling of materials utilized in finite element analysis, types of components utilized in idealization, and nonlinear solution techniques are all covered in Chapter five. Chapter six presents a conclusions summary of the present work and recommendations to work in the future.

CHAPTER TWO

Literature Review

2.1 Introduction

Because of its great structural efficiency and excellent aesthetics, box-girder bridges, both straight and horizontally curved, are frequently utilized all over the world. Many investigations have been performed on approaches for determining ultimate loads for straight hollow beams. Ultimate loads and nonlinear response for reinforced concrete horizontally curved box beams with an opening in flanges or webs have not been thoroughly investigated. The purpose of this chapter is to go through the previous studies available on (horizontally curved beams, straight and curved box girders) with and without openings unstrengthen or strengthened with RPC or CFRP laminates, particularly those beams which are under the combined effect of bending, shear and torsion.

2.2 Experimental and Analytical Studies on Reinforced Concrete curved Beams.

(Chu & Thelen, 1963) presented plastic analysis for circular curved balcony girders fixed supports at both ends and maintained the cross section of a solid beam with a considered to be influenced angle less than 180 degrees constant and tested to a distributed load perpendicular to the plane of the curved beam. To calculate the ultimate load in this work, in the same approach that any other plastic analysis, the following requirements must be fulfilled: (a) static equilibrium, (b) criteria of yielding, (c) law of flow, and (d) mechanism and compatibility conditions. At a region where a plastic hinge was developed, a surface of yielding of synchronous bending and torsion has been depicted by:

$$m_o^2 + t_o^2 = 1 \qquad 2.1$$

The following equation was used to satisfy the flow law requirement:

$$\tan \gamma_o = \frac{to}{mo.\alpha\, o} \qquad 2.2$$

where

$m_o = M / M_P$, $t_o = T / T_P$, $\alpha_o = T_P / M_P$

M: applied bending moment at cross section.

T: applied torsional moment at cross section.

M_P: plastic bending capacity of cross section.

T_P: plastic torsional capacity of cross section.

γ_o: angle between the axis of rotation at the plastic hinge and the vector radius.

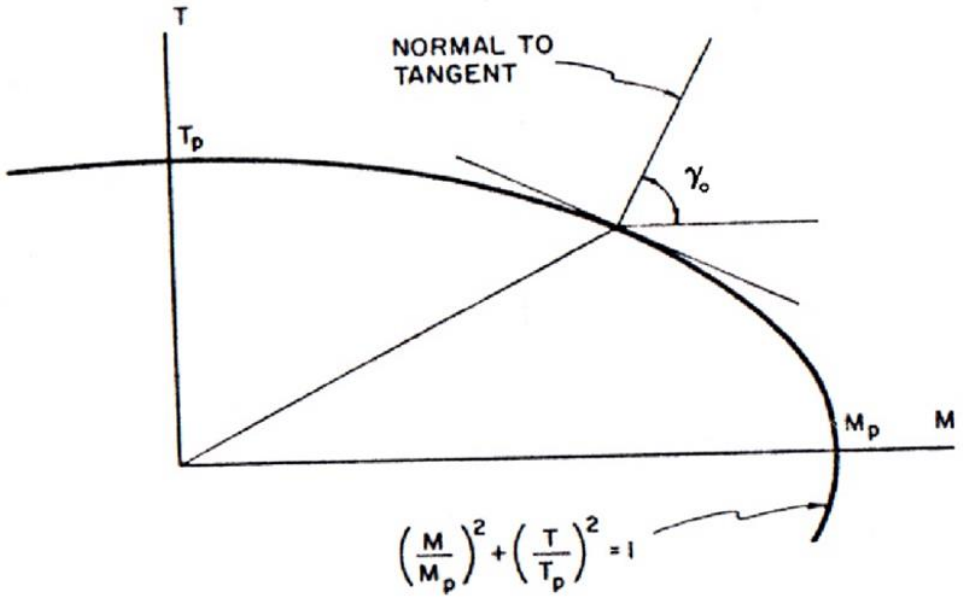

Figure (2.1) yield surfaces for combined bending and torsion, at a section where a plastic hinge was formed.

Figure 2.1 illustrates the yield surface under effect of combined bending and torsion, at a section where a plastic hinge was formed. The general method of analysis was examined, the various mechanisms of failure were investigated, and the results of the load capacity of curved beams were presented in a chart to facilitate their application.

(Jordaan et al., 1974) presented a study to develop a plastic methods of analysis for the determination of collapse load for reinforced concrete curved beams and subtending a central angel less than 180 degrees. The plastic evaluations for single point loads, in addition to uniformly distributed loads, were extended in this work to include two focused loads applied at different locations of the beam span. Formation of plastic hinge was expected at that cross section of the curved in plan beam where the internal moments meet the identical yield requirement and flow law as in equations (2.1) and (2.2).

Four curved in plan and six straight solid beams were examined in experimental section of this research. At any location, all of the specimens had constant moment and torque capacity. At the supports, the beams were completely restricted.

All curved beams have identical radius and subtended angle. The curved beams were categorized into two groups based on the amount of reinforcement. One sample from each group was subjected to one-concentrated load and the other specimens were subjected to two-point load.

Straight beams were categorized into two groups as well. The reinforcement in these two groups was equivalent to that in the curved beams group. Each group had one beam examined under bending, however the other two specimens were examined for torsion, combination bending and torsion, respectively. The purpose of testing straight specimens was to determine

the flexural and torsional capacities of each kind of cross section, as well as to check the yield criteria-provided interaction relationship. It was concluded in this article that the plastic theory could provide a reasonable estimate for pattern of the failure (position and sort of plastic hinges), however for certain patterns, the predicted maximum load was conservative, while for others, it was higher than the practical maximum load.

(H E I Badawy et al., 1977) formulated two yield criteria to represent the behavior of a reinforced concrete section under the combined action of bending, torsion and shear, and the analysis was modified to include the effect of shear. They tested seven straight solid and eight curved beams, and the results were compared with the modified analysis. In the test on curved beams, the plastic hinge locations and consequently the modes of failure were recognized from the crack patterns, the deformed shape of the beam and the measured reinforcement strains. The workers observed the plastic hinges either torsion-shear hinges, flexural hinges, or bending-torsion-shear hinges. The analysis of the test results and the comparison with the results predicated by the plastic theory indicates the following four conclusions:

1. The methods of plastic analysis can be applied to reinforced concrete curved beams.

2. An analysis using the first criterion gives a good predication of the ultimate load, mode of failure and the internal forces. Whereas an analysis using the second criterion establishes a lower bound for the ultimate load and the internal forces. The dimensionless equations for these two surfaces are

$$\frac{m^2+t^2}{1-v^2} = 1 \qquad 2.3$$

for the first yield criteria and

$$\frac{m^2+t^2}{(1-v)^2} = 1 \qquad 2.4$$

for the second yield criteria

where: $m = M/M_P$, $t = T/T_P$, $v = V/V_P$, M, T, and V are the bending moment, torsion and shear respectively; and M_p, T_p, and V_p are the corresponding plastic capacities of the cross-section in pure bending, torsion, and shear.

3. In a curved beam, two forms of internal force redistribution occur: one due to crack and the other related to the development of a plastic hinge.

4. The study effectively predicts the influence of modes of failure.

(Hammouda E I Badawy et al., 1977) presented an experimental study to investigate the validity of plastic analysis methods for reinforced concrete horizontally curved beams that including shear effect. Eight curved and seven straight beams were tested. Each curved beam had a radius of (2.21 m) and a subtended angle of (75) degree as shown in Figure 2.2. Each curved beam was designed to be tested under effect of single concentrated load. Four curved beams were reinforced identically but were tested under different end conditions. In the other curved beams, both the transverse reinforcement and the end conditions were varied. The straight beams were reinforced according to the reinforcement of the curved beams and were tested under different combinations of bending, torsion and shear. The results of the straight beams were used to determine the intersection point of the two yield criteria (proposed in an earlier investigation) with the bending, torsion, and shear axes and to check the validity of yield surfaces. This paper concluded that an analysis using the first criterion gives a good predication of the ultimate load, mode of failure, and the internal forces, whereas an analysis using the second criterion might establish a lower bound for the ultimate load and the internal forces.

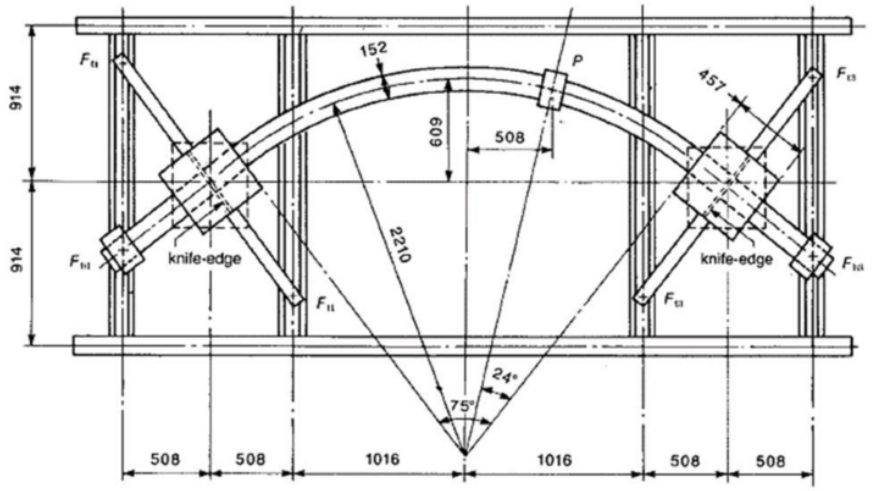

Figure (2.2) Geometry of Test Specimens **(Badawy,1977)**.

(Scordelis et al., 1982) presented a comparison of experimental and numerical analysis to study behavior of two spans, four cells, reinforced concrete box girder bridge. Experimental work included fabricate three large scale (1:2.8), the cross-sectional and longitudinal span dimensions of the models were identical, one was straight, one was curved, and one was skewed in the plane. The samples had same dimensions (21 m) length, (3.7 m) wide and (0.52 m) deep. These The samples were tested with three types of loading (dead load, working loads, and overloads, including loading to failure). Same amounts of steel reinforcement were used in the straight and curved models, but for skew model the amount used was less. Numerical analysis was provided by utilazing finite element analysis method adopted by using computer programs named (FINPLA2) for the straight box girder model and (CELL) used for both curved and skew box girder bridge models. They concluded that the structural response to point loads at mid span sections of the straight and curved box girder models was similar, the skew box girder had a different structural behavior and was directly dependent on the change in the location of transverse applied concentrate load, and that all three box girder models showed excellent response with

high overload capacities before ultimate failure. Also, they found good agreement between numerical and experimental results.

(Ali & Hemzah, 2014) presented an experimental and numerical F.E. analysis by utilizing ANSYS package program to investigate the behavior and performance of solid reinforced concrete horizontally curved beams with and without openings. Unstrengthen and strengthened externally by CFRP laminates or internally by steel reinforcement. Experimental work was included fabrication and testing of fourteen reinforced concrete curved beams divided into two group. The first group consist ten of semicircular beams (one without opening and nine with openings), while the second group consisted of four full circular reinforced concrete beams (one without opening and three with openings). The variables considered in the experimental program were included: geometry of circular beam, location of opening through profile of beam, presence of internal strengthening by reinforcing steel(stirrups) and external strengthening by CFRP laminates for beam around openings. The beams were tested under effect of point loads at top edge of each midspan. Numerical work was included a three-dimensional nonlinear finite element model using the computer program ANSYS version 12.1 suitable for the analysis of the tested reinforced concrete horizontally curved beams with or without openings and unstrengthened or strengthened by(CFRP) laminates or reinforcing steel) under incremental loading, as well as a parametric study for many variables such as location of opening through the beam profile size and type of opening and U shape strengthening using CFRP laminates.

It was concluded that the presence of opening had a considerable effect on the behavior and ultimate load capacity of semicircular and full circular beams. In contrast, the strengthening of these opening by internal steel reinforcement or external CFRP laminates restored ultimate load capacity.

Moreover, concluded that the FEM analysis and modeling had gave a good agreement with experimental results.

(Sasidharan & Johny, 2015) analyzed various curved box girder models by ABAQUS software with different radius of curvature and span. The ratio of span to depth is maintained constant. The depth of the models is varied according to a span to depth ratio of 16. The parametric analysis is used to detect changes in responses in terms of flexural and shear stresses, in addition to deflection at mid span. The following conclusions are drawn from the findings of the study of a curved single cell rectangular box girder:

- The graph plotted between reaction and radius of curvature shows that reaction decreases with increase in radius of curvature and with decrease in span length.
- The bending stress indicates a reduction by increasing the radius of curvature.
- Reduction in radius of curvature increases the shear stress.

2.3 Experimental and Analytical Studies on Reinforced Concrete Box Beams.

(Arendts, 1969) Presented a manner for the full determination of the deflection, moments and shearing forces, in the simply supported concrete straight multi-cell box girder bridges subjected to externally applied vertical concentrated loads. This method involved the replacement of the actual cellular structure of the concrete box girder by a uniform plate with structural characteristics identical to those of the real girder. Three parameters were studied; the ratio of the width to the span of the girder, a stiffness parameter reflecting the relative flexural and torsional rigidities of

the structure, and an effective width which is a function of the bridge's edge beam geometry.

It was found that the use of this theoretical expressions yield an accurate and simple way for the complete determination of load distribution in concrete box girder bridges. Also, concluded that the better load distribution is achieved in most cases of a bridge (multi cell box girder) by, smallest practical ratio of the width to the span of the girder (W/L) ratio, a low stiffness parameter value for bridges without inner diaphragms, the least flexural rigidity - transverse shearing rigidity ratio for bridges without inner diaphragms, and the maximum transverse shearing rigidity and edge configuration for bridges with diaphragms if W/L0.5, and an edge configuration with less top edge flange cantilevering if W/L>0.5.

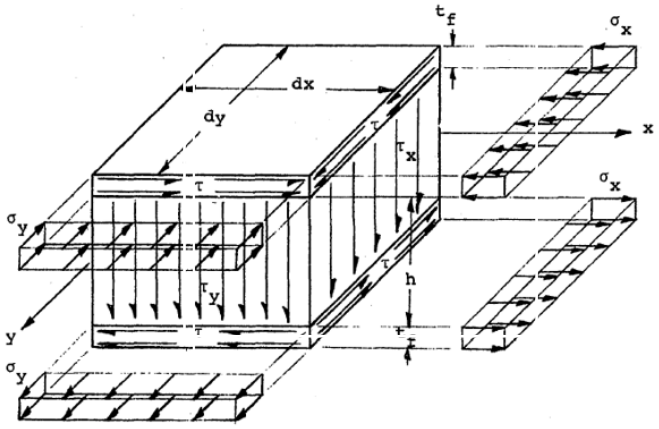

$\mathbf{t_f}$: flange thickness.
$\boldsymbol{\sigma_x, \sigma_y}$: Normal stress in the direction of x, y, respectively.
$\boldsymbol{\tau_x, \tau_y}$: Vertical shearing stress in the core media normal to x and y, respectively.

Figure (2.3) Stress distribution on typical plates **(Arendts, 1969)**

Also noted that specific loads and moments do not conform to these assumptions, yet they can be utilized as design guidelines.

Finally, it was found that the most considerable change in the distribution of moments, shear forces and quantities of deflection was the aspect ratio

W/L, the stiffness parameter. Therefore, the effect of effective width was not as great as the effect of W/L and stiffness parameter, on the distribution of load.

(Seible & Scordelis, 1983) developed a numerical method of analysis to determine the nonlinear response, collapse mechanisms and ultimate failure loads of multi-cell RC (reinforced concrete) box girder bridges under gradual increasing static loads. The study includes development of analytical model based on three-dimensional grillage of arbitrary plan geometry and constant height. A computer program (NOBOX) based on the proposed analytical scheme which also based on a mixed model formulation at the element level, had been developed and tested on numerous numerical examples, and the analytical results indicated good agreement with experimental results obtained from large scale model tests on RC box girder bridges. Interaction between different design quantities such as torsional and flexural shear in the vertical webs was incorporated using a circular interaction relationship for cracking and ultimate shear failure. Other interactions such as torsional shear forces in the top and bottom slabs with axial forces in the flanges due to longitudinal bending are difficult to establish and were not considered in this investigation. A straight, two span, four cell RC box girder bridge model was experimentally tested up to failure at the University of California, Berkeley, to illustrate the suggested analytical model for nonlinear analysis of multi-cell RC box girder bridges. Displacement and force redistributions due to structural deterioration, as well as ultimate failure loads, collapse mechanisms and plastic deformations can be predicted.

(Luo et al., 2003) based on classic thin plate theory, Presented a method for the calculation of moments on upper slab in single-cell box girders, which included representing the influence of constraint of the box girder

web on transverse flexure of the top plate by an elastically clamped plate analysis, elastically clamped boundary conditions mean that the analytical model built with two sides as a simply supported with elastically clamped plates and two sides as a simply supported only as shown in Figures 2.4 and 2.5.

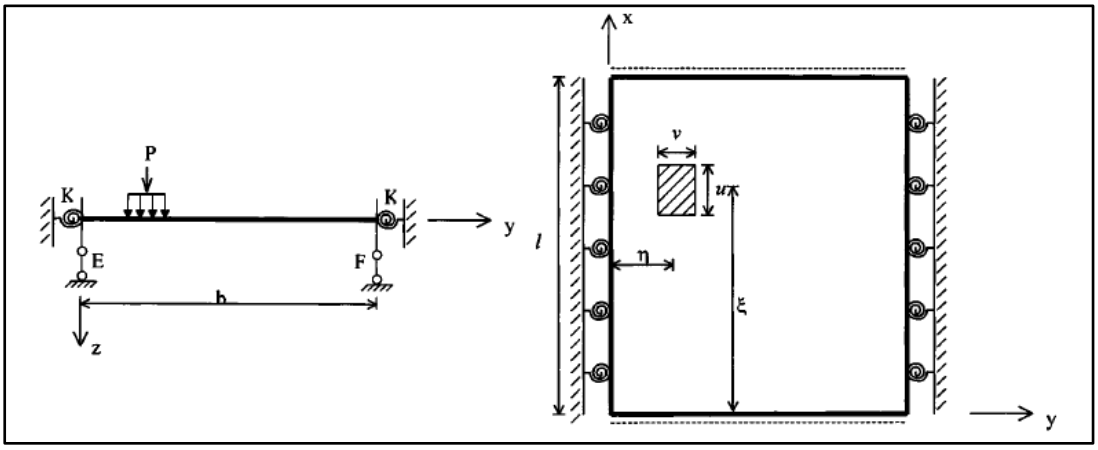

Figure (2.4) Elastically clamped plate (**Luo et al, 2003)**

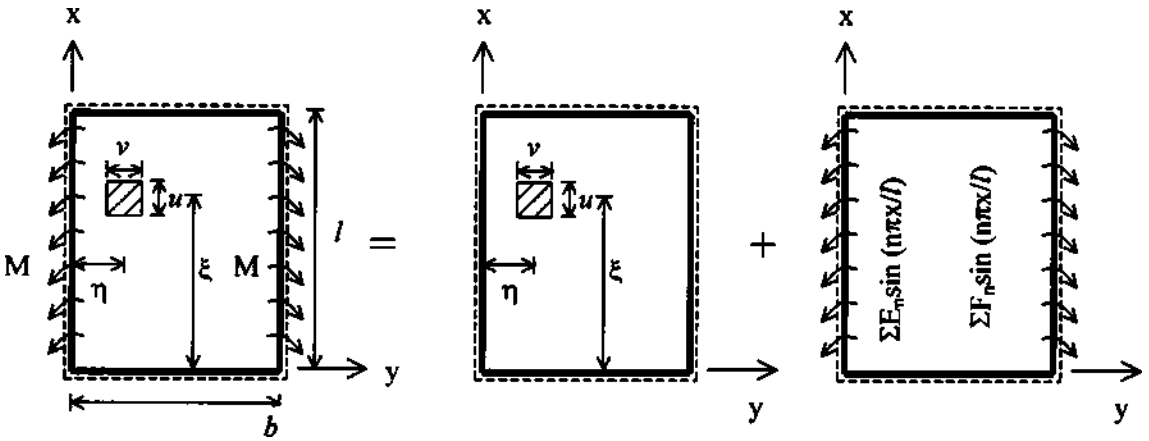

Figure (2.5) Decompositions of elastically clamped plate under local distributed load for top slab (**Luo et al, 2003)**

It was found that the proposed approach establishes a new logical way to the study of top flange of box girder bridges, especially that of wide bridges. It was noted that the results derived from the simply supported and the clamped methods for longitudinal and transverse moments of top slab of box girder represented a higher and lower limit for the elastically clamped

determinations. Also they concluded that the elastically clamped method was very close to finite strip approach which considered as an effective and accurate approach

(Al-Nuaimi & Bhatt, 2005) presented an experimental and Computational study for reinforced concrete hollow beams. Test beams having a cross section of 300x300 mm, a hollow core of 200x200 mm, and a length of 3800 mm were used in the experiment. Computational study was by finite element model for idealization of reinforced concrete hollow beams using 2D plane elements. A comparison was done between experimental result for eight reinforced concrete hollow beams and computational results (non-linear predictions produced by a 2D in-house FE program) for criteria (load displacement relationship, iongitudinal steel strain, transverse steel strain, failure load, crack pattern and mode of failure). The results from the 2D in-house finite element program showed a good agreement with experimental results.

(Kurian & Menon, 2007) presented a modified theoretical formulation and experimental work to predict the collapse load of simply supported single cell concrete rectangular box girder bridges under distortion and bending. Modification was presented (it is assumed that in addition to bending and yielding in the vertical plane, there is transverse bending accompanied by yielding of transverse rebars at all four web-flange junctions of the box girder) to the theory that found by **(Spence & Morley, 1975)** which includes estimation of collapse load under pure bending, in the other word assuming that all the rebars in the webs and bottom flange have yielded in tension).

The equation that used to estimate collapse load under pure bending by **(Spence & Morley, 1975)** are shown below:

$$P = \frac{4}{L}(F_b h + 2F_w h_1) \qquad 2.5$$

The modified equation that used to estimate collapse load under pure bending and distortion are shown below:

$$\left(\frac{P}{2} + P_d\right) b = \frac{4F_b b_1 h}{L} + \frac{4F_w h_1 b}{L} + 4m_c L \qquad 2.6$$

Where:

P= collapse load; L= length of span; b= width of box girder; $F_b$and F_w= total yield force of the reinforcement provided in the bottom flange and one web, respectively; h=distance from the centroid of the bottom flange steel to the centroidal axis of the top flange; h_1=distance of the centroid of the web steel to the centroidal axis of the top flange; b_1=distance of the centroid of the bottom flange steel from the centroidal axis; and m_c= corner plastic moment (per unit width).

Experimental work included casting four reinforced concrete box girders with length 5 m, width of upper and bottom flanges was (1540 mm and 900 mm) respectively, thickness of webs, upper and bottom flanges were 60 mm, and total depth 500 mm. These girders were tested under concentrated load with different amounts of eccentricity on upper flange as shown in Figure 2.6, which develop a lateral torsion in the cross section of beam.

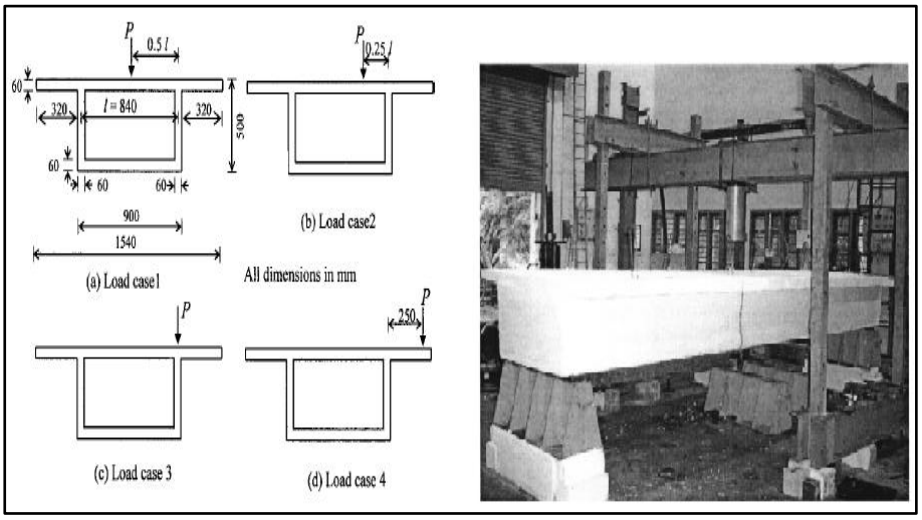

Figure (2.6) Cases study and test **(Kurian & Menon, 2007)**

They found that the results of the experimental work on concrete box girders showed the valuable confirmation of the suggested modified theory to predict the failure load. In addition, they concluded that the collapse load that found by proposed modified theory much close to the results of the experimental works.

(Galal & Yang, 2009) presented an experimental and analytical investigation on the behavior of haunched thin- walled reinforced concrete girders and box girders. When haunched thin-walled girders are independently examined under two load circumstances: first one as centric load and second one as an eccentric load resulting in simultaneous bending, torsion, and shear, the experimental plan is intended to examine the effect of bottom slabs on the response of girders. Five samples with identical section sizes as shown in Figure 2.7 were manufactured into three models varying in length of bottom slabs to evaluate the its effect.

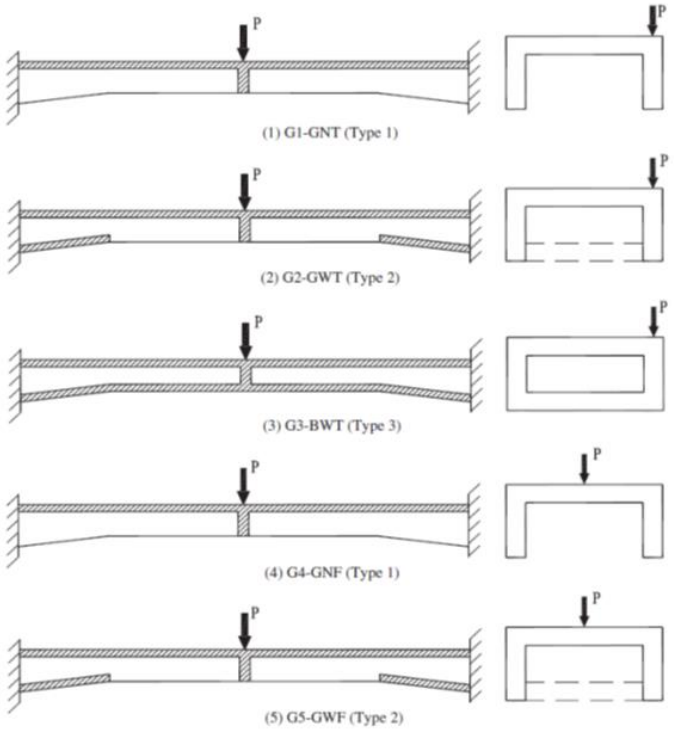

Figure (2.7) Loading cases of the five tested girders **(Galal & Yang, 2009)**

Analytical finite element part of this research represent by utilizing computer program ADINA (2005), which takes into account shape and substance nonlinearity.

This investigation showed that load eccentricities significantly reduced the ultimate loads and the ductility of the girders with open sections. However, when the open section was converted to a full-span box section, the behaviors of the girders were considerably improved. It was concluding the following

(1) Subjecting the tested girders without bottom slabs and with bottom slabs at haunched parts to eccentric load, rather than centric load, decreased their observed initial cracking load by about 25% and 17% and decreased their load-carrying capacity by 16% and 8%, respectively.

(2) For girders subjected to centric and eccentric loads, different failure processes were noticed: centric loads led to plastic flexural failure, whereas eccentric loads led to brittle failure of shear and torsion.

(3) The inclusion of a bottom slab considerably reduces the effect of load eccentricity on girder behavior.

(4) Bottom slabs for all the length across the span had a minor influence on girders under loads without eccentricity.

(5) Models created with ADINA were able to capture the non-linear behavior of girders that were tested.

(Gupta et al., 2010) presented a parametric study on the behavior of straight box girder using finite element method. It was investigated that the behavior of box girders with various cross section geometries (rectangular, trapezoidal, and circular) and depths (2,2.4,2.8) m, as illustrated in Figure 2.8. Three-dimensional 4-noded shell elements were used to evaluate the performance of box-girders in the SAP-2000 software. The linear analysis

was done under dead and live loads of Indian Road Congress Class 70R loading, for both with and without eccentricity at midspan. They presented a further computational work for deflection, bending stresses for both longitudinal and transverse axis and shear lag of cross sections.

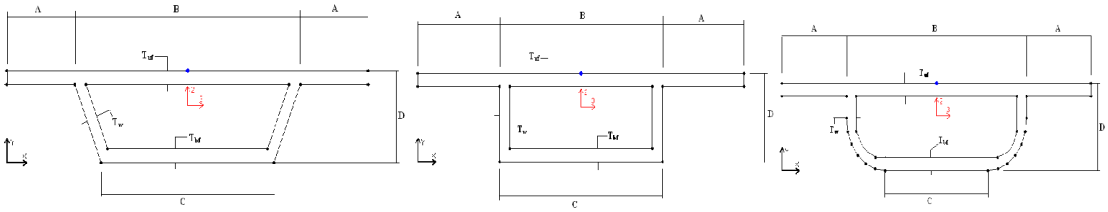

(a) (b) (c)

Figure (2.8) (a) Rectangular, (b) Trapezoidal and (c) Circular cross-section of box girder bridge **(Gupta et al., 2010)**

They concluded that the longitudinal bending stress for rounded corners box girder was15% more than trapezoidal and rectangular for the same cross sectional area. Also it was found that the flexural stress is lowest in rectangular box girder as well as the deflection was highest in rounded corners girder under the dead load and live load (centrally & eccentrically) cases and lowest in rectangular girder. As a result, it may be inferred that among these three sections, the rectangular section is the stiffest.

(**Hawas,2015** studied the effect of the external strengthening on the behavior of reinforced concrete box girders using CFRP sheets. An experimental work included casting ten reinforced concrete box girders, two variables were studied, the length and position of CFRP sheets. The length of strengthening sheets was taken (L/4, L/2 and L) depended on the length of span (L) and the position of strengthening sheets was taken in bottom surface, side surface, and combined (bottom and side surface). The specimens were tested as a simply supported under two concentrated loading.

The cracking and ultimate loads increase from (10%, 20% to 26%) with increase the length of strengthening sheets (from L/4, L/2 to L) respectively for constant position. Also, change the position of strengthening (bottom, side and combined) increased the ultimate strength (20%, 15% and 24%) respectively for constant length L/2. On the other hand, the deflection at mid span and under load decreased due to the increase in the flexural stiffness of the girder.

(Jabbar et al., 2016) investigated by using the finite element method the influence of different dimensions for square web opening in the straight box beams on the structural response of the beams under pure torsional, flexural, and cyclic loadings. Then, compared to the solid beam with no presence of openings. Two types of concrete were employed High-strength concrete and ultra-high performance concrete. This study consisted of five different sections of the beam and each labeled as: the solid section specimens, hollow section specimens, and hollow section specimens including square openings with arrange of sizes 100×100mm, 200×200 mm, and 300×300 mm. Figures 2.9 and 2.10 illustrate geometry and dimensions of reinforced concrete beam and modeled beams, respectively.

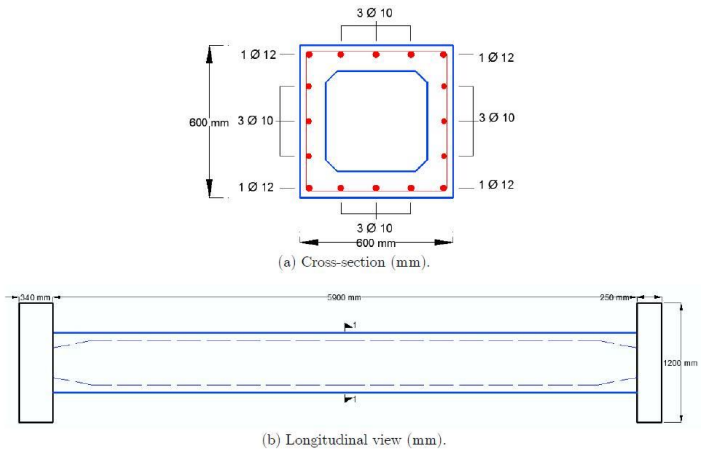

Figure (2.9) Geometry and Dimensions of Reinforced Concrete Beam **(Jabbar et al., 2016)**

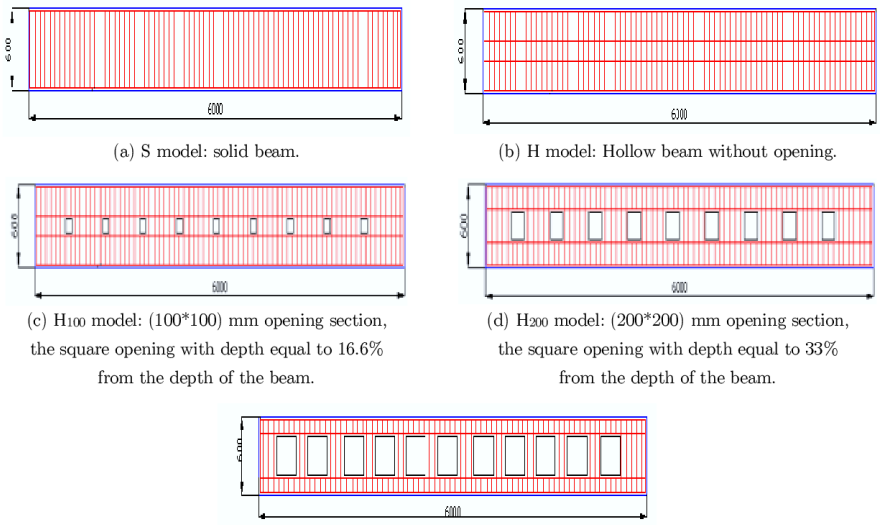

(a) S model: solid beam.

(b) H model: Hollow beam without opening.

(c) H_{100} model: (100*100) mm opening section, the square opening with depth equal to 16.6% from the depth of the beam.

(d) H_{200} model: (200*200) mm opening section, the square opening with depth equal to 33% from the depth of the beam.

(e) H_{300} model: (300*300) mm opening section, the square opening with depth equal to 50% from the total depth of the beam.

Figure (2.10) Modeled Beams **(Jabbar et al., 2016)**

It was concluding that the pure torsional load indicated that the strength of the hollow section specimen was greater than that of hollow section specimen has 100 mm openings by roughly 1.8% for the high strength concrete and 12% for the ultra high performance concrete. As well as, in a comparison to the hollow section specimen, the ultimate strengths in hollow section specimens 200mm and 300mm square opening were decreased to about 32% to 82% for the high strength concrete and 35% to 75% for the ultra high performance concrete, respectively. In addition, the results for stress and strain in the box beam with opening were increased compared to box beams without opening.

The ultimate loads indicated a reduction 24% and 42% for beams under the effect of flexural load for the high strength concrete and ultra high performance concrete, respectively, compared with those of the solid section specimens. The hollow section specimen with 100mm openings behaved almost the same with the hollow section specimen without

opening. While, the capacity was decreased in hollow section specimens consisting 200mm and 300mm square openings.

With regards to cyclic load, the ultimate load was reduced by about 38% for both hollow section specimen without opening and with 100mm openings for high strength concrete, while the reduction was about 20% and 40% for hollow section specimen without opening and that with 100mm, respectively, for ultra high performance concrete, compared with that of the solid section specimen. The amount of energy absorbed was highly reduced in both box beams with and without an opening, reflecting a reduction in performance of beam subjected to cyclic loads.

(Bhagwat et al., 2017) presented results of analysis of three different cross sections of reinforced concrete straight box girder (rectangular, trapezoidal and circular) using finite element package for CSi Bridge 2017. Three depths (2, 2.4, and 2.8 m) were used, as well as the width of the box girder, cross sectional area, and span length in all cases were kept constant. The effect of changing the shape of the section was examined on the one hand and changing the depth of section on the other on longitudinal bending stresses and deflection.

It was concluding that the inverse relationship between (longitudinal bending stresses and deflection) for depth. Also, they found that the longitudinal bending stresses and deflection were the lowest in rectangular box girder and were the highest in the circular box girder, that means rectangular shape of box girder had strength and stiffness more than trapezoidal and circular box girder.

(Alawsh & Mehdi, 2018) presented experimental and numerical investigation to study the behavior of reinforced concrete straight box girders that were made from hybrid concrete normal strength concrete (NSC) and high strength concrete (HSC).The experimental work consisted

of ten reinforced concrete box girders, five specimens of them were made of a rectangular cross section and another five specimens were made of a trapezoidal cross section, examined as simply supported beam subjected to two concentrated force. The effect of hybrid technique on box beams was investigated, with two specimens cast as homogeneous NSC and full HSC box girders and three specimens cast by using hybrid concept (HSC in upper flange only, HSC in upper flange and half depth of webs, and HSC in bottom flange and total depth of webs) box girders for each cross section. The data of experiment indicated that using of hybrid technique enhanced the general behavior of box girders with respect to the box girder that made from homogenous concrete (full NSC), the ultimate load of rectangular specimens increased by about (16, 21, and 27) % and the ultimate load of trapezoidal specimens increased by about (18, 29, and 23) %, when using HSC in upper flange only, upper flange and half depth of webs, and bottom flange and total depth of webs respectively. The ultimate load of rectangular and trapezoidal hybrid specimens decreased by only about 7% and 9% as average respectively, in comparison to homogenous specimen (full HSC).

The numerical work, was consist the modeling and analyzing the tested specimens using a nonlinear analysis. A computer program (ANSYS V16.1) was utilized to achieve this analysis. The numerical results were in good accordance with the experimental data. A parametric study was carried out to investigate the effect of changing the location of HSC layer, the slope of web in trapezoidal box girder and the existence of end diaphragms.

Results revealed that employing HSC in the top flange and total depth of web for rectangular and trapezoidal box girders yielded the optimum results., reduce the slope of the web with the vertical axis by about (0.25 % and 0.32 %) raises the ultimate load by about (1.4%) and (3.6%), respectively.

2.4 Experimental and Analytical Studies on Beams (Girders) with Openings

2.4.1Transverse Openings

(Burton, 1965) investigated the effects of inclusion duct on the behavior of reinforced concrete continuous T-beams. The study examined experimentally two specimens of T-cross section (one solid and the other with ducts). The data displaced that the two tested beams performed differently. Moreover, it was found that the design equations for ultimate strength contained in ACI-1963 Building code can safely be applied to wide shallow beams of the type used in this study with opening.

(Nasser et al., 1967) reported tests on reinforced concrete beams with openings and made the following assumptions: -

1. The chords of a vierendeel panel are considered to behave similarly to the top cord and bottom cord member at the opening.
2. When the openings are not subjected to transverse force, the cross members have central flexural regions at their mid spans.
3. The shear of the chords produces a diagonal stress accumulation at the corners, resulting in a force double the amount of the basic shear force.

The researcher looked at nine rectangular beams based on the above assumptions. His conclusions based on the beams' experimental test results were as follows:

a- Rectangular reinforced concrete beams including large openings respond identically to Vierendeel concept.

b- Adequately reinforced large opening in rectangular beams do not result in reducing the ultimate capacity of the beams, but it reduces its stiffness.

(Hanson, 1969) studied experimentally a T-beams reinforced longitudinally. The specimens contained square openings and were tested to simulate the joist on either side of a continuous support. Many parameters were taken into account in this study, but the main parameters were the size and horizontal and vertical locations of the opening. However, as the opening represents a source of weakness, the failure plane always passes through the opening, except when the opening is very close to the support so as to bypass the potential inclined failure plane. Figure 2.11 shows schematically some typical shear failures of beams containing square and circular openings.

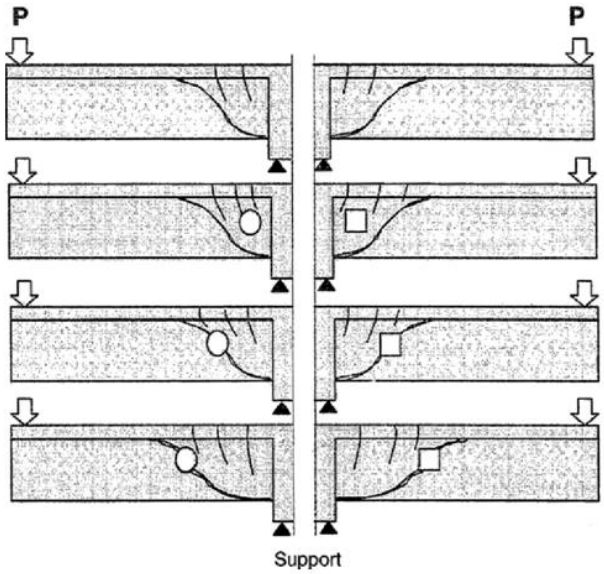

Figure (2.11) Typical Shear Failure of a Beam with Small Openings Containing no Shear Reinforcement **((Hanson, 1969), (Somes & Corley, 1974))**

(Somes & Corley, 1974) reported an identical investigation of **(Hanson, 1969)** however, the shape of openings was circular in this case. It was observed that the openings close to the support caused no loss in resistance in both situations (square and circular opening). Whenever the openings are out of the support, the strength gradually decreases till it reaches the steady

value. The opening's vertical position has little effect. However, increasing the size of the opening corresponds to a nearly linear drop in ultimate load. Nonetheless, there seems to be an opening size under which shear resistant does not decrease. For square openings, this dimensions parallels to roughly quarter of the beam depth, while for circular openings, it is equivalent to approximately 33% the depth of the beam. It was also found that by introducing stirrups for both sides of the opening, the resistance of a longitudinally strengthened specimen may be completely restored. Figure 2.8 depicts failures of shear for beams with square openings or circular openings schematically.

(Jamal, 1978) examined experimentally eleven reinforced concrete beams with opening. This study concentrated on the assessing the influence of an opening in the flexural zone and the shear zone, the position of the opening through the depth of section and the influence of additional reinforcement on the capacity. It was found that an opening in the flexural zone dose not reduce the flexural capacity of the beam up to (h/d) ratio equal to (2/3), where h is the depth of the opening and (d) is the effective depth of the beam. However, the opening did reduce the stiffness of the beam and its energy absorption capacity. When the opening was located in the shear zone a significant reduction in capacity resulted. Also, if it is not properly reinforced can lead to a very premature type of failure can occur. This study offered methods of evaluating the capacity of beams with an opening in any zone and also generalization to the case of uniformly loaded beams.

(M Abdul Mansur & Hasnat, 1979) examined experimentally the effects of small openings by casting twenty-two reinforced concrete beams, that have been subjected to torsion. According to nominal concrete strengths, the beams were divided into three groups. The first and third groups

investigated the influence of a 76mm hole size, while the second group investigated the effect of four various opening diameters (51mm, 76mm, 102mm, and 127mm) to analyze the influence of opening size. Longitudinal and transverse reinforcement were performed no all test specimens. The ACI Code 318-77 theoretical predictions are discovered with near accordance to exist test data.

(M A Mansur & Paramasivam, 1984) examined ten beams have equally located transverse circular opening that subjected to flexural and twisting. The specimens were separated into two categories CA and CB, based on the size of cross section for each category which as 175×350mm and 200×400mm, respectively. Area and distribution of reinforcing for all groups were maintained fixed. Group CA organized into three beams with varying opening sizes that were subjected to pure torsion. The opening size was kept the same for group CB, but the twisting to flexural ratio was changed from pure twisting to pure flexural. Steel strains, deformations and maximum crack width were all measured after each increment of the load. The results indicated that, the torsional strength and stiffness of a beam diminishes as the opening size increased. Depending on test outcomes, the twisting resistance of a beam is increased due to existing of a small amount of flexural moment. However, at significant bending moments, a rise in the bending moment causes a decrease in beam resistance of twisting. This is in line to results of previous studies.

(Mohammed A Mansur et al., 1985) examined experimentally twelve beams designed by the proposed method of the ACI Code 318-83, under effect of point load to study the flexural response of reinforced concrete beams containing large rectangular openings, these openings were subjected to bending and shear. The essential variables were the length,

depth, eccentricity and location of openings, and the amount and arrangement of corner reinforcement. It was concluding that at a particular load both the maximum crack width and maximum beam deflection increase with an increase in opening length, opening depth, or moment shear ratio at the center of the opening. Also, diagonal bars as corner reinforcement were found to be more effective in crack and deflection control than vertical stirrups. It was concluded that, a suitable quantity of corner reinforcement was recommended.

(M A Mansur, 1992) evaluating the influence of large rectangular web openings on behavior of beams with one span, two spans and three spans in terms of deflection response. The beams were analyzed using the direct stiffness approach. The beams were regarded as structural elements with multiple portions, and an equivalent stiffness for the portions crossed by the openings had been established. The outcomes of the experiment were in good agreement with the expected deflections derived from direct stiffness method. The approach also provides a relatively realistic representation. It was found that the opening caused a redistribution of moments and internal forces in the continuous beams.

(Tan & Mansur, 1996) suggested useful procedure for complete analysis and design of reinforced concrete beams with large web opening. Also it was suggested the guidelines to facilitate the selection of the size and location of web openings. Generally, the following should be considered:

• Chords should be positioned with a substantial enough concrete surface to create the maximum compressing region for flexure and enough height to supply convenient shear reinforcing.

• Openings height should less than half the depth of the beam.

• Supports or point loads should be no closer than one-half the beam depth distant.

For structural analysis of reinforced concrete beams with openings, they showed that in the case of a statically determinate beam, shear force and bending moment envelopes can be obtained from statics. For continuous beams, they suggested method can be followed, that is, the member containing an opening is considered as a nonprismatic beam with different cross sectional properties: those of a solid section and of the equivalent section for opening segments. It was recommended a design process for the opening segment which is based on the observed Vierendeel behavior of chord members at an opening.

The response and design of a beam with web opening under predominant shear were described by **(M A Mansur, 1998)**. Some suggestions for identifying the opening as large or small are proposed based on the observed structural behavior. Two alternative failure mechanisms have been recognized as small openings; both types of failure are termed as beam type and frame type, respectively, which need to be treated separately for the entire design. An inclined failure plane of 45°, identical to a solid beam, may be considered in beam-type failure, with the plane crossing through the center of the opening, as illustrated in Figure 2.12. (a). As illustrated in Figure 2.12, failure of frame type is caused by the creation one independent oblique crack in each chord which connecting the two solid beam parts of beam (b). With the exception of assessing the net area via the opening, the highest shear permitted in the section to prevent inclined failure of compression which considered identical to solid beam in the suggested technique.

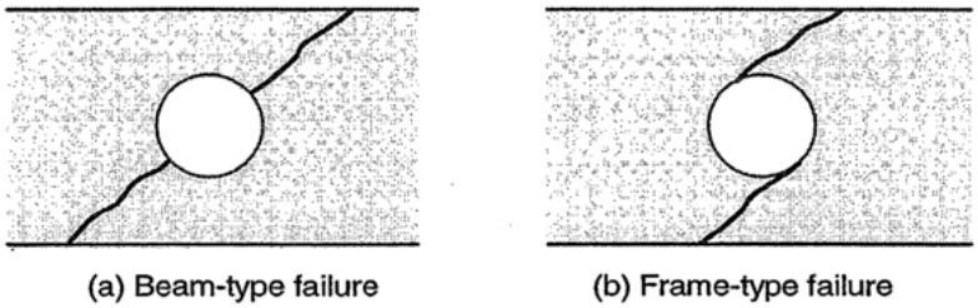

Figure (2.12) Modes of Failure for Small Opening, **(M A Mansur, 1998)**

(Al-Dolaimy, 2011) presented experimental and F.E. analysis by utilizing ANSYS computer program (version 9.0, 2004). The experiment work includes tested eight continuous reinforced concrete beams with cross-section of (150x250mm) and total length (3300mm) with two spans (clear span is 1500 mm) were tested under two-point loads. Six beams, each beam contains one opening, three of which have dimensions (200x100 mm) and the three other have dimensions (140x140mm). The location of opening was in the zone of maximum moment and maximum shear

The experimental results indicated that the use of CFRP sheet to restore the reinforced concrete continuous beams with web openings led to significant improvement on overall behavior such as crack width, deflection and increase in the ultimate load capacity. Moreover, the inclined strengthening model indicates a stiffer response compared with other strengthened model. The use of CFRP as externally strengthening system decrease the crack width, but, it cannot change the formation of inclined crack.

In the other hand, three dimensional finite element analysis was used to investigate the performance of the reinforced concrete member strengthened by CFRP laminate. The comparison between the experimental and theoretical results showed reasonable agreement and asserted the validity of the numerical analysis and methodology developed in this study

(Saksena & Patel, 2013) Investigate the effect of small circular opening on the shear and flexural and ultimate strength of beams. The main variables of the study are the changes of diameter and the position of opening. First beam was solid and was used as reference for comparison with other beams with an opening. Second beam had opening of 110mm (0.55D) at L/8 distance, third beam had opening of 90mm (0.45D) at L/8 distance. Beam number four and beam number five had openings as mentioned above at L/4 distance. The tested beams have been loaded as simple beam with two concentrated and symmetrical load. It was concluding that when the diameter of opening increased, the reduction of ultimate strength increased and patterned of cracking as well as mode of failure of the beam changed. Also, it was recommended that the usage of diagonal reinforcement and stirrups in top and bottom of opening for increasing the ultimate shear strength of the beam. Also, concluded that the most critical position of opening to reach the ultimate strength in beams is near the support and also the best place for the location of opening in these beams is in middle of a beam (flexure zone).

(Ramadan et al., 2015) using the finite element package ANSYS for straight solid beam to examine the behavior of simply supported and continuous RC beams with openings loaded by either a uniformly-distributed load, or a single, central concentrated load. The objective is to supply easier design suggestions for RC beams with openings. Published studies that is relevant, both experimental and theoretical, is compiled and critically assessed for this purpose. Then, to complement the previously published study, a large number of reinforced concrete beams have openings are examined by finite element software ANSYS. Beams used in this investigation were chosen to survey the influence of the following:

(1) opening location;

(2) boundary conditions: The findings of two hinged supports beams are compared to hinged-roller and fixed-fixed beams;
(3) span-to-depth ratio: For both hinged-hinged and hinged-roller support conditions, the performance of beams with span-to-depth ratios of 5.8 and 11.8 is investigated;
(4) reinforcement ratio for tension: The reinforcement proportions are studied, extending from the minimum to the highest code limitations;
(5) Detail of tension reinforcement development on hinged supports.
Generally, beams with openings close to supports fail due to shear mode, but beams with openings in the middle span fail due to flexure or shear-flexure modes, based on the kind of applied force (uniform or concentrated). However, quarter-point openings are more crucial to beam resistance than central openings. When the opening height ratio h0/D=0.20 and the opening length ratio L0/L=0.05, for any amount of tension reinforcement, the influence of opening presence may be neglected for specimens have central openings under uniform load. When the tension reinforcement ratio is less than 0.4max, the opening size restrictions are h0/D=0.50 and L0/L=0.20. Some design codes and research utilize simplified and empirical design procedures.

2.4.2 Vertical Openings

There is a limited literature related to reinforced concrete beams with vertical openings.

(Aziz & Ajeel, 2010) studied the shear behavior of reinforced concrete T-beams with vertical opening or cold joints in a different location of the flanges. Eight simply supported T-beams were tested under the effect of single point load. The examined specimens were constructed without transverse reinforcement, to ensure shear failure mode. One of beams was

made without any openings or cold joints (control beam) while the other beams were casted with openings or cold joints in different locations. The variables of this work were the number and location of slab openings and cold joints. It was concluded that, the presence of flange openings reduces the shear capacity about (22% to 32%) for beams containing one opening and about (17%-39%) for beams containing two openings. For beams containing cold joints, the shear capacity decreased about (27%), when compared to the specimen without opening (control).

(Dawood & Al-Jazaeri, 2014) presented an experimental study to assess the shear strength of reinforced concrete T-beams with openings in flange and strengthened by CFRP Laminates. This study was analogous to **(Aziz & Ajeel, 2010)** study, but CFRP Laminates have been used to strength the flange of the T-beam specimens having openings. In this work, an experimental investigation carried out including seven tested beams, one of them were constructed without any openings (control beam), second, third and fourth beam were constructed with openings in different locations, the other beams were constructed with openings and strengthened by CFRP laminate as shown in Figure 2.13.

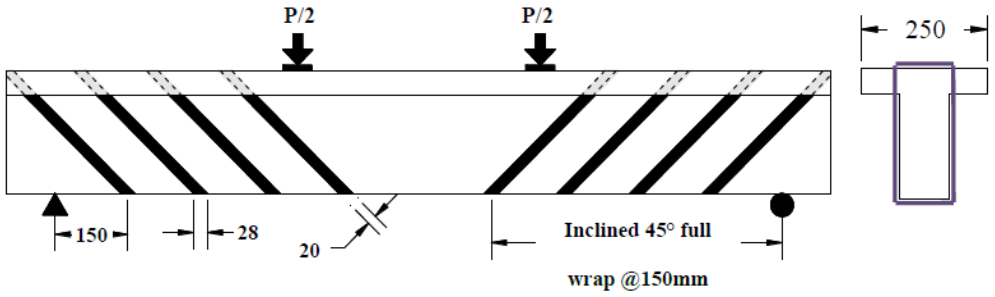

(a)

Figure (2.13) (a)Strengthening Schemes of T- Beams with Openings (b) Openings Location **(Dawood & Al-Jazaeri, 2014)**

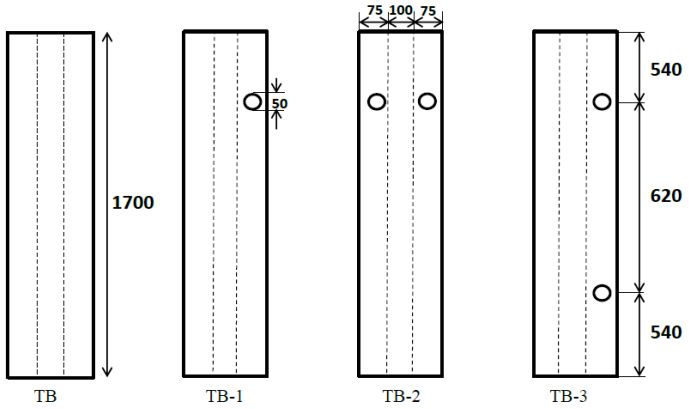

(b)

Figure (2.13) continue

It was found that, the using of CFRP laminate has significant effect on overall behavior such as the ultimate load, crack width, and deflection. The ultimate shear capacity of the strengthened specimens was improved by about (70-80) % as a comparison with beams containing openings.

The above two studies investigate the presence of opening in flanges of T-beams only and do not study the effect of the vertical opening when it penetrates the entire depth of the web, and their possibility to obstruct the reinforcement bars. In fact, in the slab-beam system, flange considers as a portion of the slab, and there are many codes deal with openings in slabs. With regard to vertical openings crossing the entire depth of the beam's web.

In 2016 **Silva et al.** presented a practical and computational study on reinforced concrete beams including multiple vertical openings. Five beams with rectangular cross section (150*100) mm were examined under effect of two point loads. All tested beams has a total span of 620 mm and total length of 800 mm. One of them was without opening representing a control specimen and all the other were with three adjacent circular openings of 25 mm diameter (25% of the beam width) passing vertically through the web

without intersect the reinforcement and located in different position (0, 60, 210, and 310) mm from the support. While, the failure mode of control specimen was flexural, it was found that when the openings located at mid span, the beam failed by shear, unexpectedly. For beam with openings located at the support, it failed by flexural without effected in the ultimate load. The failure mode of all other specimens was shear. The openings located at 60 mm from the support reduces the ultimate load by 19% as a comparison with control beam. The experimental specimens were analyzed by finite element method using ABAQUS software. It was found that the beams with vertical openings had their principal tensile stresses increased for the region where the beams were failed by diagonal tensile. It was thought that, this reason justifying the shear failure of the beam with openings at mid span.

(Hamzah & Ali, 2020) presented experimental and numerical investigation on a simply supported reinforced concrete straight solid beams with vertical and horizontal openings. The experimental part consisted of casting and testing fourteen reinforced concrete beams under effect of two point loads, which are divided into two groups, first group designed for flexural failure, while the second group was designed for shear failure. With a total length of 2000 mm, a square cross-section of 200×200 mm was kept for all specimens. The size of the opening was kept constant; its dimensions were 30% of the beam width or height. This work studied the shape of openings (square and circular), and the replacement description of the reinforcement that will prevent the penetration of opening.

It was concluded that, the presence of square vertical openings reduces the maximum capacity of load by about 15% for first group (mid-span) and 8% for second group (mid-shear span). However, it has a slight influence on the deflection at the service load, especially for second group (mid-shear

span). With regard to shape of opening, found that the vertical circular openings shows lowest influence than square openings with respect to these results for beams of both groups. With regard to second part of this work, a three-dimensional finite element model, utilizing software package ABAQUS/standard 2017 to simulate reinforced concrete beams of experiment work. It was found that, the studied reinforced beams predicted by FEM were in good agreement with the experimental results.

(Muneer, 2021) investigate experimentally the effect of vertical and transverse opening on reinforced concrete deep beams. Nine specimens were devoted to study the effect of opening axis direction, location of openings, and their shape, while other four specimens were concentrated to evaluate two proposed technical methods to restore strength and other serviceability requirements. The first by replacing concrete around the openings with RPC and the second by utilizing internal steel reinforcement around the openings.

It was found that the vertical openings with 33% of width decrease both first cracking loads and ultimate loads about (13%) and (12%), respectively with beam-type failure of openings. It was also found that the beams having vertical openings with a circular shape exhibited a slightly reduction in the ultimate load capacity than square openings, while beams with rectangular openings had largely reduction in ultimate load compared to other shapes of openings. It was concluded that the vertical openings had less effect in shear zone than transverse openings. It was found also, that the use of RPC and internal steel reinforced around the vertical openings gave a good result to restore strength and enhance deflection and cracking patterns.

2.5 Summary and Concluding Remarks

Although several experimental and computational studies on the response of reinforced concrete beams including openings have been conducted, only a few studies for the effects of openings on reinforced concrete box beams have been found. Some observations in this regard might be summarized as follows:

1- The following is a summary of the experimental and theoretical works on the behavior of concrete beams with openings:

• With regards to the behavior of concrete beams with opening, numerous experimental and theoretical studies have been done. The most of these researches focused on straight members such as simply supported beams, continuous beams, and deep beams with openings.

• The majority of experimental and numerical studies were carried out the behavior of reinforced concrete beams with openings were focused on transverse openings, while a few studies were found about the effects of vertical openings.

• Few studies were about different strengthening techniques of beams with openings by utilizing of FRP.

2- The following is a summary of the experimental and theoretical research on concrete box beam behavior:

• The majority of experimental and numerical studies were carried out the reinforced concrete box beams straight and curved without opening.

• No available experimental study is found on horizontally curved box beams with transverse or vertical openings.

• No available study is found on restoring of strength of horizontally curved box beams with opening using hybrid concrete.

• No available experimental study is found on horizontally curved box beams under repeated load.

3-The overall response of a curved beams with openings as described in the preceding literature, the following can be summarized:

• The existence of web opening reduces the ultimate load and crack width of beams, in addition stiffness of post-cracking.

• The opening corners are susceptible to wider cracking unless further reinforcing is supplied to minimize the propagation of cracks.

• Multiple opening performance is preferable in terms of strength and serviceability. To avoid premature failure, the space between adjacent openings should be equal or more than one-half of the entire beam depth, and the post should be sufficiently strengthened.

• The strength and stiffness of the beam are reduced as the opening size is increased in terms of length or depth of the opening. The eccentricity of the opening, on the other hand, has a slight influence on strength and stiffness.

• Using CFRP laminate around the openings minimized deflection of beam, controlled the cracks around openings, enhanced the ultimate load capacity of the beam, and altered the failure mode of beam.

It is obvious from the literature that no technical information on horizontally curved reinforced concrete box beams with openings is available and how to restoring strength and serviceability requirements. The current study contributes to the understanding of how reinforced concrete circular curved box beams with and without vertical and transverse

openings behave overall, and how to restoring strength and serviceability requirements under effect of monotonic and cyclic loads.

CHAPTER THREE

EXPERIMENTAL WORK

3.1 General

Even though the utilize of reinforced concrete curved box beams in architectural designs provides significant benefits, the creation of laboratory models of such structures appears to be a complex, costly, and time-consuming operation. Despite this, the structural response of fifteen circular curved box beams made of reinforced concrete with and without presence of opening, strengthened and unstrengthened under the influence of two concentrated loads was investigated experimentally in this work.

This chapter presents, standard tests of material properties used in this study. Then, this chapter describes the casting specimens, test technique, and measuring devices in detail.

3.2 Experimental Program

3.2.1 General Description

A number of tests done on a range of construction materials as part of the current experimental program, control samples (cubes and cylinders), and fifteen reinforced concrete semi-circular continuous curved box beam specimens, in addition to a pilot specimen.

The tested specimens were made of normal strength self-compacting concrete (SCC), in addition to using (reactive powder concrete RPC around openings) or external strengthened by EBR- CFRP laminates around opening for strengthened specimens.

The experimental program included three main groups as illustrated in Table (3.1): -

Group (I) consists of continuous circular curved box beams with **vertical** opening unstrengthened or strengthened by RPC or EBR-CFRP laminates and tested under monotonic loading.

Group (II) consists of continuous circular curved box beams with **transverse** opening unstrengthened or strengthened by RPC or EBR-CFRP laminates and tested under monotonic loading.

Group (III) consists of continuous circular curved box beams with **transverse** opening unstrengthened or strengthened by RPC or EBR-CFRP laminates and tested under repeated loading.

For the considered three groups, fifteen models of circular curved box beams specimens having same geometry and supports condition were tested and includes the main variables; direction of opening axis, location of opening through profile of curved beams, strengthening by (i.e., replacement of ordinary concrete by reactive powder concrete RPC around openings) cast monolithically, strengthening by EBR-CFRP laminates around opening and subjected to monotonic or repeated loading.

Figure 3.1 illustrates the naming convention used to identify each one of circular curved box beams specimens, while Figure 3.2 show the flow chart of tested circular curved box beams. Table 3.1 lists the designations and details of all circular curved box beam specimens that have been tested.

Notice there is two control specimens without opening $CB_1.L_1$ for monotonic loading and the other $CB_{12}.L_2$ for repeated loading.

Table (3.1) Designation and Details of Tested Circular Beam Specimens.

Groups	Specimen Designation	Direction of Opening	Location of Opening	Type of Strengthening	Type of Loading
Pilot CB	CB.P	---	---	---	Monotonic Loading
Group(I) CBs with vertical opening	$CB_1.L_1$	---	---	---	Monotonic Loading
	$CB_2.V37.L_1$	Vertical	37°	---	
	$CB_3.V60.L_1$	Vertical	60°	---	
	$CB_4.V82.L_1$	Vertical	82°	---	
	$CB_8.V60.S_1.L_1$	Vertical	60°	S1(Hybridization of Concrete by RPC Around Opening)	
	$CB_{10}.V60.S_2.L_1$	Vertical	60°	S2(EBR- CFRP Laminates Around Opening)	
Group(II) CBs with transverse opening	$CB_5.T37.L_1$	Transverse	37°	---	Monotonic Loading
	$CB_6.T60.L_1$	Transverse	60°	---	
	$CB_7.T82.L_1$	Transverse	82°	---	
	$CB_9.T60.S_1.L_1$	Transverse	60°	S1(Hybridization of Concrete by RPC Around Opening)	
	$CB_{11}.T60.S_2.L_1$	Transverse	60°	S2(EBR- CFRP Laminates Around Opening)	
Group(III) CBs with transverse opening	$CB_{12}.L_2$	---	---	---	Repeated Loading
	$CB_{13}.T60.L_2$	Transverse	60°	---	
	$CB_{14}.T60.S_1.L_2$	Transverse	60°	S1(Hybridization of Concrete by RPC Around Opening)	
	$CB_{15}.T60.S_2.L_2$	Transverse	60°	S2(EBR- CFRP Laminates Around Opening)	

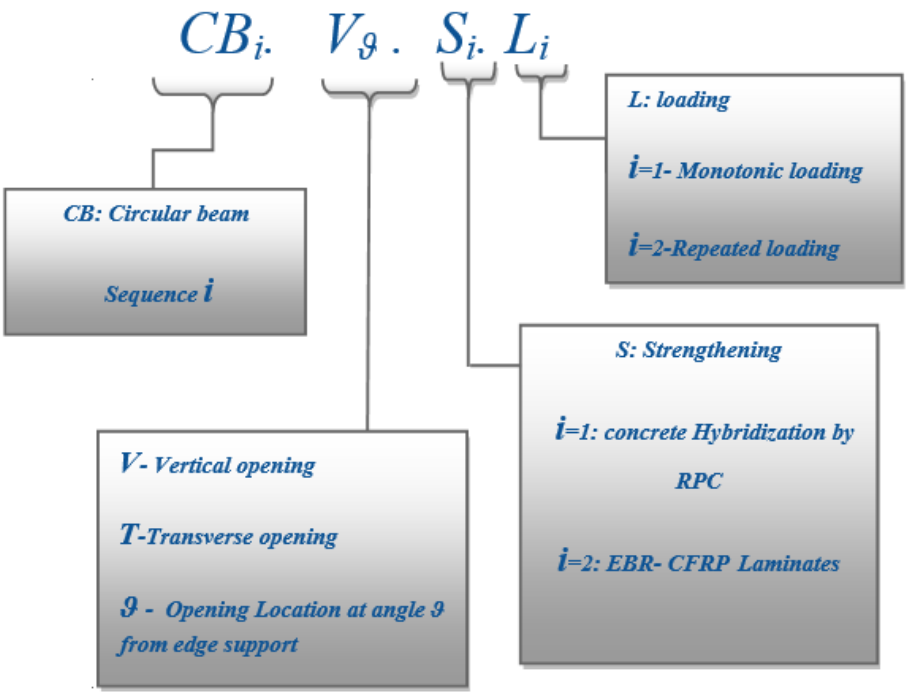

Figure 3.1 Circular Box Beam Specimen Identification.

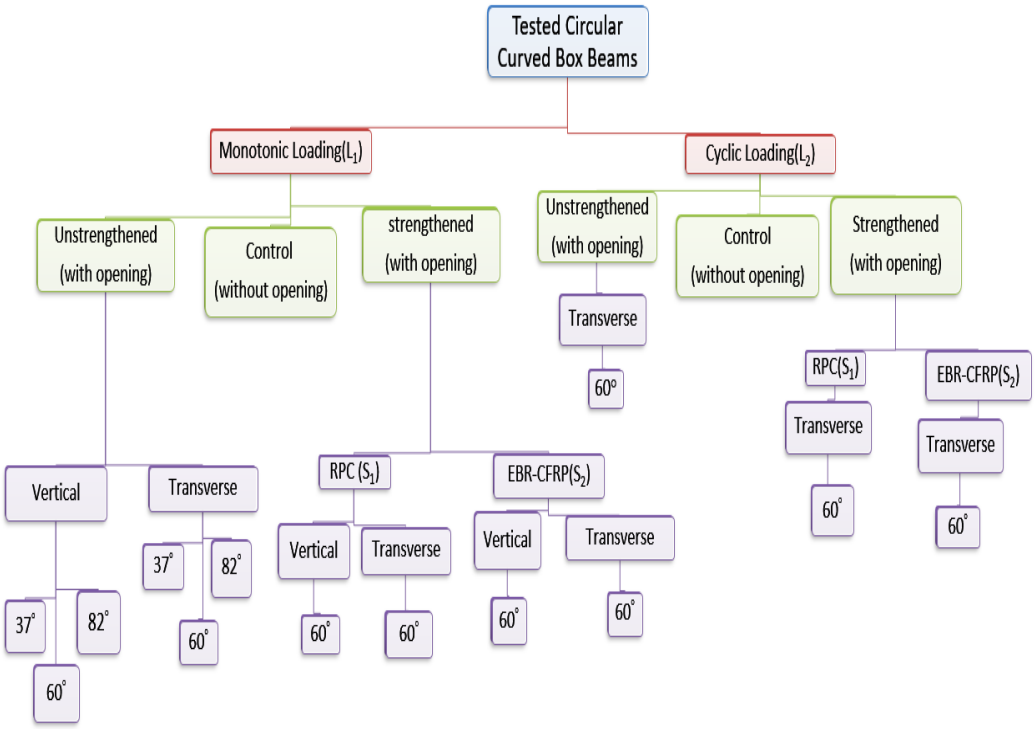

Figure 3.2 Tested Circular Curved Box Beams Flow Chart.

3.2.2 Description of Tested Circular Beams

Two-span semicircular continuous curved box beams simply supported at the external edges and in the center, has a radius 1150 mm measured to the center line of cross section of the box beam, and having cross section of dimensions 250 mm overall depth and 250 mm width with a top flange width 360mm. The cross section of the beam includes hole with dimensions (130×130) mm to represent a box beam along the beam length, as shown in Figure 3.3. The ends of all beams extended 50 mm beyond the support's centerlines. These beams tested under the effect of two point loads located at mid of each span (angle 45°). Steel reinforcement (6Ø12) mm deformed bars provided for top negative moment regions, (4Ø10) mm for bottom positive moment regions and (6Ø10+2 Ø8) mm as longitudinal torsion reinforcement with clear cover of 20 mm. The closed stirrups of Ø8 mm reinforcing bar placed at 90mm center to center from angle (0) to angle (40°), and placed at 45mm center to center from angle (40°) to angle (90°) along the beam length for each span, noting that the angle measured from exterior support toward the interior support (see Appendix B).

All circular beam specimens of the three groups had openings with dimensions of (80*80 mm), 33% of width or depth, respectively, and a control beam without openings was provided to each group.

3.2.2.1 Circular Curved Box Beams without Opening

Three curved beams were casted, The pilot beam CB.P is represented by one of them and the other two represent a control box beams $CB_1.L_1$ and $CB_{12}.L_2$ of the same type under monotonic and repeated loading, respectively. The pilot specimen, which is identical to the control specimen, it was utilized to check the machines and system for loading test that would

be employed in this work. for the test of other circular curved box beams under effect of monotonic and repeated loads.

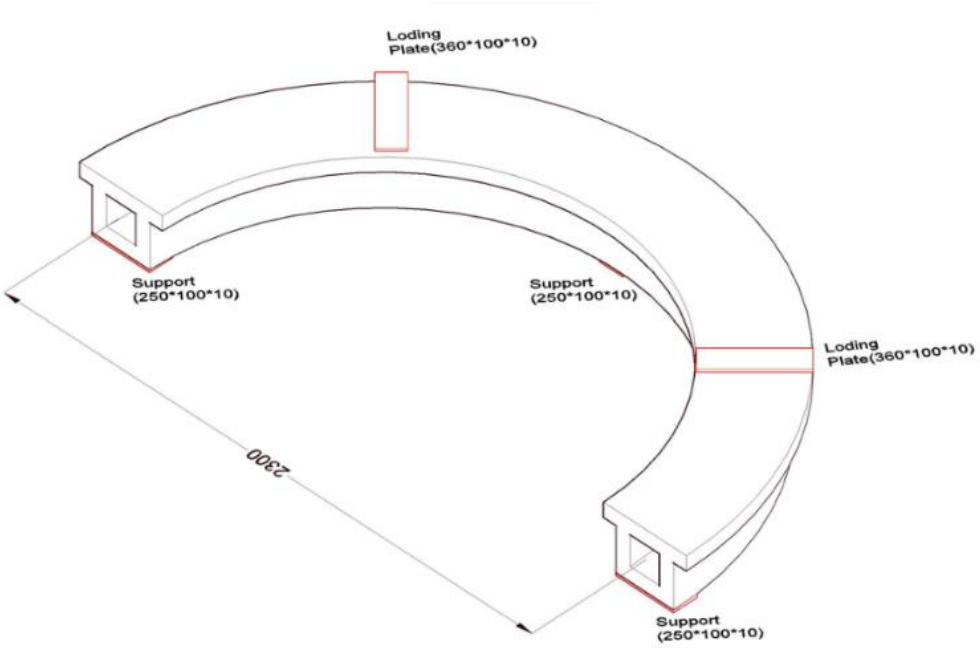

(a)

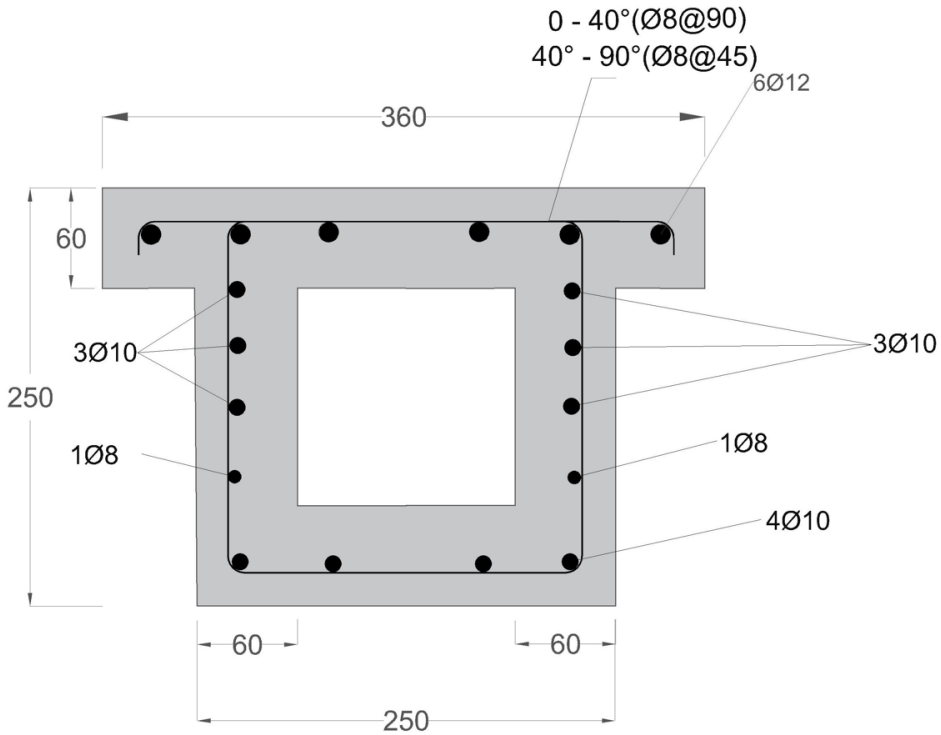

(b)

Figure (3.3) Details of Specimens (all units in millimeters): (a) Geometry, Supports and Loading (b) Cross Section and Reinforcement

3.2.2.2 Circular Curved Beams with Vertical Openings (Group I)

This group consists of five circular curved box concrete beams. specimen $CB_2.V37.L_1$ is characterized by two vertical openings, both positioned at a distance of d/2 measured from the applied load towards the exterior support (angle 37° measured from exterior support to the center of opening) Figure 3.4, specimen $CB_4.V82.L_1$ is characterized by two vertical openings, located on the two sides of the interior support, spaced by a distance of d/2 (angle 82° measured from exterior support to the center of opening). The last three circular beams were with a two vertical opening each positioned at angle (60°) measured from exterior support to the center of opening, specimen $CB_3.V60.L_1$ without any strengthening around opening, specimen $CB_9.T60.S_1.L_1$ was strengthened with RPC and specimen $CB_{10}.V60.S_2.L_1$ has been strengthened by EBR-CFRP sheets as showed in Table 3.1, to be tested under monotonic load.

3.2.2.3 Circular Curved Beams with Transverse Openings (Group II)

This group consists of five circular curved box concrete beams. specimen $CB_5.T37.L_1$ is with a two transverse opening each positioned at distance d/2 measured from point load toward exterior support (angle 37° measured from exterior support to the center of opening) Figure 3.5, specimen $CB_7.T82.L_1$ is characterized by two transverse openings, spaced symmetrically on both sides of the inner support by a distance of d/2 (angle 82° measured from exterior support to the center of opening). The last three specimens were with two transverse opening each positioned at angle (60°) measured from exterior support to the center of opening, specimen $CB_6.T60.L_1$

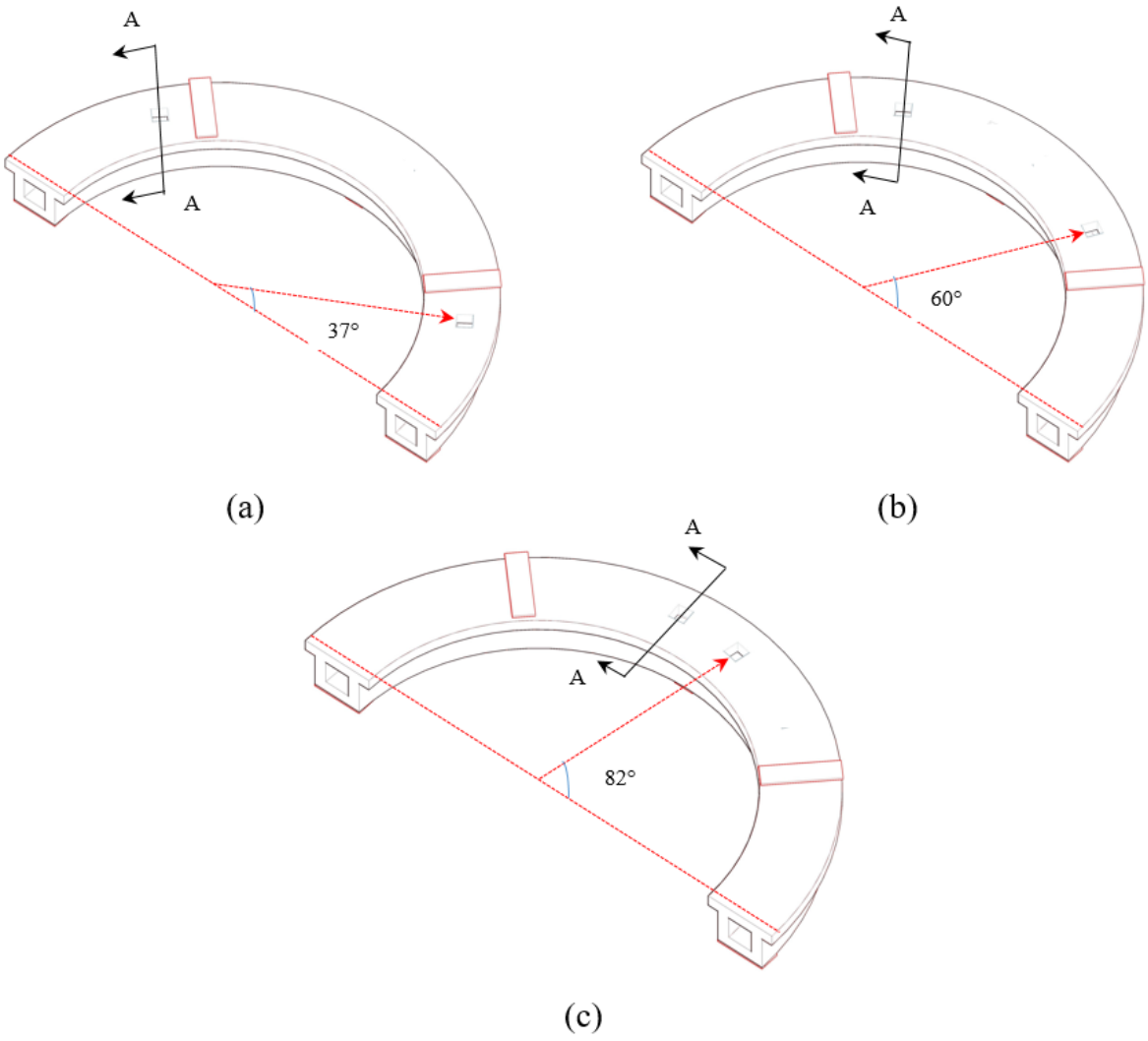

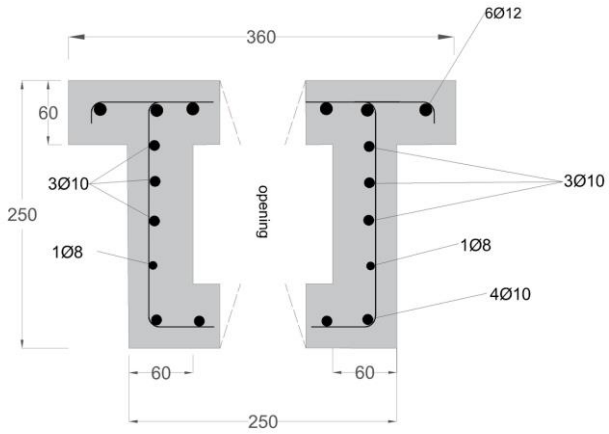

(d)

Figure (3.4) Vertical Openings (Group I) (all units in millimeters): (a) Specimen with Openings at angle 37° (b) Specimen with Openings at angle 60° (c) Specimen with Openings at angle 82° (d)Section A-A through Opening

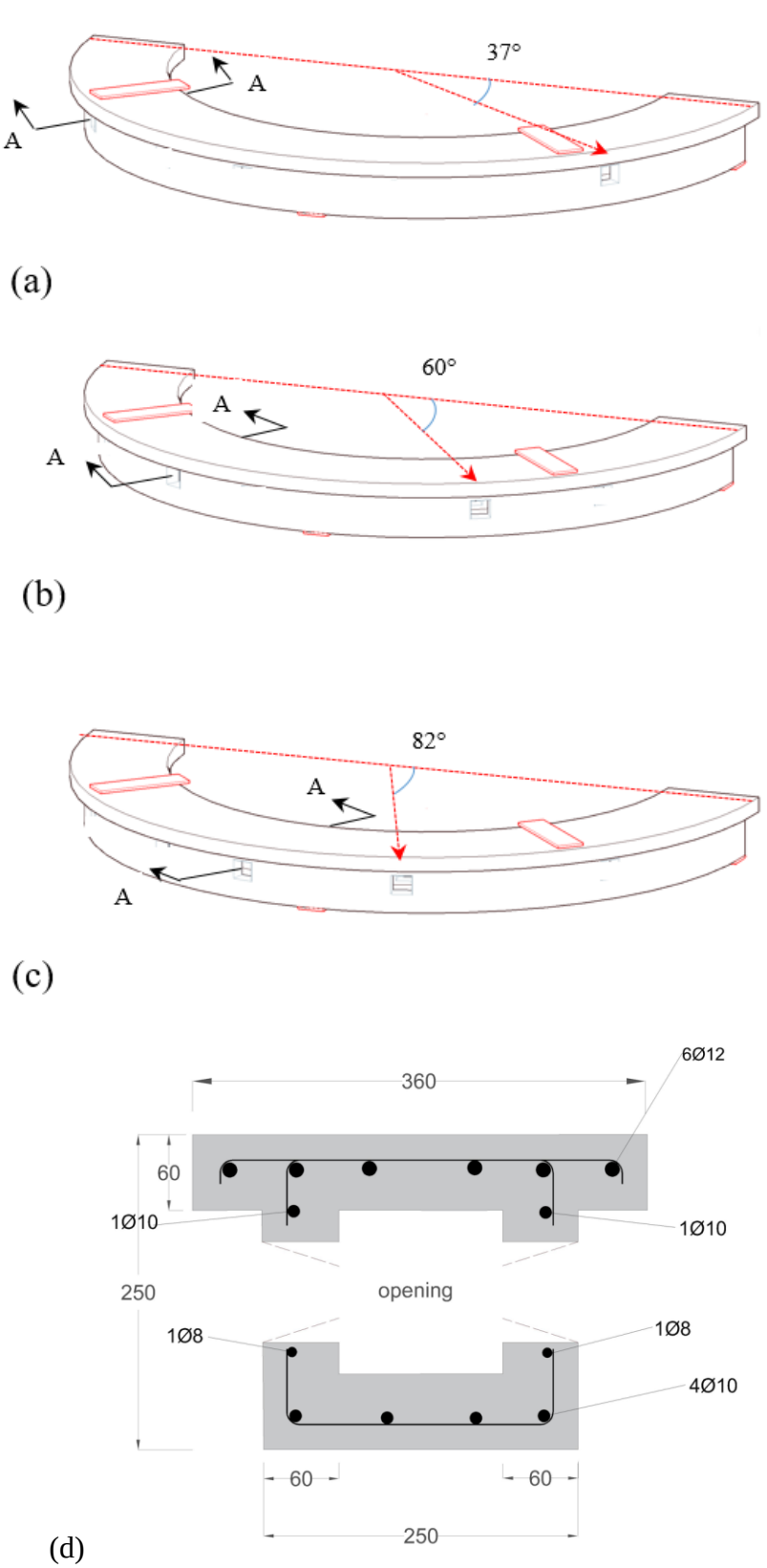

Figure (3.5) Transverse Openings (Group II) (all units in millimeters): (a) Specimen with Openings at angle 37° (b) Specimen with Openings at angle 60° (c) Specimen with Openings at angle 82° (d)Section A-A through Opening

without any strengthening around opening, specimen $CB_8.V60.S_1.L_1$ was strengthened with RPC and specimen $CB_{11}.T60.S_2.L_1$ strengthened by EBR-CFRP sheets as showed in Table 3.1, under effect of monotonic load.

3.2.2.4 Circular Curved Box Beams Under Repeated Load (Group III)

This Group consists of one curved beam without opening $CB_{12}.L_2$ similar to control beam of (Group I) but under effect of cyclic load and three circular curved box beams each one consists two transverse opening each located at angle (60°) measured from exterior support to the center of opening. Specimen $CB_{13}.T60.L_2$ specimen without any strengthening around opening, specimen $CB_{14}.T60.S_1.L_2$ was strengthened with RPC around opening and specimen $CB_{15}.T60.S_2.L_2$ strengthened by EBR-CFRP sheets as illustrated in Table 3.1.

3.2.3 Strengthening Techniques

The strength-restoring mechanism was carefully selected based on the crack pattern and mode of failure. The design of concrete hybridization (RPC and NSC) was proposed through this experiment, while design specification of ACI Committee 440-2002 was satisfied for EBR-CFRP laminates. Location of opening at angle (60°) was kept constant for all strengthened specimens.

3.2.3.1 Strengthening by Concrete Hybridization

The strengthening schemes for specimens $CB_8.V60.S_1.L_1$, $CB_9.T60.S_1.L_1$ and $CB_{14}.T60.S_1.L_2$ aimed to restore the overall structural behavior. The reactive powder concrete (RPC) was cast monolithically with NSC as a hybridization of concrete around opening for the entire section of the beam at a distance of 125 mm on both edges of vertical and transverse opening, as shown in Figures 3.6 – 3.7.

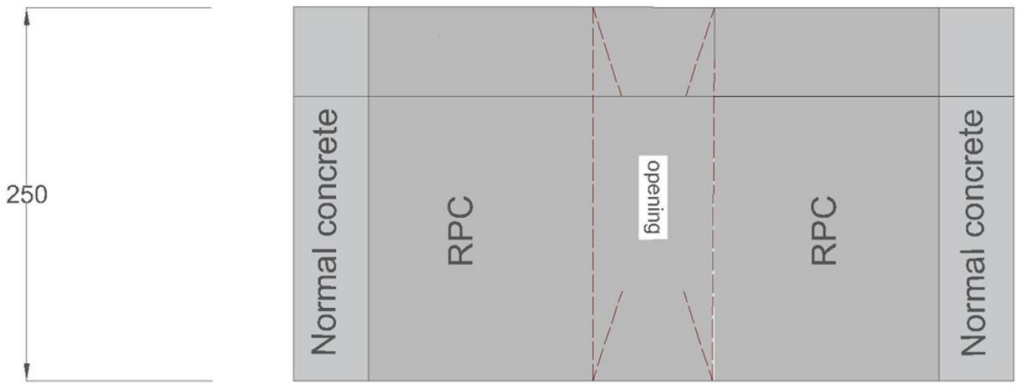

(a)

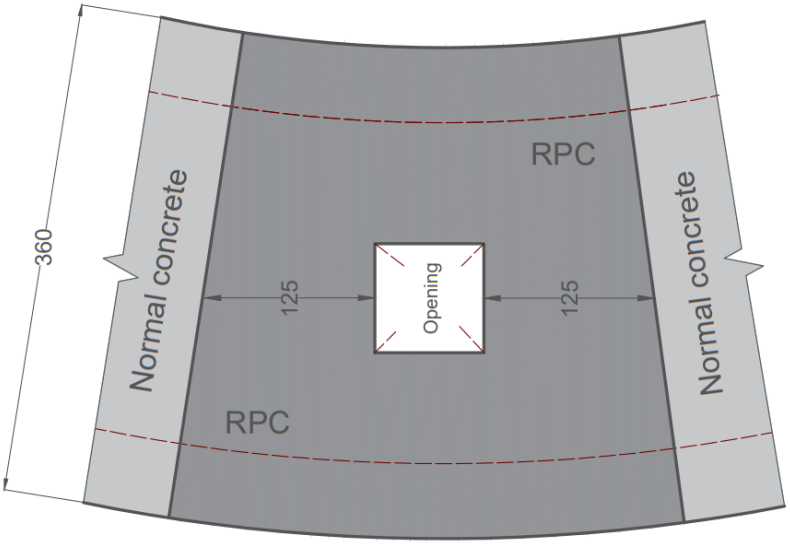

(b)

Figure (3.6) Details of Strengthening Schemes by using RPC (all units in millimeters) for Specimen $CB_8.V60.S_1.L_1$: (a) Front View; (b) Top view

3.2.3.2 Strengthening by EBR-CFRP Laminates

For specimen $CB_{10}.V60.S_2.L_1$, utilizing 0.17mm thickness of U wrap of EBR-CFRP laminates with 80 mm width on both sides of the opening and 120 mm width of U wrap for bottom and top chord of opening,

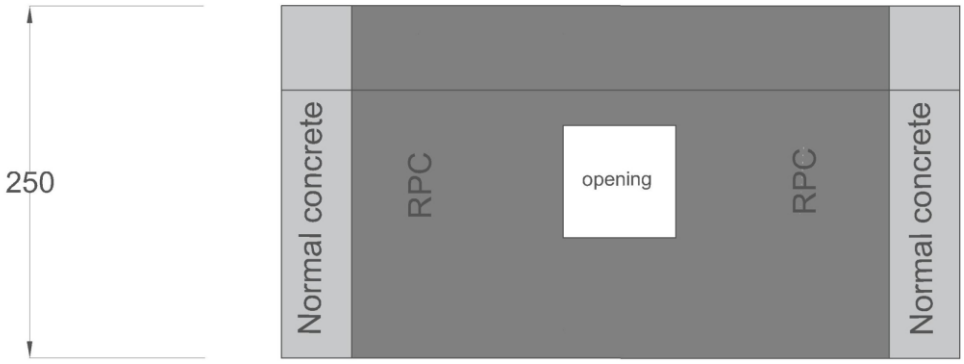

(a)

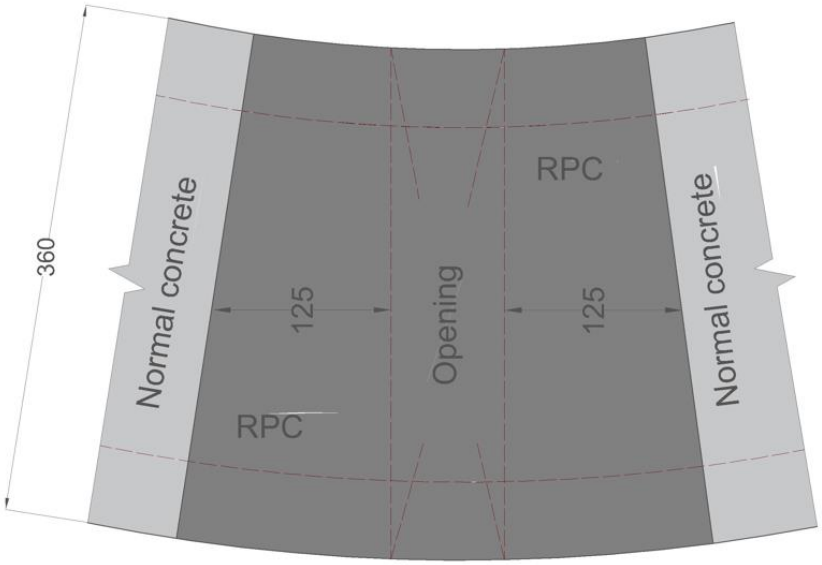

(b)

Figure (3.7) Details of Strengthening Schemes by using RPC (all units in millimeters) for Specimens $CB_9.T60.S_1.L_1$ and $CB_{14}.T60.S_1.L_2$: (a) Front View; (b) Top view

as shown in Figure 3.8, while for specimens $CB_{11}.T60.S_2.L_1$ and $CB_{15}.T60.S_2.L_2$, 0.17mm thickness of U wrap of EBR-CFRP sheets with 100 mm width on both sides of the opening and 120 mm width of U wrap for bottom and top chord of opening, as illustrated in Figure 3.9.

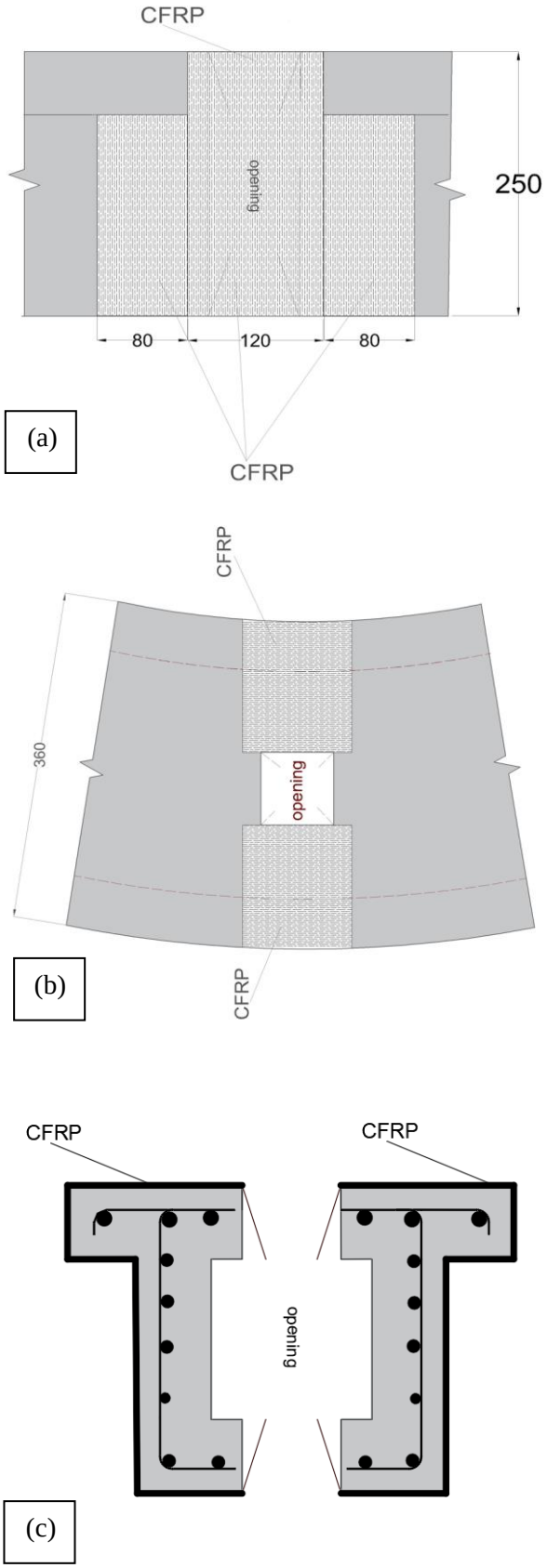

Figure (3.8) Strengthening Schemes (all units in millimeters) for Specimen $CB_{10}.V60.S_2.L_1$: (a) Front View; (b) Top view (c) Cross Section through Opening

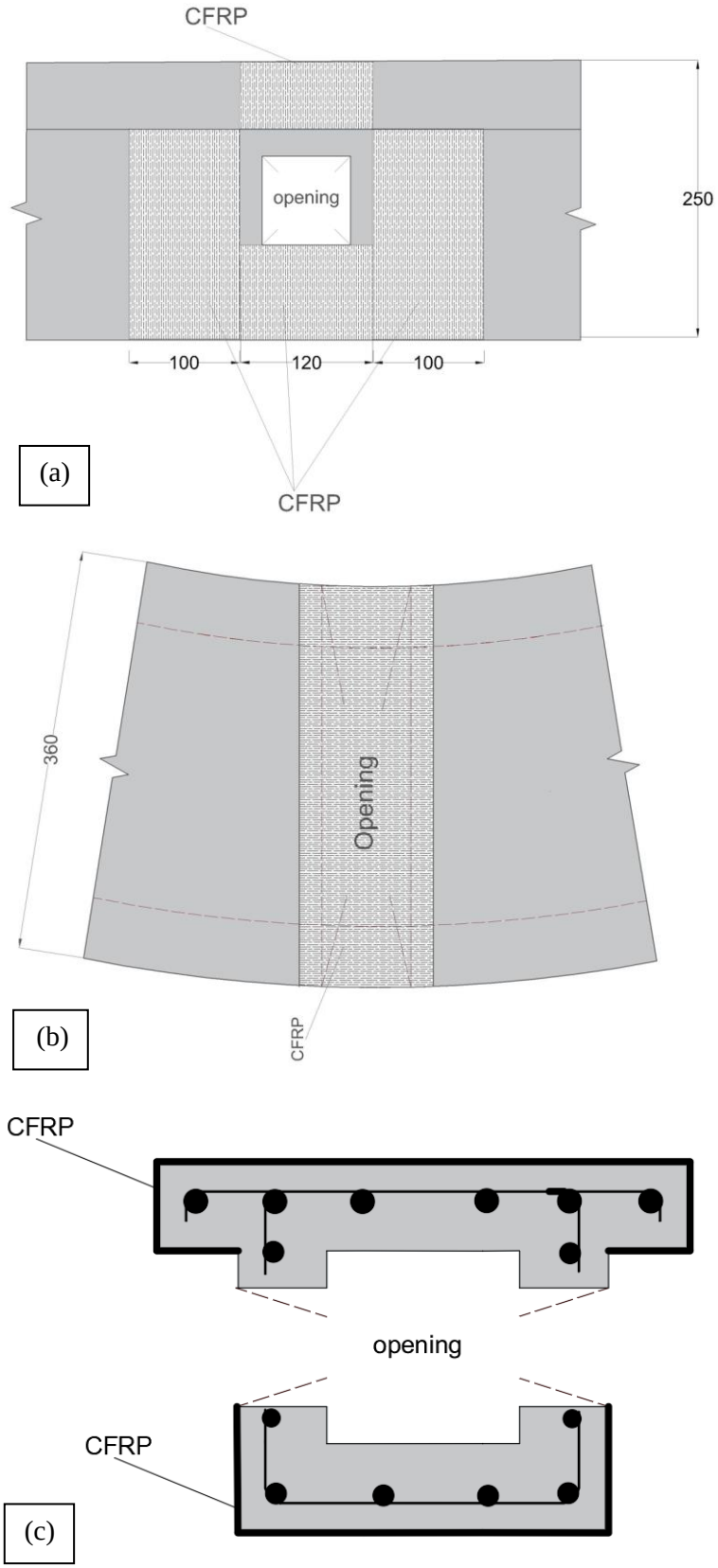

Figure (3.9) Strength Restoring Schemes (all units in millimeters) for Specimens $CB_{11}.T60.S_2.L_1$ and $CB_{15}.T60.S_2.L_2$: (a) Front View; (b) Top view (c) Cross Section through Opening

3.3 Material Properties of Tested Specimens

3.3.1 Self-compacting concrete

Cement, natural gravel, natural sand, lime stone powder, high range water reduction admixtures (HRWRA), and water are among the materials used in the production of self-compacting concrete (SCC). The materials mentioned above were examined in the laboratory of Materials Engineering College and Engineering College of Babylon University.

3.3.1.1 Cement

All of the beams were cast with ordinary Portland cement (Type I) produced in Iraq by the Lafarge company commercially marketed as (Crista). Table 3.2 lists the cement's chemical and physical characteristics. The properties satisfy the Iraqi standard requirements for ordinary Portland cement (IQ. S No. 5/1984). The mechanical and chemical characteristics of the employed cement were investigated in Materials Engineering College at Babylon University.

Table (3.2) Chemical and Physical Properties of Cement.

Chemical Properties		
Oxides	**Test Results**	**Limits of IQS No.5:1984**
CaO%	61.20	----------
SiO2%	21.40	----------
Al2O3%	4.34	----------
Fe2O3%	2.86	----------
MgO%	2.17	≤ 5%
SO3%	2.41	≤ 2.5% if C3A < 5% ≤ 2.8% if C3A > 5%
Free laminate%	1.30	≤ 4%
Loss on Ignition%	3.9	≤ 4%
Insoluble residue%	0.82	≤ 1.5%
L.S.F	0.89	0.66 – 1.02

Table (3.2) Continue

Physical Properties		
Setting time, min, initial Final	160 210	≥ 45 min ≤ 600 min
Fineness (Blaine) in cm^2/g	3560	≥ 2500
Compressive strength (MPa) 3 days 7 days	 20.43 27.1	 ≥ 15 ≥ 23
Soundness (autoclave),%	0.48	≤ 0.8

3.3.1.2 Coarse Aggregate (Gravel)

The current investigation utilized rounded gravel from Al-Nibaey with a 12.5 mm maximum particle size. The gravel was washed and cleaned numerous times with water before being dried in the open air. The aggregate grading and limitations established by Iraqi Requirements No.45/1984 are listed in Table 3.3.

Table (3.3) Coarse Aggregate Properties

No.	Sieve Size (mm)	%Passing	
		Course aggregate	IQ.S No. 45/1984
1	19	100	90-100
2	14	100	----
3	10	83.24	85-100
4	5	0	0-10
5	2.36	0	----
	Sulphate content SO_3 = 0.095% (specification requirements up to 0.1%)		

3.3.1.3 Fine Aggregate (Sand)

In this study, natural sand from the Karbala (Obeidi) plant with a maximum particle size of 4.75 mm was chosen. To reduce humidity saturation, the sand was spreading out and allowed to dry in the open air,

before being used, which might have a considerable effect on water content. The sand gradation comes between the higher and lower levels of Iraqi Specifications (IQ.S 45/1984) Zone (2) and ASTM C 33/C 33M. Table 3.4 lists the properties of sand, which has been examined in the college of Material Engineering at Babylon University.

Table (3.4) Sand Properties

No.	Sieve Size (mm)	%Passing		
		Fine aggregate	IQ.S No. 45/1984 Zone (2)	ASTM C 33/C 33M
1	9.5	100	100	100
2	4.75	99	90-100	95-100
3	2.36	81.1	75-100	80-100
4	1.18	64.41	55-90	50-85
5	0.6	35.81	35-59	25-60
6	0.3	14.41	8-30	5-30
7	0.15	7.52	0-10	0-10
	Sulphate content SO_3 = 0.18% (specification requirements up to 0.5%)			

3.3.1.4 Superplasticizer

For the production of Self-Compacting Concrete (SCC), superplasticizers (high range water reducers) are usually used to achieve the high workability needed. A high range water reducing agent (HRWRA) superplasticizer made by sika company called Sika ViscoCrete -5930-L which meets ASTM C-494 Types A and F used in this work. The characteristics of Sika ViscoCrete -5930-L are listed in Table 3.5.

Table (3.5) Technical Description of Sika ViscoCrete -5930-L*

properties	Sika ViscoCrete -5930-L
Appearance/ Color	Brownish liquid
Specific gravity	1.085 ± (0.01) g/cm3
PH	4 - 6
Total chloride ion content	Nil

*Supplied by the manufacturer

3.3.1.5 Limestone powder (LSP)

The major component of finely ground limestone powder was calcium carbonate (CaCO3). This powder, which had been brought from the local market, was known as (Al-Gubra) and utilized for enhancing fluidity and cohesiveness, also increase workability and density of the Self-Compacting Concrete (SCC). The results of the chemical analysis are shown in Table 3.6, which done in the Environmental Laboratory of Babylon University.

Table (3.6) Chemical test of (LSP)

Oxide	CaO	SiO_2	Al_2O_3	Fe_2O_3	MgO	SO_3	L.O.I
Content %	53.96	3.62	0.03	0.167	0.59	0.58	44.21

3.3.1.6 Water

Ordinary clean tap water was used in this work for both mixing and curing of all specimens.

3.3.2 Reactive Powder Concrete (RPC)

Reactive powder concrete was used in this study for strengthening purpose around openings of circular curved box beams, in attempt to restore structural behavior characteristics.

3.3.2.1 Cement

Sulfate resistance cement Iraqi manufacturing by Lafarge company commercially known (Al-Jesser) was used throughout this investigation for casting of Reactive Powder Concrete (RPC). The chemical and physical characteristics of the cement are given in Table 3.7. The properties match

the Iraqi requirement for sulfate resistance cement (IQS No.5:1984). The mechanical and chemical properties of the cement that was utilized have been assessed in Materials Engineering College at Babylon University.

Table (3.7) Cement Chemical and Physical Test Results.

Chemical Results		
Oxides	**Test Results**	**Limits of IQS No.5:1984**
CaO%	61.20	----------
SiO2%	23.00	----------
Al2O3%	3.33	----------
Fe2O3%	3.15	----------
MgO%	2.17	≤ 5%
SO3%	2.34	≤ 2.5% if C3A < 5% ≤ 2.8% if C3A > 5%
Free laminate%	1.30	≤ 4%
Loss on Ignition%	1.08	≤ 4%
Insoluble residue%	0.82	≤ 1.5%
L.S.F	0.79	0.66 – 1.02
Physical Results		
Setting time, min, initial Final	79 274	≥ 45 min ≤ 600 min
Fineness (Blaine) in cm^2/g	3155	≥ 2500
Compressive strength (MPa) 3 days 7 days	 20.43 27.1	 ≥ 15 ≥ 23
Soundness (autoclave),%	0.56	≤ 0.8

3.3.2.2 Fine Aggregate (Sand)

Same natural sand from Karbala (Obeidi) factory which used in this study to producing (SCC), was used to produce (RPC) mixture after sieving it to get pass from 0.6 mm only.

3.3.2.3 Silica Fume

MasterRoc MS 610 densified silica fume manufactured by BASF chemical company was utilized to produce RPC mixture in this investigation. Silica fume alters the porosity structure of concrete by filling in gaps between cement grains as particle packing or micro-filling, and by reacting with the

calcium hydroxide result of cement hydration to create more binder substance (calcium silicate hydrate) (C-S-H). Silica Fume considered as a powder much finer than cement, used as a partial substitute of cement or as a concrete enhancement addition. Typical properties of silica fume utilized in this study are listed by Table 3.8.

Table (3.8) Typical properties of silica fume*

properties	MasterRoc MS 610
Form	Powder
Color	Grey
Density	0.55 - 0.7 kg/l
Chloride content	<0.1%

*Supplied by the manufacturer

3.3.2.4 Steel Fibers

Micro steel fibers (type WSF0213) available in the market were employed in this research, as shown in Plate 3.1. This sort of steel fibers was made by a company in Jiangxi Province (Mainland), China according to (ASTM A820-11). It is utilized in the present study with volume fraction (V_f =2.0%) and aspect ratio (L_f/D_f) =65. The properties of the steel fibers are introduced by Table 3.9.

Plate (3.1) Steel Fibers Used in this Study

Table (3.9) Properties of Steel Fibers*

Type	Property	Specifications
WSF0213	Density	7850 kg/m^3
	Tensile strength	>2850 MPa
	Modulus of Elasticity	203 GPa
	Form	Micro steel fiber (straight)
	Average length	12-14 mm
	Nominal diameter	0.2-0.25 mm
	Aspect ratio (Lf/Df)	65

* Supplied by the manufacturer.

3.3.2.5 Superplasticizer

A Superplasticizer used throughout this work to produce (RPC) mixture was MasterGlenium 54, made by BASF chemical company. It is a modified polycarboxylic-ether-based high-performance concrete superplasticizer. ASTM C-494 has been classified this Superplasticizer as type F & G. Typical properties of MasterGlenium 54 utilized in this study are listed in Table 3.10.

Table (3.10) Typical properties of MasterGlenium 54 *

properties	MasterGlenium 54
Form	Whitish to straw coloured liquid
Relative density	1.07
pH	5-8

*Supplied by the manufacturer

3.3.2.6 Water

Ordinary clean tap water was utilized in this study for casting and curing of RPC.

3.3.3 External Bond Reinforcement (EBR) Scheme

3.3.3.1 Carbon Fiber Reinforced Polymer (CFRP) Laminate

Unidirectional, woven, carbon fiber fabric **Sika Wrap 300C** manufactured by Sika Company, Swiss was utilized for technique of strengthening specimens with openings. The main technical properties of the used (CFRP)

Laminates (**Sika Wrap 300C)** are presented in Table 3.11 as supplied by the manufacturer

Table (3.11) Technical Properties of (CFRP) Laminates *

Properties	Sika Wrap 300C
Fiber type	High strength carbon fibers
Fabric orientation	0° (Unidirectional)
Areal weight	300 g/m^2± 5%
Fiber density	1.80 g/m^3
Fabric design thickness	0.17 mm (based on total carbon content)
Tensile strength of fibers	3900 N/mm^2(nominal)
Tensile modulus of fibers	230,000 N/mm^2(nominal)
Strain at break of fibers	1.5% (nominal)
Fabric length /roll	≥ 50 m
Fabric width	600 mm

* Supplied by the manufacturer

3.3.3.2 Epoxy Sikadur-330

Epoxy resin (Sikadur-330) made by Sika Company was employed for this study to paste the CFRP Laminate on the surface of concrete around the opening of **CB** specimens. This material consisted of 2-component, thixotropic epoxy based impregnating resin and adhesive (Resin part A+ Hardener part B). Technical properties of epoxy material are displayed as given by the company in Table 3.12.

Table (3.12) Technical Properties of Epoxy Resin Materials*

Properties	Sikadur-330
Colors	Component A: white paste Component B: grey paste Components A + B: light grey paste
Density (kg/l) mixed	~1.30 kg/l (mixed component A + B mixed) (+23 °C)
Mixing ratio by weight	A:B 4:1

Table (3.12) Continue

Tensile strength (MPa)	~30 N/mm^2 (7 d, +23 °C)
Full cure, days	7 (+35 °C)
E-modulus in Tension (MPa)	~4500 N/mm^2 (7 d, +23 °C)
Thermal Expansion Coefficient	4.5×10^{-5} 1/K (Temperature range -10 °C min. / +40 °C max.)

* Supplied by the manufacturer.

3.3.4 Steel Reinforcement

Three sizes of reinforcement were tested (Ø12, Ø10 and Ø8), deformed bars of diameter (Ø12mm, Ø10mm) for main longitudinal reinforcing (circumference) and deformed bars with diameter (Ø8mm) for closed stirrups as shown in plate 3.2. The reinforcement bars were examined according to ASTM-A615/A-615M-05a. Table (3.13) shows the results of tensile test for used bars, the tensile stress were carried out utilizing the machine which specified for this purpose in Lab of College of Materials Engineering at University of Babylon.

Table (3-13) Properties of Reinforcing Steel Bars.

Nominal Diameter (mm)	**Measured Diameter (mm)**	**Yield Strength Fy,(MPa) ***	**Ultimate Strength Fu,(MPa)**	**Modulus of Elasticity (GPa) ****	**(%) Elongation**	**ASTM A615/A615M-05a**
						Min. Elon.(%)
8	7.89	460	487.3	200	9.43	≥7
10	9.88	544	651.2	200	12.83	≥7
12	11.92	560	645.8	200	14.33	≥7

*****Each value is an average of three specimens (each 30 cm length).

******Assumed value.

Plate (3.2) Testing Machine of Steel Reinforcing Bars

3.4 Concrete Mix Design

3.4.1 Self-compacting concrete (SCC)

3.4.1.1 Mix Proportion of Self-compacting concrete

Because of the tight areas and challenging geometry of the box section, self-compact concrete used for cast the specimens. The quantities of the mixture were established using the European Self Compacting Concrete Guidelines (EFNARC).

Several trial mixes with various proportions were done for the purpose of getting characteristics that are essential of the concrete, and the adequate mix was selected as the mixture, from which the beams would be casted. The self-compact concrete mixture was provided to reach normal concrete strength (around 40 MPa) in 28 days.

Slump flow (**D** and **T50**), **V-Funnel**, and **L Box** tests were carried on the fresh concrete to assess its properties, as illustrated in Plate 3.3.

Plate (3.3) Slump flow, V-Funnel and L Box tests

The trial mix was prepared by selecting the quantity of each component to be blended together according EFNARC recommendations. Then, the fresh concrete is evaluated for fresh SCC properties such as segregation resistance, filling ability, and passing ability. If the selected mix successfully created SCC, three cubes were cast and tested for compressive strength at the age of 28 days. For the final selected mix, three cubs and three cylinders were cast to assess the mechanical characteristics. Table 3.14 lists the test results of fresh concrete.

Table (3.14) Fresh concrete test results

Slump flow and T_{500}		Limitations according to EFNARC	Characteristic
d_{max} =770	767.5	SF_3(760 to 850) mm	Flow and filling ability
$d_{perp.}$ =765			
T_{500}	3	>2 sec	Viscosity and flow ability
L-box		Limitations	Characteristic
H_1 =110mm	PA= 0.92	≥ 0.80 with three-rebar	Passing ability
H_2 =102mm			
V-funnel		Limitations	Characteristic
T_v Sec	9.5	(9 to 25) sec	Viscosity and flow ability

Table 3.15 shows the final mix proportions.

Table (3.15) Mix Proportion of Self-Compacting Concrete

Materials	Proportions of mix(kg/m^3)	Constituent	EFNARC (Kg/m^3)
Cement	350	Powder	380-600
Limestone powder	100		
Coarse aggregate	830	Coarse aggregate	750-1000
Fine aggregate	830	Fine aggregate	(48-55) % of total aggregate weight
Water	150.5	Water	150-210
Superplasticizer	8	------	------
W/c ratio	0.43	------	------
w/p ratio	0.334	------	------

3.4.1.2 Mixing Procedure of Self-compacting concrete

(Emborg & Concrete, 2000) mixing technique is used to obtain the necessary workability and homogeneity of SCC mixes in this experiment. The following points explain this procedure:

1. The fine aggregate is combined with 0.33 quantity of water in the mixer and mixed thoroughly minute.
2. Another 0.33 of the water is added to the cement and mineral admixtures. The mixture is then blended for one minute.
3. After that, the coarse aggregate is added together with the remaining 0.33 of the water and 0.33of the super plasticizer dose, and the mixture is mixed for 1.5 minutes before being let to rest for 0.5 minute.
4. The remaining 0.667 dose of the superplasticizer is then added and blended within 1.5 minutes.
5. After that, the mixture is ejected, tested and cast; the total mixing time is about 5 minutes.

3.4.2 Reactive Powder Concrete (RPC)

3.4.2.1 Mix Proportion of Reactive Powder Concrete

Reactive powder concrete was used as a hybridization to restore the strength of SB spacemen with openings. During the current study, many trial mixes were carried out and then tested at age of 28 days, as listed in table 3.15. The selected mixture ratios which denoted in Table 3.16 were adequate to give an acceptable compressive strength about 120.7MPa and a suitable workability.

3.4.2.2 Mixing Procedure of Reactive Powder Concrete

For reactive powder concrete, cement, silica fume and fine sand were mixed in dry case for 2 minutes dissipate the particles of fine sand throughout the cement and silica fume particles. The superplasticizer was dissolved in water, and the solution was incrementally added throughout the mixing process, followed by 7-8 minutes of mixing. Steel fibers were uniformly distributed into the mixture within 2 minutes.

Table (3.16) Trail Mixes Proportion of RPC

Trail No.	**1**	**2**	**3**	**4**	**5**	**6**	**7 selected**
Cement (kg/m^3)	853	853	869	858	960	950	950
Silica fume (kg/m^3)	214	214	217	215	240	210	210
Sand ($kg/m^{3)}$	1069	1069	1091	1077	1040	1050	1050
Steel fiber (kg/m^3)	157(2%)	157(2%)	117(1.5%)	157(2%)	157(2%)	157(2%)	157(2%)
w/ binder (%)	18	17.5	17.5	15	16	15	16
Superplasticizer (%)	1.5	2	2	3.5	4	3	4
Flow %	82	144	132	220	220	220	220
f_c' (28 days)MPa*	91.2	86	80.14	93.6	96.87	101.5	120.7

* $f_{C\,(RPC)} = 1.0\, f_{cu}$ **(De Larrard et al., 1994)**

The total time of mixing for one batch around 10 minutes from adding the solution of water and superplasticizer to the mix.

3.5 Reinforcement Steel Framwork Preparation

In order to reinforce the curved beam, a steel reinforcement cage should carry out by tying the longitudinal reinforcement with the transverse stirrups around them. The stirrups were radially distributed, to insure that the stirrups were correctly and accurately placed in their position the steel mold was marked on outer and inner circumference as illustrate in Plate 3.4 to ensure accurate radial arrangement of the stirrups on the main reinforcement, then spacing of 90mm and 45mm were achieved on the center main reinforcement.

Plate (3.4) Preparation of Cage of Steel Reinforcement

3.6 White Polystyrene Preparation

To represent box beam, an additional process was required which is the manufacturing of the inside form. This process was done by using 2.7cm and 1.7cm thick white polystyrene cut accurately by using CNC machine to take the shape and radius of the curved box beam with the dimensions of the hole (130×130mm). This was achieved by placing four layers of 2.7cm and one layer 1.7cm white polystyrene to represent the depth of the hole (130mm). Then to protect the polystyrene during casting, it was warped by using a sticky tape. The polystyrene curve was fixed inside the steel cage and spaced equally by using spacers as illustrated in plate 3.5.

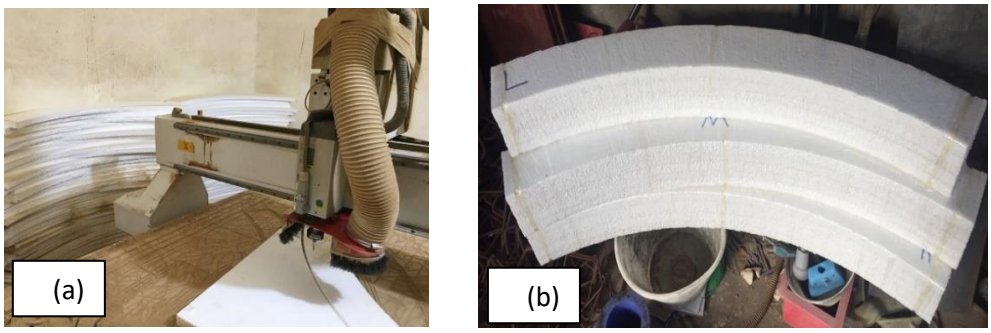

Plate (3.5) White Polystyrene Operation

(a) Cutting of White Polystyrene (b)Preparation of White Polystyrene

3.7 Formwork Preparation

Two steel formworks have been used for casting test specimens. The formworks are manufactured from the semicircular base, two semicircular moveable sides and two moveable end plate by using a CNC- machine. Thickness of steel plate used in the manufacturing was (3mm). All the parts of molds are fixed with each other by 16mm diameter bolts and the details are shown in Plate 3.6.

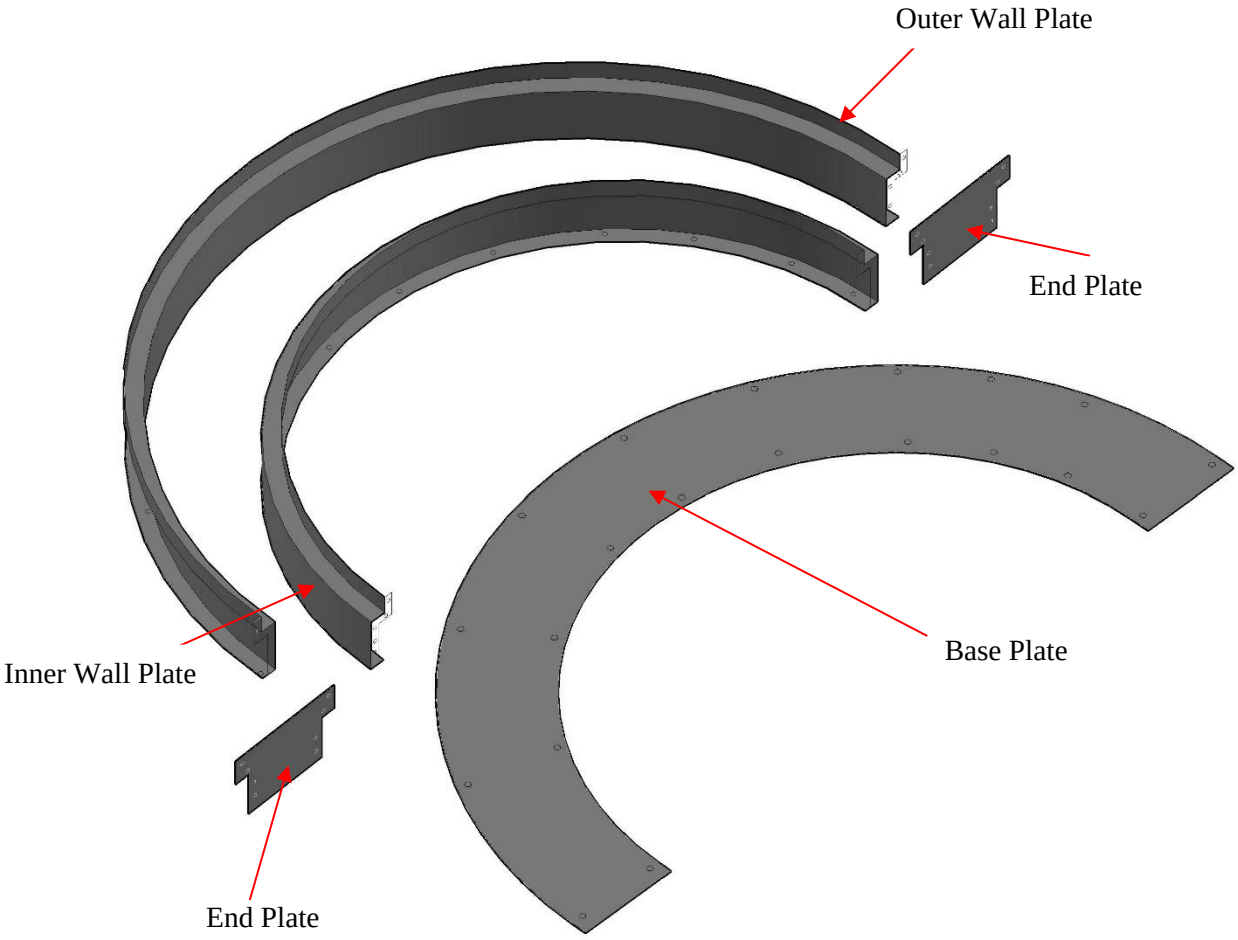

(a)

(b)

Plate (3.6) Semicircular Molds and Tools

(a) Steel Mold Layout (b)Steel Mold Photos

3.8 Casting and Curing of Tested CB Specimens

The molds of circular curved box beams specimens, cubes and cylinders were treated with oil before casting to prevent adhesion with concrete after

hardening. Reinforcement cages were prepared, then the white cork curve was fixed inside the steel cage and spaced equally by using spacers, consequently the steel cage with cork were placed inside the molds. Furthermore, circular curved box Beams specimens with opening, the wooden cubes were placed and fixed accurately on the cork by using steel hub before putting steel cage with cork in the mold. The hybrid concrete of strengthened CB specimens was manufactured from two separated mixtures of concrete (SCC and RPC) cast in the same time (monolithically) with using wood plate of thickness (4mm) to isolate them. RPC were cast into three layers with two minutes of vibration, then the concrete surface (top face of last layer) of RPC was leveled and finished by a steel trowel.

Plate (3.7) Preparation and Casting Operation of Test Specimens
(a)Reinforcement Configuration (b) Fixing of White Cork
(c) Fixing of Wood Opening (d) Assemblage the Reinforcement with Molds
(e) Cast of Self-Compact Concrete (f) Cast and Vibrating of RPC
(g) Molds Removing (h) Curing of Specimens

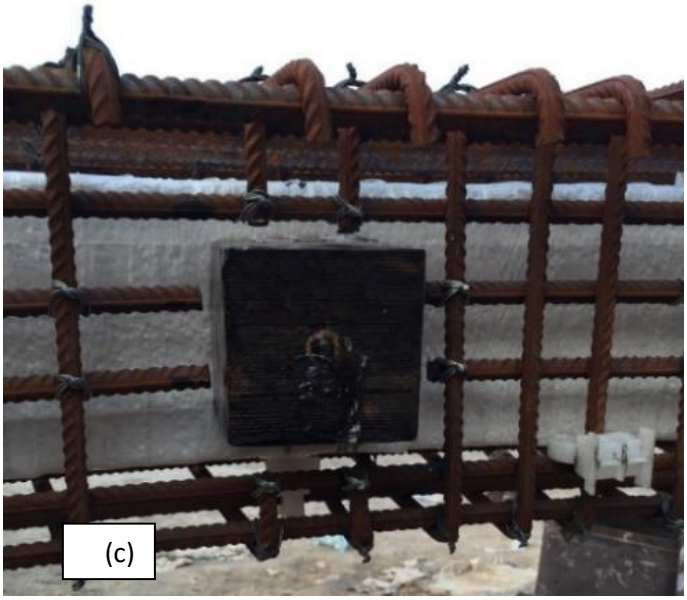

Plate (3.7) Continue

Plate (3.7) Continue

Plate (3.7) Continue

After 24 hours of casting, the burlap sacks were set over CB specimens with mold and remained moist for up to 24 hours. After 48 hours of casting, CB specimens were extracted from the molds, while ensuring that the CB specimens remain moist throughout the curing period (28 days) by moist burlap sacks, as shown in plate 3.7. Following 28 days of curing, all specimens were dried in air and CFRP laminates technique was installed to CB specimens that were externally strengthened by CFRP laminate, as illustrated later in Section 3.10.

3.9 Control Samples

Concrete cubes (150×150×150) mm, (50×50×50) mm for compressive strength and concrete cylinders (100×200) mm for splitting tensile strength were left in the molds for 24 hours. After that, they were removed from the molds and set in a basin full of clean water. After 28 days, they were taken out of the container and tested with each CB specimen at the same time for each type of concrete (SCC and RPC) according to the standard

specifications (**ASTM-C496-11**, **BS1881-116-83**) to obtain the compressive strengths and splitting tensile by using a universal testing machine, as appeared in Plate 3.8.

Plate (3.8) Test of Control Samples

(a) Compressive strength test (b) Splitting Tensile strength test

3.10 Installation of CFRP Laminates

The efficiency of strengthening of concrete structures with EBR- CFRP sheets based on the interaction between the CFRP and the concrete. The processes below were followed to achieve effective bonding:

(1) An electrical hand grinder was used to grind the surface of the concrete to make the aggregate visible and achieve a clean and smooth surface devoid of any impurities such as dirt and cement laitance.

(2) Before applying the composite, the concrete surfaces were cleansed with water and left to dry. This way cleaned the surface specimen from loose particles and contaminations.

(3) To minimize concentration of stress in the CFRP at the corners of the specimens, the beam corners were tapered (radius of about 15 mm). CFRP

will rupture at corners due to this stress concentration before reaching its maximum strength.

(4) Using a trowel or brush, Sikadur-330 mixed resin is applied to the ready surface. in an amount of (0.7 to 1.2 kg/m^2), based on the coarseness of the concrete surface.

(5) For all specimens, the Sika Wrap 300C cloth was cut into strips using scissors to the desired width and length.

(6) With the plastic roller, press the Sika Wrap 300C fabric into the resin until the resin has been pressed out of the roving.

(7) An extra resin layer of roughly (0.5 kg/m^2) can be placed as a covering layer, this will serve as a binder for additional cementitious coatings.

(8) After allowing the epoxy to harden for several days, the specimens will be ready to test (see Plate 3.9).

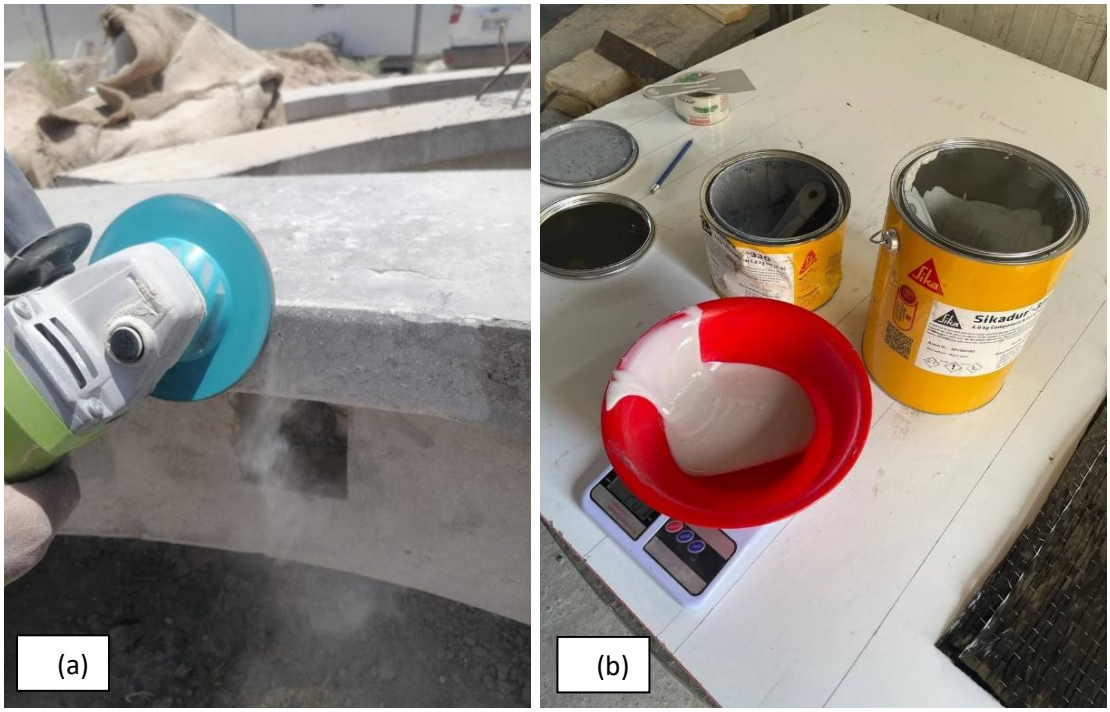

Plate (3.9) Application of CFRP Laminates on Concrete Element
(a) Grinded and Rounded of Concrete Surface and Corners (b) Preparation of Resin
(c) Cutting of Sika Wrap to Appropriate Size (d) Placing of the Fabric in to Concrete

Plate (3.9) Continue

3.11 Instruments and Testing Procedure

3.11.1 Testing Machine

The universal hydraulic testing apparatus was used to test the circular curved box beams specimens. The testing machine has a capacity of (2000 kN) available in the Structural Laboratory of the Faculty of Engineering, University of Karbala, as displayed in Plate 3.10. This apparatus was constructed from 30 mm thick steel sections and consist of a 32 mm thickness moveable braced support (two plates) that is movable up and down by a scroll placed at the machine's top. Two steel rods with a diameter of 50 mm are inserted into holes to secure the plates to the frame.

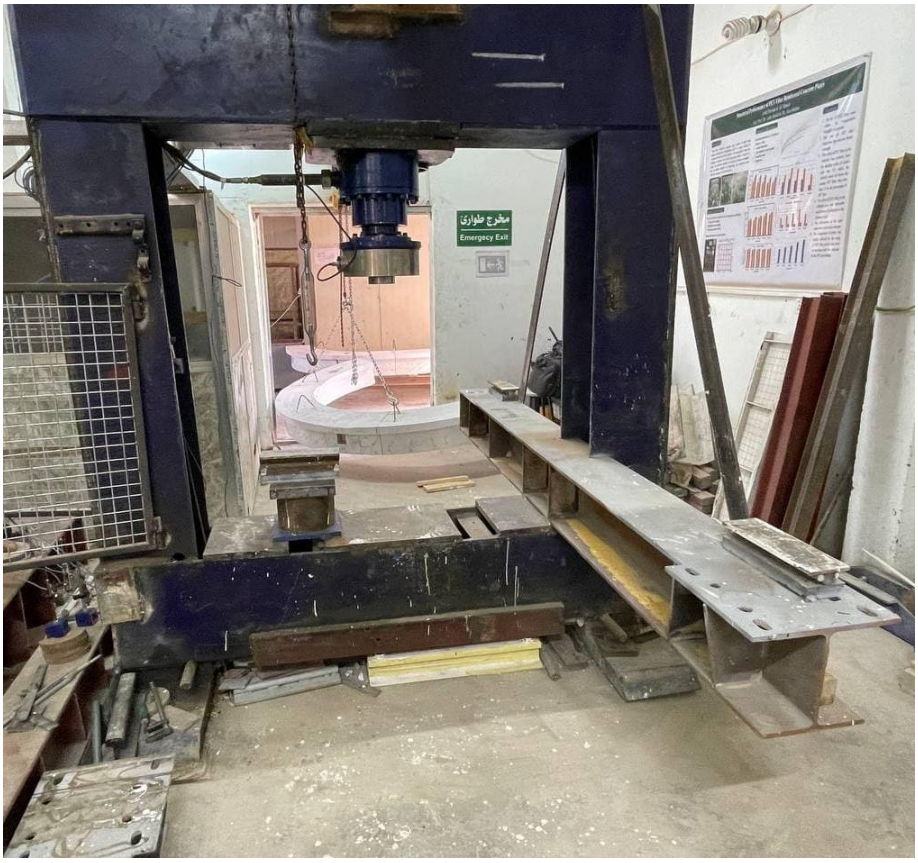

Plate (3.10) Loading Machine Used in the Tests

3.11.2 Supporting and Loading Conditions

Circular curved box beams specimens were subjected to static or repeated loads using a universal test machine, as displayed in plate 3.11. The supporting system included hinged ends on the outside and a roller on the inside. For hinged end, steel shaft with a diameter of 25mm is fixed by welding to the lower base plate, whereas two shafts with a diameter of 12 mm are welded to the top base plate (to make grove). To restrict relative movement and create a firm base beam that holds the supports, the supported plates was welded to a W-shape steel beam. The roller support be manufactured of one rod with 25mm diameter fixed by weld to the lower base plate and upper base plate was putted free upon shaft of lower base plate. Figure 3.10 displays the support conditions details.

Plate (3.11) Test Setup

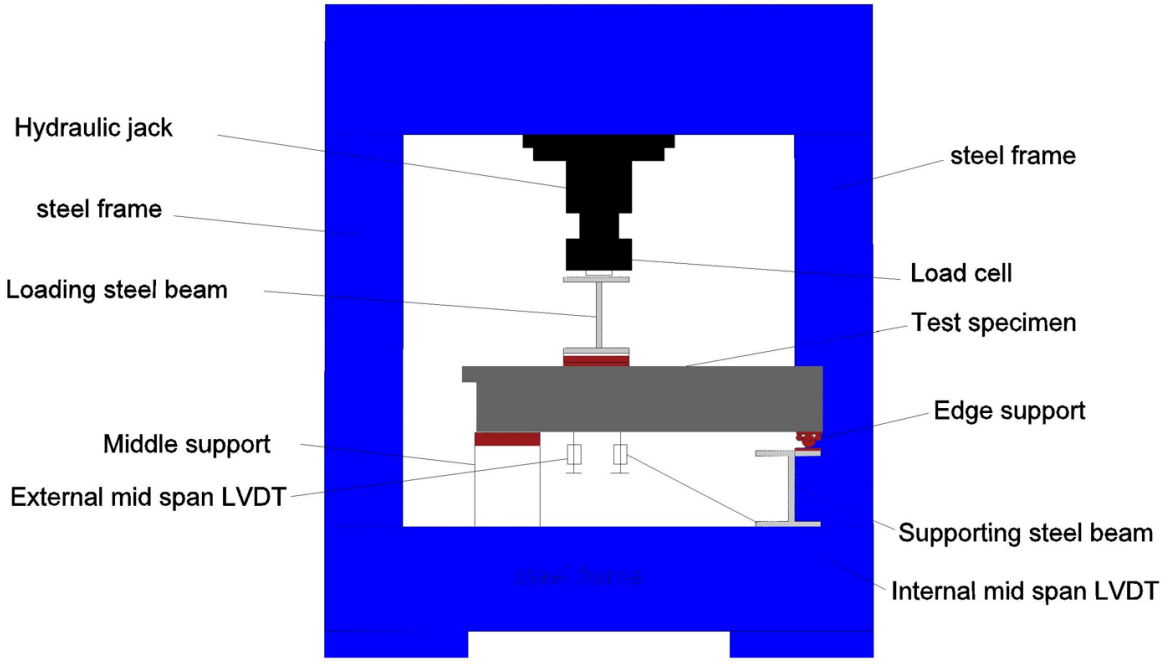

(a)

Figure (3.10) Test Setup Layout (a)Side View Schematic Drawing (b) Top View Schematic Drawing

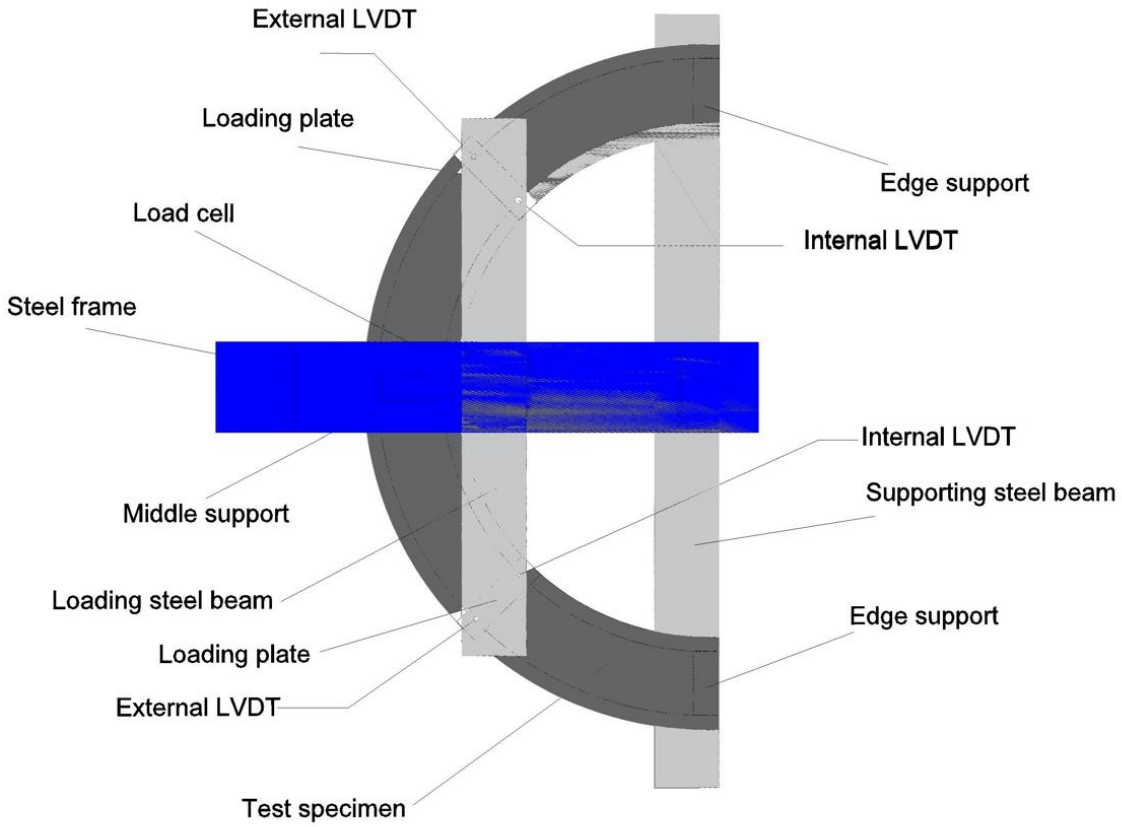

(b)

Figure (3.10) Continue

All of the semicircular beams were tested under two-point loading, with the load applied at midspan of each panel.

3.11.3 Test Instruments

Through each test, instruments were used to record the structural behavior of specimens in the loading stages. Plate 3.12 shows the instruments used in testing of CB specimens. The intent of using each measuring instrument in the examination can be shown as follows;

- LVDTs of 0.01mm precision to measure vertical deflection at midspan the of CB specimens.
- Crack meter (Microscope WF10X–18 mm) to measure the crack width.

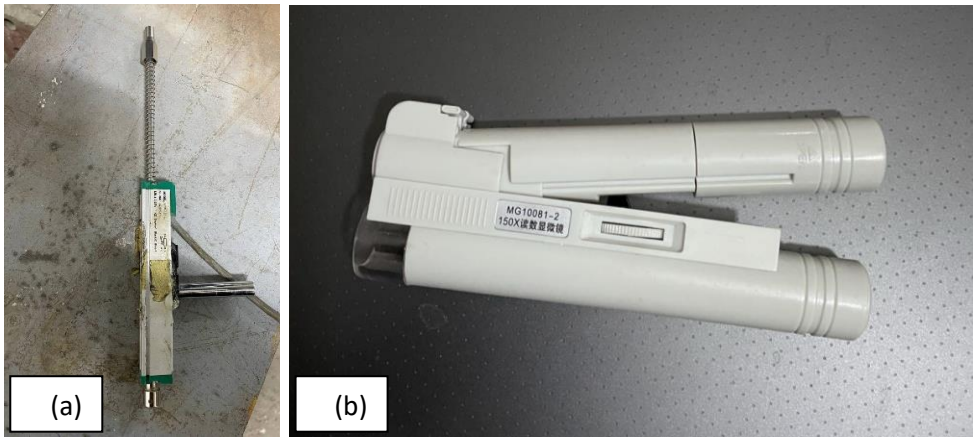

Plate (3.12) Instruments used in Testing
(a) LVDT (b) Crack meter

3.11.4 Loading History

Four Circular curved box beams specimens were subjected to repeated loading condition in one direction. The load sequence for all cyclic loaded specimens was according to the considered loads of the similar specimens under monotonic loading condition, as shown in Figure 3.11. The loading history consisted of 10 cycles of repeated loads of varying intensities, where the specimen loaded gradually each 10 kN up to the maximum load level in that particular cycle and then unloaded.

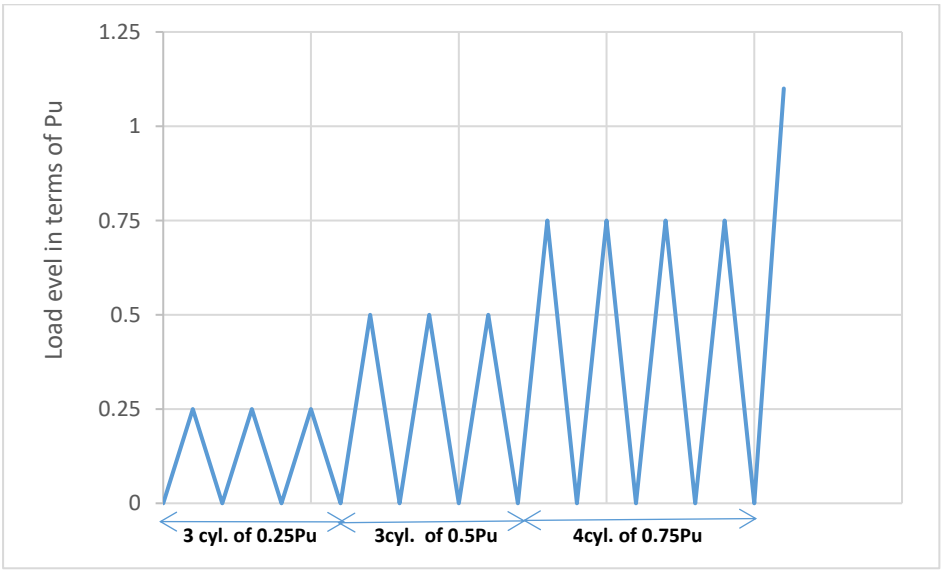

Figure (3.11) Typical Loading History of Repeated Loaded Specimens.

3.11.5 Testing Procedure

To observe the cracks development, all specimens painted by white color. Initially, one pilot specimen was tested to check the devices and loading test system before starting in the test program of CB specimens. In the preliminary test, the pilot CB specimen was subjected to static loading up to failure.

All of the CB specimens tested under two-point loading, with the load applied at midspan of each panel, as shown previously in Figure 3.10.

The CB specimens were positioned on the testing machine's supports, and then the LVDTs were calibrated and fitted at the midspan of the CB specimens. Following that, the specimens were loaded at a steady rate (every10KN along the static loading specimens). Readings of deflection was recorded continuously with the applied load by a data logger connected with the hydraulic testing machine. Specimens that were subjected to repeated loading were evaluated using a loading history according to static loads for identical specimens as illustrated in Figure 3.11. For all CB specimens, the first cracking loads was recorded, then the crack width was measured at every 25 kN. Pate 3.13 demonstrate some steps of testing program.

Plate (3.13) Test Program of Specimens
(a) Marking the path of cracks (b) Recording the crack width

CHAPTER FOUR

Experimental Results and Discussion

4.1 General

In this chapter, the general response and observation of the tested horizontally circular curved concrete beams with and without openings (control beam), and strengthened by hybrid concrete or externally bonded reinforcement with CFRP laminates subjected to monotonic or repeated loading were reported and discussed. To accomplish this objective, an experimental program has been performed, as described in the previous chapter.

Load versus deflection and torsional moment versus rotation at the mid-span of horizontally curved concrete beams were recorded for each specimen during the experimental program. As well as, cracking and ultimate loads, cracking patterns, cracks width, failure modes, ductility ratios, accumulated energy absorbed and stiffness degradation were recorded. Photographs for the tested curved beams were taken to show the cracks pattern and failure modes. In this chapter, the analysis and discussion for the recorded data of test results, general behavior and test observations are reported.

4.2 Mechanical Properties of Control Samples

After 28 days, three standard concrete cubes of (150×150×150) mm and (50×50×50) mm for compressive strength of normal concrete and reactive powder concrete respectively, and standard concrete cylinders of (100×200) mm for splitting tensile strength were taken out of the container and tested for each type of concrete (normal concrete and reactive powder concrete) according to (**BS1881-116-83** and **ASTM-C496-11**).

Table (4.1) Mechanical Properties of Control Samples.

Type of Test / CB Designation		Cubic Compressive Strength (MPa)f_{cu}	Cylinder Compressive Strength (MPa)*f'_c	Tensile Splitting Strength (MPa)f_t	Modulus of Elasticity, Ec(MPa)**
$CB_1.L_1$	NC_{SCC}	52.72	42.18	4.22	30524
$CB_2.V37.L_1$	NC_{SCC}	52.88	42.3	4.88	30568
$CB_3.V60.L_1$	NC_{SCC}	51.18	40.94	3.92	30072.7
$CB_4.V82.L_1$	NC_{SCC}	51	40.80	4.24	30021.2
$CB_5.T37.L_1$	NC_{SCC}	48.87	39.1	3.51	29389
$CB_6.T60.L_1$	NC_{SCC}	52.23	41.79	4.70	30383
$CB_7.T82.L_1$	NC_{SCC}	51.72	41.38	4.47	30233.8
$CB_8.V60.S_1.L_1$	NC_{SCC}	50.78	40.62	3.73	29954.9
	RPC	126.34	126.34	9.59	46534
$CB_9.T60.S_1.L_1$	NC_{SCC}	51.98	41.58	4.08	30288
	RPC	121.13	121.13	9.12	45564
$CB_{10}.V60.S_2.L_1$	NC_{SCC}	50.20	40.17	3.80	29788.5
$CB_{11}.T60.S_2.L_1$	NC_{SCC}	50.26	40.21	3.67	29803.3
$CB_{12}.L_2$	NC_{SCC}	52.83	42.27	4.75	30557.2
$CB_{13}.T60.L_2$	NC_{SCC}	52.33	41.86	4.45	30408.67
$CB_{14}.T60.S_1.L_2$	NC_{SCC}	51.68	41.34	4.06	30219.2
	RPC	122.91	122.91	8.79	45900
$CB_{15}.T60.S_2.L_2$	NC_{SCC}	51.82	41.45	4.63	30259.4

$f'c_{(NC)}$= 0.8 fcu (MPa) (**BS8110 − 85**)

$f'c_{(RPC)}$=1.0 fcu (MPa) **(De Larrard et al., 1994)**

$Ec_{(NC)}$=4700 $\sqrt{f_c'}$ (MPa) (ACI 318R − 19**)

$Ec_{(RPC)}=4140\sqrt{f'_c}$ (MPa) **(Habeeb et al., n.d., 2016)**

The mechanical properties of concrete samples at test days are demonstrated in Table (4.1), where each value represents the average of three samples.

4.3 Structural Response of Tested Specimens

4.3.1 General Behavior

In general, there are three phases of load-deflection and torsional moment-twisting angle response: elastic un-cracked, elastic-cracked and ultimate stages, the first stage ended as cracks were formed.

At the un-cracked phase, the deflection and twisting angle linearly increased in all specimens throughout the loading, due to elasticity of materials in the compression and tension rezones. After cracking (cracked phase), the load-deformation relationship (deflection and twisting angle) was linear, but with a steeper slope than before. After latter phase, the slope decreased largely and the deflection and twisting rotation rose dramatically up to failure with a slight increase in loading level. The discussion of results obtained for each group is presented in the following sections and illustrated in Figures (4.1 to 4.30).

During the first phases of loading, at lower load levels, all of the circular beams tested were devoid of cracks and behave elastically. The deformations were proportionate to the applied loads. Subsequently, there were little stressed, and then the whole cross section was capable of sustaining the imposed loads. More cracks appeared as the load increments increased.

There are five different types of cracks that have been developed, flexural cracks, torsional-shear cracks, flexural-shear cracks, diagonal cracks at corners of openings and oblique shear cracks. The specimen experienced

damage in the form of flexural cracks during the experiment above internal support at the top face of the beam where the maximum negative moment, flexural cracks under load at bottom face of midspan positive moment, torsional-shear crack appears diagonally between interior support and points of loading and diagonal cracks at corners of openings.

4.3.2 Pilot Specimen

The pilot specimen (CB. P) was constructed without openings to make sure everything is in order to test process supports and load positions, LVDTs and its place, in addition the overall test incremental load applications under monotonic load. Torsional-shear failure at ultimate load about (391 kN) occurred, due to several torsional-shear cracks started in the regions between middle support and applied load.

4.3.3 Control Specimens

Specimen $CB_1.L_1$

This specimen was constructed without openings, which considered as control specimen for the test groups that subjected to monotonic loading.

The beam was loaded gradually each 5 KN until failure, the first flexural crack was observed in the top face of maximum negative moment (internal support) at load of about 50 kN. At load 60 kN, the first positive flexural crack at bottom face of midspan appears. As the load reaches the value of 100 kN, first torsional -shear inclined cracks initiated in the positions between interior support and points of loading. As the load was increased further, several flexural cracks observed at top face near internal support and at bottom face near midspan, and torsional-shear in the positions between interior support and points of loading. Torsional-shear cracks spread spirally with an angle about 45° and began to increase in length and number more than flexural crack with load increments, spatially between interior support and points of loading.

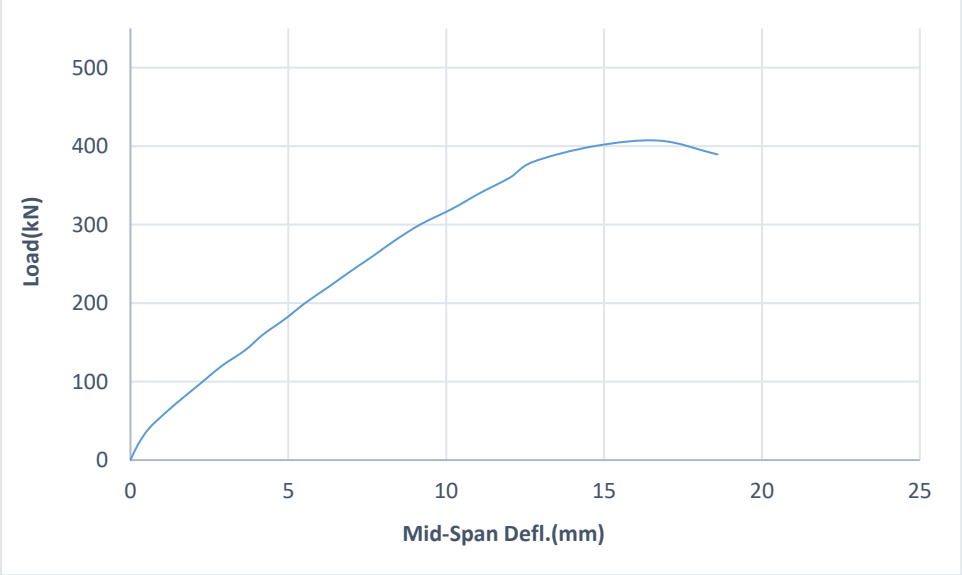

Figure (4.1) Load-Midspan Deflection Curve for Specimen **$CB_1.L_1$**

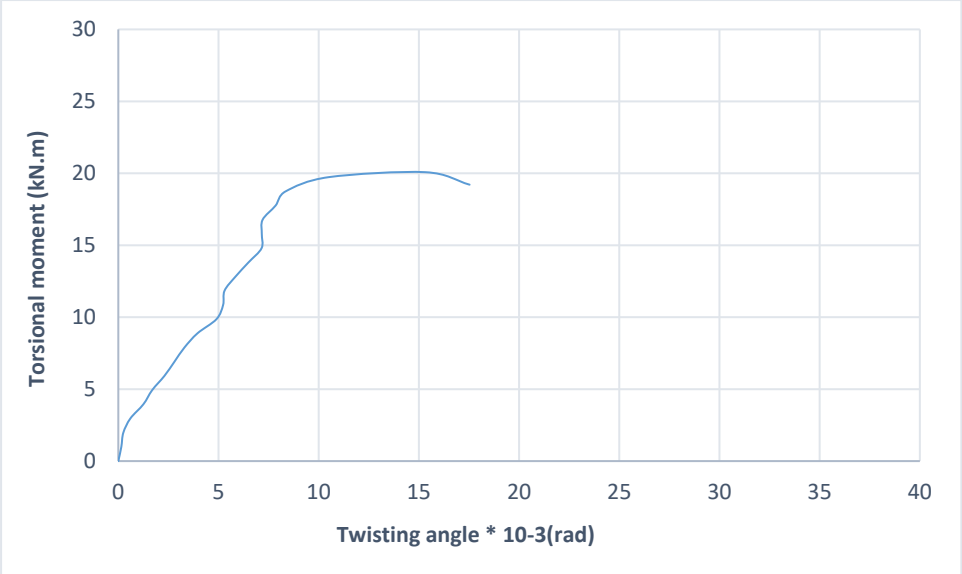

Figure (4.2) Torsional moment-Midspan Twisting Angle Curve for Specimen **CB1.L1**

At high load stages before failure (around 370 kN), it can be noticed that width, length and number of torsional-shear cracks increased more than flexural cracks. Finally, torsional-shear failure at ultimate load about 407.25 kN occurred.

Plate (4.1) Specimen **$CB_1.L_1$**

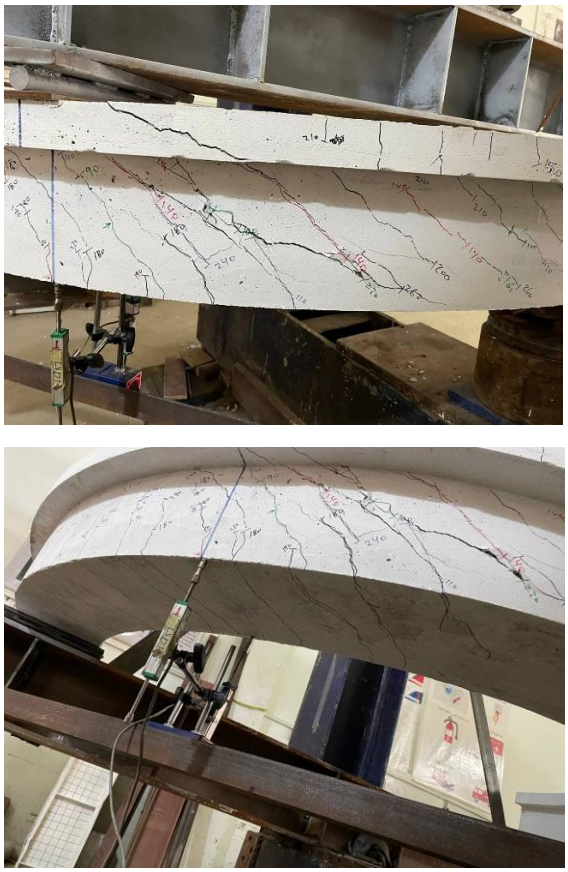

Plate (4.2) Mode of Failure and Cracks Pattern for Specimen **$CB_1.L_1$**

Figures 4.1and 4.2 show load deflection curve and Torsional moment-angle of twisting curves at midspan, respectively, while Plates 4.1and 4.2, show mode of failure and cracks pattern.

Specimen $CB_{12}.L_2$

This specimen was made without openings, which taken into consideration as control specimen for the test group that subjected to repeated loading. First flexural cracking of this circular beam that subjected to cyclic loading, is formed above internal support in the top face of beam where maximum negative moment within the first cycle at load of 40 kN. At load about (60 kN in the first cycle), the first flexural crack due to positive moment at bottom face of midspan appears. While continuing to increase the applied load within the first cycle and at the value of about 90 kN, first torsional - shear inclined cracks appeared in the locations between middle support and applied load.

As the load was increased further in the form of repeated loading (loading –unloading), several flexural cracks observed at top face near internal support and at bottom face near midspan, and torsional-shear in the positions between interior support and points of loading in a manner similar to specimen $CB_1.L_1$.

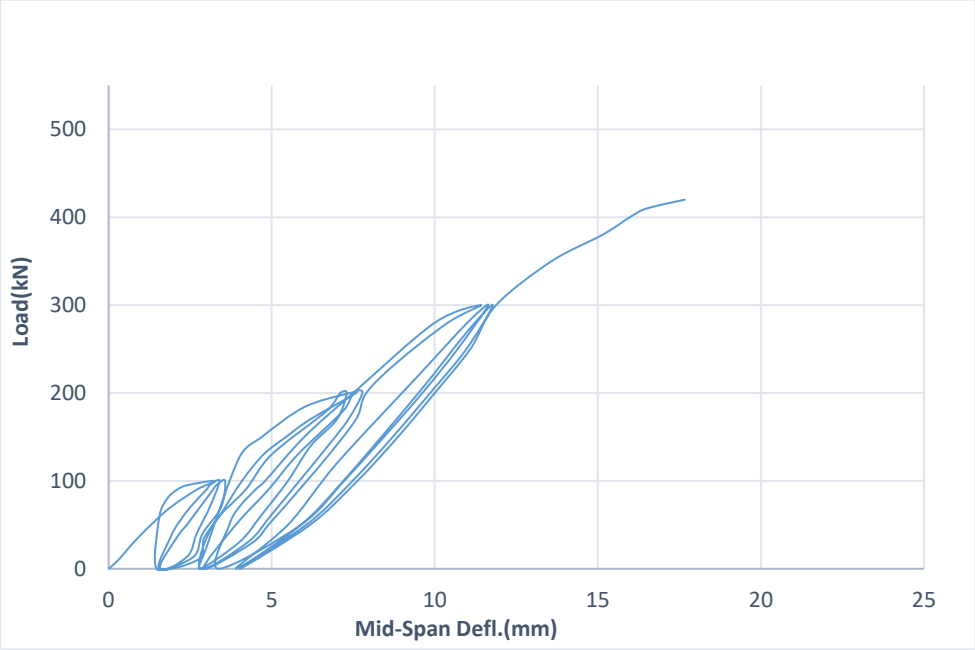

Figure (4.3) Load-Midspan Deflection Curve for Specimen **$CB_{12}.L_2$**

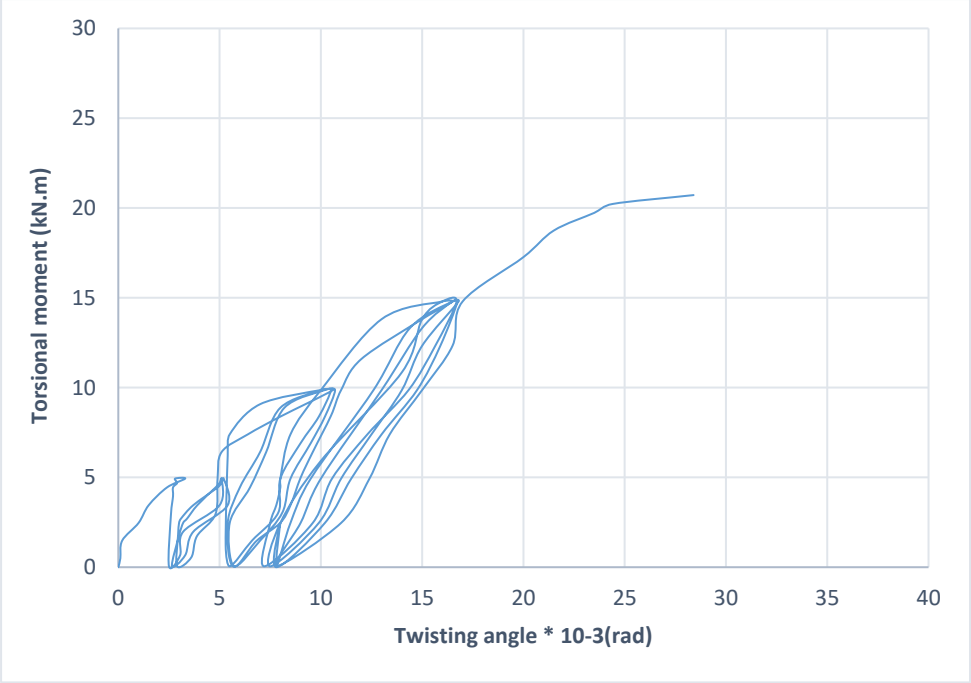

Figure (4.4) Torsional moment-Midspan Twisting Angle Curve for Specimen **CB12.L2**

Plate (4.3) Specimen **$CB_{12}.L_2$**

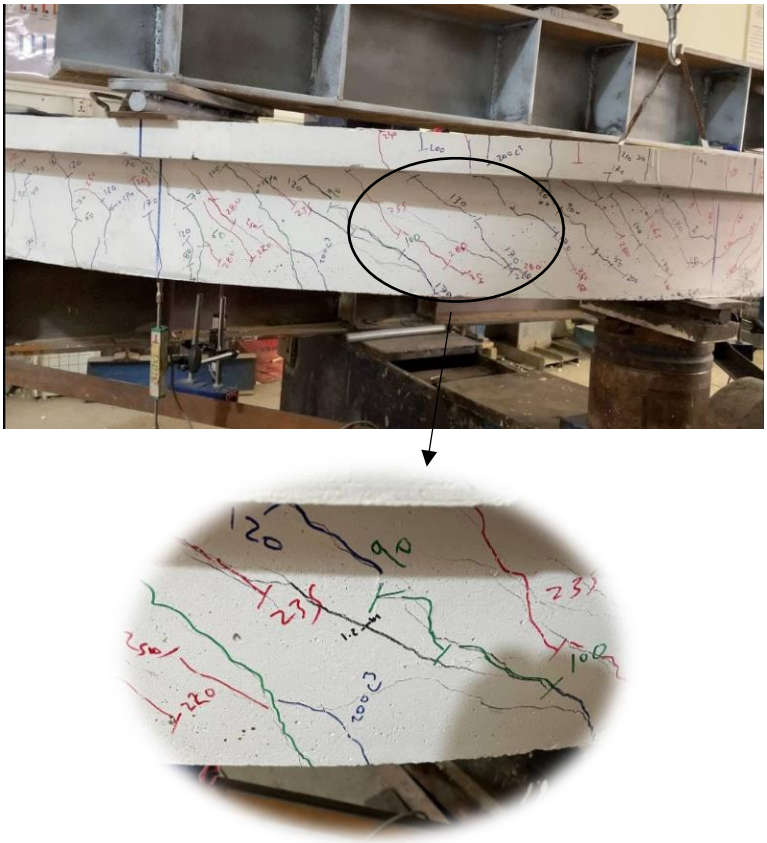

Plate (4.4) Mode of Failure and Cracks Pattern for Specimen **$CB_{12}.L_2$**

As a further progress in the frequency of cycles within the same level of load, a slight increase in the length and width of some cracks were observed. Lastly, torsional-shear failure at an ultimate load of about 421.20 kN took place. Figures 4.3 and 4.4 clarify load-deflection and Torsional moment - angle of twisting curves for midspan, respectively, while Plates 4.3 and 4.4, depicts failure mode and cracks pattern at Failure.

4.3.4 First Test Group (CBs with Vertical Openings)

In this test group, five specimens were fabricated of circular curved box beams with vertical opening unstrengthening or strengthened by RPC or CFRP laminates and tested under monotonic loading.

4.3.4.1 Unstrengthened specimens

Specimen $CB_2.V37.L_1$

The circular beam $CB_2.V37.L_1$ includes vertical opening between the applied load and exterior support spaced at distance d/2=125 mm from the applied load(37° measured from exterior support to the center of opening) and without strengthening, as shown in Plate (4.5). The load was progressively raised until the first flexural crack appeared at a load of around 40 kN, which was seen at the top face above the inner support where highest negative moment region. The slanted crack appeared in one corner of lower vertical opening at load of 50 kN. At load of 60 kN, the first flexural crack at bottom face of midspan appears where positive moment region. Torsional-shear cracks start to appear at load of 70 kN at mid-distance between load and middle support where maximum torsional force zone. As the load was increased further, several flexural cracks at top face (internal support), bottom face (midspan) and torsional-shear cracks at positions between the applied loads and internal support were initiated. Continue moving of flexural cracks upward and downward, oblique cracks of torsional-shear developed in length and numbers. Moreover, inclined cracks growing in width and length, and onset at other corners of lower vertical openings. Finally, while no diagonal crack was appeared in corners of upper vertical opening at ultimate load was about 385.74 kN, torsional-shear failure occurred in zones between interior support and points of loading. It can be concluded, that the presence of vertical openings at an angle (37°) reduce the ultimate load capacity (compared with control beam) by about 5%, also slight lack was noticed in flexural and torsional stiffness. Figures 4.5 and 4.6 exhibit load-deflection and Torsional moment -angle of twisting curves for midspan, respectively while, Plates 4.5 and 4.6, displays failure mode and types of crack.

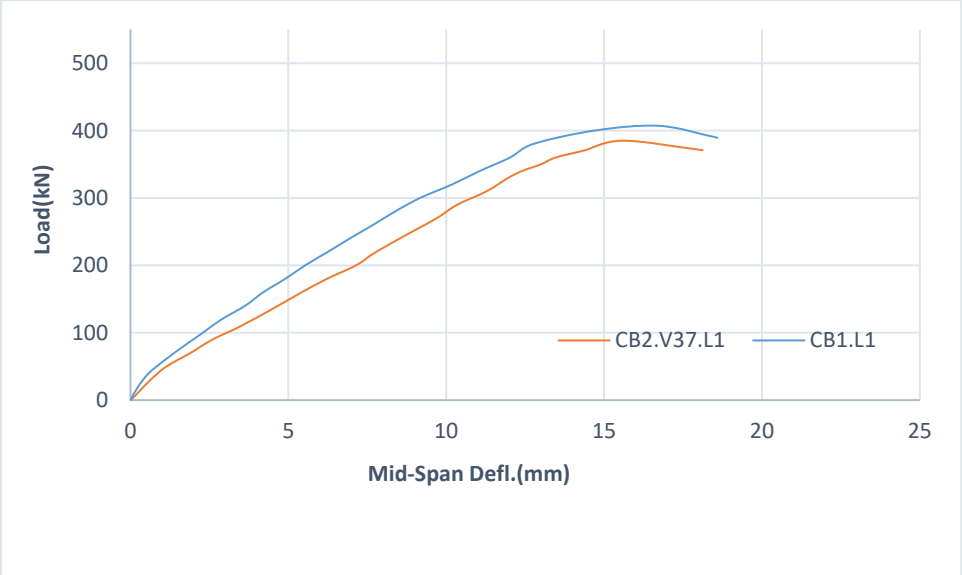

Figure (4.5) Load-Midspan Deflection Curve for Specimens (**$CB_1.L_1$**and **$CB_2.V37.L_1$**)

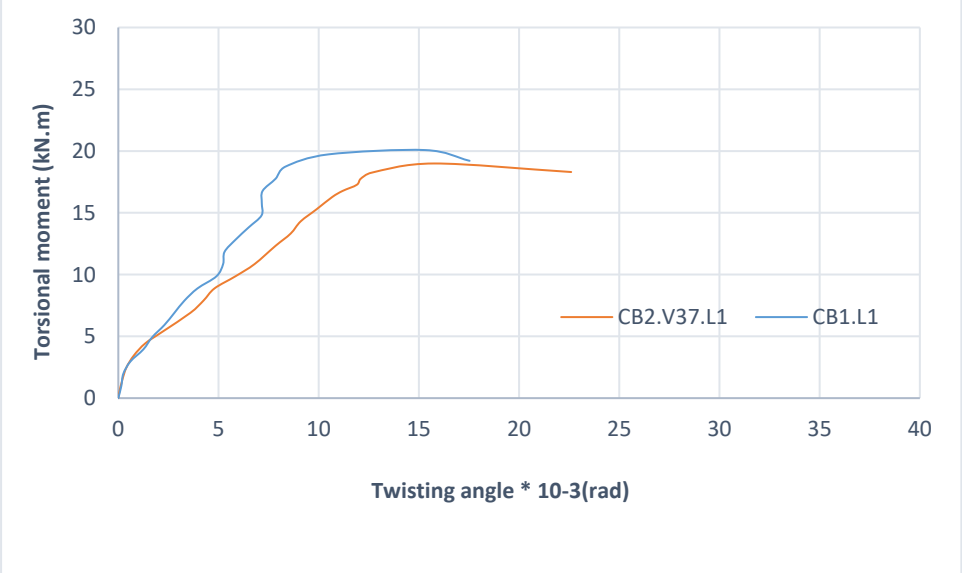

Figure (4.6) Torsional moment-Midspan Twisting Angle Curve for Specimens (**$CB_1.L_1$**and **$CB_2.V37.L_1$**)

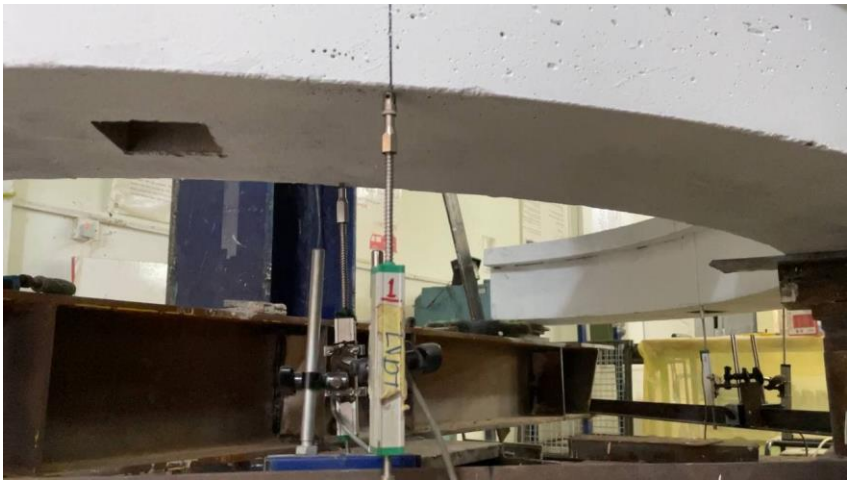

Plate (4.5) Specimen **$CB_2.V37.L_1$**

Plate (4.6) Mode of Failure and Cracks Pattern for Specimen **$CB_2.V37.L_1$**

Specimen $CB_3.V60.L_1$

The $CB_3.V60.L_1$ beam includes vertical opening positioned exactly at angle 60° measured from exterior support to the center of opening (in zone between the applied loads and internal support) and without strengthening, as shown in Plate (4.7). The load was started and continued to increase until the first flexural crack formed with a load of around 40 kN which was noticed at the top face of the flange above the interior support where the highest negative moment zone. At load step of 60 kN the first flexural crack at bottom face of midspan appears due to maximum positive moment. Torsion-shear cracks occurred when the load was increased to 80 kN, while the first visible inclined cracks at the corners of lower and upper vertical openings at load 90 kN were created. The increasing of applied load was accompanied by an increase in the number, width and length of flexural and Torsional-shear cracks.

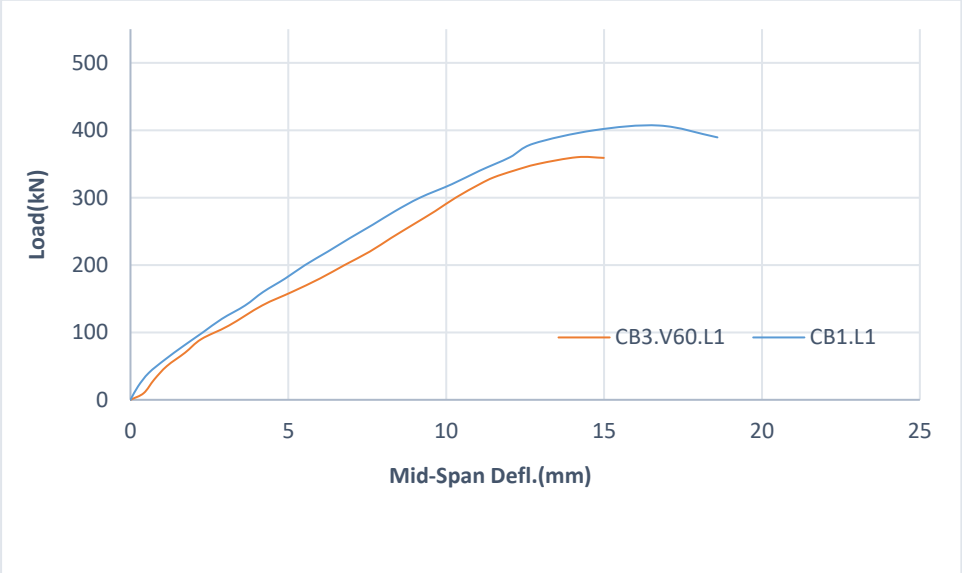

Figure (4.7) Load-Midspan Deflection Curve for Specimens (**$CB_1.L_1$**and **$CB_3.V60.L_1$**)

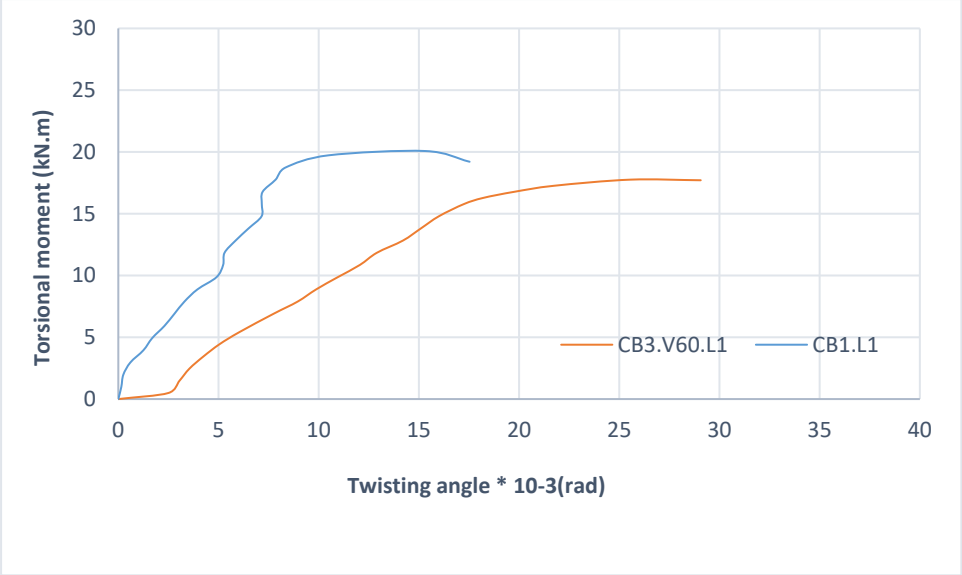

Figure (4.8) Torsional moment-Midspan Twisting Angle Curve for Specimens (**$CB_1.L_1$**and **$CB_3.V60.L_1$**)

Plate (4.7) Specimen **$CB_3.V60.L_1$**

Plate (4.8) Mode of Failure and Cracks Pattern for Specimen **$CB_3.V60.L_1$**

Finally, rapid propagation of diagonal cracks at the corners of lower vertical opening convert the mode of failure from torsional-shear to frame type failure when reached the load of 360.3 kN, however no considerable deformation in the upper vertical openings. It can be concluded, that the presence of vertical openings at an angle (60°) reduce the ultimate load capacity (compared with control beam) by about 11.5%, also reduced flexural and torsional stiffness of the beam. Figures 4.7 and 4.8 illustrate load-deflection and Torsional moment -angle of twisting curves at midspan, respectively, and Plates 4.7 and 4.8 depicted mode of failure and types of crack of the Specimen.

Specimen $CB_4.V82.L_1$

The $CB_4.V82.L_1$circular beam includes vertical opening spaced at distance d/2=125 mm from face of internal support (82° measured from exterior support to the center of opening) and with no presence of strengthening, as displayed in Plate (4.9). During the initial phases of load, the beam deformation was within elastic limits, and load was incrementally raised until the first flexural crack appeared at a load of 40 kN in the region of tension above middle support. As the load was increased further, first crack initiated which was observed in corners of the upper vertical opening with a load of roughly 60 kN, because of a concentration of stresses at these corners. At load step of 70 the first flexural crack at bottom face of midspan appears where maximum positive moment region. Diagonal torsional-shear cracks occurred at the place of maximal torsional moment between applied load and middle support with further load increments (100 kN). Many flexural and Torsional-shear cracks developed as the load was increased. At a high stages of load increment, torsional-shear cracks propagated rapidly, while no considerable increase in the width of diagonal crack in the corners of upper vertical openings. The beam $CB_4.V82.L_1$was failed due to forming large oblique torsional-shear cracks in zones between interior support and points of loading at ultimate load of about 400.55 kN. Noted that no diagonal cracks in the corners of the lower vertical openings until failure, this was due to subjected to a compression state. It can be noticed, that the presence of vertical openings at an angle (82°) caused very slight reduction in the ultimate load capacity (compared with control beam) was about 1.5%, also slit lack were observed in flexural and torsional stiffness in the beam. Figures 4.9 and 4.10 illustrate load-deflection and Torsional moment -angle of twisting curves for midspan, respectively, and Plates 4.9 and 4.10, display mode of failure and types of crack.

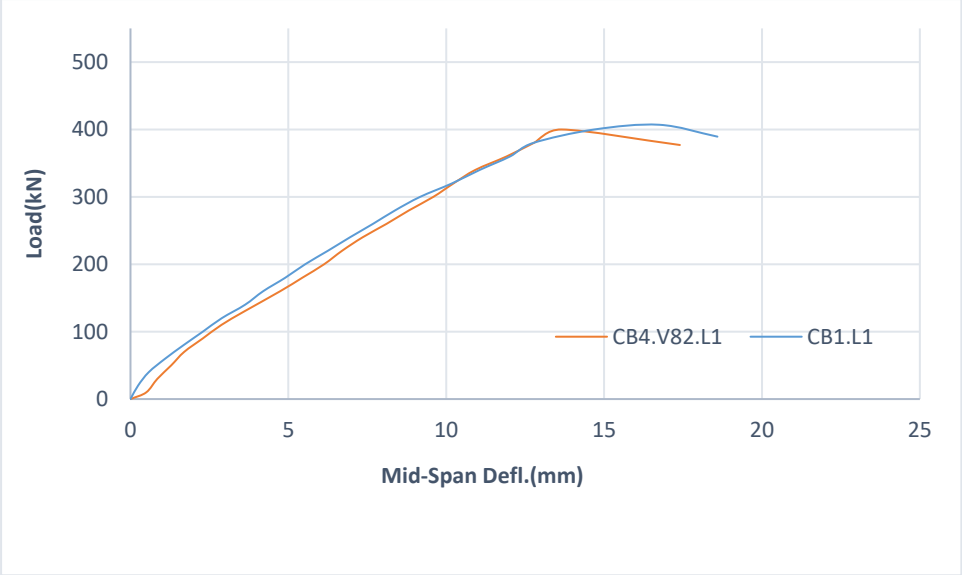

Figure (4.9) Load-Midspan Deflection Curve for Specimens (**$CB_1.L_1$**and **$CB_4.V82.L_1$**)

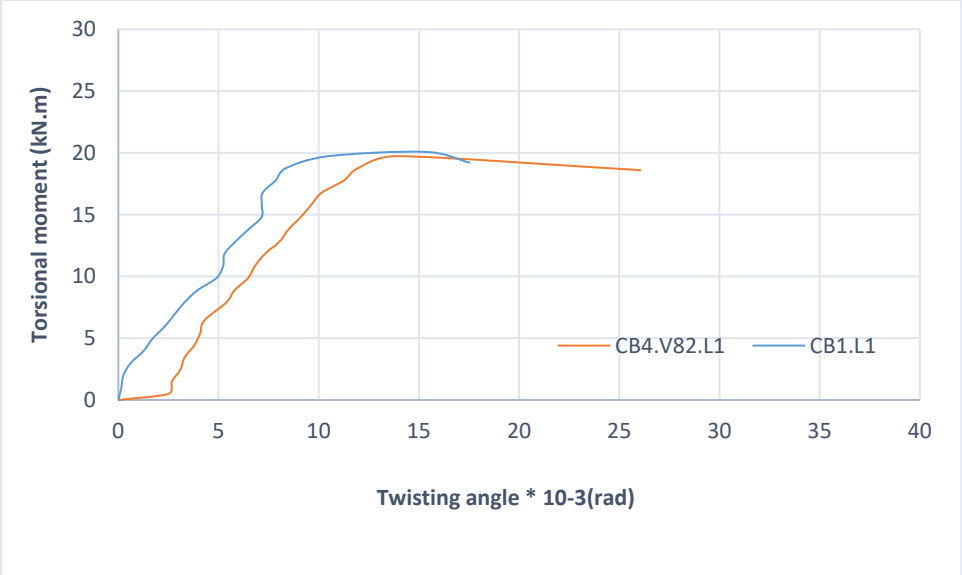

Figure (4.10) Torsional moment-Midspan Twisting Angle Curve for Specimens (**$CB_1.L_1$**and **$CB_4.V82.L_1$**)

Plate (4.9) Specimen **$CB_4.V82.L_1$**

Plate (4.10) Mode of Failure and Cracks Pattern for Specimen **$CB_4.V82.L_1$**

4.3.4.2 Strengthened specimens

Specimen $CB_8.V60.S_1.L_1$

The $CB_8.V60.S_1.L_1$ beam includes vertical opening positioned exactly at angle 60° measured from exterior support to the center of opening (in zone between the applied loads and internal support) and strengthened by hybridization of concrete around opening and for the entire section of the beam, using RPC cast monolithically at a distance of 125 mm on both edges of vertical opening , as shown in Plate 4.11. In this Specimen, flexural crack was first noticed at the top face of specimen above interior support where maximum negative moment with a load roughly 59.2 kN. At load 80 kN, first flexural crack was initiated at maximum positive moment under applied load. At a load of 120 kN, inclined torsional-shear cracks formed in the region between the applied load and the middle support, flexure cracks developed across these increments, due to high strength and ductility of RPC, no corner cracks occurred at the vertical opening. As load increased further, torsional-shear cracks began to appear at load 160 kN in RPC. Fine corner cracks at lower vertical opening was noticed at load of 190 kN, while in upper vertical opening appeared at 250 kN. Increasing in length, number and width of flexural and torsional-shear cracks were noticed as load as increase, while cracks in RPC zones maintain its length and width (no serious change) until failure. The ultimate load capacity was about (427 kN), which was increased by about 4.8% and 18.5% when compared with specimens $CB_1.L_1$ and $CB_3.V60.L_1$ respectively. As mode of failure, the beam was failed due to flexural positive moment near midspan. Figures 4.11 and 4.12 depict load-deflection and Torsional moment -angle of twisting curves at midspan, respectively, also Plates 4.11and 4.12, displayed failure mode and pattern of cracks.

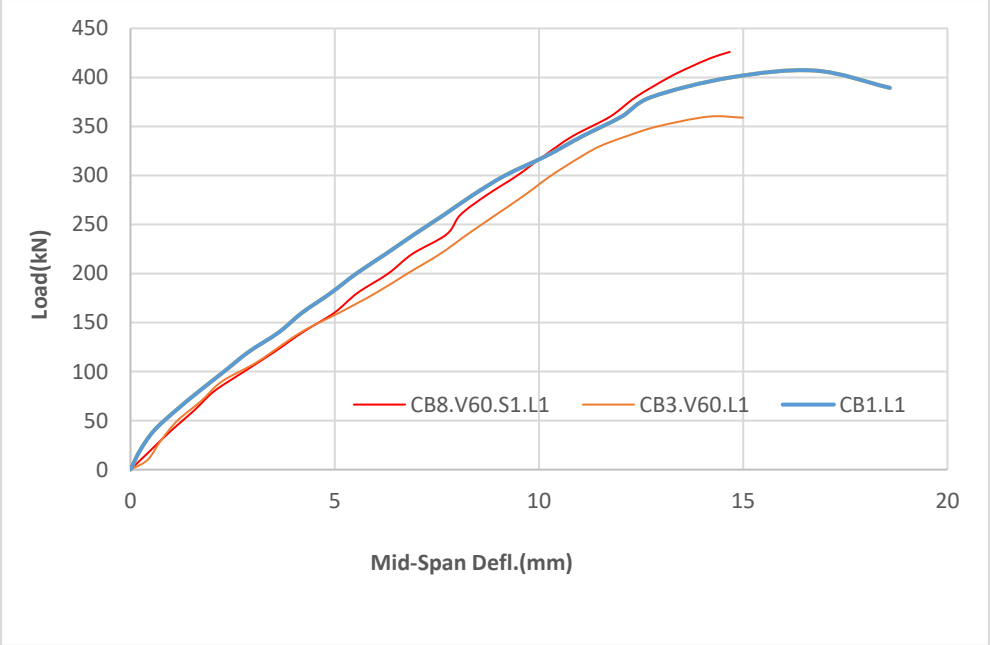

Figure (4.11) Load-Midspan Deflection Curve for Specimens (**$CB_1.L_1$**, **$CB_3.V60.L_1$**and **$CB_8.V60.S_1.L_1$**)

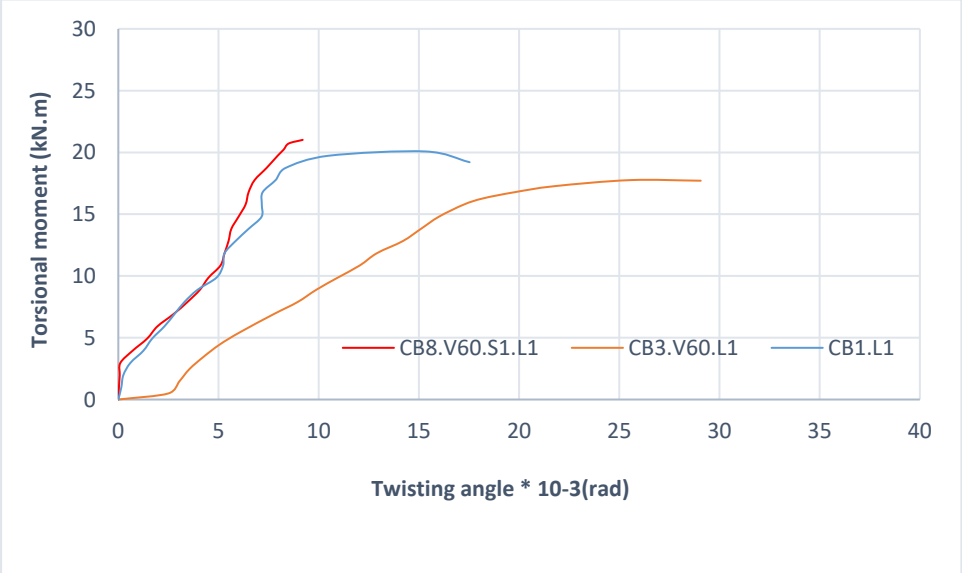

Figure (4.12) Torsional moment-Midspan Twisting Angle Curve for Specimens (**$CB_1.L_1$**, **$CB_3.V60.L_1$**and **$CB_8.V60.S_1.L_1$**)

Plate (4.11) Specimen **$CB_8.V60.S_1.L_1$**

Plate (4.12) Mode of Failure and Cracks Pattern for Specimen **$CB_8.V60.S_1.L_1$**

Specimen $CB_{10}.V60.S_2.L_1$

The circular beam $CB_{10}.V60.S_2.L_1$ beam includes vertical opening positioned exactly at angle 60° measured from exterior support to the center of opening (in zone between the applied loads and internal support), strengthened by 0.17mm thickness of U wrap EBR-CFRP laminates with 80 mm width on both side of the opening and U wrap of 120 mm width for upper and lower chords of opening, as shown in Plate 4.13. As usual, this specimen was incrementally loaded until the flexural first crack was appear with a load around 60 kN at top face of beam above middle support where maximum negative moment zone and at maximum positive moment zone at midspan. When load reaches 110 kN, torsional-shear cracks start to appear at zones between the load and the middle support. As load increased further and at load of about 150 kN due to confinements of CFRP laminates, diagonal crack at external corner of the lower vertical opening towards midspan was observed, while no diagonal cracks at corners of the upper vertical opening was appeared until the load was reached 350 kN, also flexural and diagonal torsional-shear cracks was propagated (increase in number, length and width) through these increments. At stages of loading above 350 kN, corner cracks at the opening and torsional-shear cracks did not propagate when reaches the CFRP laminates and prevent it from extending through until failure taken place because of the confinements of CFRP laminates. Figures 4.13 and 4.14 depict midspan load-deflection and midspan Torsional moment -angle of twisting curves, respectively. As shown in plate 4.14, a frame type failure happened owing to torsional moment which cause deboning of CFRP laminates at load of 415.56 kN which was larger than the control specimen $CB_1.L_1$ by about 2% and 15.3% when compared with the specimen $CB_3.V60.L_1$.

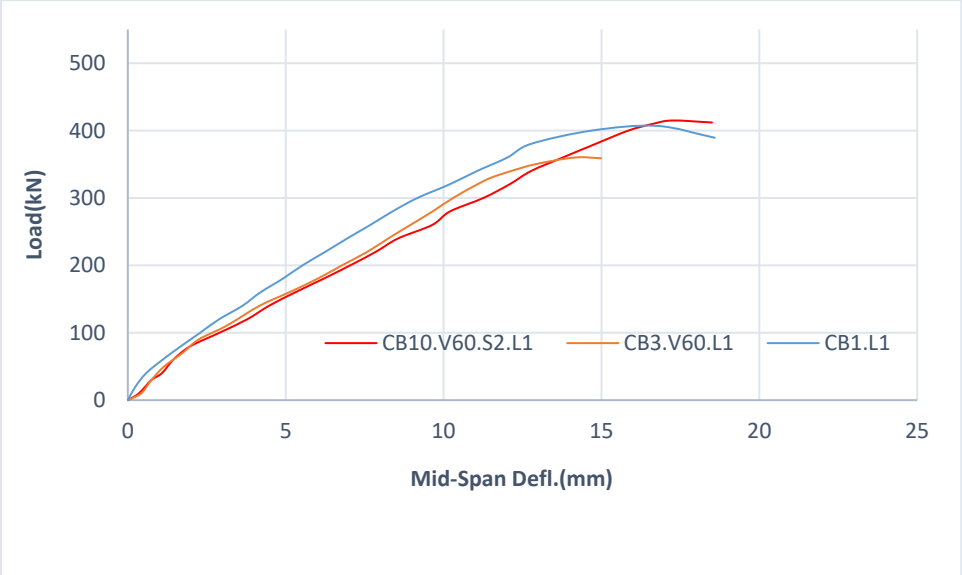

Figure (4.13) Load-Midspan Deflection Curve for Specimens (**$CB_1.L_1$**, **$CB_3.V60.L_1$**and **$CB_{10}.V60.S_2.L_1$**)

Figure (4.14) Torsional moment-Midspan Twisting Angle Curve for Specimens (**$CB_1.L_1$**, **$CB_3.V60.L_1$**and **$CB_{10}.V60.S_2.L_1$**)

Plate (4.13) Specimen **$CB_{10}.V60.S_2.L_1$**

Plate (4.14) Mode of Failure and Cracks Pattern for Specimen **$CB_{10}.V60.S_2.L_1$**

4.3.5 Second Test Group (CBs with Transverse Openings)

In this test group, five test specimens were manufactured of circular curved box beams with Transverse opening unstrengthening or strengthened by RPC or CFRP laminates and tested under monotonic loading.

4.3.5.1 Unstrengthened specimens

Specimen $CB_5.T37.L_1$

This beam includes transverse opening between the applied load and exterior support spaced at distance d/2=125 mm from the applied load (37°measured from exterior support to the center of opening) and without strengthening, as shown in Plate 4.15. The load was raised gradually up to the first flexural crack appearing at a load of about 39 kN at the top face of the beam above the interior support where the maximum negative moment position. At load step of 65 kN, the first flexural crack at bottom face of midspan appears in region of maximum positive moment. Torsion-shear cracks developed between load and internal support where the maximum torsional and shear force after increasing the load to 75 kN. The diagonal crack was appeared in lower corner of transverse opening at load of 85 kN. As the load was increased further, several flexural cracks at top face (internal support), bottom face (midspan), another crack occurs at the opposite corners of the opening also torsional-shear cracks developed between the concentrated load and the mid support. Finally, torsional-shear cracks propagated rapidly more than diagonal cracks at corners of transverse openings, then failure occurred in zones between mid support and loading applied at load of about 401 kN which was less than that for $CB_1.L_1$ by about 1.5%. Figures 4.15 and 4.16 illustrate load-deflection and Torsional moment -angle of twisting curves for midspan, respectively, and Plate 4.16, depicts failure mode and pattern of cracks.

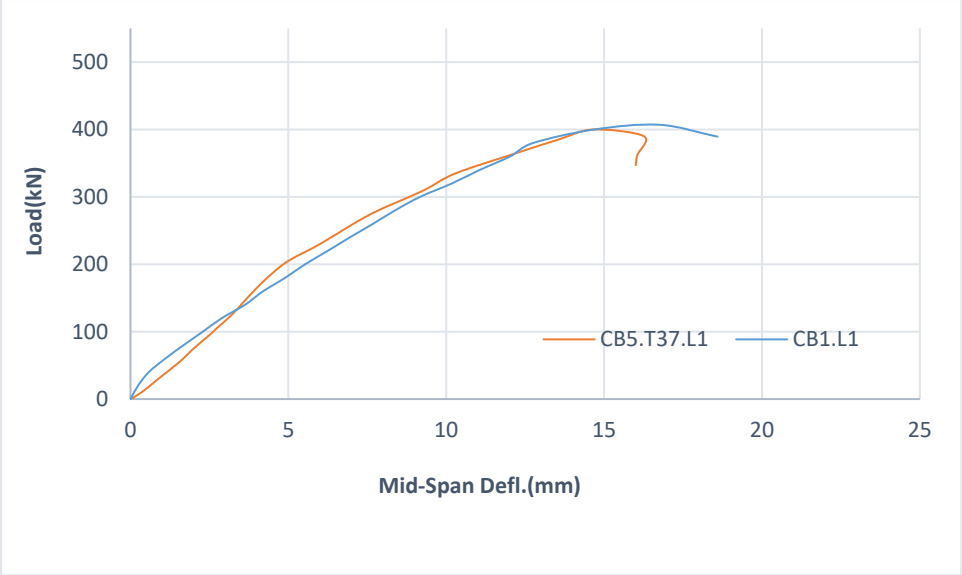

Figure (4.15) Load-Midspan Deflection Curve for Specimens (**$CB_1.L_1$**and **$CB_5.T37.L_1$**)

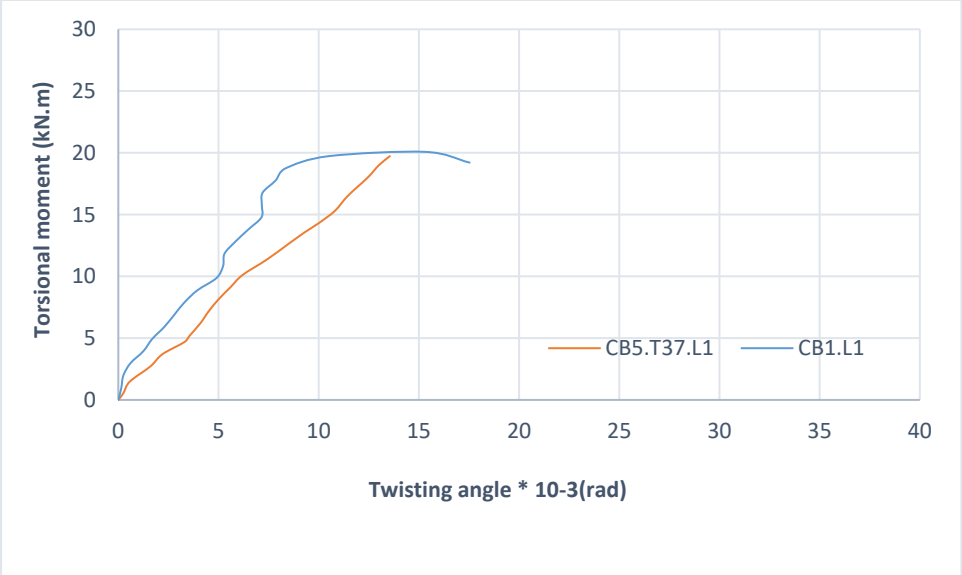

Figure (4.16) Torsional moment-Midspan Twisting Angle Curve for Specimens (**$CB_1.L_1$**and **$CB_5.T37.L_1$**)

Plate (4.15) Specimen **$CB_5.T37.L_1$**

Plate (4.16) Mode of Failure and Cracks Pattern for Specimen **$CB_5.T37.L_1$**

Specimen $CB_6.T60.L_1$

The $CB_6.T60.L_1$ beam includes transverse opening positioned exactly at angle 60° measured from exterior support to the center of opening (in zone between the applied loads and internal support) and unstrengthen, as illustrate in Plate 4.17. The specimen was loaded gradually until the first crack appears at a load of 50 kN at the skew corners (beam type) of the transverse opening, also flexural crack was noticed at top face of flange above the middle support in position of maximum negative moment. After increasing the load to 80 kN, the flexural crack at bottom face of midspan developed, as well as torsional-shear cracks began to appear. The increasing of applied load was accompanied by an increase in the number, width and length of flexural and Torsional-shear cracks. Simultaneously, rapid propagation of diagonal cracks at the corners of transverse opening, frame type failure mode at opening zone was occurred.

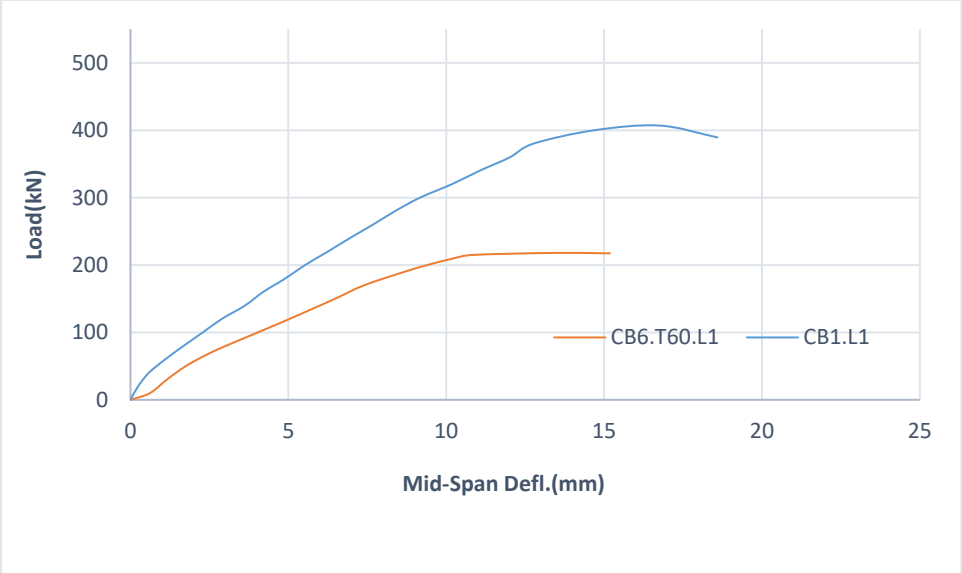

Figure (4.17) Load-Midspan Deflection Curve for Specimens (**$CB_1.L_1$**and **$CB_6.T60.L_1$**)

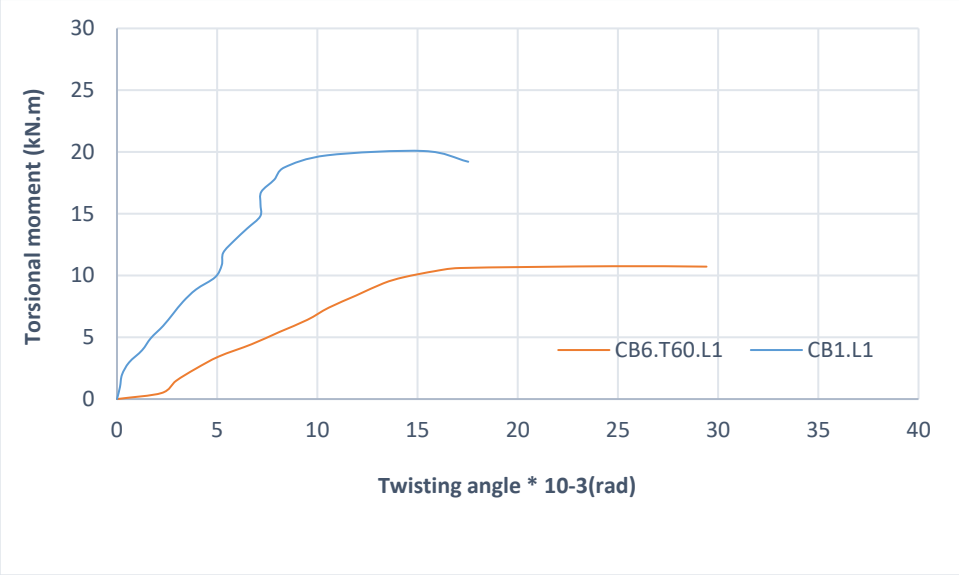

Figure (4.18) Torsional moment-Midspan Twisting Angle Curve for Specimens (**$CB_1.L_1$**and **$CB_6.T60.L_1$**)

Figures 4.17 and 4.18 presented midspan load-deflection and Torsional moment -angle of twisting curves, respectively. Plate 4.18 shows mode of failure the and the crack pattern of the beam at ultimate load of 218 kN, which indicated a large reduction by about 46.4% when compared with a control $CB_1.L_1$.

Plate (4.17) Specimen **$CB_6.T60.L_1$**

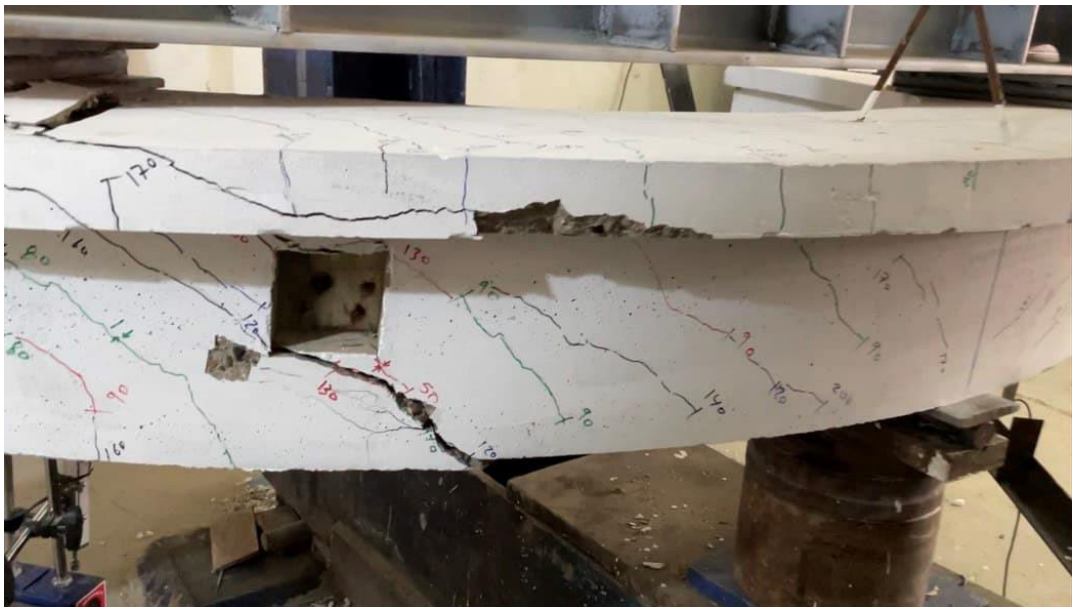

Plate (4.18) Mode of Failure and Cracks Pattern for Specimen **$CB_6.T60.L_1$**

Specimen $CB_7.T82.L_1$

The $CB_7.T82.L_1$ circular beam includes transverse opening spaced at distance d/2=125 mm from face of internal support (82° measured from exterior support to the center of opening), with absence of strengthening, as displayed in Plate 4.19. During the initial phases of load, the beam displacement was within elastic limits, when the load was progressively raised, at a load of 58 kN, the first cracks due to flexure tend to develop at top face of beam above mid support. As the load was increased further, first cracks monitored in the upper and lower skew corners of the transverse openings as a result of the concentration of stresses at these corners with load of about 80 kN. At load step of 90 kN, the flexural first crack at bottom face of midspan occurs in region of maximum positive moment. Slanted torsional-shear cracks developed between point load and interior support where the position of highest torsional moment with additional load increments (140 kN). After more load increment, several flexural and torsional-shear cracks were initiated, while corner cracks at openings were increased in length and width. The ultimate load of beam $CB_7.T82.L_1$was about 331.48 kN by forming sudden shear cracks at top and bottom cords of the opening (frame type failure) near internal support. It can be noticed, that the presence of transverse opening at an angle (82°) caused a reduction in the ultimate load capacity (compared with control beam) was about 18.66%, also a clear reduction was observed in flexural and torsional stiffness of the beam. Figures 4.19 and 4.20 illustrate midspan load-deflection and Torsional moment -angle of twisting curves, respectively, as well as Plate 4.20, depicts failure mode and pattern of cracks.

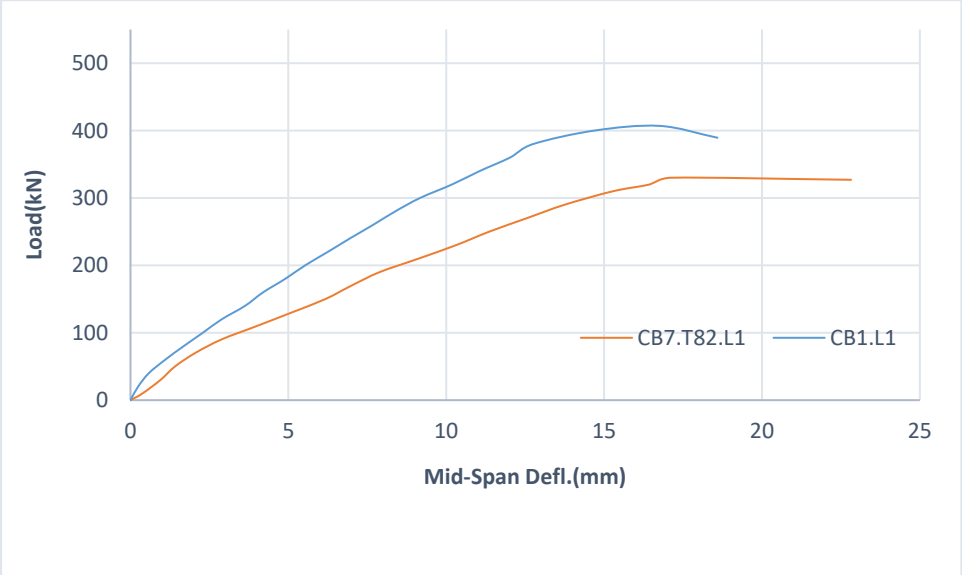

Figure (4.19) Load-Midspan Deflection Curve for Specimens (**$CB_1.L_1$**and **$CB_7.T82.L_1$**)

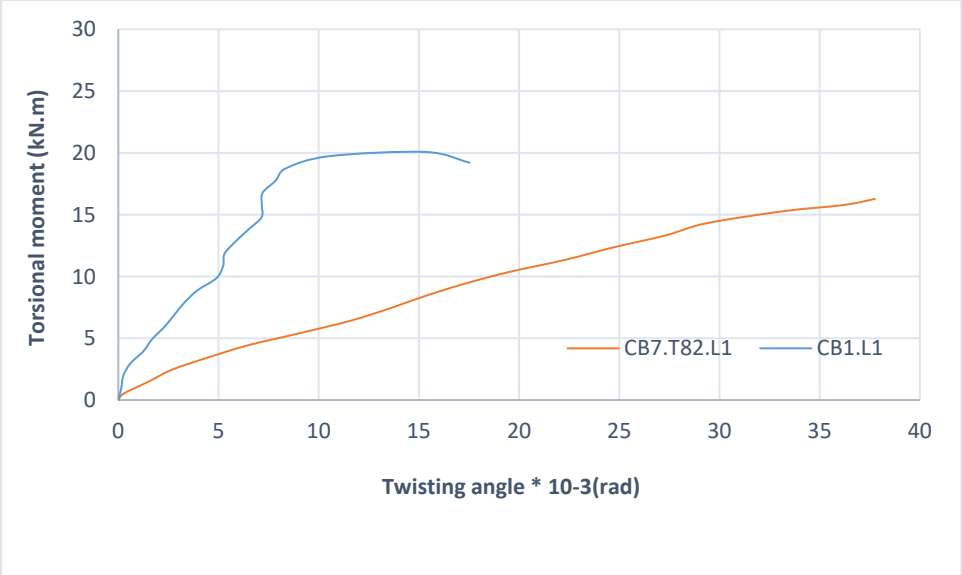

Figure (4.20) Torsional moment-Midspan Twisting Angle Curve for Specimens (**$CB_1.L_1$**and **$CB_7.T82.L_1$**)

Plate (4.19) Specimen **$CB_7.T82.L_1$**

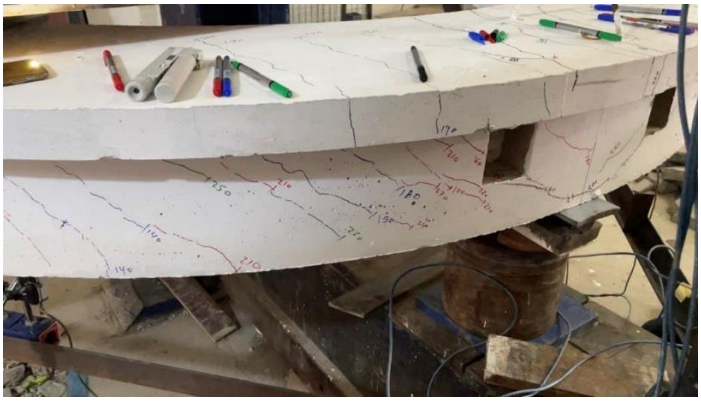

Plate (4.20) Mode of Failure and Cracks Pattern for Specimen **$CB_7.T82.L_1$**

4.3.5.2 Strengthened specimens

Specimen $CB_9.T60.S_1.L_1$

The $CB_9.T60.S_1.L_1$beam includes transverse openings positioned exactly at angle 60° measured from exterior support to the center of opening (in zone between the applied loads and internal support) and strengthened by hybridization of concrete using RPC cast monolithically at a distance of 125 mm on both edges of opening , as shown in Plate 4.21. While the load increased gradually, the flexural first crack appeared at the top face of the specimen above interior support in the zone of a maximum negative moment with a load of around 65 kN. At load 80 kN, first flexural crack was initiated at maximum positive moment under applied load, while at load step of 90 kN first cracks in RPC observed in the top and bottom skew corners of the transverse openings. Inclined torsional-shear cracks started to appear at the region between the middle support and loading when the load reaches 120 kN. As load increased further, torsional-shear cracks began to appear at load 170 kN in RPC zones around transverse openings. Increasing in length, number and width of flexural and torsional-shear cracks were noticed as load as increase, while cracks in RPC zones maintain its fine length and width (no considerable deformation) until failure because of high strength and ductility of RPC. At last, the beam failed due to flexural positive moment near midspan at load of 512.65 kN, an increase was observed by about 25.9% and 135% when compared with the Specimens $CB_1.L_1$and $CB_6.T60.L_1$ respectively . Figures 4.21 and 4.22 shows midspan load-deflection and Torsional moment -angle of twisting curves, respectively, and Plate 4.22, depict failure mode and pattern of cracks.

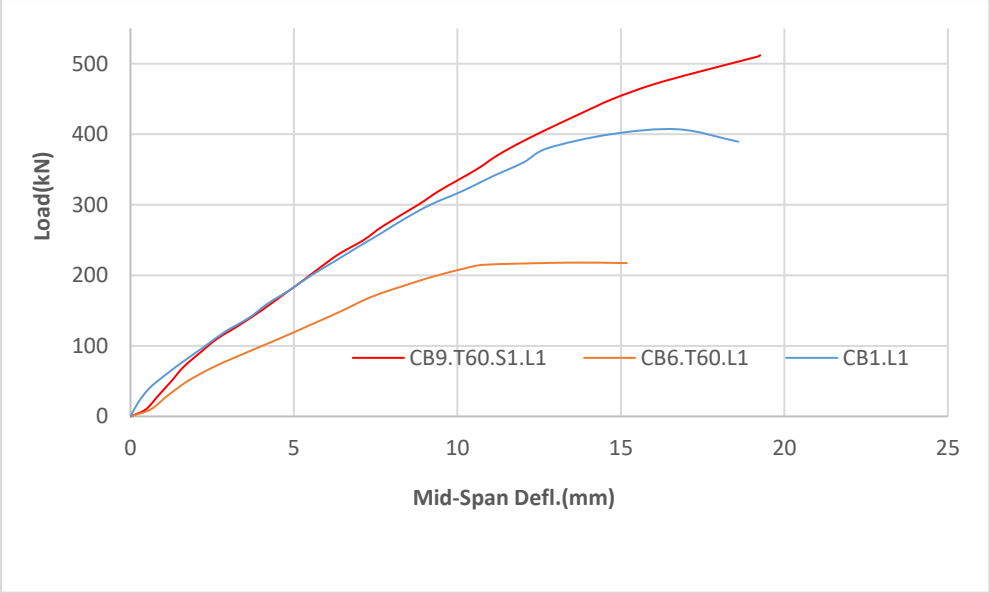

Figure (4.21) Load-Midspan Deflection Curve for Specimens (**$CB_1.L_1$**, **$CB_6.T60.L_1$** and **$CB_9.T60.S_1.L_1$**)

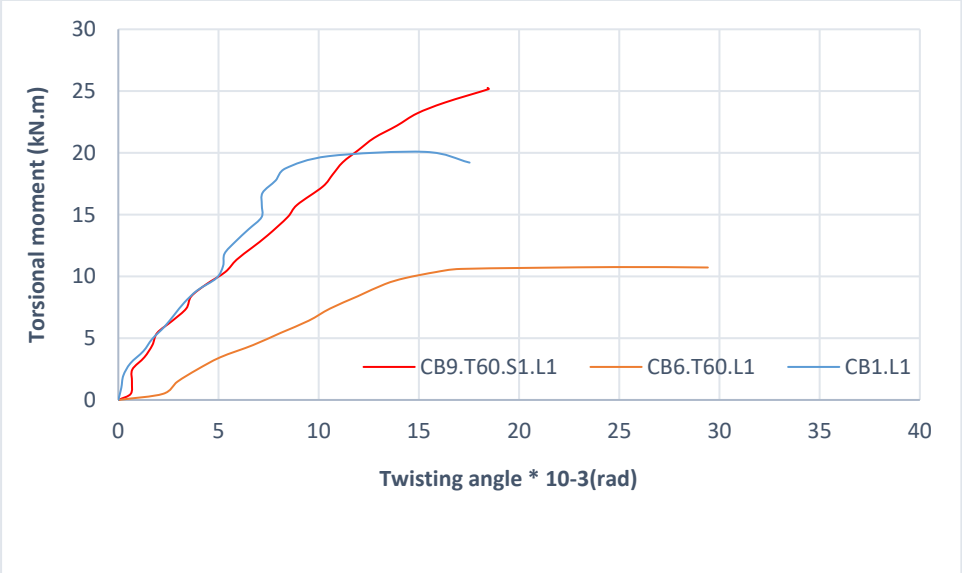

Figure (4.22) Torsional moment-Midspan Twisting Angle Curve for Specimens (**$CB_1.L_1$**, **$CB_6.T60.L_1$** and **$CB_9.T60.S_1.L_1$**)

Plate (4.21) Specimen **$CB_9.T60.S_1.L_1$**

Plate (4.22) Mode of Failure and Cracks Pattern for Specimen **$CB_9.T60.S_1.L_1$**

Specimen $CB_{11}.T60.S_2.L_1$

The circular beam $CB_{11}.T60.S_2.L_1$ beam includes transverse opening positioned exactly at angle 60° measured from exterior support to the center of opening (in zone between the applied loads and internal support) and strengthened using 0.17mm thickness of U wrap of EBR-CFRP laminates with 100 mm width at both side of the opening and U wrap of 120 mm width for upper and lower chords of opening, as shown in Plate 4.23. As usual, this circular beam was loaded incrementally until the flexural first crack was noticed at 60 kN at maximum negative moment zone above interior support. Also, the inclined crack was observed at top corner toward the point of loading of the transverse opening because of stresses concentration at this corner at a load of 70 kN, while flexural crack at maximum positive moment zone at midspan was initiated at load of 80 kN. While the load reaching of 110 kN, oblique torsional-shear cracks started to appear at zones between the applied load and the interior support. Through further increased in the loading, numerous flexural, torsional and skew corners were propagated (increase in number, length and width). It should be noted that corner cracks at the opening and torsional-shear cracks did not propagate when reaching the CFRP laminates and prevent its extension through until failure occurs because of the confinements of CFRP laminates. Figures 4.23 and 4.24 displays midspan load-deflection and torsional moment -angle of twisting curves, respectively. Finally, beam type failure happened due to torsional moment which cause deboning of CFRP laminates at load of 301.54 kN, as shown in plate 4.24. It can be concluded, that the ultimate load capacity for $CB_{11}.T60.S_2.L_1$ beam still less than that for control Specimen $CB_1.L_1$ by about 25.9%, while an increase was noticed about 38.3% as a comparison with Specimen $CB_6.T60.L_1$.

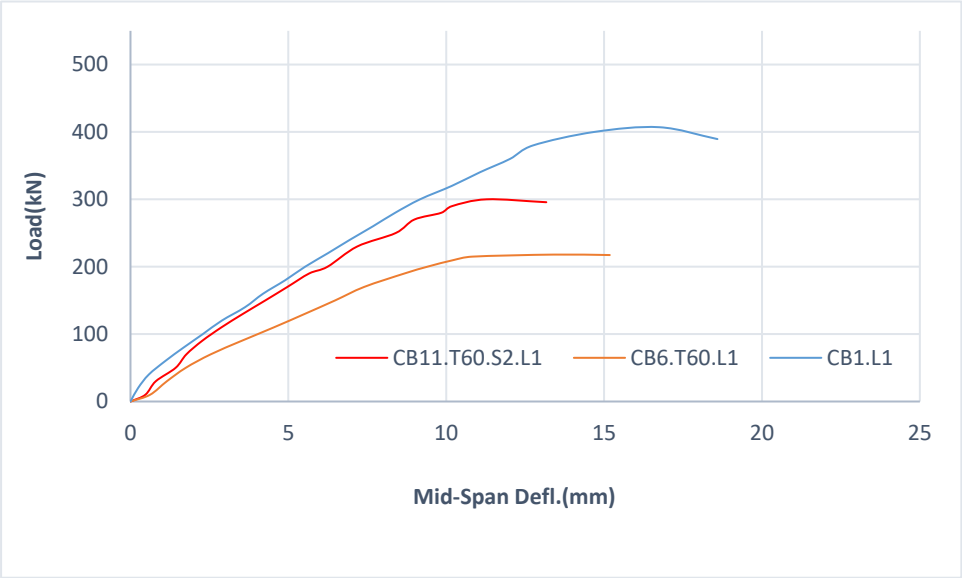

Figure (4.23) Load-Midspan Deflection Curve for Specimens (**$CB_1.L_1$**, **$CB_6.T60.L_1$**and **$CB_{11}.T60.S_2.L_1$**)

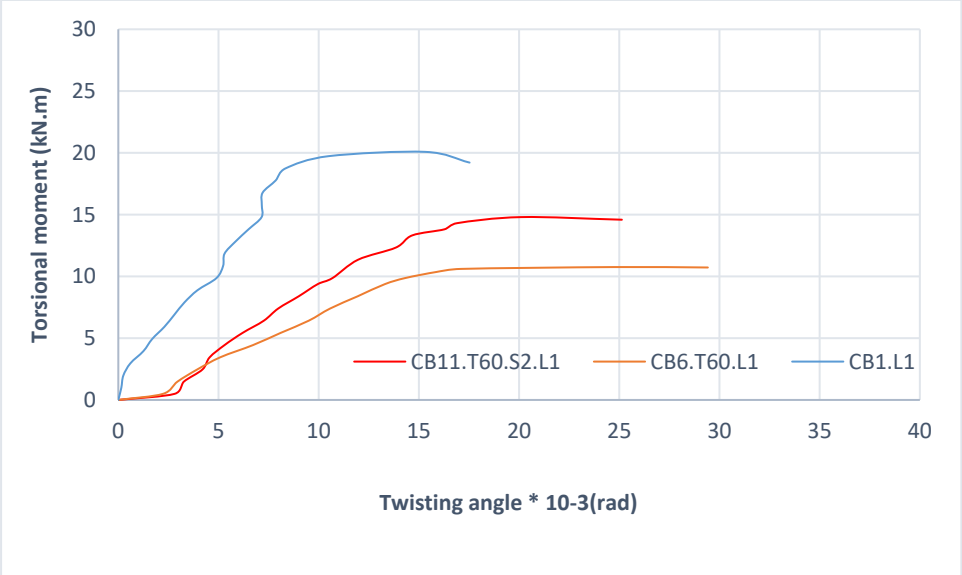

Figure (4.24) Torsional moment-Midspan Twisting Angle Curve for Specimens (**$CB_1.L_1$**, **$CB_6.T60.L_1$** and **$CB_{11}.T60.S_2.L_1$**)

Plate (4.23) Specimen **$CB_{11}.T60.S_2.L_1$**

Plate (4.24) Mode of Failure and Cracks Pattern for Specimen **$CB_{11}.T60.S_2.L_1$**

4.3.6 Third Test Group (CBs with Transverse Openings Under Cyclic Loading)

In this test group, three test specimens were manufactured of circular curved box beams with Transverse opening unstrengthening or strengthened by RPC or EBR-CFRP laminates and tested under repeated loading.

Specimen $CB_{13}.T60.L_2$

The $CB_{13}.T60.L_2$ beam includes transverse opening positioned exactly at angle 60° measured from exterior support to the center of opening (in zone between the applied loads and internal support) and without strengthening, as shown in Plate 4.25. First flexural cracking of this circular beam that subjected to cyclic loading, was formed in the top face of maximum negative moment (internal support) within the first cycle at load of 50 kN, while an opposite corner (beam type) of the transverse opening were observed within the third cycle at a load of 55 kN. After increasing the load to 65 kN in the fourth cycle, the flexural crack was noticed at bottom face of midspan of beam where region of maximum positive moment, but Torsional-shear cracks appeared at a load of 75 kN within the same cycle. As the load continues to rise through repeated loading (loading – unloading), several flexural and torsional-shear cracks were noticed, as a further progress in the frequency of cycles within the same level of load, a slight increase in the length and width of some cracks were observed. Finally, rapid propagation of diagonal cracks at the corners of transverse opening caused a frame type failure mode at opening zone. Figures 4.25 and 4.26 display midspan load-deflection and torsional moment -angle of twisting curves, respectively. Plate 4.26 shows mode of failure at ultimate

load of 239 KN in addition to pattern of crack, caused a reduction in the ultimate load capacity compared with control beam $CB_{12}.L_2$ about 43.26%

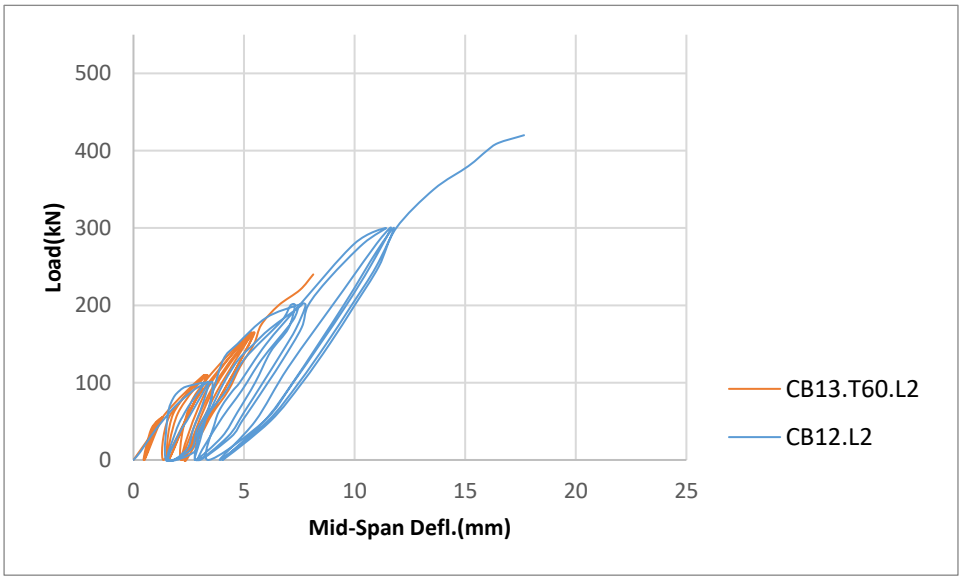

Figure (4.25) Load-Midspan Deflection Curve for Specimens (**$CB_{12}.L_2$** and **$CB_{13}.T60.L_2$)**

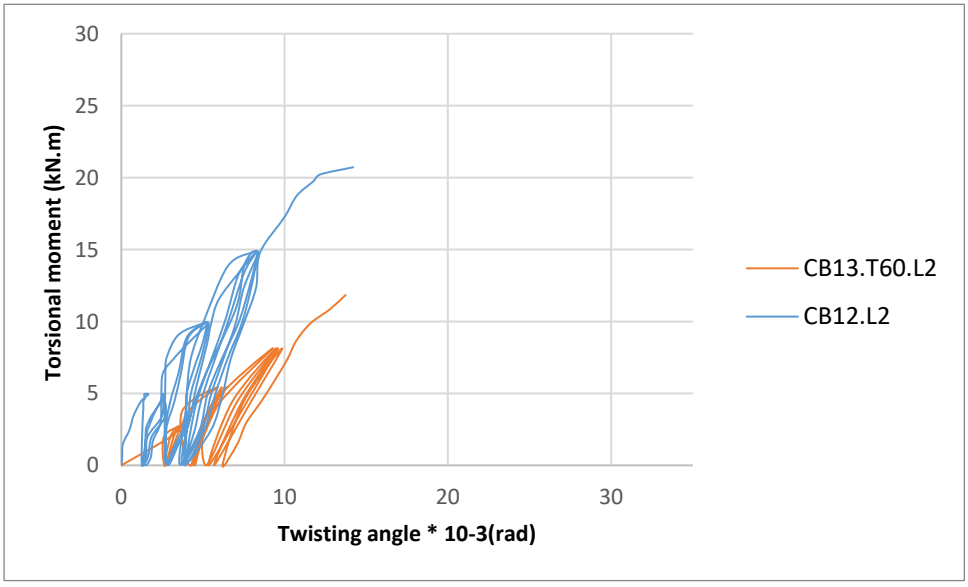

Figure (4.26) Torsional moment-Midspan Twisting Angle Curve for Specimens (**$CB_{12}.L_2$** and **$CB_{13}.T60.L_2$)**

Plate (4.25) Specimen **$CB_{13}.T60.L_2$**

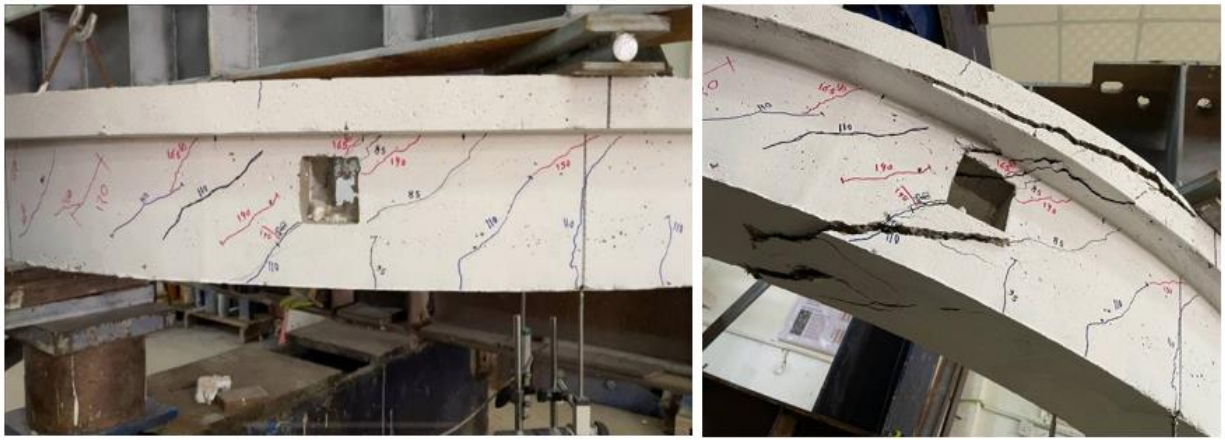

Plate (4.26) Mode of Failure and Cracks Pattern for Specimen **$CB_{13}.T60.L_2$**

Specimen $CB_{14}.T60.S_1.L_2$

The $CB_{14}.T60.S_1.L_2$ beam includes transverse openings positioned exactly at angle 60° measured from exterior support to the center of opening (in zone between the applied loads and internal support) and strengthened by hybridization of concrete around opening and for the entire section of the beam, using RPC cast monolithically at a distance of 125 mm on both edges of opening , which illustrated in Plate 4.27. While the load incrementally raised within the first cycle, flexural crack was first noticed at the top face of beam above interior support where maximum negative moment with a load of around 42 kN, but at load 80 kN first cracks in RPC were observed in bottom corner of the transverse openings toward midspan. Within the first cycle, inclined torsional-shear cracks starting occur at the region between the concentrated load and the middle support with a load of 110 kN, also this level of load first flexural crack was initiated at maximum positive moment under applied load. As load increased further in next cycles, inclined crack was observed in the opposite top corner toward point of loading of the transverse opening, also many torsional-shear cracks were propagated in and out of RPC zones. Increasing in length, number and width of flexural and torsional-shear cracks were noticed as load as increase, while cracks in RPC zones maintain its fine width (no considerable propagation) until failure due to high strength and ductility of RPC. Finally, at ultimate load which reached 508 kN within end cycle, the beam was failed due to maximum shear at interior support. An increase observed by about 20.6% and 112.55% when compared to the specimens $CB_{12}.L_2$ and $CB_{13}.T60.L_2$ respectively. Figures 4.27 and 4.28 illustrate midspan load-deflection and Torsional moment -angle of twisting curves, respectively. Plate 4.28, display failure mode and patterns of crack.

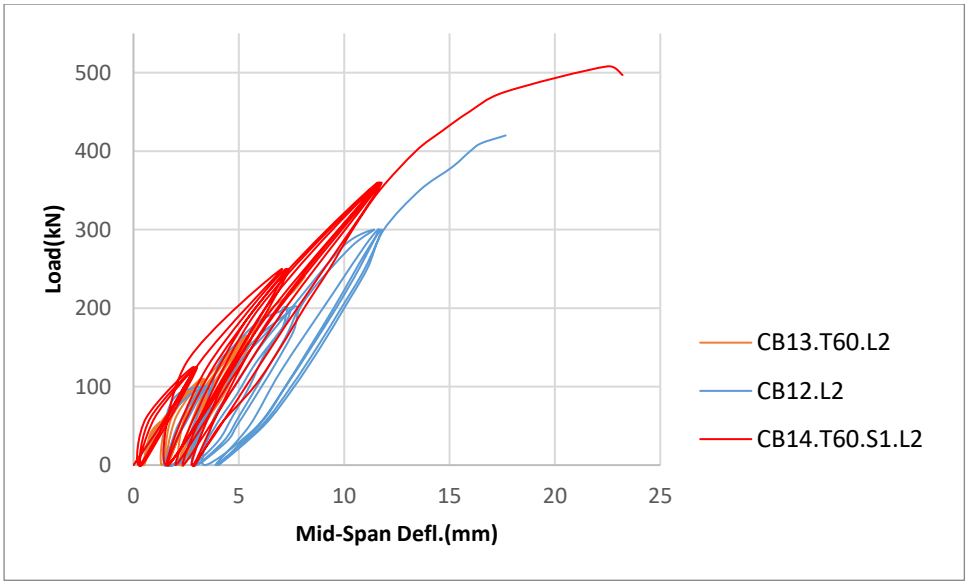

Figure (4.27) Load-Midspan Deflection Curve for Specimens (**$CB_{12}.L_2$, $CB_{13}.T60.L_2$** and **$CB_{14}.T60.S_1.L_2$**)

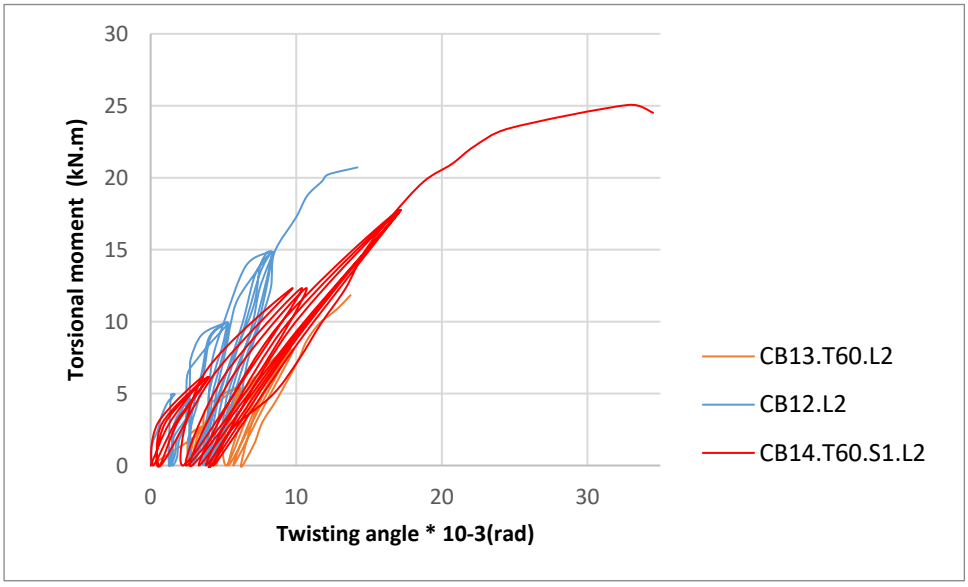

Figure (4.28) Torsional moment-Midspan Twisting Angle Curve for Specimens (**$CB_{12}.L_2$, $CB_{13}.T60.L_2$** and **$CB_{14}.T60.S_1.L_2$**)

Plate (4.27) Specimen **$CB_{14}.T60.S_1.L_2$**

Plate (4.28) Mode of Failure and Cracks Pattern for Specimen **$CB_{14}.T60.S_1.L_2$**

Specimen $CB_{15}.T60.S_2.L_2$

The circular beam $CB_{15}.T60.S_2.L_2$ beam includes transverse opening positioned exactly at angle 60° measured from exterior support to the center of opening (in zone between the applied loads and internal support) and strengthened utilizing 0.17mm thickness of U wrap of CFRP laminates with 100 mm width on both sides of the opening and U wrap of 120 mm width for upper and lower chords at opening region, as shown in Plate 4.29. This beam subjected to repeated loading and loaded gradually within first cycle up to initiating of the flexural crack through load of 50 kN at zone above middle support. Within first cycle inclined crack was observed in the top corner toward point of loading of the transverse opening because of concentration of stresses at this corner at 60 kN of load level, while crack due to flexure at zone of midspan where maximum of positive moment was initiated at load of 75 kN. In the fourth cycle and at a load of about 100 kN, torsional-shear cracks began to appear at zones between the mid support and concentrated load. As the repeated loading continued, several flexural, torsional and skew corners were propagated (increase in number, length and width), also it should be noted that corner cracks at the opening and torsional-shear cracks did not propagate when extends to CFRP laminates which restrict its extension through until failure takes place because of the confinements of CFRP laminates. Figures (4.29) and (4.30) present midspan load-deflection and Torsional moment -angle of twisting curves, respectively. Finally, frame type failure was happening because of the torsional moment which cause deboning of CFRP laminates within the last cycle at a load of 287.3 kN, as shown in plate (4.30). It can be concluded, that the ultimate load capacity for $CB_{15}.T60.S_2.L_2$ beam still less than that for control specimen $CB_{12}.L_2$ by about 31.8%, while an increase was about 20.2% as a comparison with specimen $CB_{13}.T60.L_2$.

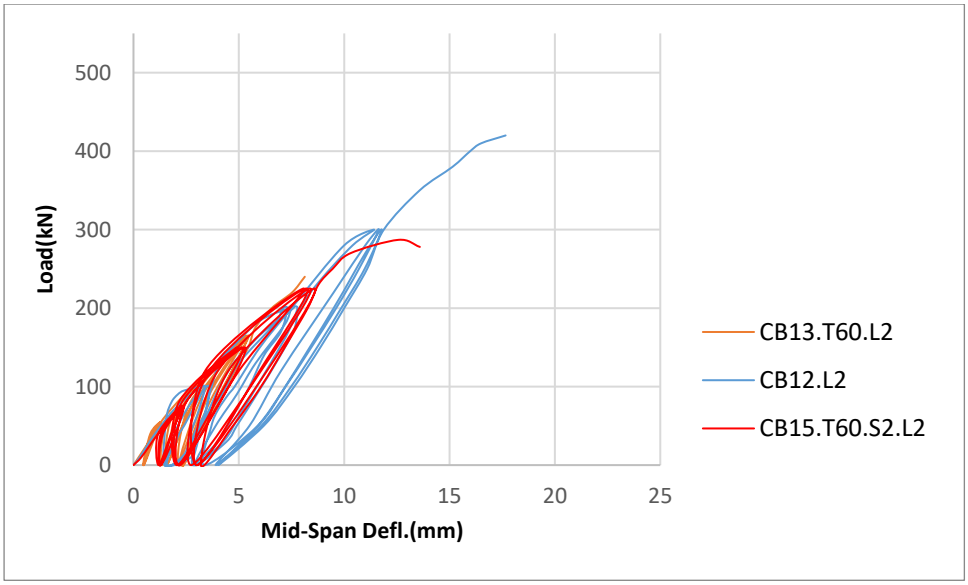

Figure (4.29) Load-Midspan Deflection Curve for Specimens (**$CB_{12}.L_2$, $CB_{13}.T60.L_2$** and **$CB_{15}.T60.S_2.L_2$**)

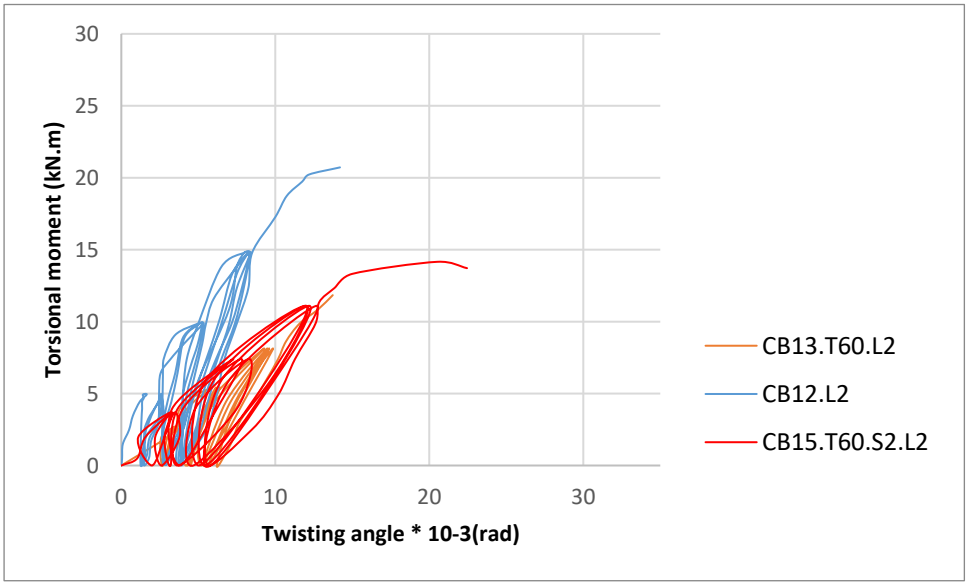

Figure (4.30) Torsional moment-Midspan Twisting Angle Curve for Specimens (**$CB_{12}.L_2$, $CB_{13}.T60.L_2$** and **$CB_{15}.T60.S_2.L_2$**)

Plate (4.29) Specimen **$CB_{15}.T60.S_2.L_2$**

Plate (4.30) Mode of Failure and Cracks Pattern for Specimen **$CB_{15}.T60.S_2.L_2$**

4.4 Effect of Considered Variables on Structural Response

4.4.1 Cracking Load and Cracking Pattern

As a summary of the experimental results, the first cracking loads of flexural, torsional-shear and corners of opening cracks, Table 4.2 shows the percentage of decrease or increase for all of the examined CB specimens compared to the control specimens.

In general, the circular beams with vertical opening and without strengthning under monotonic load ($CB_2.V37.L_1$, $CB_3.V60.L_1$and $CB_4.V82.L_1$) exhibited a decrease in first cracking load for flexural and torsional-shear by an average (20)% and (0-30%) compared to the control $CB_1.L_1$, respectively, due to presence of openings which caused a reduction of beam stiffness. While, those beams with strengthning around vertical opening under monotonic load ($CB_8.V60.S_1.L_1$and $CB_{10}.V60.S_2.L_1$) showed an improvement in the flexural cracking load with 18% and 20% respectively, and for torsional-shear by about 20% and 10% respectively, compared to the control $CB_1.L_1$, also an increase was observed in first cracking load at corner of opening for $CB_8.V60.S_1.L_1$and $CB_{10}.V60.S_2.L_1$ by about 110% and 60%, respectively compared to the $CB_3.V60.L_1$.

The circular beams with unstrengthened transverse opening under monotonic load ($CB_5.T37.L_1$ and $CB_6.T60.L_1$) exhibited a reduction in first cracking load for flexural and torsional-shear by an average (0-22)% and (0-25%) compared to the control $CB_1.L_1$,while no reduction was noticed in cracking load of torsional-shear for specimen $CB_7.T82.L_1$. The strengthened circular beams with transverse opening under monotonic load (CB9.T60.S1.L1and CB11.T60.S2.L1) showed an improvement in the cracking load of flexural with 18% and 20% respectively, and for torsional-shear by about 20% and 10% respectively, compared to the control $CB_1.L_1$.

As a first cracking load of corner of opening, strengthened specimens

Table 4.2 Cracking Load, Ultimate Load and Failure Modes of the of Tested CB Beams

CB Designation	**Cracking Load, kN**			$\frac{P_{cr\,(i)} - P_{cr(r)}}{P_{cr(r)}} \times 100\%$		$\frac{P_{cr\,(i)} - P_{cr(r1)}}{P_{cr(r1)}} \times 100\%$	**Ultimate Load, kN**	$\frac{P_{u\,(i)} - P_{u(r)}}{P_{u(r)}} \times 100\%$ $\frac{P_{u\,(i)} - P_{u(r1)}}{P_{u(r1)}} \times 100\%$	**Mode of Failure**
	Flex.	**Tor.**	**Corner**	**Flex.**	**Tor.**	**Corner**			
$CB_1.L_1$	50	100	---	---	---	---	407.25	--- ---	torsional-shear at 60°
$CB_2.V37.L_1$	40	70	50	-20	-30	---	385.74	-5 ---	torsional-shear at 60°
$CB_3.V60.L_1$	40	80	90	-20	-20	---	360.3	-11.5 ---	frame type at opening
$CB_4.V82.L_1$	40	100	60	-20	0	---	400.55	-1.5 ---	torsional-shear at 60°
$CB_8.V60.S_1.L_1$	59	120	190	18	20	110	427	4.8 18.5	flexural at mid-span
$CB_{10}.V60.S_2.L_1$	60	110	150	20	10	60	415.56	2 15.3	frame type at opening
$CB_5.T37.L_1$	39	75	85	-22	-25	---	401	-1.5 ---	torsional-shear
$CB_6.T60.L_1$	50	80	50	0	-20	---	218	-46.5 ---	frame type at opening
$CB_7.T82.L_1$	58	140	80	16	40	---	331.48	-18.6 ---	frame type at opening

Table 4.2 continue

$CB_9.T60.S_1.L_1$	65	120	90	18	20	80	512.65	25.9 135	flexural at mid-span
$CB_{11}.T60.S_2.L_1$	60	110	70	20	10	40	301.54	-26 38.3	frame type at opening
$CB_{12}.L_2$	40	90	---	---	---	---	421.2	--- ---	torsional-shear at 60°
$CB_{13}.T60.L_2$	50	75	55	25	-17	---	239	-43.25 ---	frame type at opening
$CB_{14}.T60.S_1.L_2$	42	110	80	5	22	45.4	508	20.6 112.6	shear at interior support
$CB_{15}.T60.S_2.L_2$	50	100	60	25	11	9	287.3	-31.79 20.2	frame type at opening

i :-Considered CB, r :- Control $CB_1.L_1$ or $CB_{12}.L_2$

r1:- $CB_3.V60.L_1$ or CB6.T60.L1 or $CB_{13}.T60.L_2$

$CB_9.T60.S_1.L_1$and $CB_{11}.T60.S_2.L_1$ showed a clear increase by about 80% and 40%, respectively compared to the $CB_6.T60.L_1$.

The cracking load for unstrengthened circular beam specimen under repeated loading $CB_{13}.T60.L_2$ was decreased especially torsional-shear by about17% compared to the control specimen $CB_{12}.L_2$, while the strengthened specimens ($CB_{14}.T60.S_1.L_2$ and $CB_{15}.T60.S_2.L_2$) exhibits a rise in the cracking load of flexural with 5% and 25% respectively, and for torsional-shear by about 22% and 11% respectively, compared to the control $CB_{12}.L_2$, also an increase in the first cracking load of corner of opening by about 45.4% and 9% respectively, as result of enhanced flexural rigidity of beams.

4.4.2 Ultimate Strength and Failure Modes

The following paragraphs, summarized a comparison of ultimate load capacity for all test specimens which listed in Table 4.2.

In Group I, the circular beams without strengthening and with vertical opening under effect of monotonic load ($CB_2.V37.L_1$, $CB_3.V60.L_1$and $CB_4.V82.L_1$) indicated a reduction in ultimate load capacity by about (5%, 11.5% and 1.5%) compared to the control CB1.L1, respectively. While, the strengthened circular beams with vertical opening under monotonic load ($CB_8.V60.S_1.L_1$and $CB_{10}.V60.S_2.L_1$) noticed an increase in ultimate load capacity by about (4.8% and 2%) compared to the control $CB_1.L_1$and about (18.5% and 15.3%) when compared to the $CB_3.V60.L_1$, respectively.

In Group II, the unstrengthened circular beams with transverse opening under monotonic load ($CB_5.T37.L_1$, $CB_6.T60.L_1$and $CB_7.T82.L_1$) exhibited an decrease in ultimate load capacity by about (1.5%, 46.5% and 18.6%) compared to the control $CB_1.L_1$, respectively. While, the strengthened circular beam with transverse opening under monotonic load ($CB_9.T60.S_1.L_1$) showing a rise in the capacity of ultimate load by roughly 25.9%, the strengthened specimen($CB_{11}.T60.S_2.L_1$) showed a reduction by about 26% compared to the control $CB_1.L_1$ .But, when compared the ultimate load capacity of strengthened specimens $CB_9.T60.S_1.L_1$and $CB_{11}.T60.S_2.L_1$ to the unstrengthened specimen $CB_6.T60.L_1$, an increase achieved was about (135% and 38.3%), respectively.

In Group III, the circular beam without strengthening and with transverse opening under effect of cyclic load $CB_{13}.T60.L_2$ exhibited a reduction in ultimate load by by nearly 43.25% as a comparison to the control beam under cyclic loading $CB_{12}.L_2$. The strengthened circular beam with transverse opening under cyclic load $CB_{14}.T60.S_1.L_2$ exhibits an increase in ultimate load capacity by about 20.6% compared to the control $CB_{12}.L_2$, while the strengthened specimen $CB_{15}.T60.S_2.L_2$ showed a reduction about

31.79%. On the other hand, when compared the ultimate load capacity of strengthened specimens ($CB_{14}.T60.S_1.L_2$ and $CB_{15}.T60.S_2.L_2$) to the specimen $CB_{13}.T60.L_2$, an increase achieved was about (112.6% and 20.2%) respectively.

From the above paragraphs and Table 4.2, it can be concluded that the RPC Hybridization technique achieved greater improvement compared to EBR-CFRP laminate technique.

4.4.3 Deformation Response

In this experimental work, deformations represent a deflection and twisting at midspan of the circular beams. Deformations response of circular beams could be described by the load-midspan deflection relationships as well as torsional moment- midspan twisting relationships at service loads (approximately 65% of maximum load).

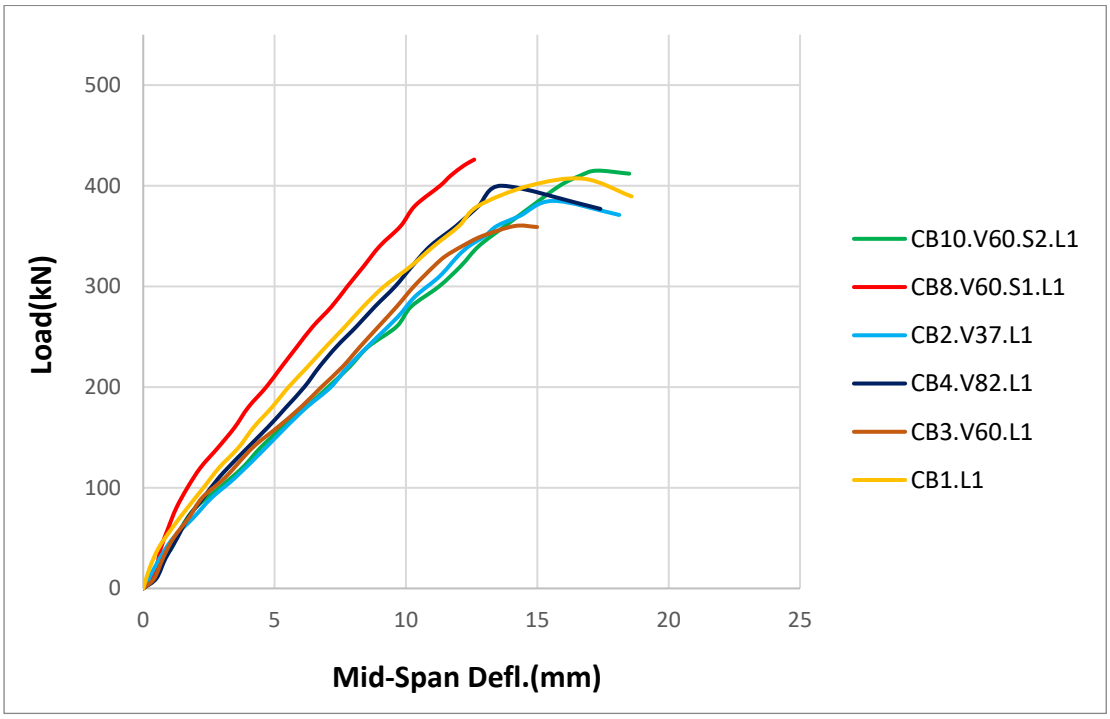

Figure (4.31) Load-Midspan Deflection Response for CBs of Group I

In this section, the load-midspan deflection curves of CBs specimens subjected to monotonic load were showed and compared to each other within the test groups. Furthermoe, the service defelection, twisting and

their contrast percentages compared with the reference specimens listed in Table 4.3. Figures 4.31-4.34 represent the load-midspan deflection and torsional moment- midspan twisting response of test group, they were as follows:

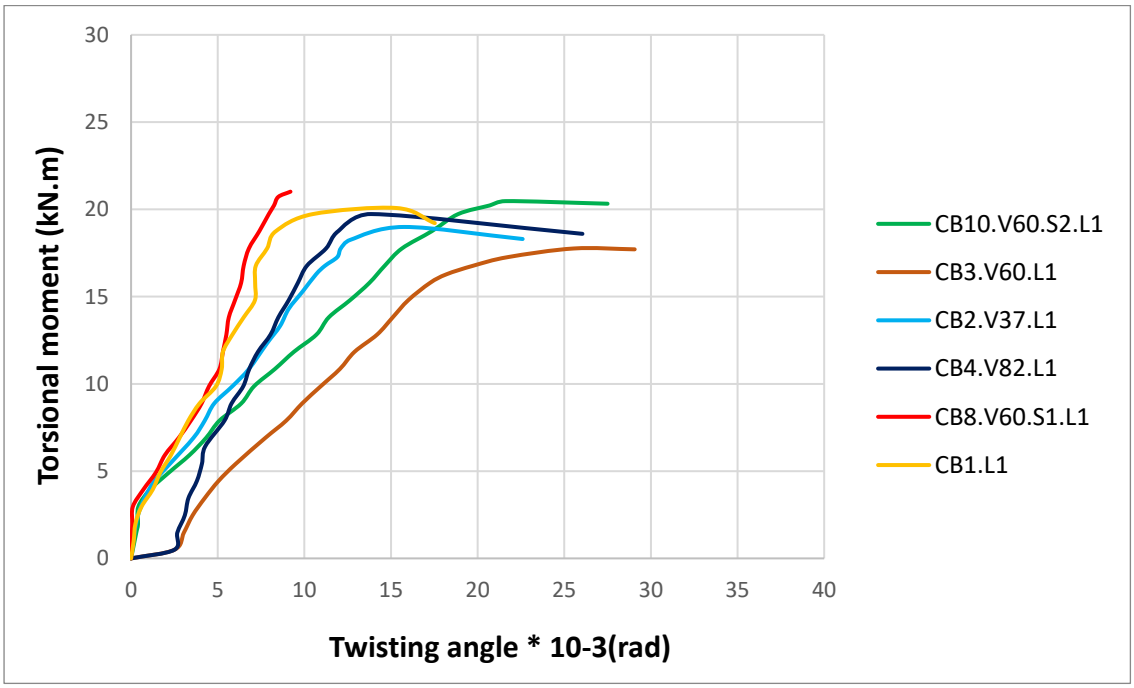

Figure (4.32) Torsional moment-Midspan Twisting Angle Response for CBs of Group I

For circular beams CBs (Group I), the specimens without strengthening ($CB_2.V37.L_1$, $CB_3.V60.L_1$and $CB_4.V82.L_1$) showed a clear increase in service midspan deflection and midspan twisting with a range (5-20.63) % and (35-140.65) % respectively, noticed that this increase corresponding to the reduction in fluxtural rigidity and torsional rigidity compared to control CB.

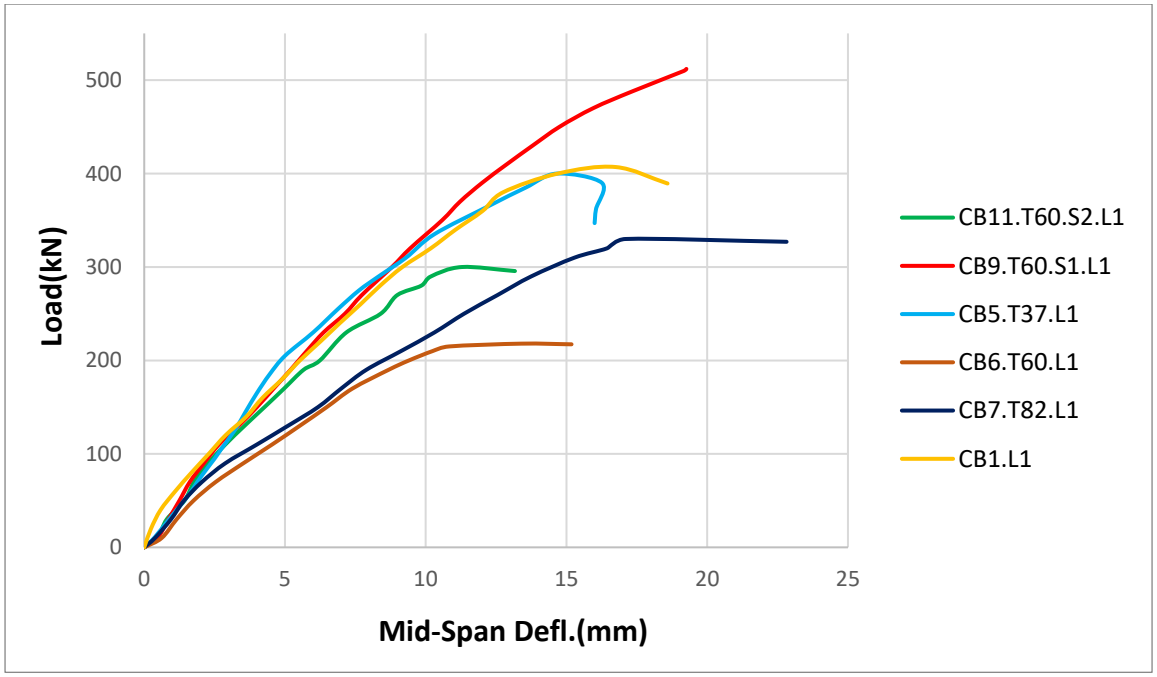

Figure (4.33) Load-Midspan Deflection Response for CBs of Group II

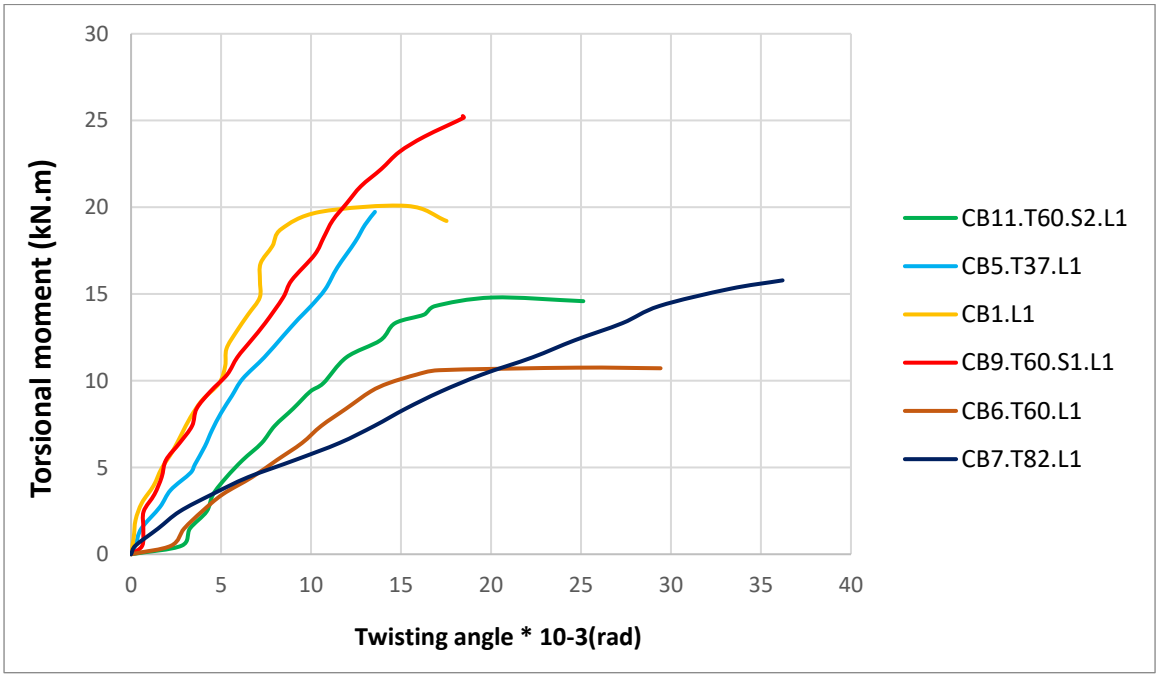

Figure (4.34) Torsional moment-Midspan Twisting Angle Response for CBs of Group II

The strengthened specimen $CB_8.V60.S_1.L1$by using RPC hybridization technique, exhibited a reduction in service midspan deflection 15.63% and

service midspan twisting decreased by about 8.13%, because high strength and toughness of RPC compensated the lost fluxtural and torsional rigidity due to presence of opening, and also restricting formation of early cracks around opening. While the strengthened specimen $CB_{10}.V60.S_2.L_1$ by using CFRP laminate technique, showed an increase in service midspan deflection and midspan twisting by about 21.9% and 75.6% respectively,this was corresponding to an increase in ultimate load capacity of the mentioned specimen compared with the control $CB_1.L_1$, as shown in table 4.3.

Table (4.3) Service Deformations of Tested CBs.

CB Designation		**Service Deflection, Δs (mm)***	$\frac{\Delta s_i - \Delta s_r}{\Delta s_r} \times 100\%^{(**)}$	**Service Twisting, θs (Radian)$\times 10^{-3}$**	$\frac{\theta s_i - \theta s_r}{\theta s_r} \times 100\%^{(**)}$
$CB_1.L_1$		8	---	6.15	---
Group I	$CB_2.V37.L_1$	9.65	20.63	8.4	36.6
	$CB_3.V60.L_1$	9.1	13.75	14.8	140.65
	$CB_4.V82.L_1$	8.4	5	8.3	35
	$CB_8.V60.S_1.L_1$	6.75	-15.63	5.65	-8.13
	$CB_{10}.V60.S_2.L_1$	9.75	21.9	10.80	75.6
Group II	$CB_5.T37.L_1$	7.9	0	9	46.34
	$CB_6.T60.L_1$	***	---	***	---
	$CB_7.T82.L_1$	12.55	56.88	26.8	335.77
	$CB_9.T60.S_1.L1$	7.5	-6.25	7.1	15.44
	$CB_{11}.T60.S_2.L_1$	8.95	11.88	14.2	130.9

* (Pser.=0.65 $P_{ult.}$) **(Jeffrey, 2003)**

** Δs_r= Service deflection of the control CB,
Δs_i=Service deflection of the considered CB

*** Ultimate load less than the serverse load of control $CB_1.L_1$

For CBs (Group II), the unstrengthen specimens $CB_5.T37.L_1$ and $CB_7.T82.L_1$ showed an increase in service midspan deflection and midspan

twisting with a range (0 -56.88) % and (9-26.8) % respectively, compared to the control $CB_1.L_1$. The unstrengthen specimen $CB_6.T60.L_1$ failed at a load lower that the service load of control specimen $CB_1.L_1$. The strengthened specimen $CB_9.T60.S_1.L_1$ (using RPC hybridization technique), exhibited a decrease by about 6.25% in service midspan deflection and an increase in midspan twisting 15.44 % due to effect of RPC which led to considerable increase in ultimate load capacity compared with the control $CB_1.L_1$. While the strengthened specimen $CB_{11}.T60.S_2.L_1$ (using CFRP laminate technique), showed an increase in service midspan deflection and midspan twisting by about 11.88 % and 130.9% respectively, compared with the control $CB_1.L_1$.

4.4.4 Ductility

Ductility can be defined as the ability to sustain inelastaic deformations without lossing of the load carrying capacity prior to failure. The present study examines ductility parameters by dividing vertical displacement at maximum load by vertical displacement at service load (approximately 65 percent of maximum load) **(Jeffrey,2003)**. As shown in Table 4.4, the presence of openings led to a reduction in the ductility of all restored and without restoring CBs specimens under monotonic loading.

Figure 4.35 compared the cumulative ductility values for all specimens that tested under the effect of repeated load. Since accumulated ductility up to any point of load is defined as the summation of ductility at maximum load level achieved in each cycle until the cycle in consideration, **(Muthuswamy & Thirugnanam, 2014)**.

Table (4.4) Ductility Factor of Tested CBs under Monotonic Loading.

CB Designation		Service Deflection, Δs (mm)*	Ultimate Deflection, Δu (mm)	Ductility Factor, μ ($\frac{\Delta u}{\Delta s}$)	$\frac{\mu_i - \mu_r}{\mu_r} * 100\%^{(**)}$
CB1.L1		8	16.75	2.09	---
Group I	CB2.V37.L1	8.66	15.6	1.8	-13.88
	CB3.V60.L1	8	14.14	1.77	-15.3
	CB4.V82.L1	8.11	13.65	1.68	-19.62
	CB8.V60.S1.L1	6.94	12.6	1.82	-12.92
	CB10.V60.S2.L1	9.85	17.25	1.75	-16.27
Group II	CB5.T37.L1	7.06	14.66	2.08	-0.5
	CB6.T60.L1	6.43	13.4	2.08	-0.5
	CB7.T82.L1	9.45	17.1	1.8	-13.88
	CB9.T60.S1.L1	9.86	19.26	1.95	-6.7
	CB11.T60.S2.L1	5.88	11.28	1.91	-8.6

* (Pser.=0.65 Pult.) **(Jeffrey, 2003)**

** μ_r= Ductility of the control CB

μ_i =Ductility of the considered CB

Cumulative ductility values for unstrengthened specimen $CB_{13}.T60.L_2$ increased about 2.2% compared with the control $CB_{12}.L_2$. While, for the strengthened specimens $CB_{14}.T60.S_1.L_2$ and $CB_{15}.T60.S_2.L_2$, the cumulative ductility were 10.2% and1.1% more than the control $CB_{12}.L_2$, respectively.

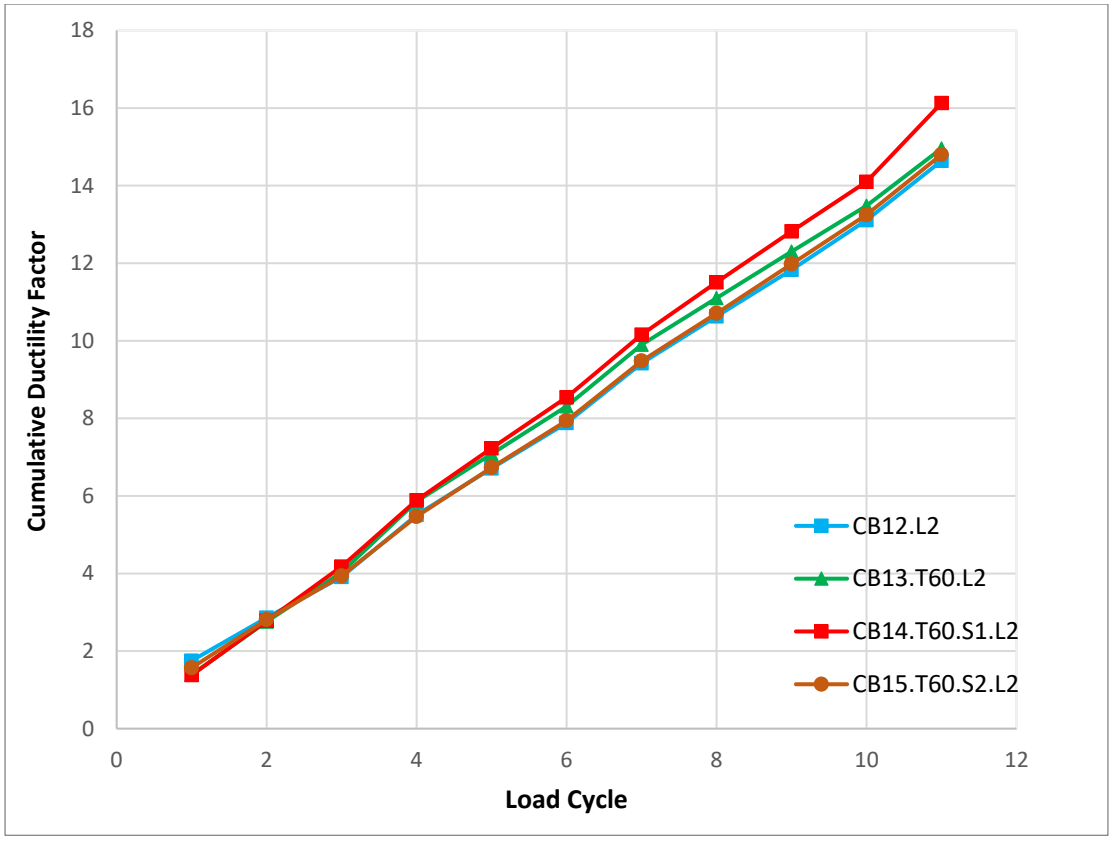

Figure (4.35) Variation of Cumulative Ductility Factor of Specimens of Group III

During the final stages of loading, the cumulative ductility value of the CB with RPC hybridization technique was higher than those of other CBs due to high ductility of reactive powder concrete, but the CB with CFRP laminate technique was very close to that of control $CB_{12}.L_2$ due to debonding of CFRP laminate.

4.4.5 Energy Absorption

When the specimen is subjected to repeated load, a certain amount of energy is taken in each cycle of load that is roughly equivalent to the work involved in straining or deforming the structure to the limit of deflection. The energy absorption amount was determined as the area under the hysteresis loop of the load-deflection diagrams **(Rajaram et al., 2010)**. The cumulative energy absorbed of the circular box beam was acquired by

adding the energy absorption amount of the beam during each cycle considered **(Muthuswamy & Thirugnanam, 2014)**.

The cumulative energy absorption values for the unstrengthened specimen $CB_{13}.T60.L_2$ decreased by about 74.8% compared with the control $CB_{12}.L_2$, due to presence of transverse opening. On the other hand, the cumulative energy absorption values for the strengthened specimens $CB_{14}.T60.S_1.L_2$ and $CB_{15}.T60.S_2.L_2$ it raised by about 28.8% for the first specimen and decreased about 48.44% for the other compared to the control $CB_{12}.L_2$, but when compared the same strengthened specimens to the unstrengthened circular beam $CB_{13}.T60.L_2$ an increase were achieved which approximately 411% and 104%, respectively.

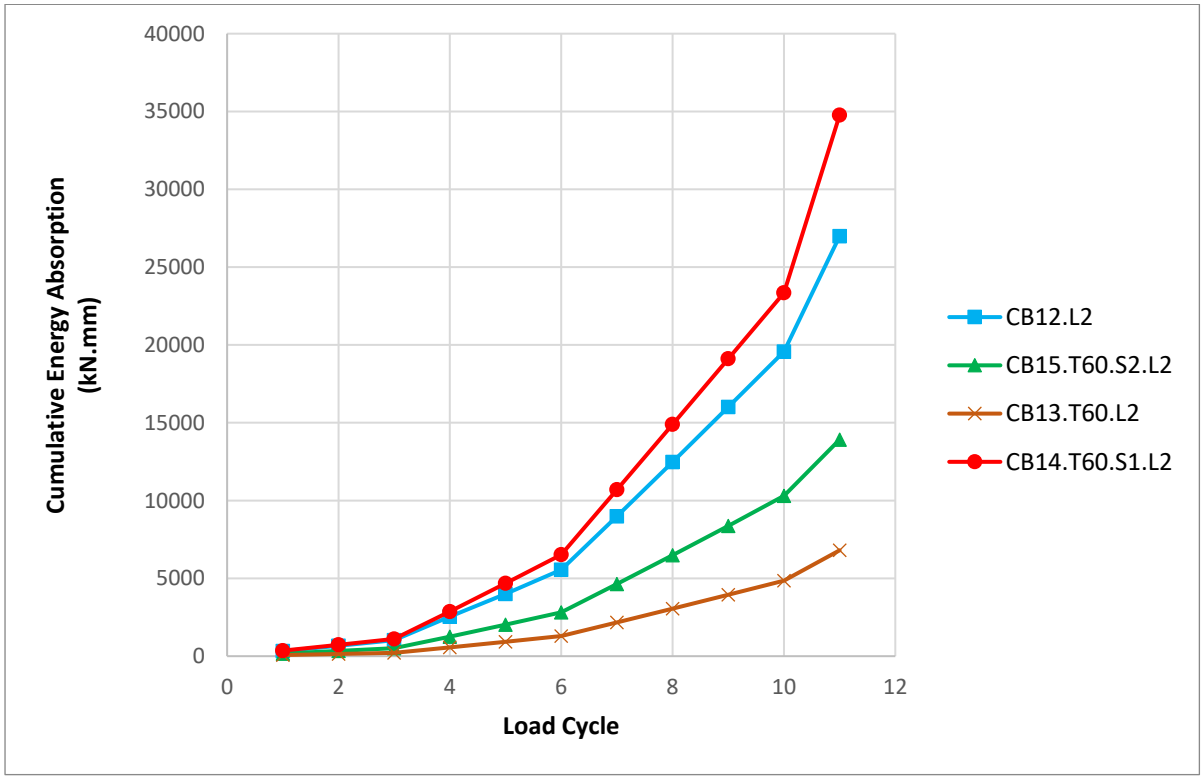

Figure (4.36) Variation of Cumulative Energy Absorption of Specimens of Group III

Figures 4.36 and 4.37 are used to compare the cumulative energy absorption capacity correspond to number of cycles for all the circular beams that tested under effect of cyclic load.

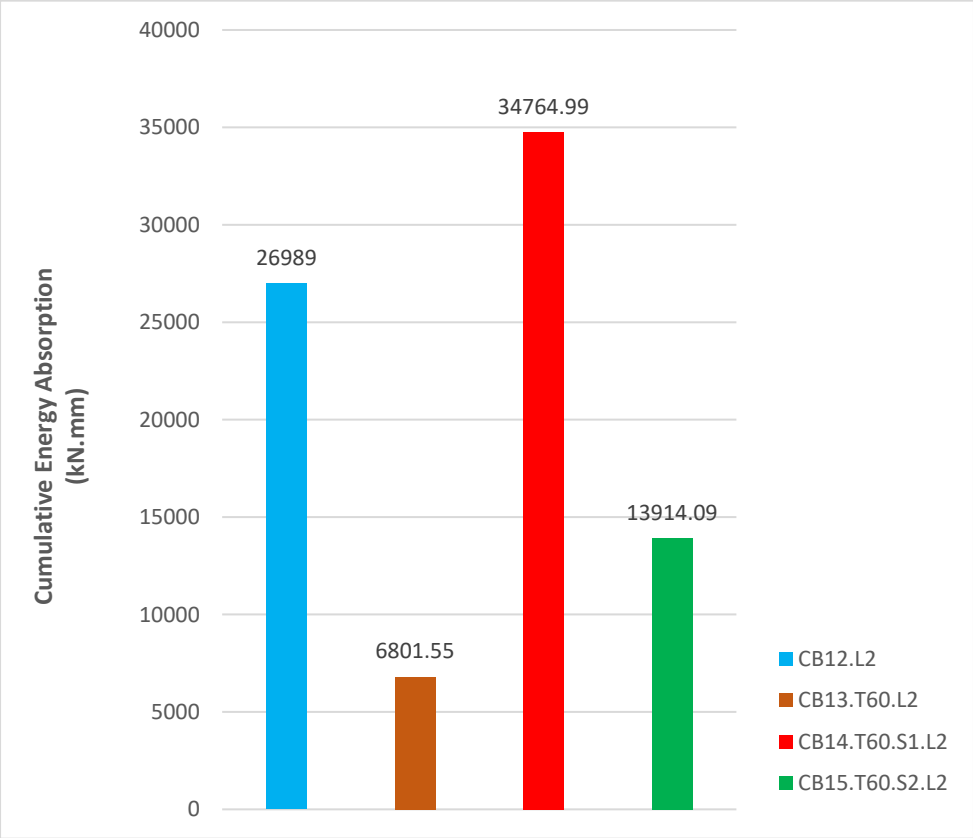

Figure (4.37) Comparison of Cumulative Energy Absorption of Specimens of Group III

The circular box beams do not dissipate much energy in the first three cycles, as can be shown. The specimens, on the other hand, exhibit a high dissipation energy in the final cycles, because greater peak loads create an additional area (dissipated energy) limited by the load-displacement curve. It was clearly observed that, the circular box beams with RPC hybridization approach had more energy dissipation capacity than that adopted the EBR-CFRP laminate approach.

4.4.6 Stiffness Criteria

Stiffness is defined as the load required for producing unit deformation in the member. The slope of the secant drawn to each cycle in the hysterical curve at loading 0.75 times the maximum load of that cycle was measured as stiffness criteria **(Muthuswamy & Thirugnanam, 2014)**. The stiffness values for the monotonic loaded circular beams are tabulated in Table 4.5.

Table (4.5) Stiffness Criteria of Tested CBs Subjected to Monotonic Loading.

CB Designation		**0.75 Pmax* (kN)**	**Deflection at 0.75Pmax (mm)**	**Stiffness,κ (kN/mm)**	**$\frac{\kappa_i - \kappa_r}{\kappa_r} \times 100\%$****
	$CB_1.L_1$	305.44	9.37	32.6	----
Group I	$CB_2.V37.L_1$	289.3	10.35	28	-14.11
	$CB_3.V60.L_1$	270.22	9.23	29.27	-10.2
	$CB_4.V82.L_1$	300.4	9.6	31.3	-3.98
	$CB_8.V60.S_1.L_1$	320.25	8.5	37.68	15.6
	$CB_{10}.V60.S_2.L_1$	311.67	11.67	26.7	-18
Group II	$CB_5.T37.L_1$	300.75	9.03	33.3	2.14
	$CB_6.T60.L_1$	163.5	7.35	22.24	-31.78
	$CB_7.T82.L_1$	248.61	11.38	21.84	-33
	$CB_9.T60.S_1.L_1$	384.5	11.77	32.67	0.21
	$CB_{11}.T60.S_2.L_1$	226.16	7.03	32.17	-1.3

* max applied load

** κ_i= Stiffness of the considered CB

κ_r = Stiffness of the control CB

Table (4.6) Stiffness Degradation for CBs Subjected to Repeated Loading.

Cycle No.	$CB_{12}.L_2$		$CB_{13}.T60.L_2$		$CB_{14}.T60.S_1.L_2$		$CB_{15}.T60.S_2.L_2$	
	Stiffness,κ (kN/mm)	Percent of Stiffness Degradation %	Stiffness,κ (kN/mm)	Percent of Stiffness Degradation %	Stiffness,κ (kN/mm)	Percent of Stiffness Degradation %	Stiffness,κ (kN/mm)	Percent of Stiffness Degradation %
1	34.88	---	35.87	---	40	---	33.28	---
2	22	36.92	31.98	10.8	38.42	3.95	27.57	17.16
3	21	39.8	31.49	12.21	35.65	10.88	26.4	20.67
4	27.57	20.95	41.25	-15	40.23	-0.6	29.15	12.4
5	21.77	37.59	28.74	19.9	32	20	25.28	24
6	20.92	40	28.45	20.7	31	22.5	24.09	27.61
7	25.9	25.75	32.4	10.8	34.13	14.68	29.2	12.26
8	22.16	36.47	27	24.8	28.42	28.95	23.83	28.4
9	21.57	38.16	26.5	26.12	27.55	31.13	23.27	30
10	21.33	38.85	25.9	27.8	28.45	28.9	22.65	31.94
11	25.4	27.18	30.5	15	29.8	25.5	24.8	25.48
Average		34.1		15.3		18.6		22.9

As a comparison with control $CB_1.L_1$, the stiffness of CBs that without strengthening under monotonic loading showed higher stiffness degradation about (14.11%, 10.2% and 3.98%) for ($CB_2.V37.L_1$, $CB_3.V60.L_1$and $CB_4.V82.L_1$) of Group I, respectively. While a degradation was about (31.78% and 33%) for ($CB_6.T60.L_1$and $CB_7.T82.L_1$), respectively, the presence of opening at an angle (37°) for specimen $CB_5.T37.L_1$ had no effect on its stiffness compared to the control $CB_1.L_1$. While the stiffness of CBs that strengthened by utilizing RPC hybridization technique around vertical and transverse opening ($CB_8.V60.S_1.L_1$ and CB9.T60.S1.L1) was enhanced by (15.6% and 0.2%), respectively,

compared to the control $CB_1.L_1$, but when compared the above specimens to $CB_3.V60.L_1$ and $CB_6.T60.L_1$ the stiffness percent increased by approximately 28.7% and 46.9%, respectively. The stiffness of CBs strengthened by using CFRP laminate technique around vertical and transverse opening $CB_{10}.V60.S_2.L_1$ and $CB_{11}.T60.S_2.L_1$, still showed a stiffness degradation about (18% and 1.3%), respectively, compared to the control $CB_1.L_1$, while when compared to CBs ($CB_3.V60.L_1$ and $CB_6.T60.L_1$) the stiffness was less about (8.9% for the first specimen) and increased by about (44.65% for the second specimen).

During unidirectional cyclic loading, the materials, i.e. concrete and steel are subjected to loading, unloading, and reloading processes. This will cause initiation of internal micro-cracks and will sometimes lead to the fatigue limit of the materials. This, in turn, increases the deformations within the beams, subsequently leading to decrease the stiffness. Therefore, it is necessary to assess degradation of stiffness in the circular beams subjected to cyclic loading. For the unstrengthened cyclic loaded specimen $CB_{13}.T60.L_2$ the stiffness decreased slowly when the load increased, also as stiffness degradation was decreased by about 55.13% as average compared to control $CB_{12}.L_2$.

On the other hand, the strengthened specimens $CB_{14}.T60.S_1.L_2$ and $CB_{15}.T60.S_2.L_2$ showed less stiffness degradation about 45.45% and 32.84 as average than the control $CB_{12}.L_2$. It can be concluded that, the using of RPC hybridization technique around transverse opening produced more stiffness- enhancing than that using CFRP laminate technique. The stiffness values for the cyclic loaded beams are tabulated in Table 4.6.

4.4.6 Width of Cracks

In general, all specimens showed similar cracks, mainly flexural cracks at first, followed by inclined torsional-shear cracks as the load increased. For

specimens subjected to monotonic load, Table 4.7 and Figures 4.38 and 4.39 describes the kind of major crack and maximum crack width at service load for control specimen $CB_1.L_1$.

Table (4.7) Type and Width of Major Crack of Tested CBs Subjected to Monotonic Loading.

CB Designation		Type of Crack	Crack Width(mm)*	$\times\frac{Wcr(i)-Wcr(r)}{Wcr(r)}$ 100%**
CB1.L1		torsional-shear	0.11	----
Group I	$CB_2.V37.L_1$	torsional-shear	0.4	263.63
	$CB_3.V60.L_1$	flexure of positive moment	0.24	118.2
	$CB_4.V82.L_1$	torsional-shear	0.28	154.5
	$CB_8.V60.S_1.L_1$	flexure of positive moment	0.14	27.27
	$CB_{10}.V60.S_2.L_1$	flexure of positive moment	0.37	236.36
Group II	$CB_5.T37.L_1$	torsional-shear	0.25	127.27
	$CB_6.T60.L_1$	Corner of opening	***	----
	$CB_7.T82.L_1$	flexure of negative moment	0.4	263.63
	$CB_9.T60.S_1.L_1$	flexure of positive moment	0.16	45.4
	$CB_{11}.T60.S_2.L_1$	Corner of opening	0.75	581.8

*****Width of major crack at service load
** Wcr(i): major crack width of considered CB
Wcr(r): major crack width of control CB.
*** Failed before service load of control CB

The largest crack width at service load of final cycle of control $CB_{12}.L_2$ for specimens subjected to cyclic loading was shown in Table 4.8 and Figure 4.4.

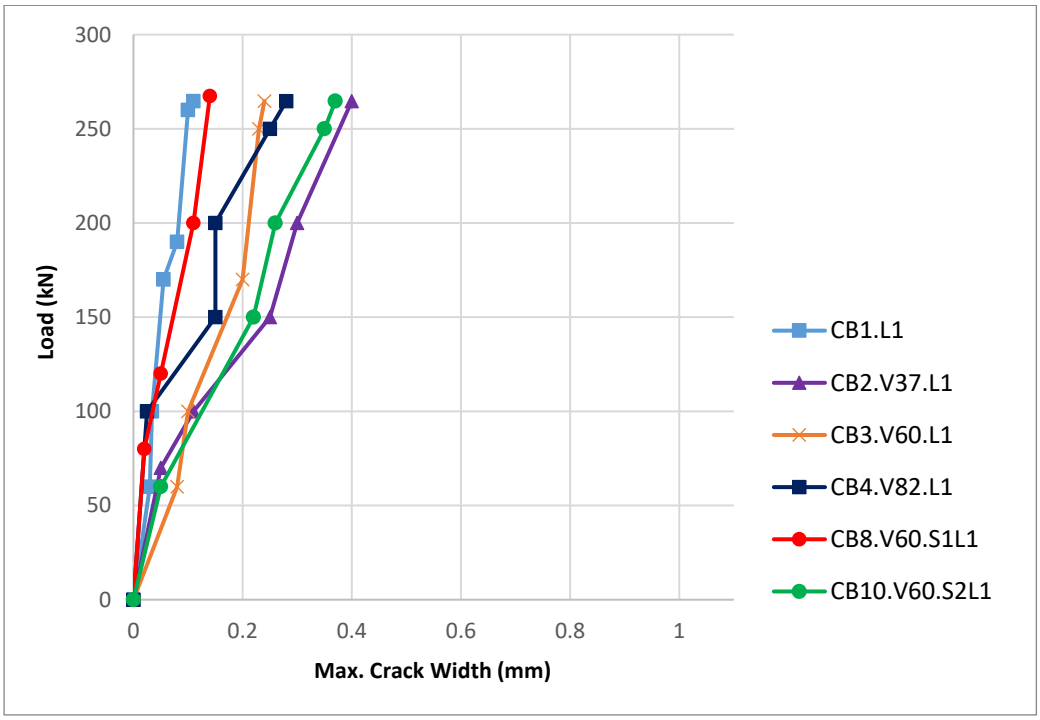

Figure (4.38) Width of Major Cracks up to Service Load for CBs in **Group (I)**

Generally, the curved beams of Group (I) that had vertical openings without strengthening exhibited an increase in cracks width at service loads by about (118.2-263.63)%, and that had strengthened with CFRF laminates by 236.36%, while the spesimen that strengthened by RPC shows relatively a slight increase by about 27.27% due to the effect of steel fibers in delaying the appearance of cracks and controlled on their widths under monotonic loading.

On the other hand, the curved beams of Group (II) that had transverse openings without strengthening shows an increase in cracks width at service loads by about (127.27-263.63)% under monotonic loading, and that had strengthened with CFRF laminates by 581.8%, while the spesimen that strengthened by RPC exhibited relatively a slight increase by about 45.4%, comparid to the control $CB_1.L_1$.

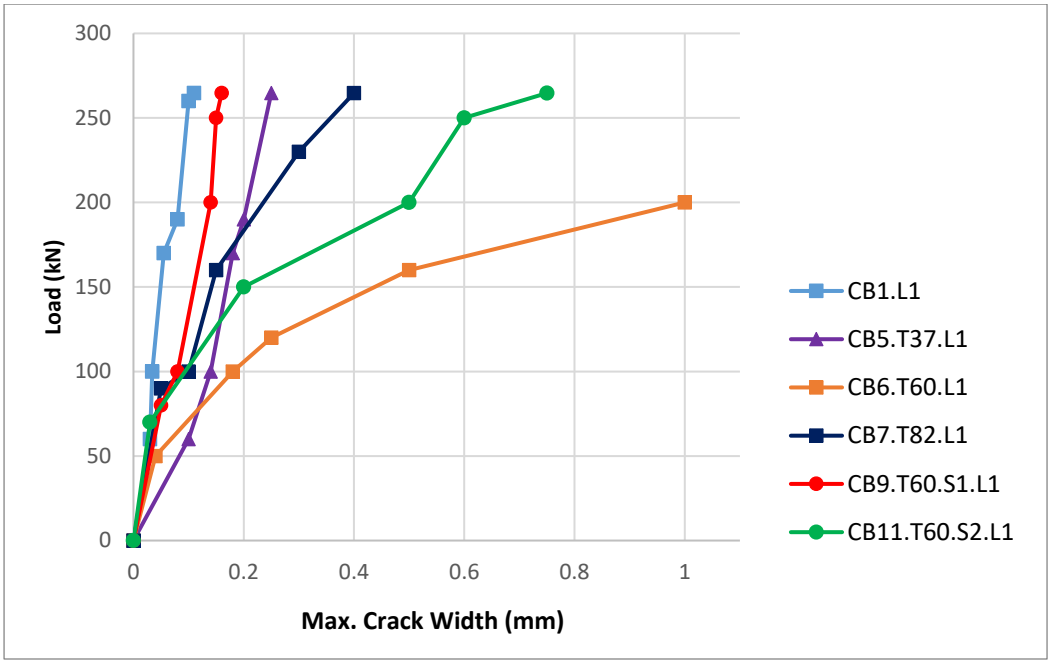

Figure (4.39) Width of Major Cracks up to Service Load for CBs in **Group (II)**

Table (4.8) Type and Width of Major Crack of Tested CBs Subjected to Repeated Loading.

CB Designation	Type of Crack	Crack Width(mm) *	$\times\frac{Wcr(i)-Wcr(r)}{Wcr(r)}$ 100%**
$CB_{12}.L_2$	torsional-shear	0.12	----
$CB_{13}.T60.L_2$	Corner of opening	1	733.3
$CB_{14}.T60.S_1.L_2$	Corner of opening	0.24	100
$CB_{15}.T60.S_2.L_2$	Corner of opening	0.76	533.3

* Width of major crack at service load of final cycle

** Wcr(i): major crack width of considered CB

Wcr(r): major crack width of reference CB

With regards to Group (III), which tested under repeted loading, largest increase 733.3% was obseved in unstrengthened specimen with transverse opening, while the strengthened specimens were showd an increase by about 100% and 533.3% for $CB_{14}.T60.S_1.L_2$ and $CB_{15}.T60.S_2.L_2$ respectively, compared to $CB_{12}.L_2$.

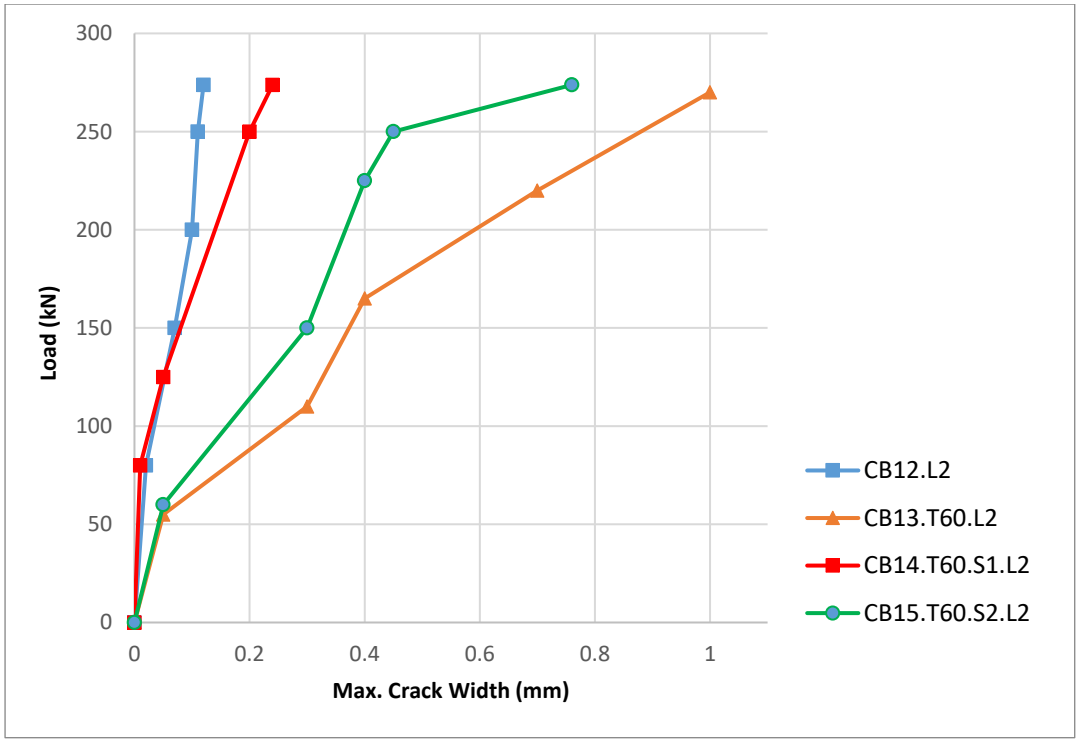

Figure (4.40) Width of Major Cracks up to Service Load of Final Cycle for CBs in **Group (III)**

CHAPTER FIVE

FINITE ELEMENT ANALYSIS

5.1 General

Finite element analysis (FEA) is a practical and cost-effective method for analyzing the complex behavior of concrete structures, particularly those with complex non-linear structural behavior. For studying structural mechanisms and conducting parametric analyses, ABAQUS is one of the most widely used commercial finite element analysis tools. ABAQUS/CAE 2017 is utilized to numerically model the response of reinforced concrete horizontally curved box beams.

Although experimental testing is the most accurate method of studying structural behavior, it has numerous drawbacks. The major difficulty is that the experimental results may change from test to test, which might be due to a variety of factors. Experimental testing is also restricted, costly, and time-consuming. Thus, FE simulation is a helpful tool for not only cross-checking experimental data but also doing parametric analysis for variables not considered in the experimental program.

The validity of the FE model will be assessed in this chapter by comparing numerical simulation results to experimental data for all specimens. The element types, constitutive model, mesh size, and boundary conditions of each component will be detailed first, followed by the specifics of the generated FE model. Finally, a parametric analysis will be carried out.

5.2 Main Meshing Elements

The elements that used in the analysis of reinforced concrete horizontally curving beams are described in this section as follows.

5.2.1 3D Solid Element

In ABAQUS, there are many different elements that may be employed, and it's essential to select the right one for the work. The three-dimensional eight-node linear brick element with reduced integration and hourglass control was chosen for the solid component (i.e. concrete (NSC and RPC)), as shown in Figure 5.1. ABAQUS, on the other hand, offers a variety of three-dimensional (3D) continuum components. The advantage of using linear brick elements over quadratic brick elements is that they may be utilized with contact, whereas quadratic brick components require longer to compute consistent nodal loads throughout the slave surface. While the aim of choosing reduced integration rather full integration is to avoid the shear locking phenomena, full integration produces poor results. So, the chosen element type is a dependable option for the majority of applications. Each three-dimensional solid element has eight nodes, each with three degrees of freedom. To simulate the steel plates in both loading and supporting positions, the three-dimensional solid element (C3D8R) was employed, similar to the concrete beam, see Appendix C.

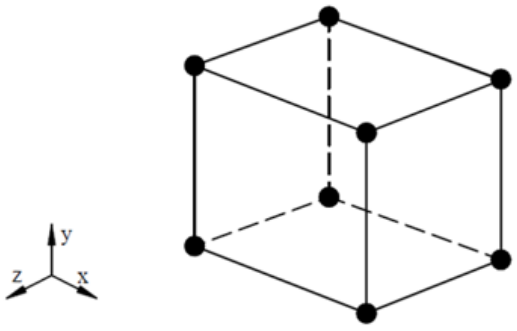

Figure 5.1 C3D8R Element type used in FE simulation (Wu, 2015) of concrete and steel plates

5.2.2 Truss Element

To represent the reinforcing bars in reinforced concrete horizontally curving beams in ABAQUS/standard, a linear 3D of two node truss element with three degrees of freedom at each node (T3D2) was utilized. Figure 5.2 illustrates truss components embedded in three-dimensional (3-D) continuum brick elements that serve as host. The translational degrees of freedom at the nodes of the embedded element are restricted and are confined to the appropriate interpolated values (shape function) in the host continuum element when the element is embedded, see Appendix C.

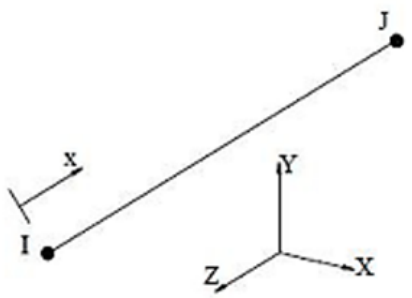

Figure 5.2 Truss element(T3D2) (Metwally, 2014)

5.2.3 Shell Element

Shell elements (S4R: A 4-node doubly curved thin or thick shell, reduced integration, hourglass control, finite membrane strains). This element has been used to simulate CFRP laminate. Furthermore, this type of element is capable to represent CFRP failure (Al-Zubaidy et al., 2013),(Faggiani & Falzon, 2010). Moreover, because they capture through the thickness shear stress without utilizing one element per layer, the continuum shell element allows for a full three-dimensional model and is more efficient in

processing than traditional brick elements (Faggiani & Falzon, 2010),(Falzon et al., 1999), see Appendix C.

5.3 Model Geometry and Boundary Conditions

For all reinforced concrete horizontally curved box beams, 3D simulations were used to provide an accurate estimate of the overall behavior and failure mechanism. Figure 5.3 depicts the geometry of the FE model generated for the control beams in three dimensions. The Z -axis indicates the beam's longitudinal direction, while the X-Y plane represents the beam's cross section.

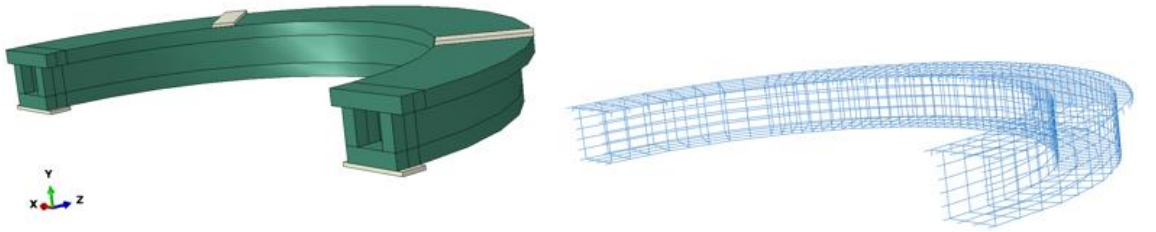

(a) CB_1L_1specimen

(b) $CB_6.T60.L_1$specimen

Figure 5.3 Three Dimensions View of Curved Beams FE model.

To model the contact type between the concrete and the reinforcement, the embedding technique was used. Steel reinforcement bars were chosen as the embedding part in this restriction, whereas the host region was used to

represent the concrete, in addition, perfect bond between concrete and steel was adopted in this work. The interaction option is used to link steel plates to the beam specimen in both loading and supporting positions. In addition, full bond is postulated for the beams with reactive powder concrete and CFRP laminates, there is full transfer of load between CFRP laminates and adhesive and between adhesive and concrete. The embedded region function in ABAQUS allows it to simulate many kinds of parts. One of the most difficult parts of the model in ABAQUS/ Standard is proper modeling of boundary conditions. The supporting condition has been modelled in the continuous simply supported beam with two spans, as described in Chapter 3, thus two exterior supports includes a hinge that constrains translations in the x and y directions, Furthermore, a middle support limiting translation in the y directions. On a demarcation line in the center of the steel plates, the actual restrictions are inserted along the width of the beam. The typical boundary conditions of the specimens utilized in the simulations are shown in Figure 5.4.

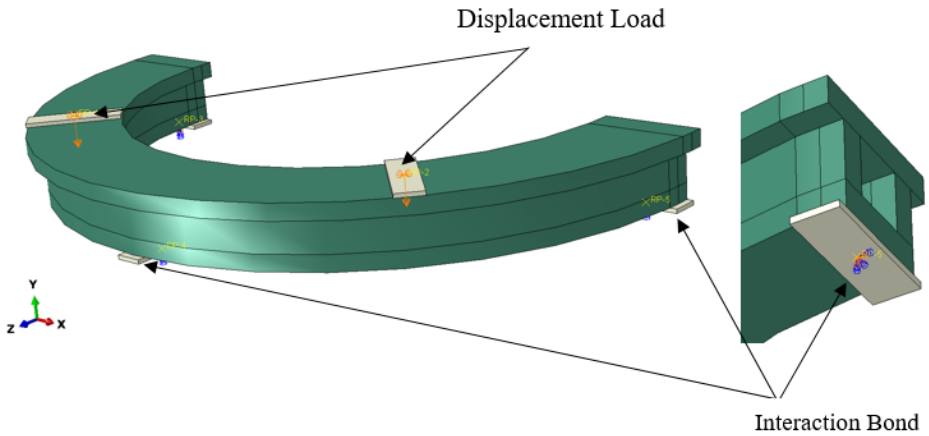

Figure 5.4 Typical Boundary Conditions and Applied Load of Modelled Curved Beams

5.4 Load

A nonlinear dynamic implicit, Quasi-static step analysis in ABAQUS/Standard was performed to examine the RC beams. Load was applied as a displacement along the width of the of loading plate at top surface, the applied displacement was 20 mm.

5.5 Convergence Investigation

Various numerical model factors that might influence the prediction of ultimate load and over all response were studied in this section on the control beam. To begin, a mesh sensitivity research was conducted to determine the best mesh sizes.

5.5.1 Effect of Mesh Size

Because of the load and boundary conditions imposed at the concrete portion, (Daud, 2015) determined that the load deflection behavior of the reinforced concrete slab is more sensitive to the concrete mesh size than the two other instances (steel & CFRP). As shown in Figure 5.5, many sizes of mesh were utilized to determine the appropriate mesh density for control curved box beams ($CB_1.L_1.$). The main goal of the convergence work is to discover the best mesh size for the model with the least number of elements and the best convergence with the experimental test findings. In selecting the optimum mesh size, the midspan deflection was used as a guideline. As illustrated in Figure 5.6, when the number of elements is increased from (9344) to (25254), the difference may be ignored for control curved box beams ($CB_1.L_1.$). So, the number of elements (9344), used for the control and other Curved Box Beams specimens.

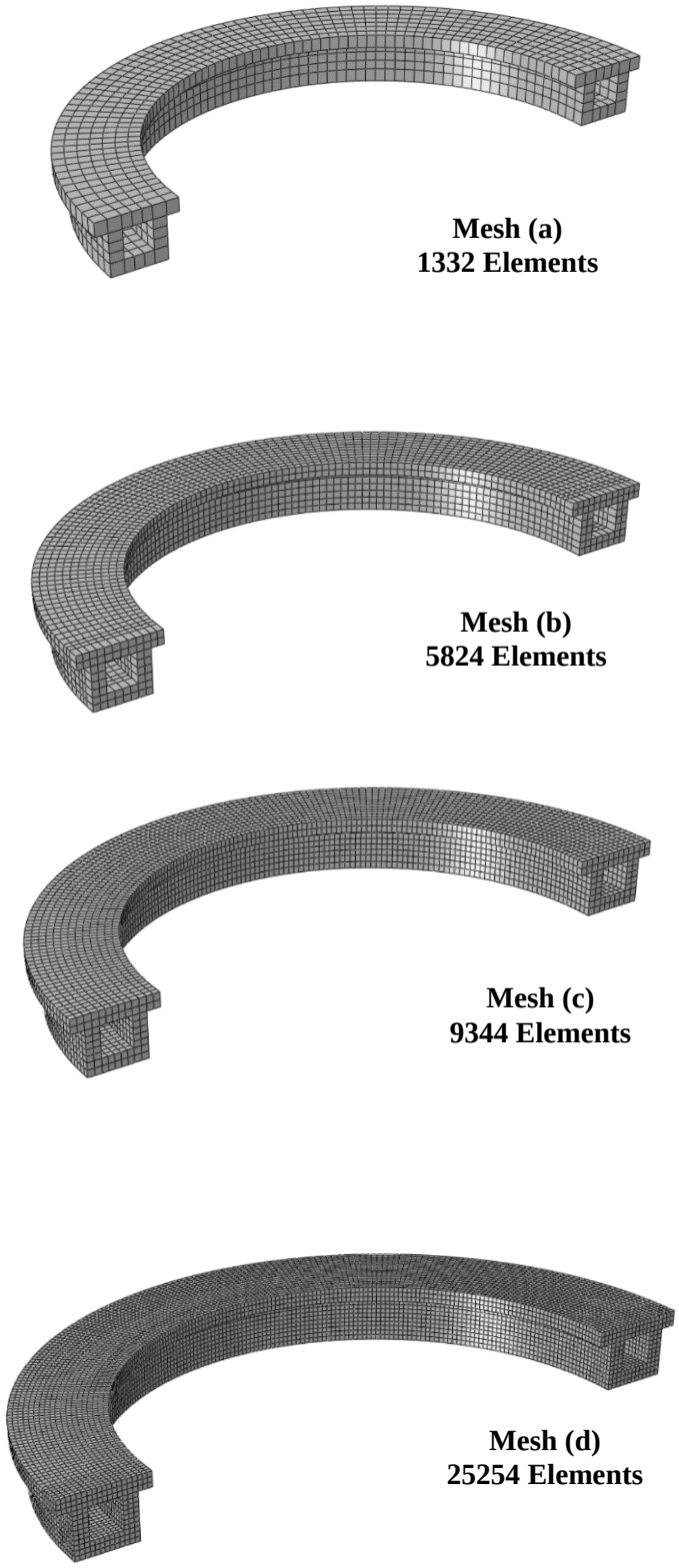

Figure 5.5 Mesh Density of the Control Curved Box Beams ($CB_1.L_1$ specimen).

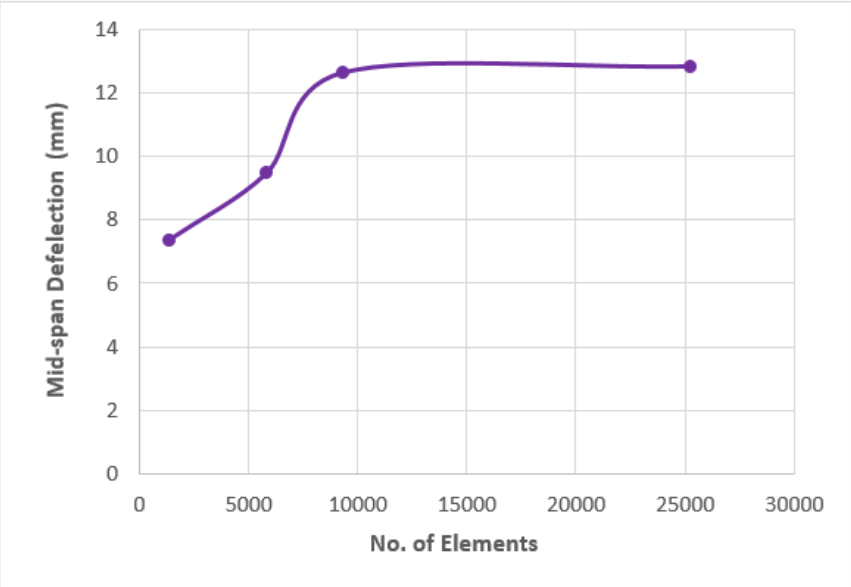

Figure 5.6 Results of Convergence Study

5.6 Finite Element Analysis Results and Discussion

In terms of load-deflection curves, torsional moment- twisting angle, load of cracking, final load, service deflection, ductility factors, and cracking patterns at failure, a comparison is done between the experimental results and numerical analysis.

5.6.1 Deformation Response

The load-deflection and torsional moment- twisting angle relationships describe the behavior of the investigated members during the loading, and it is an essential indicator of the FE model's validity. Figures 5.7 and 5.8 illustrate the load–midspan deflection for Group I and Group II, respectively, while Figure 5.9 and 5.10 show torsional moment-midspan twisting angle responses for Group I and Group II, in addition to Figure 5.11which show load–midspan deflection for Group III, generated from FEM were compared to the experimental data. The load–midspan

deflection and torsional moment-midspan twisting angle predicted by the FEM matched the actual results in most cases. Its response, on the other hand, were stiffer than those obtained from the experimental specimens. Higher stiffness in FEM might be due to a variety of factors. In the case of the experiments, the most essential factor is the formation of micro cracks owing to shrinkage of drying, handling of concrete, detrimental effect of environment, et cetera. Micro cracks are not included in FEM models (Metwally, 2014). Another factor for the simulated beams stronger initial load-midspan deflection response might be the way rebars bonds were simulated. The embedded region constraint that was employed in ABAQUS to represent the interaction between the concrete and rebars was perfect bond, as mentioned previously in the geometry model. Because the actual interaction is imperfect in real, this perfect representation may really contribute to the numerical model's misleading initial greater stiffness.

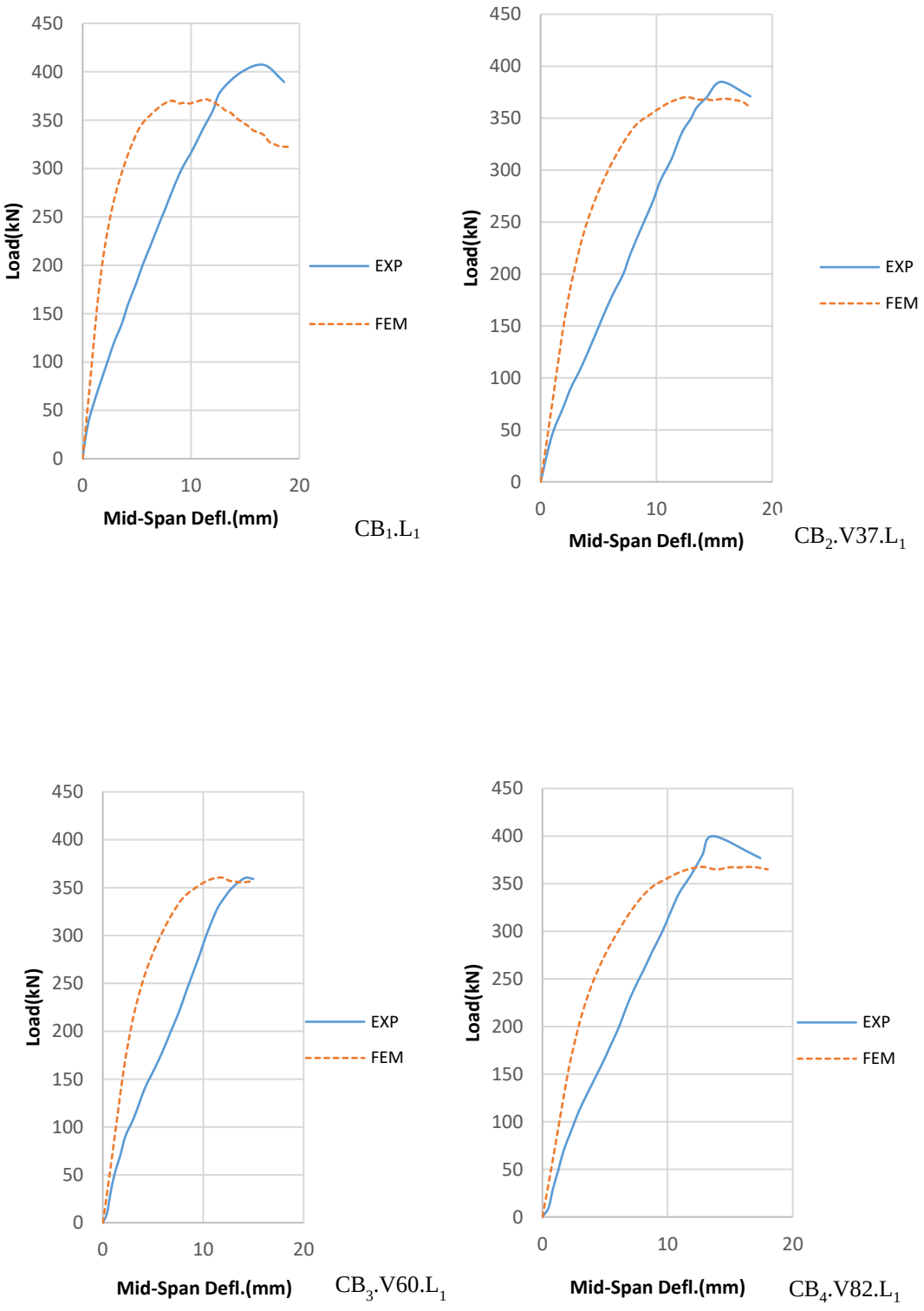

Figure 5.7 Experimental and Numerical Load-Midspan Deflection Curves of (Group I) Under Monotonic Load

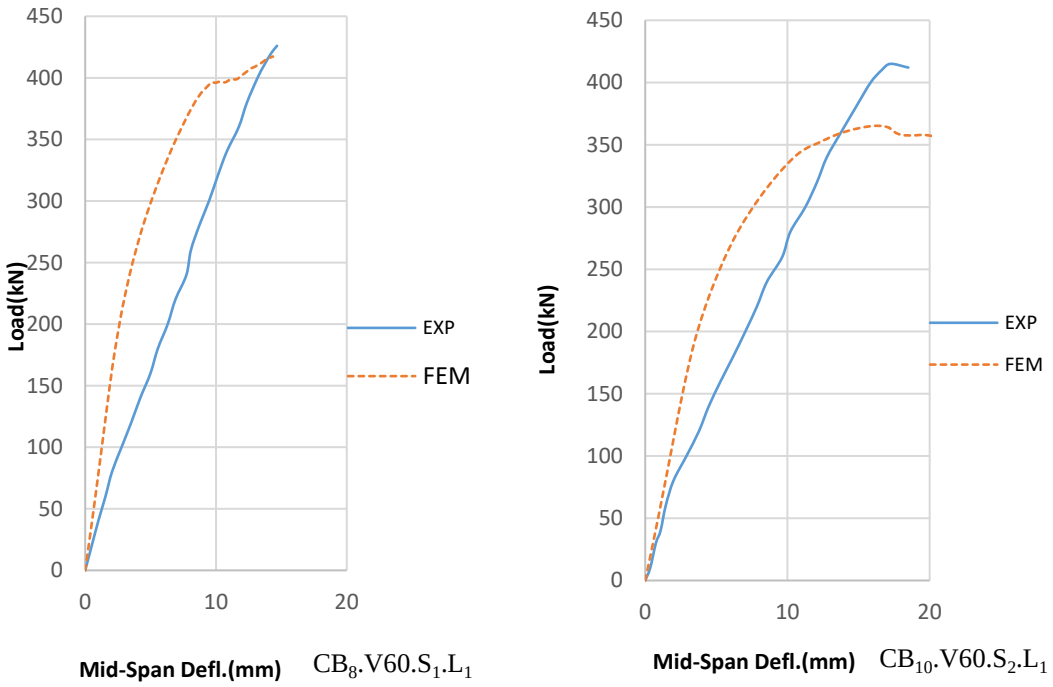

Figure 5.7 Continue

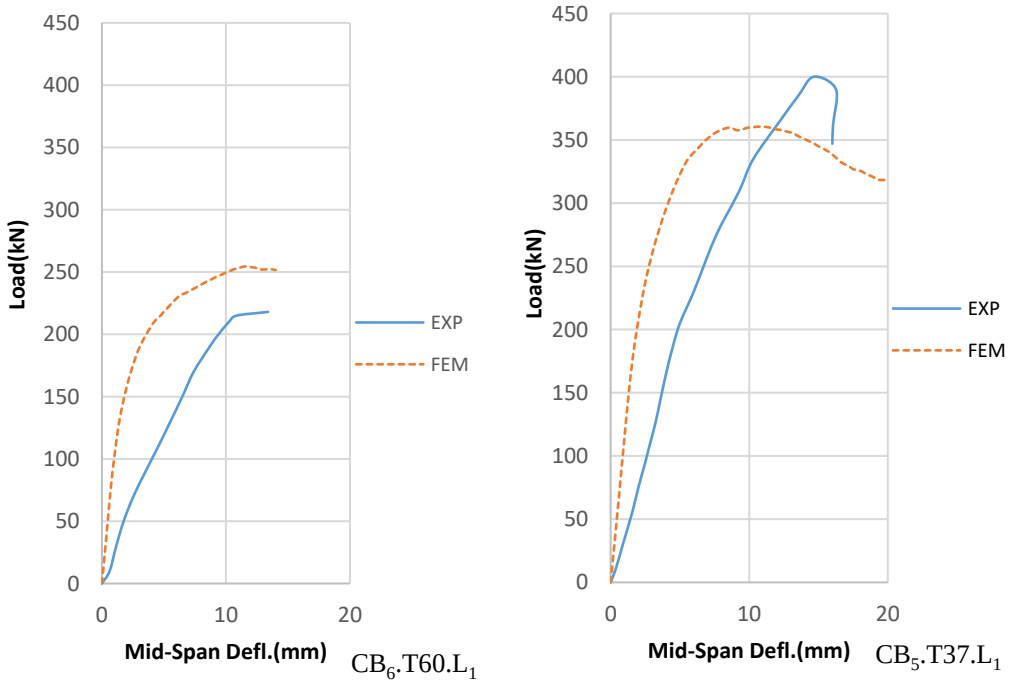

Figure 5.8 Experimental and Numerical Load-Midspan Deflection Curves of (Group II) Under Monotonic Load

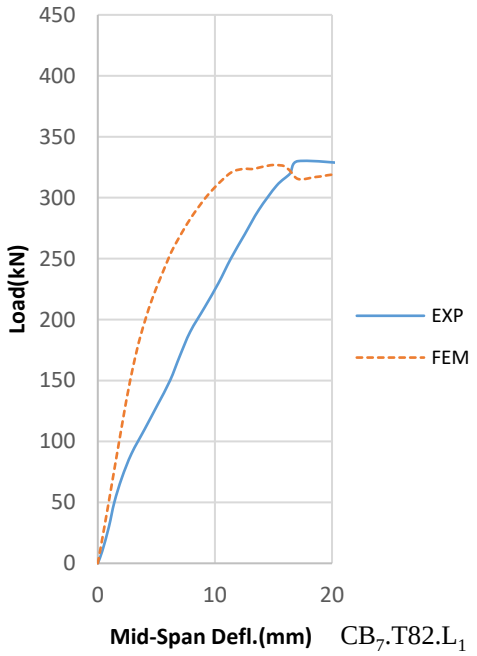

$CB_7.T82.L_1$

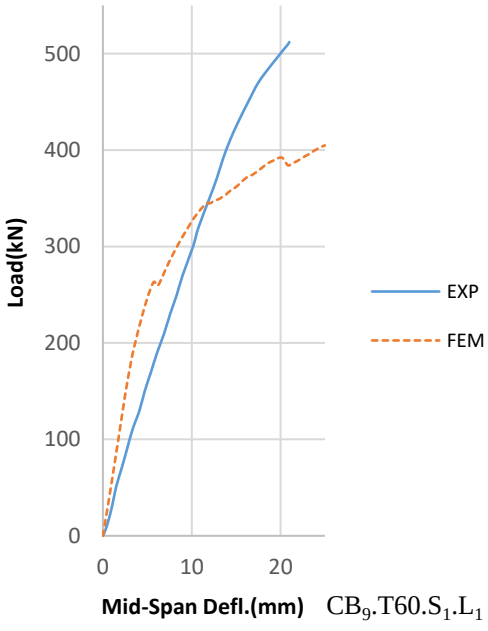

$CB_9.T60.S_1.L_1$

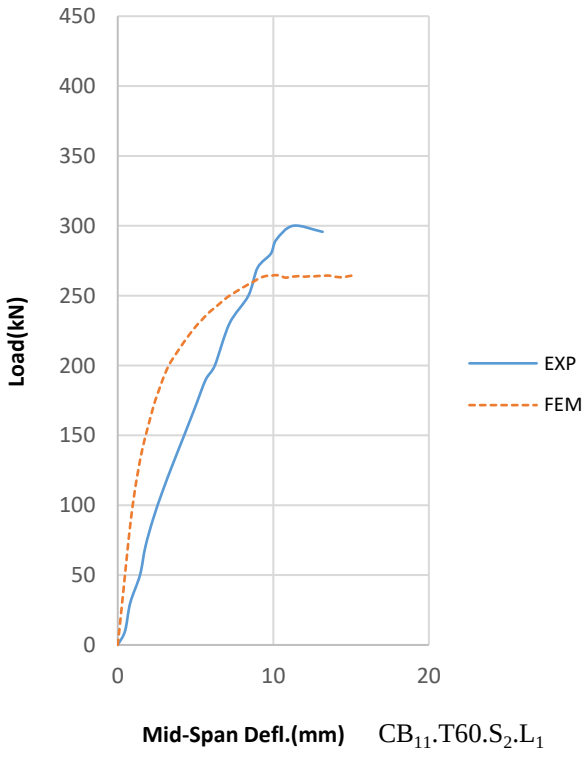

$CB_{11}.T60.S_2.L_1$

Figure 5.8 Continue

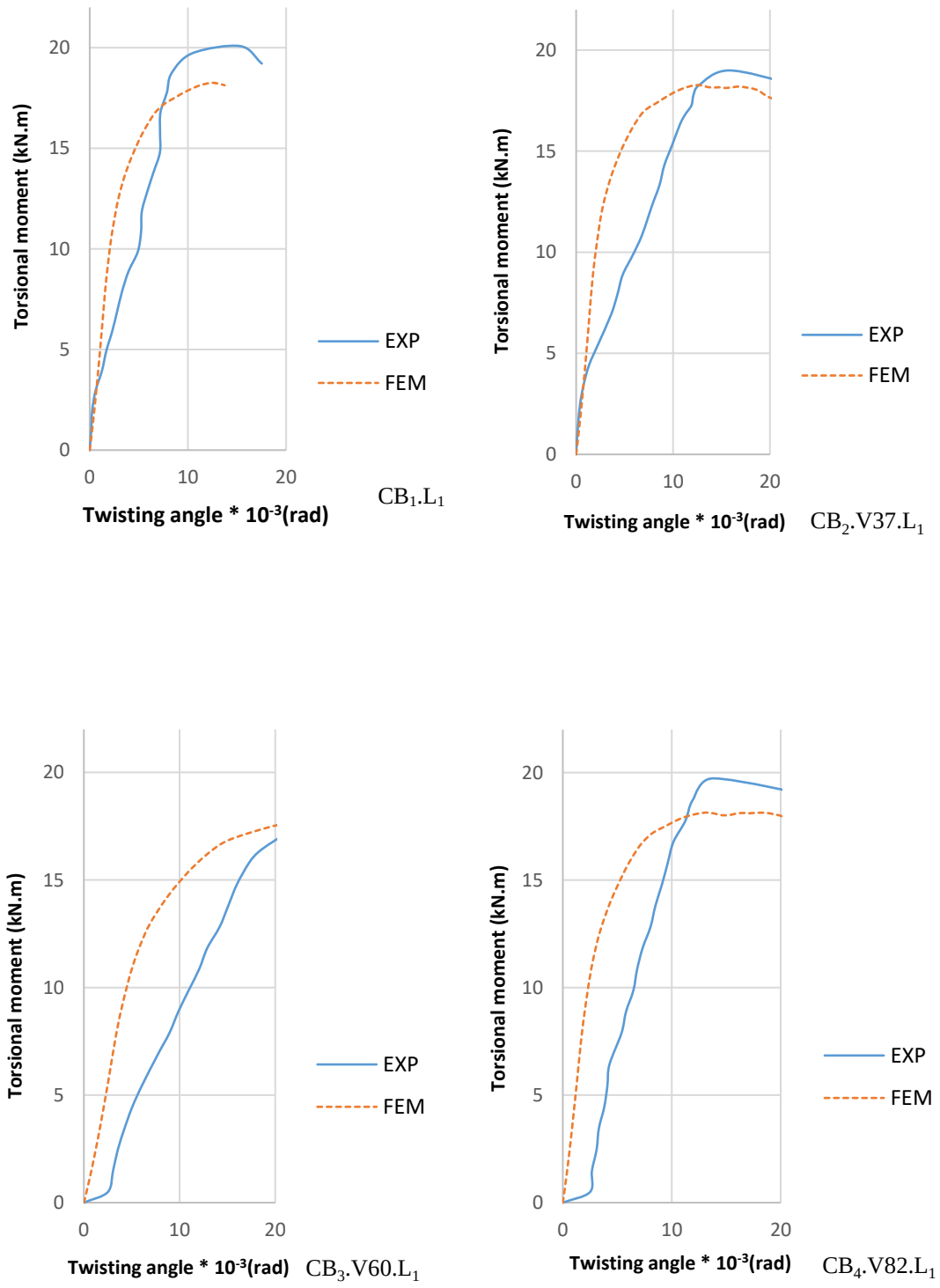

Figure 5.9 Experimental and Numerical Torsional moment-Midspan Twisting Angle Curves of (Group I)

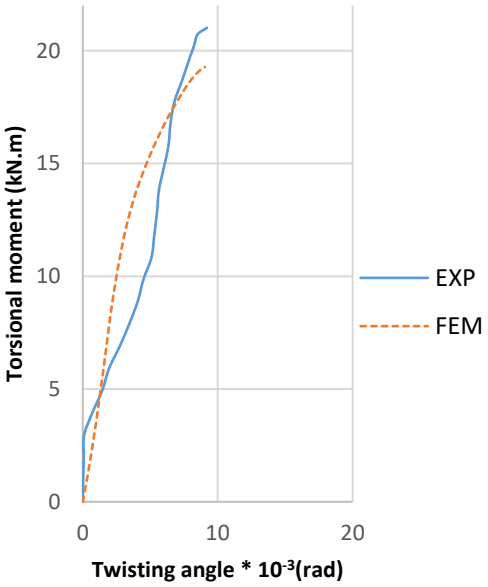

$CB_8.V60.S_1.L_1$

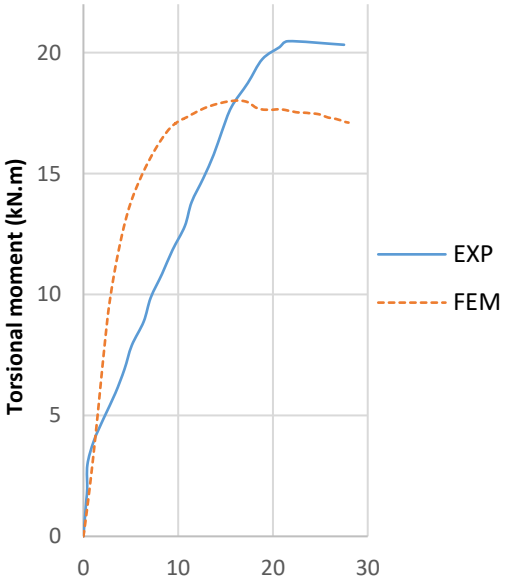

$CB_{10}.V60.S_2.L_1$

Figure 5.9 Continue

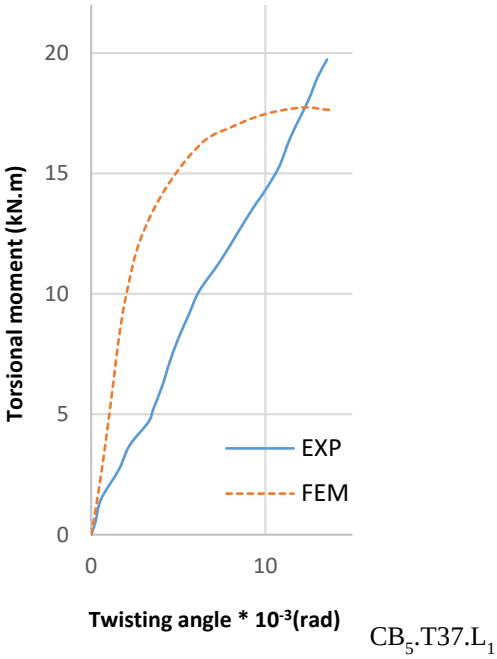

$CB_5.T37.L_1$

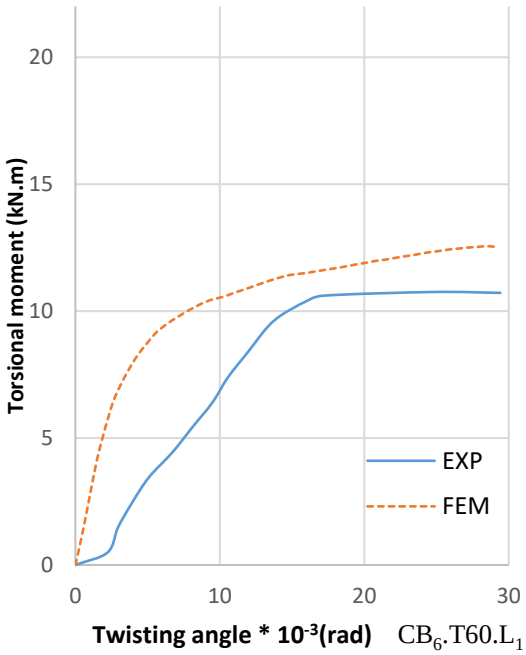

$CB_6.T60.L_1$

Figure 5.10 Experimental and Numerical Torsional moment-Midspan Twisting Angle Curves of (Group II)

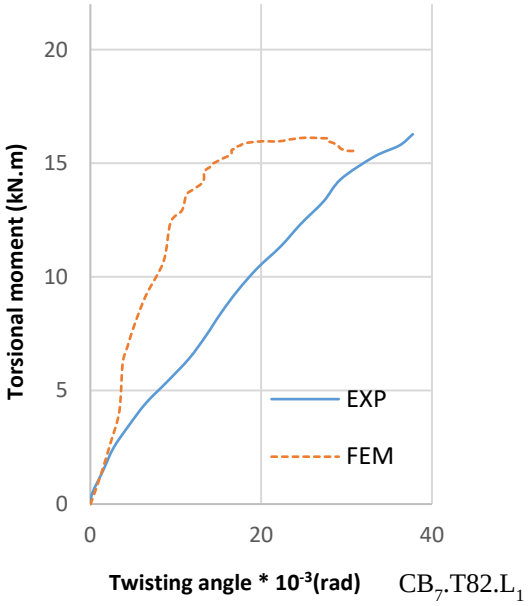

$CB_7.T82.L_1$

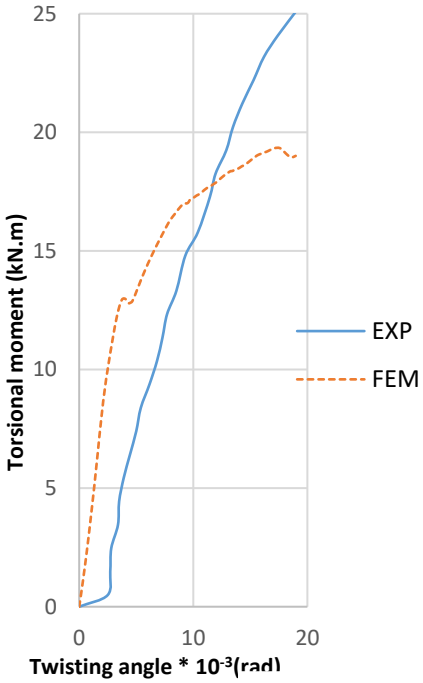

$CB_9.T60.S_1.L_1$

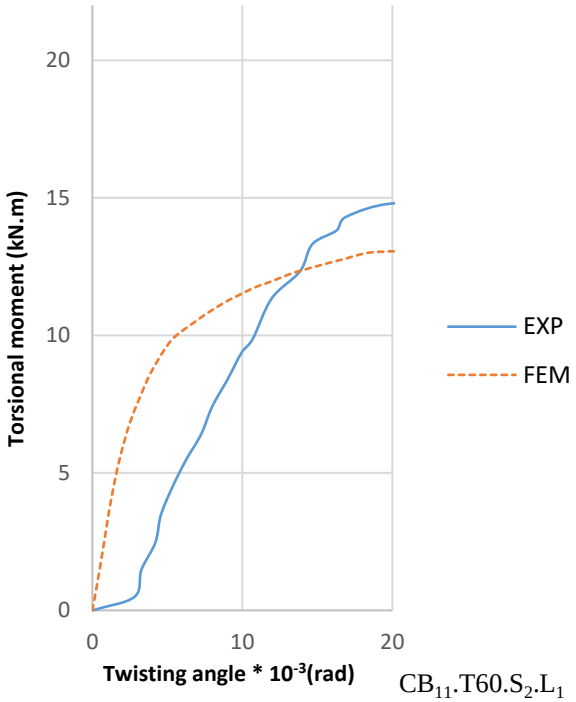

$CB_{11}.T60.S_2.L_1$

Figure 5.10 Continue

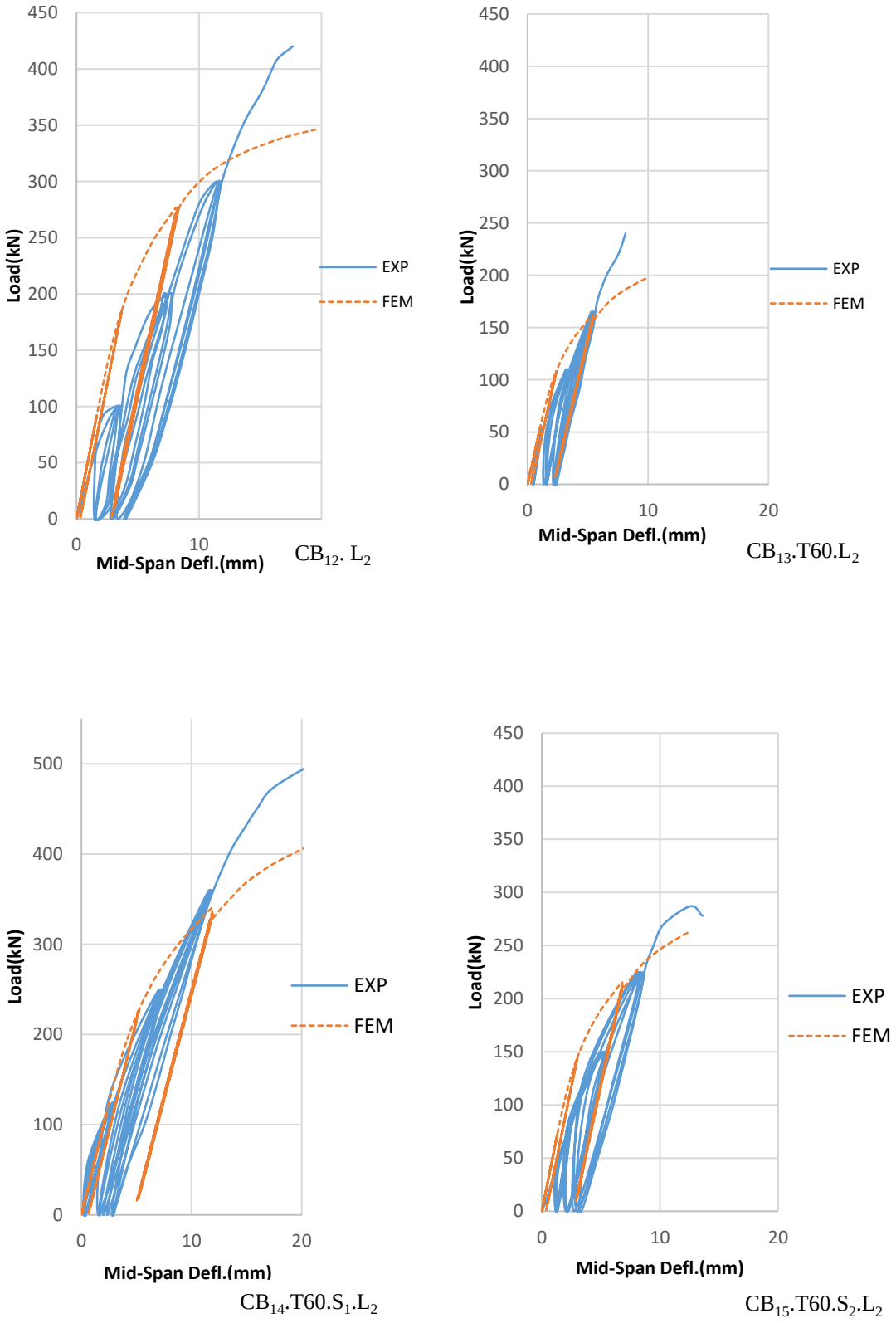

Figure 5.11 Experimental and Numerical Load-Midspan Deflection Curves of (Group III) Under Cyclic Load

5.6.2 First Cracking and Ultimate Loads

Table 5.1 shows a comparison of the experimantal and numerical results of the first cracking and ultimate loads. For numerical models, an ultimate load is the final applied load step before the solution diverges owing to multiple cracks and substantial deflections. It should be noted that the numerical findings for first cracking and ultimate loads were found to be in good agreement with the experimental values. The first cracking load calculated from numerical data for all models were as average, 5 % lower than that calculated from experimental data. The numerical ultimate loads, on the other hand, were as average 8% lower than the experimental ultimate loads for all models.

Table 5.1 Experimental and FEM Cracking and Ultimate Loads of CBs.

Beam Designation	Cracking load(KN)			Ultimate load(KN)		
	$P_{cr(FEM)}$	$P_{cr(Exp.)}$	$\frac{P_{cr(FEM)}}{P_{cr(Exp.)}}$	$P_{u(FEM)}$	$P_{u(Exp.)}$	$\frac{P_{u(FEM)}}{P_{u(Exp.)}}$
$CB_1.L_1$	47	50	0.94	371.6	407	0.913
$CB_2.V37.L_1$	36.45	40	0.91	370.3	385	0.96
$CB_3.V60.L_1$	38.77	40	0.97	360.58	360	1
$CB_4.V82.L_1$	41.18	40	1.03	367.66	400	0.92
$CB_8.V60.S_1.L_1$	58.1	59	0.98	436.9	427	1.02
$CB_{10}.V60.S_2.L_1$	55.9	60	0.93	365	415.56	0.88
$CB_5.T37.L_1$	40.65	39	1.04	360.58	400	0.9
$CB_6.T60.L_1$	44.26	50	0.88	254.28	218	1.17
$CB_7.T82.L_1$	54.13	58	0.93	319.51	330	0.97
$CB_9.T60.S_1.L_1$	64.62	65	0.99	411	512.65	0.802

Table 5.1 Continue

$CB_{11}.T60.S_2.L_1$	64.88	60	1.08	263.92	301.54	0.88
$CB_{12}.L_2$	37	40	0.93	345.97	421.2	0.82
$CB_{13}.T60.L_2$	42.66	50	0.85	198.15	239	0.83
$CB_{14}.T60.S_1.L_2$	43.82	42	1.04	416.12	508	0.82
$CB_{15}.T60.S_2.L_2$	41.57	50	0.83	263.37	287.3	0.92
Average			0.95			0.92

5.6.3 Deflection at Service Load and Ductility Index

Table 5.2 illustrates the comparison of numerical and experimental deflection at service load and ductility factor for all curved box beams. The service load is equivalent to 0.59 of the total load **(Mansur, 2006)**. The FE analysis' service deflection values and ductility factors were in accepted agreement with the experimental values. The service deflection value and ductility factor of the final cycle are specified for the repeated loaded specimens. For service deflection and ductility factor, the deviations as average were roughly 20% and 13%, respectively.

Table 5.2 Experimental and FEM Results (Service Deflections and Ductility Factors).

Beam designation	**Service Deflection (mm)**			**Ductility Factor, μ**		
	$(\Delta s)_{FEM}$	$(\Delta s)_{EXP.}$	$\frac{(\Delta s)_{FEM}}{(\Delta s)_{EXP.}}$	$(\mu)_{FEM}$	$(\mu)_{EXP.}$	$\frac{(\mu)_{FEM}}{(\mu)_{EXP.}}$
$CB_1.L_1$	3.94	5.53	0.712	3.2	3.02	1.06
$CB_2.V37.L_1$	3.98	6.2	0.65	2.54	2.51	1.01
$CB_3.V60.L_1$	4.92	7.1	0.7	2.03	1.99	1.02
$CB_4.V82.L_1$	5.09	7.0	0.73	2.38	1.95	1.22
$CB_8.V60.S_1.L_1$	4.45	6.66	0.67	2.88	1.9	1.5

Table 5.2 Continue

$CB_{10}.V60.S_2.L_1$	5.84	8.2	0.71	2.74	2.1	1.3
$CB_5.T37.L_1$	3.94	5.67	0.7	3.12	2.6	1.2
$CB_6.T60.L_1$	13.4	*	---	1.37	----	----
$CB_7.T82.L_1$	6.72	9.12	0.74	2.44	1.9	1.28
$CB_9.T60.S_1.L_1$	5.9	7.8	0.76	3.6	2.8	1.28
$CB_{11}.T60.S_2.L_1$	6.57	6.94	0.95	1.61	1.62	0.99
$CB_{12}.L_2$	8.2	10.82	0.76	2.32	1.66	1.39
$CB_{13}.T60.L_2$	*	8.13	---	---	1	---
$CB_{14}.T60.S_1.L_2$	10.6	9.35	1.1	2.07	2.4	0.86
$CB_{15}.T60.S_2.L_2$	12.57	10.3	1.22	1	1.22	0.82
Average			0.8			1.15

* Ultimate load less than the service load of control beam

5.6.4 Crack Pattern and Modes of Failure

The crack patterns generated by the FEM were quite similar to those found in the actual investigation. Figure 5.12 illustrate the crack patterns for specimens $CB_1.L_1$, $CB_3.V60.L_1$ and $CB_6.T60.L_1$, specimens with opening had more cracks at the opening vicinity than those without opening and changing the failure mode as in the experiment result. Similar to those obtained in experiments, first cracks occurred at flexural zone of negative moment for all specimens. In agreement with the experimental results, the cracks near the transverse opening of specimen $CB_6.T60.L_1$ was more than that in specimen $CB_7.T82.L_1$with vertical opening and then led to a large reduction in the ultimate load of specimen $CB_6.T60.L_1$ compared with the control specimen $CB_1.L_1$.

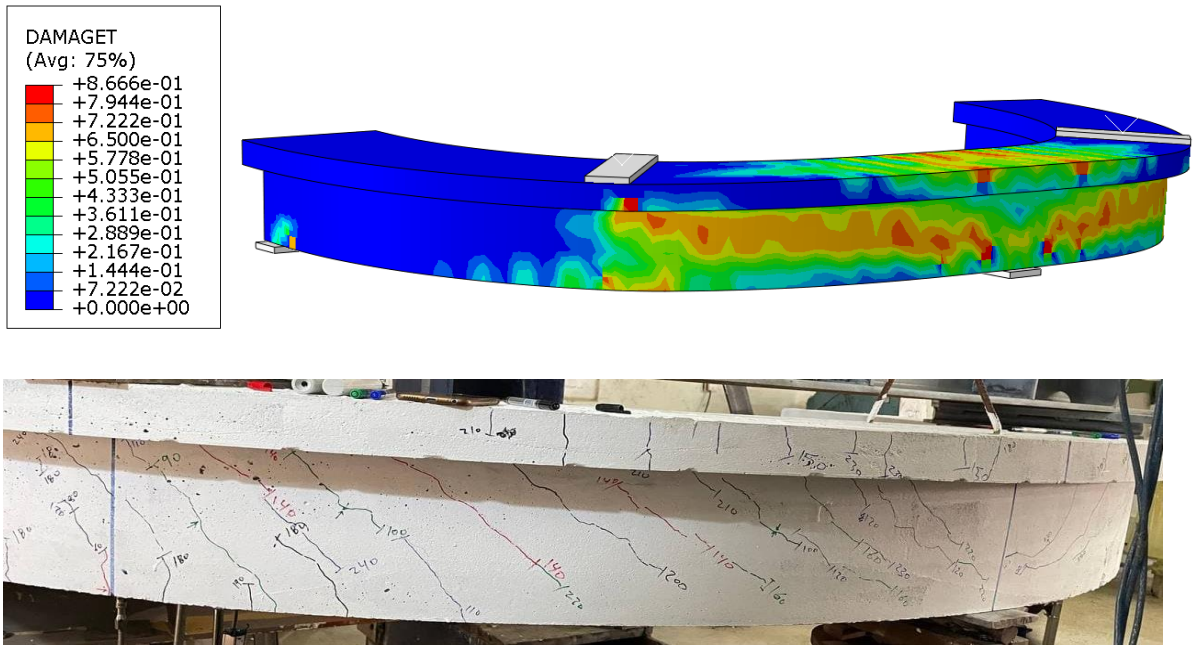

(a)

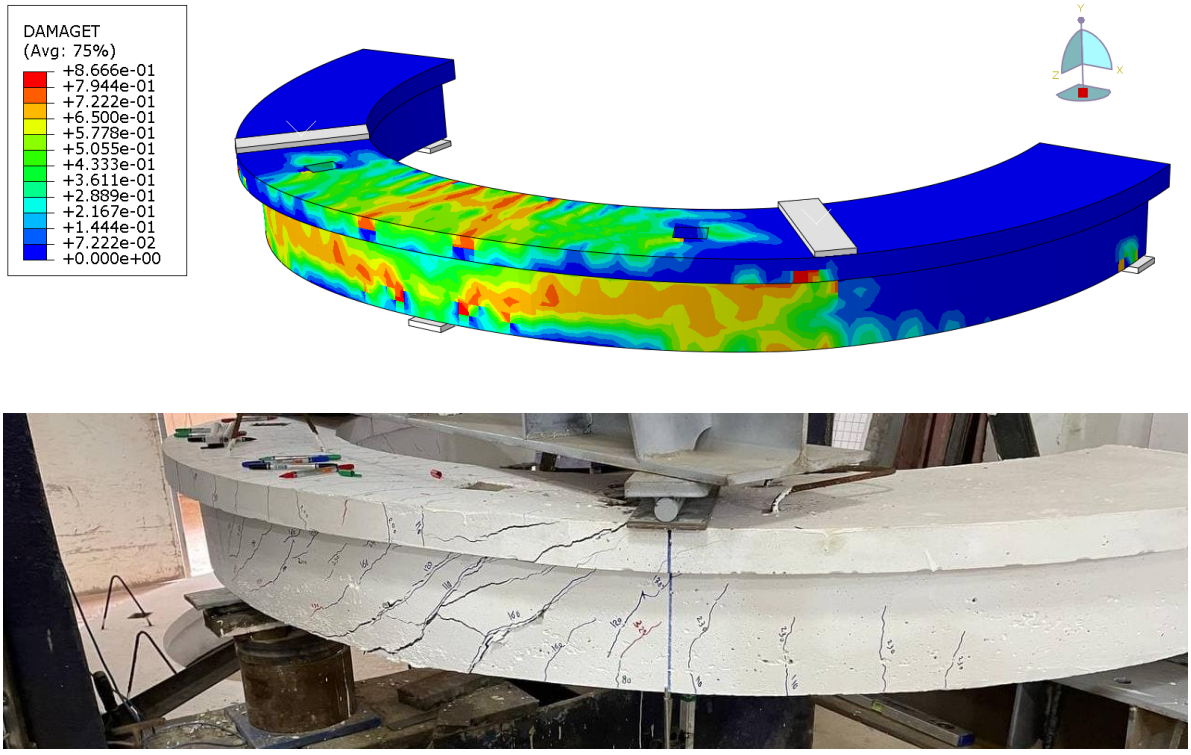

(b)

Figure 5.12 Cracking Patterns of Finite Element Model for Specimens (a)$CB_1.L_1$, (b)$CB_3.V60.L_1$and (c)$CB_6.T60.L_1$

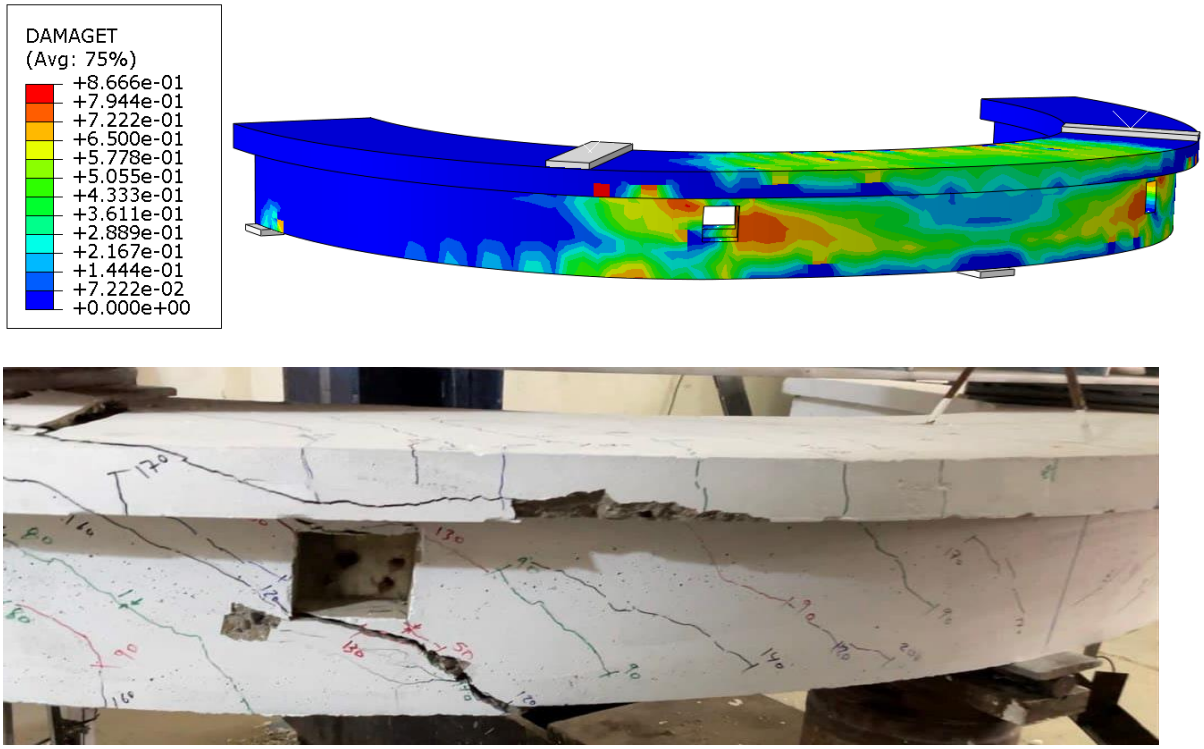

(c)

Figure 5.12 Continue

Finally, when compared to experimental observations, the reported failure mechanism determined in FEM for all specimens was identical to the experimental failure mode.

5.7 Parametric Study

Three important parameters were investigated in the experimental work, including the opening location, the direction of opening axis, and two types of strengthening in attempt to restore the strength of curved box beams with openings under monotonic and repeated load. Using the finite element simulation model in this work, which has been shown to be capable of forecasting the experimental ultimate load to within an acceptable percent and modes of damage. In order to provide a more complete and accurate knowledge of the behavior of curved box beams with openings, a parametric analysis carried out. It included the assessment of the behavior of curved box beams involving different shapes of opening and effect of curvature.

5.7.1 Effect of Opening Shape

The location and direction of axis of opening have been well studied during the experiments. Therefore, in order to get a full view of the effects of opening shape, a rectangular and circular shape of opening will be studied also for both directions. The dimensions of the rectangular opening were 64 mm depth and 100 mm length, while the circular opening was with diameter 93.3mm, which represent the equivalent area of the square opening for $CB_3.V60.L_1$ and $CB_6.T60.L_1$ specimens with the same position (at Angle 60°). Figures 5.13 and 5.14 depicts the load–midspan deflection and torsional moment-midspan twisting angle responses for vertical openings, respectively, while Figures 5.15 and 5.16 shows the load–midspan deflection and torsional moment-midspan twisting angle responses for transverse openings, respectively, calculated by FEM.

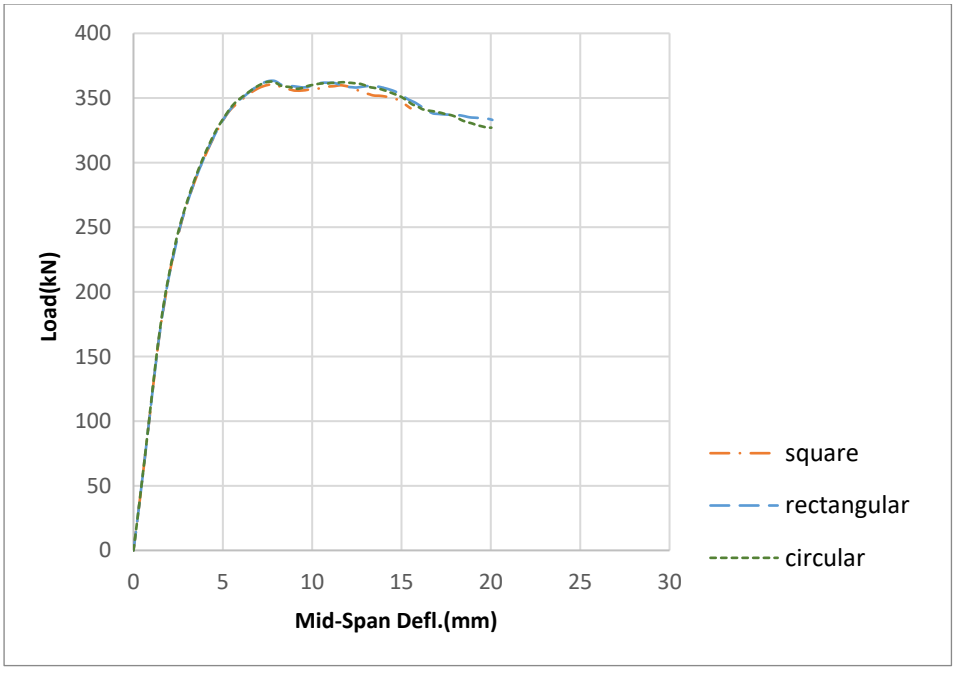

Figure 5.13 Load–Midspan Deflection Curves of FEM for Beams with Various Shapes of Vertical Openings at Angle 60°

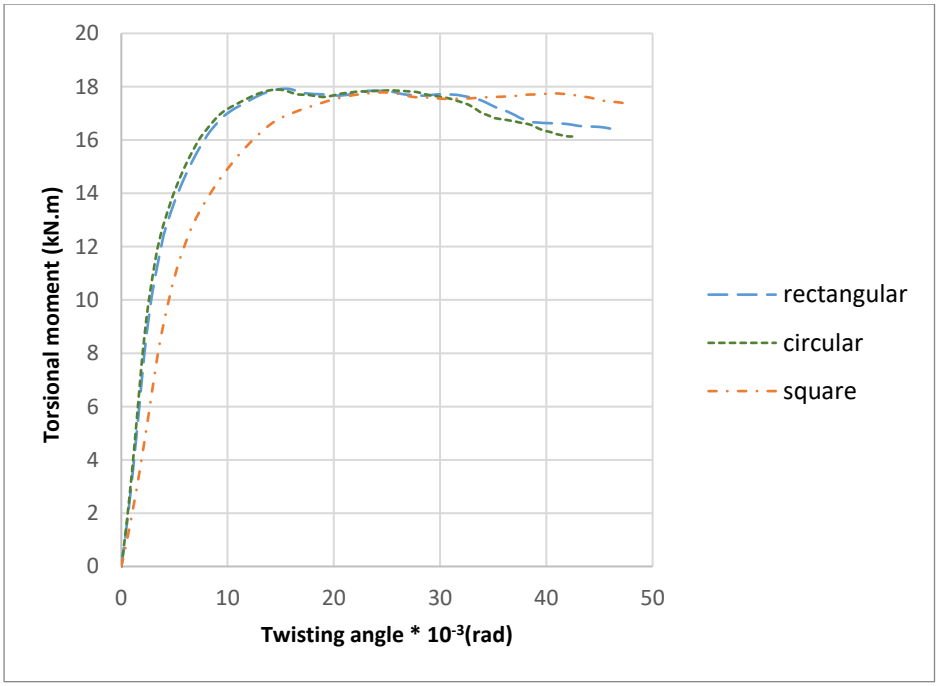

Figure 5.14 Torsional moment-Midspan Twisting Angle Curves of FEM for Beams with Various Shapes of Vertical Openings at Angle 60°

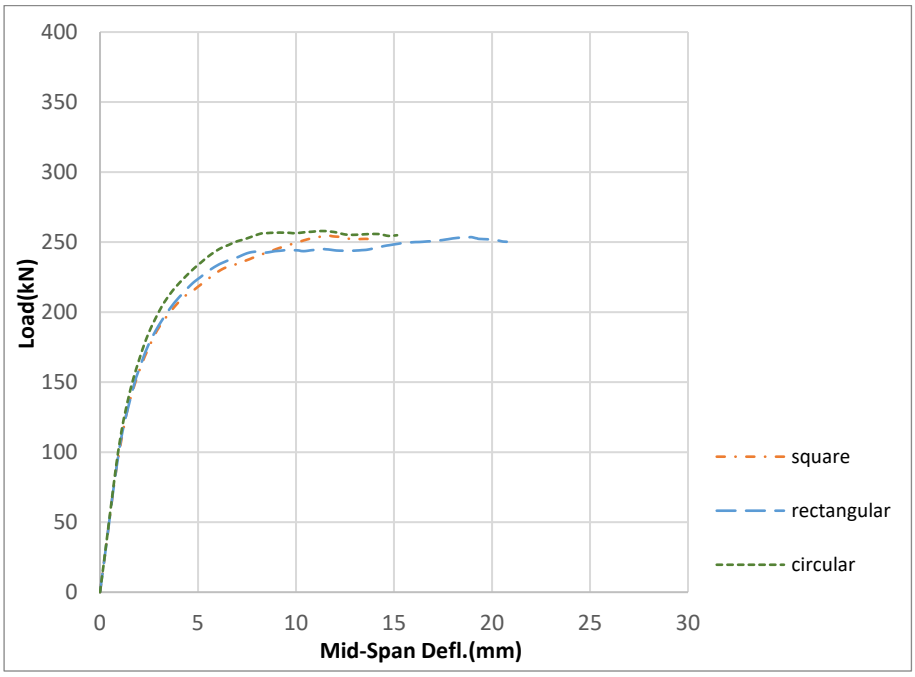

Figure 5.15 Load–Midspan Deflection Curves of FEM for Beams with Various Shapes of Transverse Openings at Angle 60°

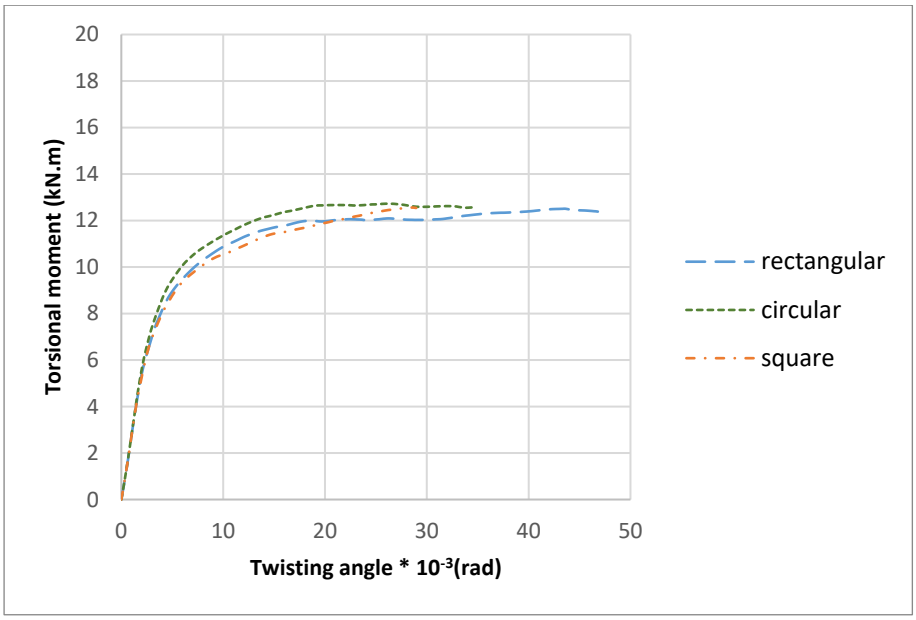

Figure 5.16 Torsional moment-Midspan Twisting Angle Curves of FEM for Beams with Various Shapes of Transverse Openings at Angle 60°

Table 5.3 Comparison of Effect of Shapes of Vertical Openings at Angle 60° by the FE Model.

Beam with specified Shapes of Openings	Numerical cracking load P_{cr} (kN)	Numerical ultimate load Pu (kN)	Variation in the cracking load relative to the (FEM) $CB_3.V60.L_1$ (%)	Variation in the ultimate load relative to the (FEM) $CB_3.V60.L_1$ (%)
(FEM) $CB_3.V60.L_1$ (square)	38.77	360.58	---	---
Par. (rectangular)	38.62	360.77	-0.38	0
Par. (circular)	38.89	360.45	0.31	0

Table 5.4 Comparison of Effect of Shapes of Transverse Openings at Angle 60° by the FE Model.

Beam with specified Shapes of Openings	Numerical cracking load P_{cr} (kN)	Numerical ultimate load Pu (kN)	Variation in the cracking load relative to the (FEM)$CB_6.T60.L_1$ (%)	Variation in the ultimate load relative to the (FEM)$CB_6.T60.L_1$ (%)
(FEM)$CB_6.T60.L_1$ (square)	44.26	254.56	---	---
Par. (rectangular)	43.82	253	-1	-0.6
Par. (circular)	44.22	258.12	0	1.4

As illustrated in Tables 5.3 and 5.4, no considerable change in cracking load for beams with rectangular or circular Vertical and Transverse openings at Angle 60° by the FE Model, compared to that with square Vertical and Transverse openings at Angle 60°.

It is observed that the presence of a circular or rectangular opening in vertical direction led to approximately the same ultimate load by FEM for beam with a square opening, while in the transverse direction the ultimate load was increased by about 1.4% for circular opening and decreased 0.6% for rectangular opening, when compared to the ultimate load of beam with a square opening at Angle 60°.

5.7.2 Effect of Curvature

To survey the influence of curvature on behavior of horizontally curved box beam, two radius of curvature of box beams were compared in the current parametric study in addition to that of experimental study (1.15m exp., 1.5m and ∞). The study carried out on curved beam without openings and that with transverse opening at angle 60°. The load- midspan deflection curves

of three cases are shown in Figures 5.17 and 5.18. As shown in Tables 5.5 and 5.6, a slight reduction in cracking load for beams without openings and those with transverse openings at Angle 60° which as average (4-6.5) % and (0-1) %, respectively, as a comparison to beams with radius of experiment (1.15 m). There was a noticeable change in overall behavior and ultimate load, which was noticed and reported. For beams without openings, ultimate load was raised roughly (10.5% and 19.41%) in beams with radius (1.5 and ∞) m, respectively, while an increase by about (14.7% and 59.4%) in beams of radius (1.5 and ∞) m respectively, for beams with transverse openings at angle 60° compared to curved box beams with radius of 1.15 m.

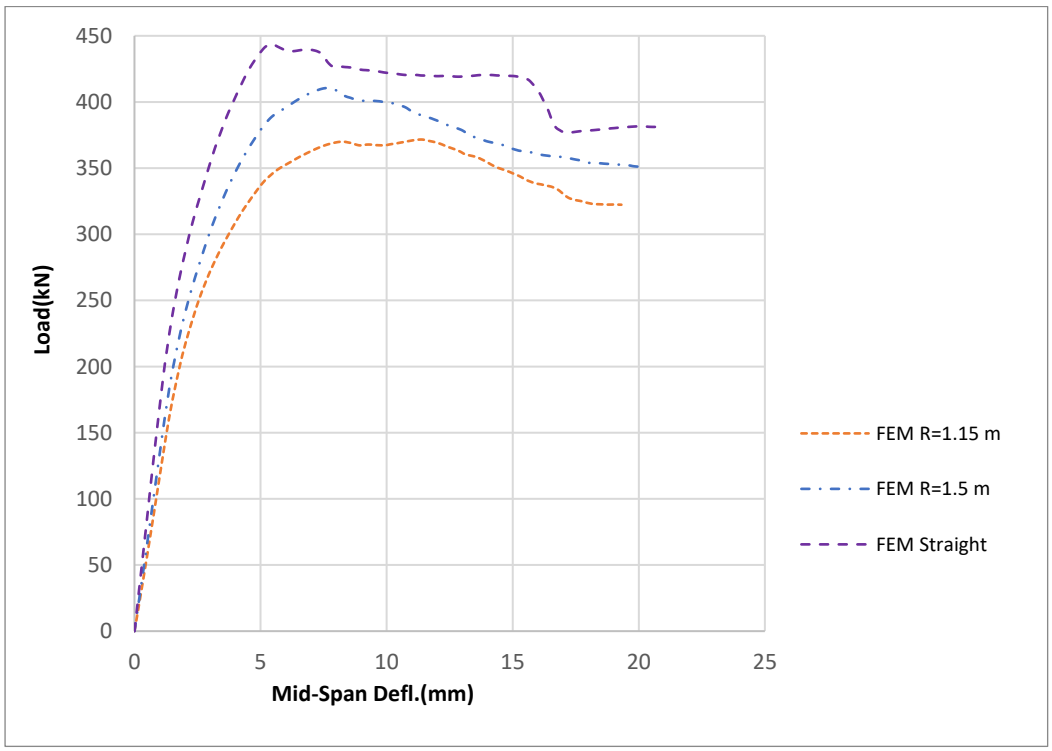

Figure 5.17 Load–Midspan Deflection Curves of FEM for Beams without Openings

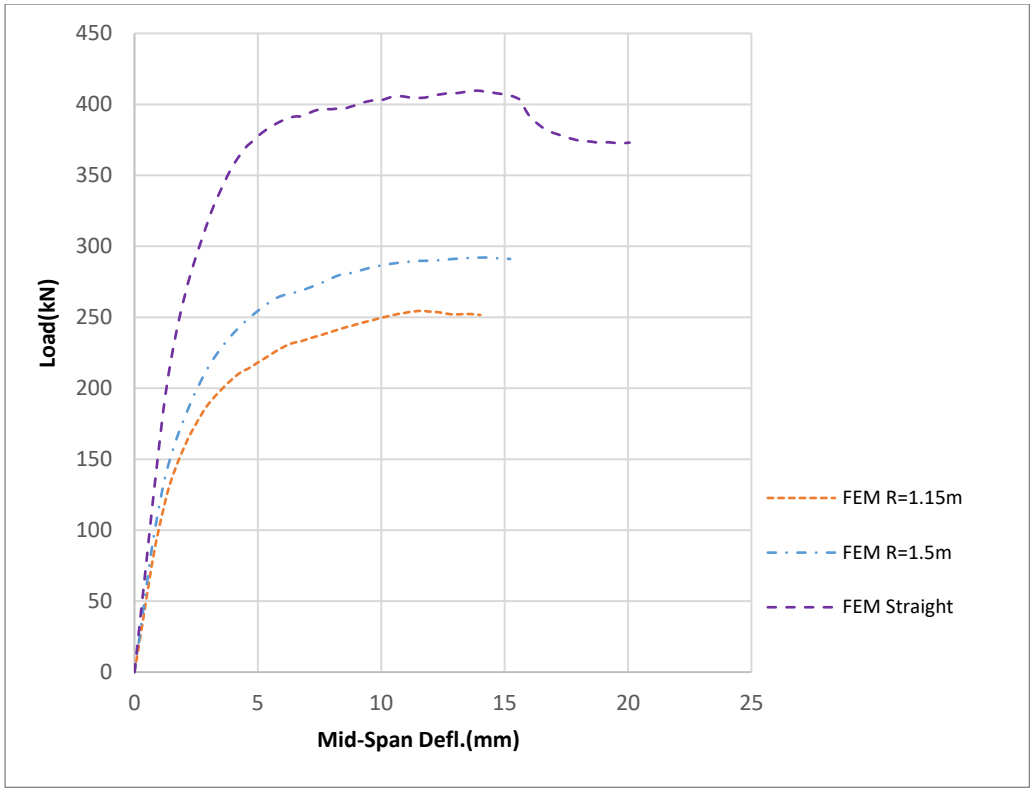

Figure 5.18 Load–Midspan Deflection Curves of FEM for Beams with Transverse Openings at Angle 60°

Table 5.5 Comparison of Effect of Curvature for Beams without Openings by the FE Model.

Beam radius	Numerical cracking load P_{cr} (kN)	Numerical ultimate load Pu (kN)	Variation in the cracking load relative to the (FEM) $CB_1.L_1$(%)	Variation in the ultimate load relative to the (FEM) $CB_1.L_1$(%)
(FEM)$CB_1.L_1$ (R=1.15m)	47	371.6	---	---
Par. (R=1. 5m)	45.12	410.61	-4	10.5
Par. (R= ∞ m)	43.95	443.74	-6.5	19.41

Table 5.6 Comparison of Effect of Curvature for Beams with Transverse Openings at Angle 60° by the FE Model.

Beam radius	Numerical cracking load P_{cr} (kN)	Numerical ultimate load Pu (kN)	Variation in the cracking load relative to the (FEM)$CB_6.T60.L_1$(%)	Variation in the ultimate load relative to the (FEM)$CB_6.T60.L_1$(%)
(FEM)$CB_6.T60.L_1$ (R=1.15m)	44.26	254.56	---	---
Par. (R=1. 5m)	43.82	292	-1	14.7
Par. (R= ∞ m)	44.23	405.78	0	59.4

5.7.3 Effect of RPC Strength

To investigate the influence of using RPC with another compressive strength on behavior of horizontally curved box beam, RPC of 200 MPa were utilized and compared to the finite element result of that of experimental, which 120 MPa. The study carried out on curved beams with transverse and vertical openings at angle 60°. The load- midspan deflection curves of two cases are shown in Figures 5.19 and 5.20. As shown in Tables 5.7 and 5.8, no changes in cracking load for beams with openings and strengthened with RPC of 200 MPa, as a comparison to beams that strengthened using RPC of 120 MPa around openings for both directions. There was a noticeable increase in ultimate load of beams strengthened with RPC of 200 MPa, which was noticed and reported, the percentage of increase was 6.4% for beams with vertical openings and 3.8% for beams with transverse openings, compared to those strengthened with RPC of 120 MPa by the FE Model.

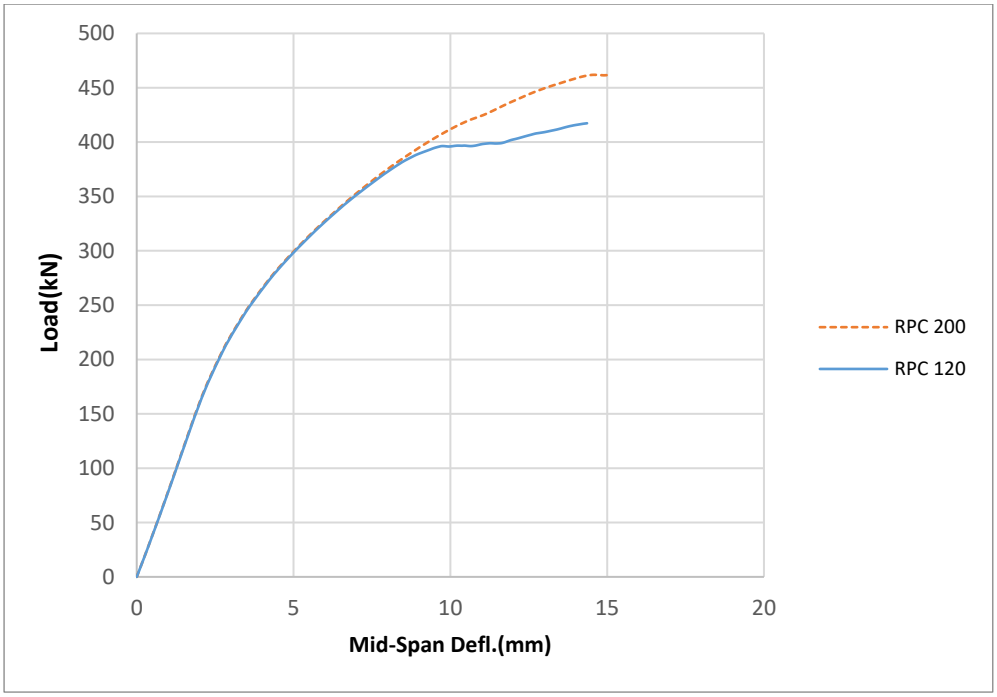

Figure 5.19 Load–Midspan Deflection Curves of FEM for Strengthened Beams with Vertical Openings at angle 60°

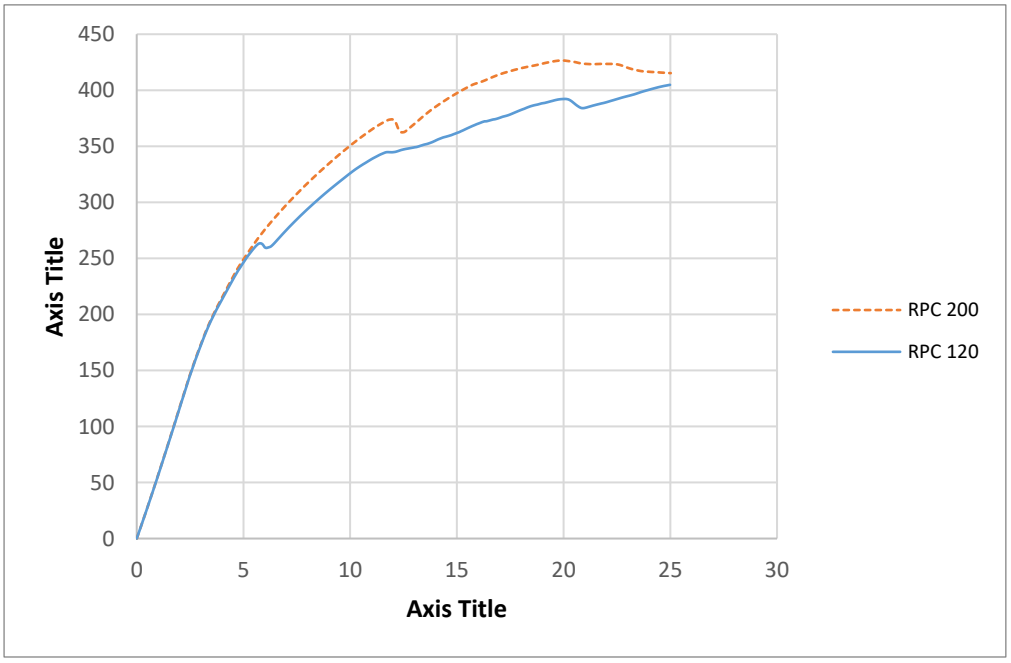

Figure 5.20 Load–Midspan Deflection Curves of FEM for Strengthened Beams with Transverse Openings at angle 60°

Table 5.7 Comparison of Effect of RPC Version for Beams with Vertical Openings by the FE Model.

Beam with RPC Used	Numerical cracking load P_{cr} (kN)	Numerical ultimate load Pu (kN)	Variation in the cracking load (%)	Variation in the ultimate load (%)
RPC 120	58.1	436.9	---	---
RPC 200	58	464.8	0	6.4

Table 5.8 Comparison of Effect of RPC Version for Beams with Transverse Openings by the FE Model.

Beam with RPC Used	Numerical cracking load P_{cr} (kN)	Numerical ultimate load Pu (kN)	Variation in the cracking load	Variation in the ultimate load
RPC 120	64.62	411	---	---
RPC 200	64.8	426.6	0	3.8

CHAPTER SIX

CONCLUSIONS AND RECOMMENDATIONS FOR FURTHER WORK

6.1 General

The essential aim of this work is to gain further about the behavior of horizontally curved reinforced concrete box beams with and without openings. Unstrengthened or strengthened by reactive powder concrete RPC around openings or external strengthened by EBR- CFRP laminates around opening. This study involved an experimental work as well as a nonlinear finite element analysis by (ABAQUS/CAE 2017 in order to forecast the maximum strength and general behavior of the specimens that have been tested. This chapter will provide the experimental and analytical, as well as some suggestions for further investigations.

6.2 Conclusions

The essential summary noticed from each phase of the study (experimental work and modeling of finite element) for horizontally curved reinforced concrete box beam with and without involving of openings, as well as strengthened using reactive powder concrete RPC around openings or external strengthen utilizing EBR- CFRP laminates will be explained in this part, which summarizes the results of a study and benefits:

6.2.1 Experimental Work Conclusions

1- The presence of vertical opening at angle 37° and 82° led to a slight reduction in the ultimate load capacity of the beam by about 5% and 1.5%, respectively.

2- The inclusion of transverse openings at angle 37° and 82° reduced the ultimate load capacity about 1.5% and 18.66%, respectively.
3- The presence of openings in both directions vertical or transverse at angle 60° had higher effect on ultimate load capacity of beam as mentioned in the two previous points, causing a reduction by about 11.5% and 46.4% for vertical and transverse openings, respectively if compared with control beam without opening.
4- The strengthening by reactive powder concrete RPC around openings at angle 60° enhanced the ultimate load carrying capacity about 4.8% and 25.9% for curved beams vertical and transverse opening, respectively, as a comparison with beam without opening, while the ultimate load carrying capacity increased by around 18.5% and 135% for vertical and transverse openings relative to curved beams that unstrengthen, respectively.
5- The external strengthening by EBR- CFRP laminates around opening at angle 60° restored the ultimate load carrying capacity with slight increase for curved box beams with vertical openings if compared with control beam without opening and still less than that for control specimen by 25.9% for curved beams with transverse opening, while the increased of the ultimate load carrying capacity about 15.3% and 38.3% when compared to curved beams with unstrengthened around vertical and transverse opening, respectively.
6- The response of curved beams that subjected to a repeated load was similar to that under monotonic load with a small reduction as a result of fatigue effect.
7- Generally, the mode of failure for specimens that unstrengthened around vertical and transverse opening at angle 37° and 82°was not affected, while at angle 60° was changed from torsional- shear failure

mode of control specimen to frame- type failure at opening zone for both monotonic and repeated load.

8- The mode of failure for specimens that strengthened by reactive powder concrete RPC around openings was changed from frame-type failure at opening to flexural failure mode near midspan, while the specimens that strengthened by external strengthening by EBR-CFRP laminates around opening failed in a manner similar to unstrengthen curved beam which is frame- type failure at opening.

9- Service deformation response in terms of measured mid-span deflection and twisting angle within service stage for all unstrengthened curved beams with opening were adversely effected (increased) when compared with the control beam with a range (5-20.63) % and (0 -18.1) % as a midspan deflection for beams with vertical and transverse opening, respectively, while as twisting angle at mid-span the range was (35-140.65) % and (46.34-335.77) % for beams with vertical and transverse opening, respectively.

10- Service deflection response at mid-span for beams strengthened by reactive powder concrete RPC around openings were decreased about 15.63 % and 6.25 % for beams with vertical and transverse opening, respectively, when compared with the control beam, while as twisting angle at mid-span the reduction was 8.13 % for beam with vertical and an increase 15.44% for beam with transverse opening, relative to the control beam.

11- Service mid-span deflection response for beams strengthened by hybrid EBR-CFRP were increased by about 21.9 % and 11.88 % for beams with vertical and transverse opening, respectively, when compared with the control beam, while the mid-span twisting angle was increased 75.6 % and 130.9% for beams with vertical and transverse opening, respectively.

12- The ductility factor for all unstrengthened curved beams with opening were decreased with a range (13.88-19.62) % and (0.5-13.88) % for beams with vertical and transverse opening, respectively, when compared with the control beam while as twisting angle at mid-span the range was (21.6-103.3) % and (43-234.1) % for beams with vertical and transverse opening, respectively. Furthermore, the ductility factor for strengthened curved box beams by hybrid concrete (reactive powder concrete RPC around openings) and by EBR- CFRP laminates around opening were not show improvement.

13- With regardes to cumulative energy absorption values for beams subjected to repeated load, unstrengthened specimen was decreased by about 74.8% compared with the control, while the cumulative energy absorption values for the strengthened specimens raised by about 28.8% for the first specimen and decreased about 48.44% for the other, but when compared the same strengthened specimens to the unstrengthened circular beam an increase were achieved which approximately 411% and 104%, respectively.

14- Stiffness Criteria for unstrengthened curved beams with openings were adversely effected (decreased) with a range (3.98-14.11) % and (0-33) %, respectively, when compared with the control beam, while for strengthen curved beams by reactive powder concrete RPC around openings showed an increase by about 15.6% and 0.21% for beams with vertical and transverse opening, respectively.

15- Width of major crack at service load for unstrengthen curved beams with vertical and transverse openings increased with a range (118.2-263.63) % and (127.27-263.63) %, respectively, when compared with the control beam, while for strengthened curved beams by reactive powder concrete RPC around openings showed an increase by about 27.27% and 45.4% for beams with vertical and transverse

openings, respectively. As strengthen curved beams by EBR-CFRP showed an increase by about 236.36% and 581.8% for beams with vertical and transverse openings, respectively.

16- The proposed approach for strengthening by reactive powder concrete RPC around openings at angle 60° achieved a beneficial result. The failure mode altered from opening mode to flexural type failure.

17- The method of design proposed for strengthening by EBR- CFRP laminates around opening at angle 60° led to good result, as increase the ultimate load capacity relative to unstrengthened beams.

6.2.2 Finite Element Analysis Conclusions

1- The ABAQUS package's numerical analysis is suitable for horizontally curved box beams with openings that are either unstrengthen or strengthened by hybrid concrete (reactive powder concrete RPC) or by EBR-CFRP laminates. The overall response of load-deformation curves (deflection and twisting) by numerical analysis was comparable to that of experimental curves. The accuracy of the numerical study was verified by a comparison with experimental data, with an average of variance of roughly 5%, 8% and 20% for cracking load, ultimate load and service deflection, respectively.

2- It is observed that the presence of a circular or rectangular openings with area equal to square opening of experiment work in vertical direction led to an approximately same ultimate load by FEM for beam with a square opening at angle 60°, while in the transverse direction the ultimate load was increased slightly for circular opening and a slight decrease for rectangular opening, when compared to the ultimate load of beam with a square opening.

3- The capacity of ultimate load of the curved beam without openings exhibits an increase by decrease the curvature (1/R) for the identical length by approximately (10.5% and 19.41%) for curvature (0.67 and 0.0) if compared to that with (1/R) = 0.87 of experiment, for curved beam with openings increased by about (14.7% and 59.4%) for curvature (0.67 and 0.0).

4- A slight increase in ultimate load of the curved beam with opening at angle 60° for both directions when using RPC with 200 MPa.

6.3 Recommendations for Further Works

1. Examining the response of horizontally curved reinforced concrete box beams with and without opening under effect of reversed cyclic loads and dynamic loads.

2. Investigating the performance of horizontally curved reinforced concrete box beams with several height/radius (h/R) ratios and/or various layout of span (like parabolic or elliptical).

3. Exploring the behavior of horizontally curved reinforced concrete box beams with different cross- sectional shapes (like trapezoidal or rectangular).

4. Experimentally investigate the effect of other types of strengthening on the performance of horizontally curved reinforced concrete box beams with openings (like near surface-mounted NSM bars or internal steel reinforcement).

5. Testing experimentally effect of other types of supports boundary conditions such as (three spans, fixed-fixed, ring beam).

References

ACI Committee 318, (2019).Building Code Requirements for Structural Concrete (ACI 318-19) and Commentary on Building Code Requirements for Structural Concrete (ACI 318R-19), Farmington Hills, Michigan.

ACI Committee 314(2016). Guide to Simplified Design for Reinforced Concrete Buildings (ACI 314R-16), Farmington Hills, Michigan.

AASHTO LRFD Bridge Design Specifications (2010), American Association of State Highway and Transportation Officials, USA, Fifth Edition.

ACI Committee 440 , (2008). Guide for the Design and Construction of Externally Bonded FRP Systems for Strengthening Concrete Structures (ACI 440.2R-08), ACI Manual of Concrete Practice, American Concrete Institute, Farming Hills, U.S.A.

ACI Committee 544, 1996 (Reapproved 2002). Guide for Specifying, Mixing, Placing, and Finishing Steel Fiber Reinforced Concrete (ACI-544.1R-96), American Concrete Institute, Detroit.

Al-Nuaimi, A. S., & Bhatt, P. (2005). 2D Idealisation of Hollow Reinforced Concrete Beams Subjected to Combined Torsion, Bending and Shear. *The Journal of Engineering Research [TJER]*, *2*(1), 53–68.

Al-Zubaidy, H., Al-Mahaidi, R., & Zhao, X.-L. (2013). Finite element modelling of CFRP/steel double strap joints subjected to dynamic tensile loadings. *Composite Structures*, *99*, 48–61.

Alawsh, N. A., & Mehdi, T. H. (2018). Behavior of Reinforced Concrete Hybrid Trapezoidal Box Girders Using Ordinary and Highly Strength Concrete. *Journal of University of Babylon for Engineering Sciences*, *26*(5), 272–278.

Alhamaidah, A. S. M. (2017). *The structural behaviour of horizontally curved prestressed concrete box girder bridges*. University of Salford.

Al-Shimmari, I.K., (2006). Nonlinear Finite Element Analysis of Reinforced Concrete Beam-Column Connection with Interface Element under Cyclic Loading, M.Sc. Thesis, Babylon University, Iraq.

Al-Dolaimy, A.T., (2011) Structural Behavior of Continuous Reinforced Concrete Beams with Openings and Strengthened by CFRP Laminates, M.Sc. Thesis, university of Babylon.

Ali, A Y. (1990). *Behavior of Lap Splices in Reinforced Concrete Beams under Inelastic Cyclic Loads*. M. Sc. Thesis, University of Technology, Iraq, December.

Ali, Ammar Yaser, & Hemzah, S. A. (2014). Nonlinear analysis for behavior of RC horizontally curved ring beams with openings and strengthened by CFRP laminates. *Jordan Journal of Civil Engineering*, *8*(4).

Arendts, J. G. (1969). *Load distribution in simply supported concrete box girder highway bridges*. Iowa State University.

ASTM C1240-04 (2004). Standard specification for the use of silica fume as a mineral admixture in hydraulic cement concrete, mortar and grout, Annual Book of ASTM Standards, American Society for Testing and Material, Vol. 04.02.

ASTM C494-05 (2005). Standard specification for chemical admixtures for concrete, Annual Book of ASTM Standards, American Society for Testing and Material.

ASTM C192/C 192M-05 (2005). Standard practice for makimg and curing concrete test specimens in the labratory, Annual Book of ASTM Standards, American Society for Testing and Material, Vol. 04.02.

ASTM C496-11 (2011). Standard specification for splitting tensile strength of cylindrical concrete specimens, Annual Book of ASTM Standards, American Society for Testing and Material, Vol. 04.02.

ASTM C615/A 615M-15a (2015). Standard specification for deformed and plain steel bars for concrete reinforcement, Annual Book of ASTM Standards, American Society for Testing and Material, Vol. 01.02.

ASTM C39-15a (2015). Standard specification for testing method for compressive strength of cylindrical concrete specimens, Annual Book of ASTM Standards, American Society for Testing and Material, Vol. 04.02.

Aziz, A. H., & Ajeel, A. E. (2010). Effect of existing flange openings and cold joints on strength of RC T-beams. *Journal of Engineering, Collage of Engineering,*

University of Baghdad, Iraq, *16*(1), 4535–4546.

Badawy, H E I, McMullen, A. E., & Jordaan, I. J. (1977). Experimental investigation of the collapse of renforced concrete curved beams. *Magazine of Concrete Research*, *29*(99), 59–69.

Badawy, Hammouda E I, McMullen, A. E., & Jordaan, I. J. (1977). Effect of shear on collapse of curved beams. *Journal of the Structural Division*, *103*(9), 1849–1866.

Barbuta, M., Gavriloaia, C., & Toma, I. O. (2009). Flexural behavior of short reinforced concrete hybrid beams â€“experiment and numerical simulations. *INTERSECTII/INTERSECTIONS*, *6*(4).

Bernard, O., Mivelaz, P., & Brühwiler, E. (1998). Investigation Of The Long Term Behaviour Of Hybrid Concrete Structures. *2nd International Ph. D Symposium in Civil Engineering, Budapest*, 1–8.

BS-1881-116 (1983). Method for determining of compressive strength of concrete cubes, British Standards Institution, London.

Bhagwat, K. K., Kulkarni, D. K., & Cholappanavar, P. (2017). Parametric study on behaviour of box girder bridges using CSi Bridge. *International Research Journal of Engineering and Technology (IRJET) V*, *4*.

Bonneau, O., Lachemi, M., Dallaire, E., Dugat, J., & Aitcin, P.-C. (1997). Mechanical properties and durability of two industrial reactive powder concretes. *Materials Journal*, *94*(4), 286–290.

Burton, K. T. (1965). Influence of Embedded Service Ducts on the Strength of Continuous Reinforced Concrete T-Beams. *Journal Proceedings*, *62*(10), 1327–1344.

Carolin, A. (2003). *Carbon fibre reinforced polymers for strengthening of structural elements*. Luleå tekniska universitet.

Chu, K.-H., & Thelen, A. (1963). Plastic Analysis of Circular Balcony Girders. *Journal of the Structural Division*, *89*(6), 159–186.

Carvalho Silva, Ricardo José, Antonio Edson de Araújo Pontes, and Rodrigo Farias da

Silva. Experimental Analysis of Reinforced Concrete Beams with Vertical Holes, *South American Journal of Structural Engineering* ASAEE, v. 13, n. 1, PP. 21-41, jan./jun. 2016

Daud, R. A. (2015). *Behaviour of reinforced concrete slabs strengthened externally with two-way FRP sheets subjected to cyclic loads*. The University of Manchester (United Kingdom).

Dawood, M. B., & Al-Jazaeri, R. A. (2014). Shear Behavior of Reinforced ConcreteT-Beams with Openings in Flange and Strengthened by CFRPLaminates. *Journal of Babylon University/Engineering Sciences*, *22*(2).

De Larrard, F., Belloc, A., Renwez, S., & Boulay, C. (1994). Is the cube test suitable for high performance concrete? *Materials and Structures*, *27*(10), 580–583.

el Ali, A. A. (2011). *EXPERIMENTAL AND THEORITICAL INVESTIGATION FOR BEHAVIOR OF CONCRETE DEEP BEAMS REINFORCED WITH CFRP BARS FAILING IN SHEAR*. BASRAH UNIVERSITY.

European federation of specialist construction chemicals and concrete systems (EFNARC), the European Guidelines for Self- Compacting Concrete; Specification, Production and Use, (2005) 1-68

Faggiani, A., & Falzon, B. G. (2010). Predicting low-velocity impact damage on a stiffened composite panel. *Composites Part A: Applied Science and Manufacturing*, *41*(6), 737–749.

Falzon, B. G., Hitchings, D., & Besant, T. (1999). Fracture mechanics using a 3D composite element. *Composite Structures*, *45*(1), 29–39.

Galal, K., & Yang, Q. (2009). Experimental and analytical behavior of haunched thin-walled RC girders and box girders. *Thin-Walled Structures*, *47*(2), 202–218.

Goodier, C. I. (2003). Development of self-compacting concrete. *Proceedings of the Institution of Civil Engineers-Structures and Buildings*, *156*(4), 405–414.

Gupta, P. K., Singh, K. K., & Mishra, A. (2010). *Parametric study on behaviour of box-girder bridges using finite element method*.

Habeeb, G. M., Dawood, M. B., & Adheem, A. H. (n.d.). *FLEXURAL BEHAVIOR OF PRECAST-PRESTRESSED CONCRETE BEAM WITH REACTIVE POWDER CONCRETE SLAB.*

Hamzah, A. S., & Ali, A. Y. (2020). *SHEAR BEHAVIOR OF REINFORCED CONCRETE BEAMS WITH VERTICAL AND TRANSVERSE OPENINGS*.

Hanson, J. M. (1969). Square openings in webs of continuous joists. *Portland Cement Assoc R & D Lab Bull*.

Hasnat, A., & Akhtanizzamam, A. A. (1987). Beams with small rectangular opening under torsion, bending, and shear. *Journal of Structural Engineering*, *113*(10), 2253–2270.

Hwang, S.-D., Khayat, K. H., & Bonneau, O. (2006). Performance-based specifications of self-consolidating concrete used in structural applications. *ACI Materials Journal*, *103*(2), 121.

Hawas, M. A. Behavior of Reinforced Concrete Box Girder Using Polymer Reinforced Fiber Strengthening, MSc Thesis, 2015

Jabbar, S., Hejazi, F., & Mahmod, H. M. (2016). Effect of an opening on reinforced concrete hollow beam web under torsional, flexural, and cyclic loadings. *Latin American Journal of Solids and Structures*, *13*, 1576–1595.

Jordaan, I. J., Khalifa, M. M. A., & McMullen, A. E. (1974). Collapse of curved reinforced concrete beams. *Journal of the Structural Division*, *100*(11), 2255–2269.

Karataş, M. A., & Gökkaya, H. (2018). A review on machinability of carbon fiber reinforced polymer (CFRP) and glass fiber reinforced polymer (GFRP) composite materials. *Defence Technology*, *14*(4), 318–326.

Kurian, B., & Menon, D. (2007). Estimation of collapse load of single-cell concrete box-girder bridges. *Journal of Bridge Engineering*, *12*(4), 518–526.

Lahlou, K., Aitcin, P. C., & Chaallal, O. (1992). Behaviour of high-strength concrete under confined stresses. *Cement and Concrete Composites*, *14*(3).

Luo, Q. Z., Tang, J., & Li, Q. S. (2003). Calculation of moments on top slab in single-cell box girders. *Journal of Structural Engineering*, *129*(1), 130–134.

Mansur, M A. (1992). Deflections of reinforced concrete beams with web openings. *ACI Structural Journal*.

Mansur, M A. (1998). Effect of openings on the behaviour and strength of R/C beams in shear. *Cement and Concrete Composites*, *20*(6), 477–486.

Mansur, M A. (2006). Design of reinforced concrete beams with web openings. *Proceedings of the 6th Asia-Pacific Structural Engineering and Construction Conference (ASPEC 2006)*, 5–6.

Mansur, M A, Lee, Y. F., Tan, K. H., & Lee, S. L. (1991). Tests on RC continuous beams with openings. *Journal of Structural Engineering*, *117*(6), 1593–1606.

Mansur, M A, & Paramasivam, P. (1984). Reinforced concrete beams with small opening in bending and torsion. *Journal Proceedings*, *81*(2), 180–185.

Mansur, M A, & Tan, K.-H. (1999). *Concrete beams with openings: analysis and design* (Vol. 20). CRC Press.

Mansur, M A, Tan, K.-H., & Wei, W. (1999). Effects of creating an opening in existing beams. *Structural Journal*, *96*(6), 899–905.

Mansur, M Abdul, & Hasnat, A. (1979). Concrete beams with small opening under torsion. *Journal of the Structural Division*, *105*(11), 2433–2447.

Mansur, Mohammad A, Ting, S. K., & Lee, S.-L. (1983). Torsion tests of r/c beams with large openings. *Journal of Structural Engineering*, *109*(8), 1780–1791.

Mansur, Mohammed A, Tan, K. H., & Lee, S. L. (1985). Design method for reinforced concrete beams with large openings. *Journal Proceedings*, *82*(4), 517–524.

Maroliya, M. K. (2012). State of Art-on Development of Reactive Powder Concrete. *International Journal of Innovative Research and Development (ISSN 2278–0211)*, *1*(8), 493–503.

Mazzolani, F. M. (2001). *The Use of FRP Materila for THE Seismic Upgrading of Existing RC Structurs*.

Metwally, I. M. (2014). Nonlinear analysis of concrete deep beam reinforced with gfrp bars using finite element method. *Malaysian Journal of Civil Engineering*, *26*(2).

Muthuswamy, K. R., & Thirugnanam, G. S. (2014). Structural behaviour of hybrid fibre reinforced concrete exterior Beam-Column joint subjected to cyclic loading. *International Journal of Civil & Structural Engineering*, *4*(3), 262–273.

Mohsen, K., Mohd, Z.J., and Payam, S. An Experimental Study on Shear Reinforcement in RC Beams Using CFRP-bars, *Scientific Research and Essays* Vol. 6, No. 16, 19 August, 2011, pp. 3447-3460

Nasser, K. W., Acavalos, A., & Daniel, H. R. (1967). Behavior and design of large openings in reinforced concrete beams. *Journal Proceedings*, *64*(1), 25–33.

O'Neil, E. F., Dauriac, C. E., & Gilliland, S. K. (1997). Development of reactive powder concrete (RPC) products in the United States construction market. *Special Publication*, *167*, 249–262.

Parashar, A., Aggarwal, P., Saini, B., Aggarwal, Y., & Bishnoi, S. (2020). Study on performance enhancement of self-compacting concrete incorporating waste foundry sand. *Construction and Building Materials*, *251*, 118875.

Paultre, P., Khayat, K. H., Cusson, D., & Tremblay, S. (2005). Structural performance of self-consolidating concrete used in confined concrete columns. *ACI Structural Journal*, *102*(4), 560–568.

Rajaram, P., Murugesan, A., & Thirugnanam, G. S. (2010). Experimental Study on behavior of interior RC beam column joints subjected to cyclic loading. *International Journal of Applied Engineering Research*, *1*(1), 49.

Ramadan, O. M., Metwally, K. G., & Shaban, W. M. (2015). Proposed recommendations for the design of reinforced concrete beams with openings. *World Congress on Advanced in Structural Engineering and Mechanics (NSEN15) Incheon, Korea*.

Rathod, A. P., & Vora, T. P. (2015). Fiber reinforced polymer reinforcement for construction-state of the art review. *Stress (Mpa)*, *276*, 517.

Richard, P., & Cheyrezy, M. (1995). Composition of reactive powder concretes. *Cement*

and Concrete Research, *25*(7), 1501–1511.

Russell, H. G., Graybeal, B. A., & Russell, H. G. (2013). *Ultra-high performance concrete: A state-of-the-art report for the bridge community*. United States. Federal Highway Administration. Office of Infrastructure ….

Sadrekarimi, A. (2004). Development of a light weight reactive powder concrete. *Journal of Advanced Concrete Technology*, *2*(3), 409–417.

Saksena, N. H., & Patel, P. (2013). Experimental study of reinforced concrete beam with web openings. *International Journal of Advanced Engineering Research and Studies-India*, *2*(3), 66–68.

Sasidharan, N. P., & Johny, B. (2015). Finite element analysis and parametric study of curved concrete box girder using Abaqus software. *International Journal of Research in Enginnering and Technology*, *4*(10), 425–429.

Scordelis, A. C., Wasti, S. T., & Seible, F. (1982). Structural response of skew RC box girder bridge. *Journal of the Structural Division*, *108*(1), 89–104.

Seible, F., & Scordelis, A. C. (1983). Nonlinear analysis of multi-cell reinforced concrete box girder bridges. *Engineering Structures*, *5*(1), 45–57.

Somes, N. F., & Corley, W. G. (1974). Circular openings in webs of continuous beams. *Special Publication*, *42*, 359–398.

Spence, R. J. S., & Morley, C. T. (1975). The strength of single-cell concrete box girders of deformable cross-section. *Proceedings of the Institution of Civil Engineers*, *59*(4), 743–761.

Subramani, T., Subramani, M., & Prasath, K. (2014). Analysis of three dimensional horizontal reinforced concrete curved beam using Ansys. *International Journal of Engineering Research and Applications*, *4*(6), 156–161.

ISIS. Reinforced Concrete Structures with Fiber Reinforced Polymers, ISIS Design Manual No. 3, Version 2, Manitoba, Canada: ISIS Canada Corporation, 2007

Tan, K.-H., & Mansur, M. A. (1996). Design procedure for reinforced concrete beams with large web openings. *Structural Journal*, *93*(4), 404–411.

Tan, K.-H., Mansur, M. A., & Huang, L.-M. (1996). Reinforced concrete T-beams with large web openings in positive and negative moment regions. *Structural Journal*, *93*(3), 277–289.

Vedenoja, K. (2017). *The assessment of openings in existing load bearing concrete structures*.

Wu, Y. (2015). *Shear strengthening of single web prestressed hollow core slabs using externally bonded FRP sheets*.

Yen, B. T., Kim, D., & Wilson, J. L. (2006). Evaluation of Displacements and Stresses in Horizontally Curved Beams. *Evaluation*, *2*, 1–2006.

Appendix A
INTRODUCTION

A.1 Mode of Failure

Mode 1 failure

Figure A.1, illustrate the assumed failure surface for mode 1 together with the internal forces developed in steel reinforcement. The skewed compression zone in this mode is assumed at the top of the beam. After some modification, assumptions and derivations, the strength in failure mode 1 due to the applied vectors **M**, **T**, and **V** acting at the midsection of the opening **(Hasnat & Akhtanizzamam, 1987)**, is obtained by the following quadratic equation, and denoted by **T1**:

$$T_1 = \frac{M_{O1} K_1}{\Delta} \left(\sqrt{\frac{1}{K_1} + \frac{1}{(\psi\Delta)^2}} - \frac{1}{\psi\Delta} \right) \qquad \text{..... A.1}$$

where $\psi = T/M$, $\lambda = M/V$,

$$K_1 = \frac{1}{1 + 2\alpha} \left(\frac{Aw \, . fyw}{s} \frac{X_1 Y_1}{M_{O1}} \right)$$

and

$$\Delta = 1 + \frac{\mu}{\psi\lambda}$$

where:

$$\mu = \frac{b^2 + bh}{2b + 4h}$$

$\alpha = h / b$

$\mathbf{x_1}$ is the width of stirrups

$\mathbf{A_w}$ is the area of one leg of the stirrups

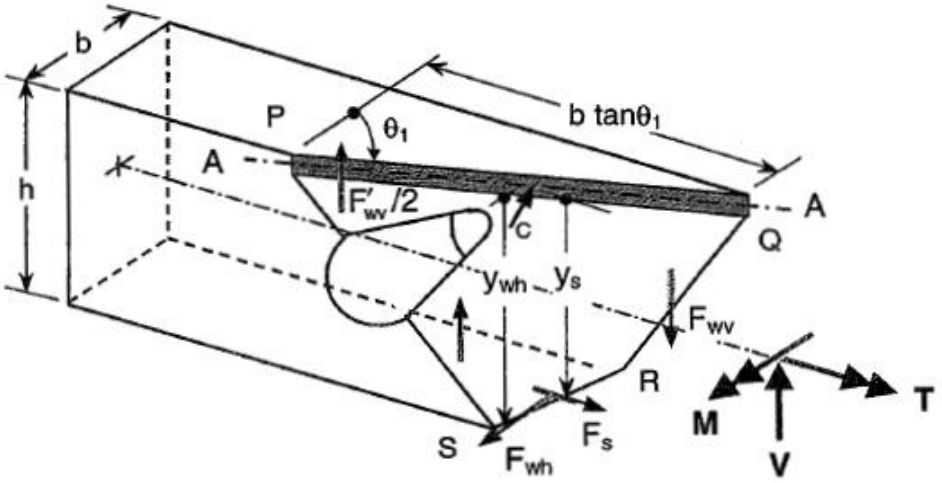

Figure (A.1) Mode 1 failure surface for beams with a small opening **(Mansur & Tan, 1999)**

Mode 2 failure

Figure A.2 illustrate the failure surface for this mode. In this failure mode, a skewed compression zone is located along a lateral side of the beam. After some modification, assumptions and derivations, the strength equation for Mode 2 is obtained by the following equation and denoted by **T2.**

$$T_2 = \frac{M_{01}}{1+\delta}\sqrt{R_2 . K_2} \quad \ldots\ldots\ldots\ldots\ldots\ldots\ldots\ldots\ldots\ldots\ldots\ldots \quad \text{A.2}$$

Where, $\delta = x_1 .V/2T$, $R_2 = M_{O2}/M_{O1}$, and

$K_2 = \frac{1}{1+\frac{2}{\alpha}} \left(\frac{Aw . fyw}{s} \frac{x_1 y_1}{M_{O1}}\right)$

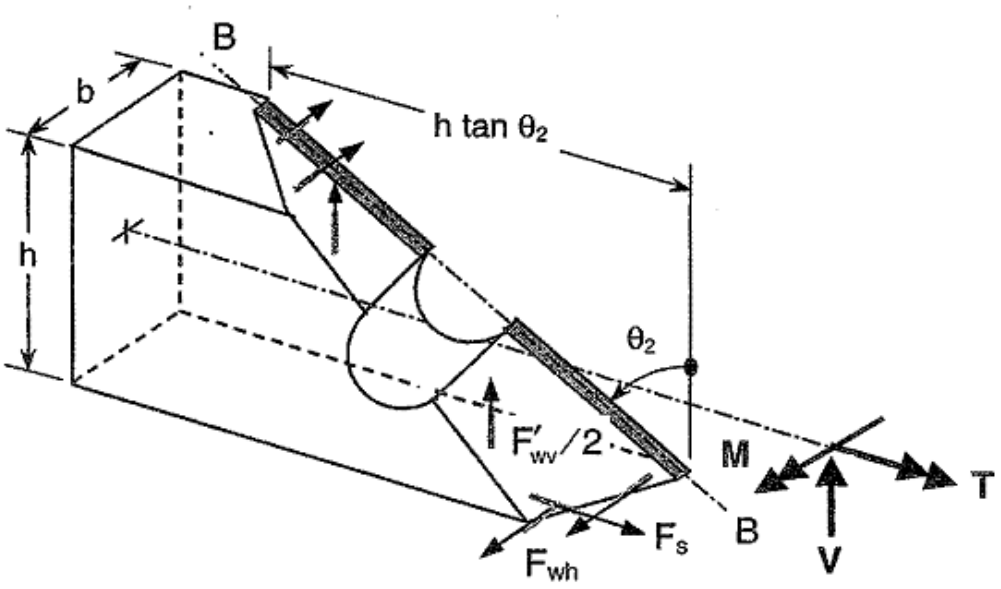

Figure (A.2) Mode 2 failure surface for beams with a small opening **(Mansur & Tan, 1999)**

Mode 3 failure

The analysis in this mode is selfsame for mode 1, except that the skewed compression zone is at the bottom instead of at the top see figure A.1. The equations for mode 1 can be employed to derive the equations for Mode 3 by twirling the beam upside down and taking M = -M, V = -V. After some modification and assumptions, the strength equation for mode 3 is obtained by the following equation and denoted by **T3**.

$$T_3 = \frac{2M_{O1}.K_1}{\Delta'}\left(\frac{1}{\psi\Delta'} - \sqrt{\frac{R_3}{K_1} + \frac{1}{(\psi\Delta')^2}}\right) \quad \text{..... A.3}$$

Where, $R_3 = M_{O3}/M_{O1}$, and $\Delta' = \mu/(\psi.\lambda) - 1$

M_{O3} : Pure flexural strength in negative bending.

Mode 4 failure

The three modes of failure described above, which can be considered a flexural type of torsional failure, usually occur when the beam contains adequate stirrups such that the main steel yields, and the full flexural strength of the beam is reached when loaded to failure.

But, when beams containing inadequate stirrups, the concrete compression zone may shear through prior to yielding of the main steel and this will precipitate failure at a load below the corresponding flexural failure load. This type of failure may be called shear-compression mode of failure. A detailed analysis to predict the strength of the beam failing in this mode is rather too complex for practical use and is hardly justified because of the limited test data available. For beams without an opening, it was found empirically **(Collins et al., 1968)** that the possibility of a shear type failure could be checked in a single step by introducing an "equivalent shear" V_{eq}", as given by A.4.

$$V_{eq} = V_u + \frac{1.6}{B} T_u \quad \text{A.4}$$

Where, ***Vu*** and ***Tu*** are the factored shear and torsion, respectively, at the section under consideration and B width of section. The shear compression strength of the beam can then be evaluated by means of the shear strength equation for a section using ***Veq*** instead of ***Vu*** to account for torsional effects. This procedure has been found to give results well on the conservative side.

A similar equation has been proposed by **(Hasnat & Akhtanizzamam, 1987)** to evaluate the shear compression strength of a beam containing a small opening. It is given as:

$$V_{eq} = V_u + \frac{1.2}{B} T_u \quad \text{A.5}$$

A.2 Design for Beam Type Failure

• Mode 1 failure

In a design situation, the factored bending moment, torsional moment, and the shear force at the center of the opening are known. Thus, M = Mu, T = Tu, and V = Vu. Designating the equivalent moment due to torsion and shear in Mode 1 failure $M_{eq\,(1)}$, that is:

$$M_{eq(1)} = (T + V_u \mu)\sqrt{1 + 2\alpha} \quad \text{A.6}$$

the required strength in positive bending becomes (M_{o1})

M_{o1} = $M_{eq\,(1)}$ + Mu A.7

The designer chooses a value of (α=h/b) if the sectional dimensions are not given or known in advance, evaluates $M_{eq\,(1)}$, and then finds the value of M_{o1}. The section and the longitudinal reinforcement must be designed for this moment using the normal flexural design procedure. The transverse reinforcement is obtained from Eq. (A.8).

$$\frac{Aw}{s} = \frac{1}{\emptyset}\left[\frac{M_{eq(1)}}{4X_1Y_1fyw}\right] \quad \text{..... A.8}$$

• Mode 2 failure

According to the Australian Code (1974), and after some substitutions yields:

M_{o2} = $M_{eq\,(2)}$ A.9

Where: $M_{eq\,(2)}$, the equivalent moment due to shear and torsion for Mode 2 failure, is given by:

$M_{eq(2)}$= Tu + Vu $\frac{x1}{2}$ A.10

AS 1480-197 4 suggests that if Mu < 0.5 $M_{eq\,(2)}$, the cross section of the beam and the area of longitudinal reinforcement should be such that the beam can withstand an equivalent bending moment, $M_{eq\,(2)}$, as given above in lateral bending. Also, the area of web steel should not be less than that given by:

$$\frac{Aw}{s} = \frac{1}{\emptyset}\left[\frac{M_{eq(2)}}{4X_1Y_1fyw}\right] \quad \text{..... A.11}$$

• Mode 3 failure

According to the Australian Code (1974), and after some substitutions yields:

M_{o3} = $M_{eq\,(3)}$ – Mu A.12

Where:

$M_{eq(3)}$ =$(Tu + Vu\,\mu)\sqrt{1+2\alpha}$ A.13

$M_{eq\,(3)}$ is the equivalent moment due to torsion and shear in mode 3 failure. Thus, if the numerical value of Mu is greater than $M_{eq(3)}$, there is no possibility of a mode 3 failure. Physically it means that any tensile stress at the top of the beam induced by $M_{eq(3)}$ is canceled by the compression due to Mu. No top steel is, therefore, required. However, nominal steel comprising at least one bar at each of the top two corners must be provided for anchorage of stirrups.

If $Mu < M_{eq\,(3)}$, there will be residual tension at the top of the beam, and top steel should be introduced according to the usual flexural theory to withstand a negative bending (that is, one of opposite sign to Mu) of magnitude ($M_{eq\,(3)}$ -Mu).

• Mode 4 failure

Similar to the Australian Code (1974) approach, Eq. (2.69) may be used to preclude a shear-compression mode of failure of a beam containing a small opening. Thus, the equivalent shear for this mode is calculated as:

$$V_{eq} = Vu + \frac{1.6}{B} Tu \qquad \text{..... A.14}$$

The transverse reinforcement is then designed to resist this equivalent shear on the basis of the normal shear design provisions by assuming that the failure plane passes through the center of opening. If the steel area, Aw, thus determined is greater than that already found during the previous design steps, the larger quantity should be adopted.

References

Hasnat, A., & Akhtanizzamam, A. A. (1987). Beams with small rectangular opening under torsion, bending, and shear. *Journal of Structural Engineering*, *113*(10), 2253–2270.

Mansur, M. A., & Tan, K.-H. (1999). *Concrete beams with openings: analysis and design* (Vol. 20). CRC Press.

Appendix B
ANALYSIS OF REINFORCED CONCRETE BEAMS

B.1Analytical Solution of Semicircular Curved Box Beam (Control Beam)

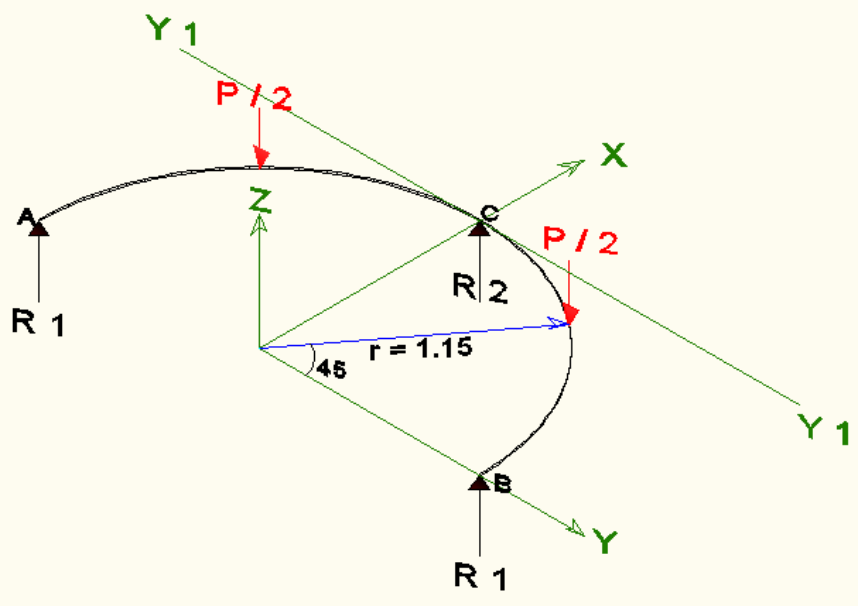

Figure (B.1) Semicircular Curved Beam Loading and Forces

As in Figure B.1, Radius of Semicircular Curved box Beam = r =1.15

Applied Load = $\frac{P}{2}$ …… for each midspan

Reaction at A , $R_a = R_b = R1$

Reaction at C, $R_C = R2$

Taking moment of forces about y_1-y_1 axis (through support C):

(Direction of θ start from exterior support toward interior support for each span)

$2 \times R1 \times r = 2 \times p/2 \, (r - r \times \sin(45))$

$R_a = R_b = R1 = 0.14645\ p$

$\Sigma Fy = 0$

$R_C = R2 = 0.7071\ p$

By taking a section before and after the applied load we can find the shear, bending
moment and torque equations.

- **Shear, Moment and Torsion calculation**

1. For $\theta < 45$

$V = 0.14645\ p$

$M(\theta) = 0.14645p \times r \times \sin(\theta)$

$T(\theta) = 0.14645\ p \times r(1-\cos(\theta))$

2. For $45 < \theta < 90$

$V = 0.14645p - 0.5\ p = -0.35355p$

$M(\theta) = 0.14645p \times r \times \sin(\theta) - 0.5p \times (r \times \sin(\theta-45))$

$T(\theta) = 0.14645p \times r(1-\cos(\theta)) - 0.5p \times r \times (1-\cos(\theta-45))$

The shear force, bending moment and torque diagrams could be drawn as shown below in Figures B.2, B.3 and B.4, respectively.

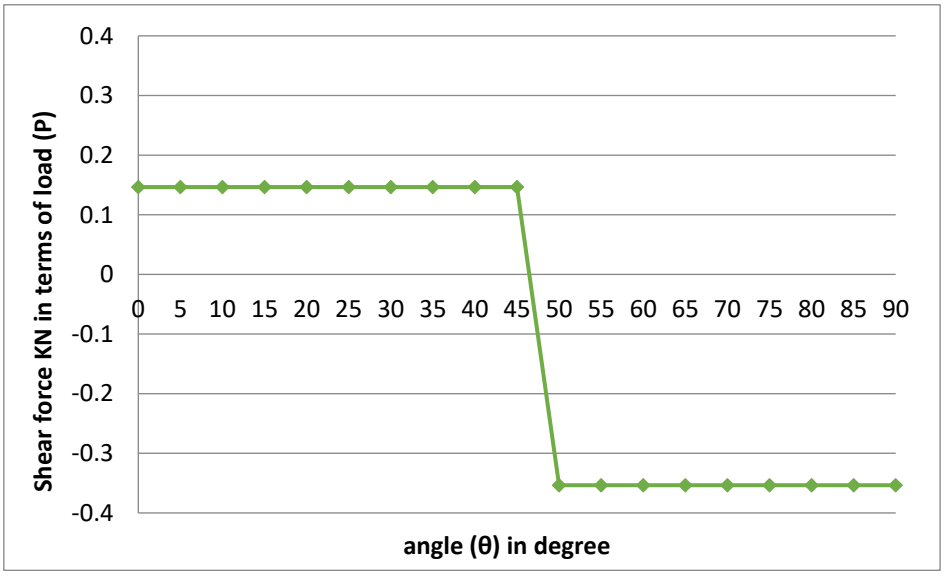

Figure (B.2) shear force diagram of semicircular beam

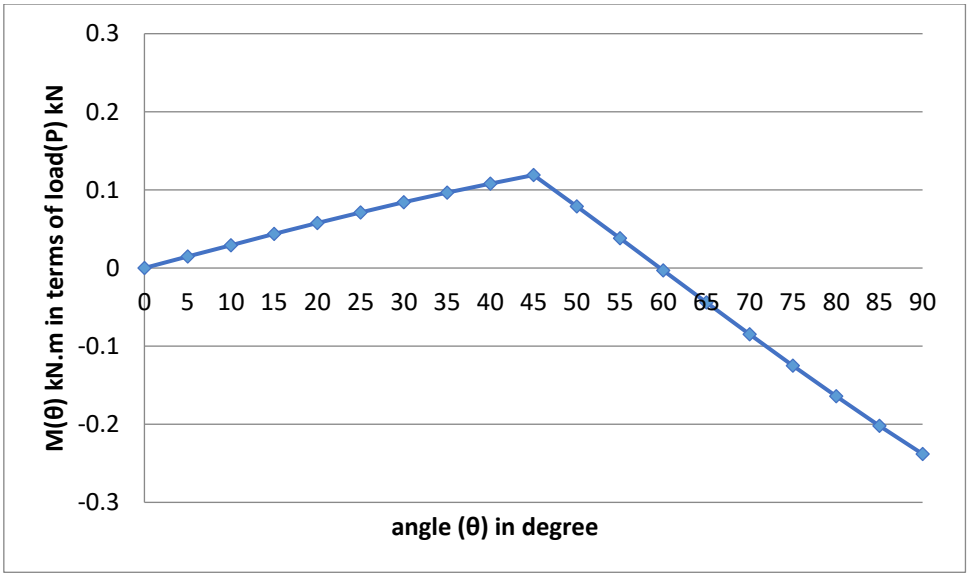

Figure (B.3) Moment diagram of semicircular beam

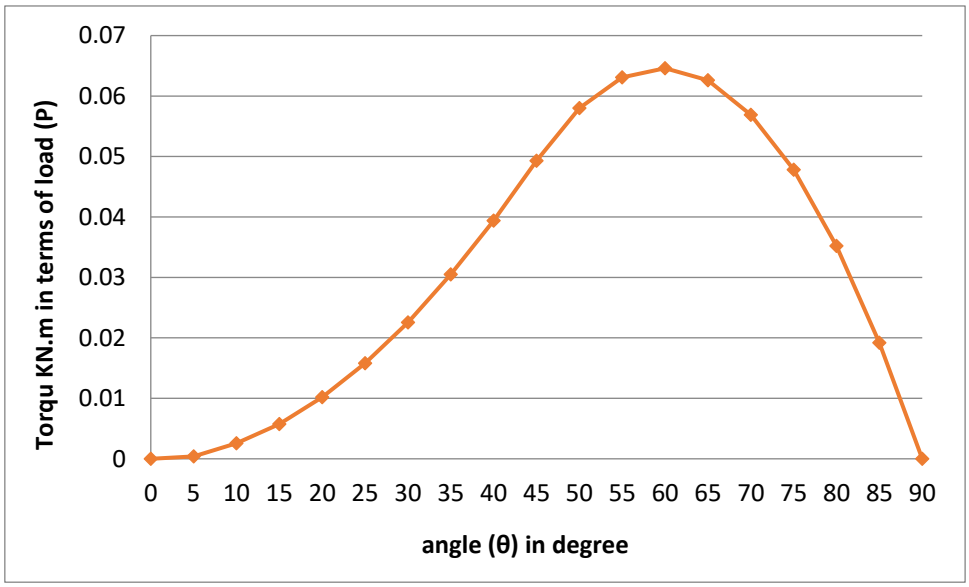

Figure (B.4) Torque diagram of semicircular beam

B.2Calculation for Control Beam

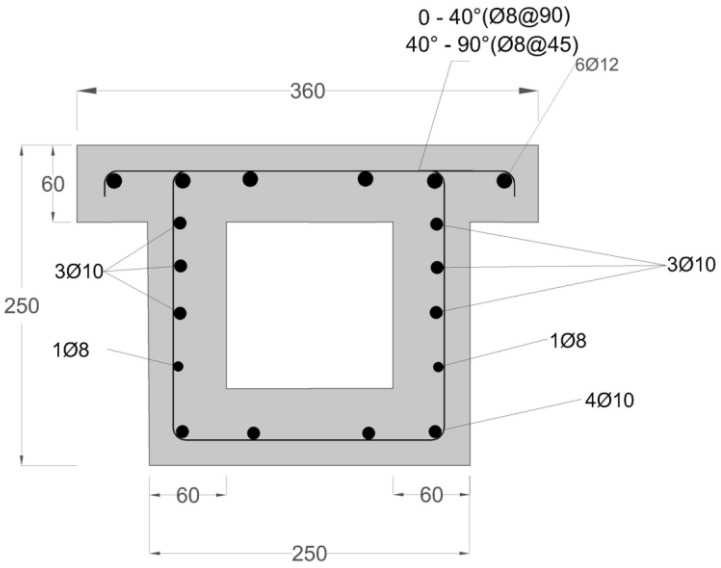

Figure (B.5) Cross Section and Reinforcement

fc'= 35 Mpa

fy = 550 Mpa

For Positive Moment

As= 4*78.5 =314mm2

$A_{comp.}$ = As fy/0.85 fc'= 5805 mm^2

A_{flang} = 360 × 60 =21600> $A_{comp.}$

Work as rectangular section

a= 5805 / 360 = 16.125mm

C= 16.125/0.85=18.97 mm

C_b= (600/600+ fy) × d=113.2 mm

C_b > C, so tension failure will occur fs= fy

$C_{max.}$=3/7 d =3/7×217=93 > C (single reinforcement)

ρ= As/bd = 314/(360×217) = 0.004 > ρ_{min} .=1.4/ fy =0.0025

$Mu^+ = \phi.\rho.b.d^2.fy(1-0.59\rho.fy/fc')$

$Mu^+=0.9\times0.004\times360\times217^2\times550(1-0.59\times 0.004\times(550/35))$

Mu^{+} = 32.32kN.m

For Negative Moment

As= 6*113 =678mm^2

$A_{comp.}$ = As fy/0.85 fc'= 12534.45 mm^2

A_{flang} = 250 × 60 =15000> $A_{comp.}$

Work as rectangular section

a= 12534.45 / 250 = 50.14mm

C= 50.14/0.85=58.98 mm

C_b= (600/600+ fy) × d=113.2 mm

C_b > C, so tension failure will occur fs= fy

$C_{max.}$=3/7 d =3/7×217=93 > C (single reinforcement)

ρ= As/bd = 678/(250×217) = 0.0125 < ρ_{max}=0.0185 =$0.85\beta_1\frac{f'_c}{f_y}\frac{\varepsilon_{cu}}{\varepsilon_{cu}+0.004}$, β_1=0.8 for fc'= 35

, ε_{cu} =0.003

Mu^{-} =ϕ.ρ.b.d^2.fy(1-0.59ρ.fy/fc')

Mu^{-}=0.9×0.0125×250×217^2×550(1-0.59× 0.0125×(550/35))

Mu^{-} = 64.4 kN.m

From bending moment diagram

Mu^{+} = 0.12 P = 32.32 ⟹ $P^{+}_{flexural}$ =269 kN

Mu^{-} = 0.235P =0.235(269)= 63.3kN.m ≈ 64.4 kN.m

For sequence of failure increase **P** by 10% = 269×1.1= 296 kN

From Shear Force Diagram we have

Vu= 0.35 P

Therefore, V= 0.35 × 296 = 103.6 kN

Vc= ϕ× 0.17×$\sqrt{fc'}$ ×b×d

Vc = 0.75× 0.17×$\sqrt{35}$×120×217/1000 = 19.64 kN

$V > \varphi Vc$

Shear reinforcement is required

$V = \varphi\ Vc + Vs$

$Vs = 103.6 – 19.64 = 83.96$ kN

$\frac{Av}{s} = \frac{83.96 \times 1000}{420 \times 217} = 0.92$

From Torque Diagram we have

$Tu = 0.0646\ P$

Therefore, $Tu = 0.0646 \times 296 = 19.12$ kN.m

The section properties as required from ACI code -318 are :

$A_g = 52200$ mm^2 (for hollow section, A_g is the area of concrete only) ACI

$A_{cp} = 69100$ mm^2

$P_{cp} = 1220$ mm

$A_{oh} = 202 \times 202 = 40804$ mm^2

$P_{oh} = 808$ mm

$A_o = 0.85\ A_{oh} = 34683.4$ mm^2

$T_{th} = 0.083\lambda \sqrt{fc'}\ \frac{A_g^2}{P_{cp}}$, $\lambda = 1$ for normal weight concrete

$T_{th} = 0.083 \times 1 \times \sqrt{35}\ \frac{52200^2}{1220} = 1.09$ kN.m $<$ T = 19.12 kN.m

$\frac{At}{s} = \frac{Tu}{2 \times Ao \times fy \times \cot\theta}$, assumed $\theta = 45$, (ACI318-19)

$\frac{At}{s} = \frac{19.12 \times 10^6}{2 \times 34683.4 \times 420 \times 1} = 0.65$

Based on the typical two-leg stirrup, this may be expressed as

$\frac{A_{(V+t)}}{s} = \frac{Av}{s} + 2(\frac{At}{s})$

$\frac{A_{(V+t)}}{s} = 0.92 + (2 \times 0.65) = 2.22$

Assume ϕ 8 mm stirrups $A_V = 50.26 * 2 = 100.52$ mm^2

S= $\frac{100.52}{2.22}$ =45.3, for torsion S_{max}= the lesser of (*Ph*/8=101 ,300) (ACI318-19)

Therefore, use ϕ 8 mm stirrups @ 45 mm

$Al = \frac{At}{s} \times Ph \times \frac{f_{yt}}{f_y} \times \cot^2\theta$= 0.65× 808× 1 × 1 =525.2 mm^2

Use (6 ϕ 10 +2 ϕ 8) =571.52mm^2 , longitudinal reinforcement for torsion

From Shear and Torque Diagram, for Region from(0 to 40°) and from (140° to 180°) we have

Vu= 0.14645 P and Tu= 0.0394 P , P= 296 kN

Vu=43.35 kN

Tu= 11.66 kN.m

$\frac{Av}{s} = \frac{(43.35-19.64)\times 1000}{420\times 217}$ = 0.26

$\frac{At}{s} = \frac{11.66\times 10^6}{2\times 34683.4\times 420\times 1} = 0.4$

$\frac{A_{(V+t)}}{s}$ = 0.26+ (2×0.4) =1.06

S= $\frac{100.52}{1.06}$ =94.83 mm , use ϕ 8 mm stirrups @ 90 mm

B.3 Design of EBR-CFRP Laminate for Strengthening of Circular Curved Beams with Opening

B.3.1 Transverse Opening (θ=60°)

Dimension of opening = (80 × 80) mm

P= 300 kN

Vu (at center of opening) = 106.065 kN

Mu (at center of opening) = 0 kN.m

Tu (at center of opening) = 19.38 kN.m

Beam Type Failure

1- Torsion

$x_o = y_0$ =250-(2×20) - (2×4) = 202 mm

$T_n=\sum_{i=1}^{4} T_i = T_u=\frac{2A_{oh}A_t f_{yt}}{s}\cos\theta$, $30< \theta <60$, $\theta= 45$ 11.82×10^6

$\frac{A_t}{s} =\frac{19.38\times10^6}{4\times40804\times3900} \times1= 0.03$ mm²/mm

s=50×0.17/0.03=283 mm, this is too mach spacing, check shear requirement.

2-Shear

$V_c = \frac{1}{6}\sqrt{f_c'}\, b_w(d-d_0)$

$V_c = \frac{1}{6}\sqrt{40} \times 120 \times (217-80) \times 10^{-3} = 17.33$ KN

$V_f = Vu - V_c$

$V_f = 106.065 - 17.33 = 88.735$ KN

$Af = \frac{88.735\times1000}{3900} = 22.75$mm²

$bf = \frac{Af}{0.17} = \frac{23}{0.17} = 135.3$ mm

use *bf* =100 mm U wrapping full depth stirrup on each side of opening, which will satisfy torsional requirement too.

Frame Type Failure

Design of bottom chord

1-*Vertical shear*

Assume identical sections

Vu= 0.5× 106.065 =53

$V_c = \frac{1}{6}\sqrt{40} \times 120 \times (85) + \frac{1}{6}\sqrt{40} \times 130 \times (60) = 18.97$ kN

$V_f = 53 - 18.97 = 34.03$ KN

$Af = \frac{34.03\times1000}{3900} = 8.73$mm²

$bf = \frac{Af/2}{0.17} = \frac{8.73/2}{0.17}$ = 25.68 mm

2-*Lateral shear*

Vuz= $\frac{T_u}{(e_t+e_{b)}}$, $(e_t+e_b) = 250 - 2 \times (20 + 8 + 6) = 182$mm

Vuz = $\frac{19.38}{0.182}$ = 106.48 kN

$V_c = \frac{1}{6}\sqrt{40} \times 60 \times 217 \times 10^{-3}$ = 13.72 KN

V_f = Vuz - V_c = 106.48 -13.72=92.75 KN

$Af = \frac{92.75 \times 1000}{3900}$ = 23.78mm^2

$bf = \frac{Af/2}{0.17} = \frac{23.78/2}{0.17}$ = 70 mm

Use 120 mm CFRP laminates U wrapping for bottom chord

For chord above opening

Use 120 mm CFRP laminates U wrapping for upper flange only as shown in figure below.

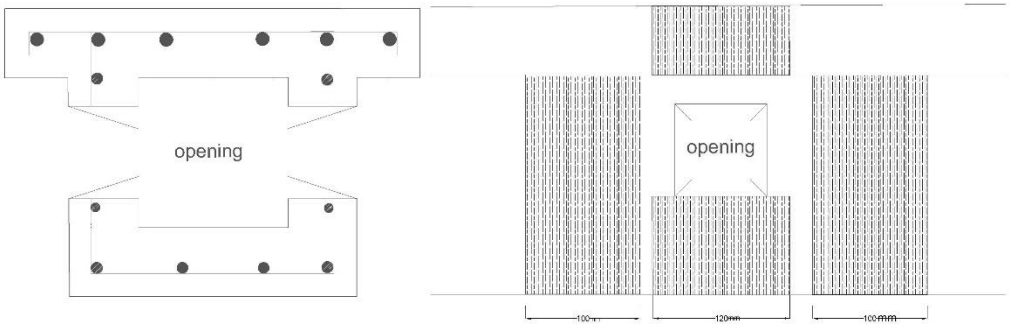

B.3.2Vertical Opening

Dimension of opening = (80 × 80) mm

P= 300 kN

Vu (at center of opening) = 106.065 kN

Mu (at center of opening) = 0 kN.m

Tu (at center of opening) = 19.38 kN.m

Beam Type Failure

1- Torsion

$x_o = y_0 = 250-(2\times20) - (2\times4) = 202$ mm

$T_n = \sum_{i=1}^{4} T_i = T_u = \frac{2A_{oh}A_t f_{yt}}{s}\cos\theta$, $30 < \theta < 60$, $\theta = 45$ 11.82×10^6

$\frac{A_t}{s} = \frac{19.38\times10^6}{4\times40804\times3900} \times 1 = 0.03$ mm^2/mm

s=50×0.17/0.03=283 mm, this is too mach spacing, check shear requirement.

2-Shear

$V_c = \frac{1}{6}\sqrt{f_c'}\, b_w(d)$

$V_c = \frac{1}{6}\sqrt{40} \times 120 \times (217) \times 10^{-3} = 27.45$ KN

$V_f = Vu - V_c$

$V_f = 106.065 - 27.45 = 78.61$ KN

$Af = \frac{78.61 \times 1000}{3900} = 20.16$mm^2

$bf = \frac{Af}{0.17} = \frac{20.16}{0.17} = 118.6$ mm

use *bf* =80 mm U wrapping full depth stirrup on each side of opening, which will satisfy torsional requirement too.

Frame Type Failure

Design of external chord

1-*Vertical shear*

Assume identical sections

Vu= 0.5× 106.065 =53

$V_c = \frac{1}{6}\sqrt{40} \times 60 \times 217 \times 10^{-3} = 13.72$ kN

$V_f = 53 - 13.72 = 39.27$ KN

$Af = \frac{39.27 \times 1000}{3900} = 10$ mm^2

$bf = \frac{Af/2}{0.17} = \frac{10/2}{0.17} = 29.62$ mm

2-*Lateral shear*

$Vuz = \frac{T_u}{(e_t + e_b)}$, $(e_t + e_b) = 250 - 2 \times (20 + 8 + 6) = 182$mm

$Vuz = \frac{19.38}{0.182} = 106.48$ kN

$V_c = \frac{1}{6}\sqrt{40} \times 250 \times (60\text{-}2\text{-}8\text{-}4) \times 10^{-3} = 7.4$ KN

$V_f = Vuz - V_c = 106.48 - 7.4 = 99.1$ KN

$Af = \frac{99.1 \times 1000}{3900} = 25.4$ mm^2

$bf = \frac{Af/2}{0.17} = \frac{25.4/2}{0.17} = 74.75$ mm

Use 120 mm CFRP laminates U wrapping for external and internal chords as shown in figure below.

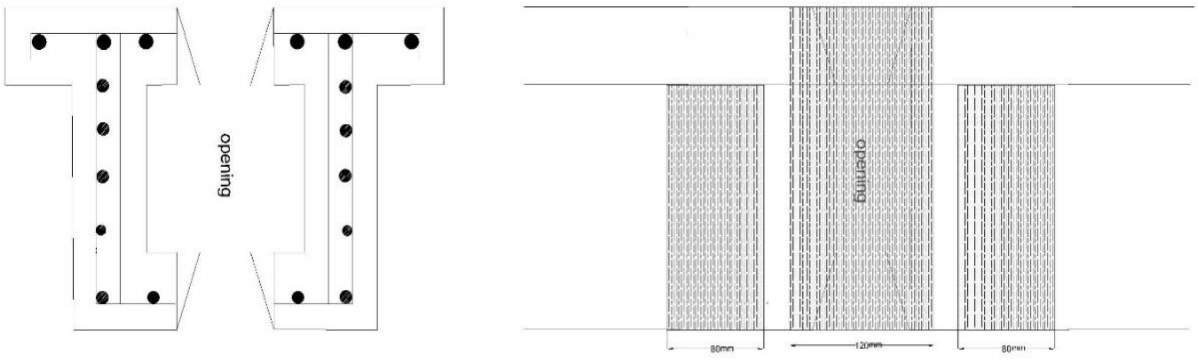

Appendix C
MODELLING OF MATERIAL PROPERTIES IN FINITE ELEMENT ANALYSIS

C.1 Introduction

The main components of a horizontally curve beam are the concrete, the steel reinforcement bars embedded inside the concrete. In addition, the EBR- CFRP sheet and the adhesive layer connecting CFRP for beams strengthened by CFRP technique. It is important to simulate the actual material behavior of each component in order to provide a realistic model of reinforced concrete horizontally curved beams, the ABAQUS material library contains excellent material models that can accurately replicate the real behavior of each component.

C.2 Material models

C.2.1 Concrete

Smeared cracking, brittle cracking mode of concrete, and damaged plasticity are three approaches to simulate concrete behavior in ABAQUS/ Standard. The smeared crack concrete model has the capacity to represent concrete in a variety of structures, including as beams, trusses, shells, and solids. Individual macro-cracks are not monitored in this model during analysis. Constitutive calculations are assigned to an integration point, which results in a loss of present stiffness and strength at that integration point. Only three cracks may form at every integration point (one in the case of uniaxial stress, two in the case of plane stress). The crack has an influence on the constitutive equations because oriented

damaged elasticity assumptions. These assumptions are implemented to describe the reversible part of the material's response after cracking failure **(Chaudhari & Chakrabarti, 2012)**. However, due to convergence difficulties produced by the lack of a cyclic/unloading response or damage to the elastic stiffness induced by plastic straining, it is difficult to make the model appropriate for 3D applications **(Daud, 2015)**. Furthermore, because of its capacity to predict the behavior of the test up to failure, the damaged plasticity model is mostly utilized in structures subjected to dynamic or cyclic stress **(Rusinowski, 2005)**. The damage plasticity model was utilized to analyze the reinforced concrete horizontally curved beam segments for the reasons stated above.

C.2.1.1 Principle of the Concrete Damaged Plasticity Formulation

Compression and tension deterioration are the two most important components of the damaged plasticity model. The elastic stiffness of the element is decreased when it plasticizes due to damaged features, and it is unable to recover its initial elastic stiffness. This is essential for cyclic loading, since the two damage parameters, *dc* and *dt*, are considered to be functions of plastic strains, temperature, and field variables, and they reflect deterioration of elastic stiffness.

$$d_t = d_t(\epsilon_t^{\sim pl}, \theta, f_i);\ 0 \le d_t \le 1 \qquad \text{C.1}$$

$$d_c = d_c(\epsilon_c^{\sim pl}, \theta, fi);\ 0 \le dc \le 1 \qquad \text{C.2}$$

where:

The subscripts *t* and *c* refer to tension and compression respectively.

$\epsilon_t^{\sim pl}$ and $\epsilon_c^{\sim pl}$ are the equivalent plastic strains.

θ is the temperature.

fi, (i=1,2,3, 4...*)* are other predefined field variables **(Lin, 2011)**.

The damage parameters can have values ranging from zero which represents the undamaged material to one which represents the damaged material (total loss of strength). Figure 5.1 presents the damage plasticity default condition. The basic tension and compression stress-strain curve is shown as a dotted line in Figure B.1, whereas the solid line depicts a high damage cyclic loading curve when the element is subjected to tension greater than its tensile strength **(Taplin & Grundy, 1999)**. Cracking, on the other hand, causes partial material deterioration and is indicated by the variable *dt*. The elastic behavior of the element after unloading can be determined by $(1 - dt)\ E_0$. The parameter w_c defines the element's elastic behavior when compressed, and $(1 - dt + w_c d_t)$ represents the modulus of elasticity in compression. It is good to remember that cracks have no effect on compression stiffness (i.e. the w_c parameter equals unity). The parameter w_c, on the other hand, equals zero when full deterioration and compression stiffness equals tension stiffness. Similarly, the parameter d_c (which describes losses in original properties that occur in the crushing section) may be used to represent compression damage, and the parameter w_t can be used to describe initial characteristics under tension.

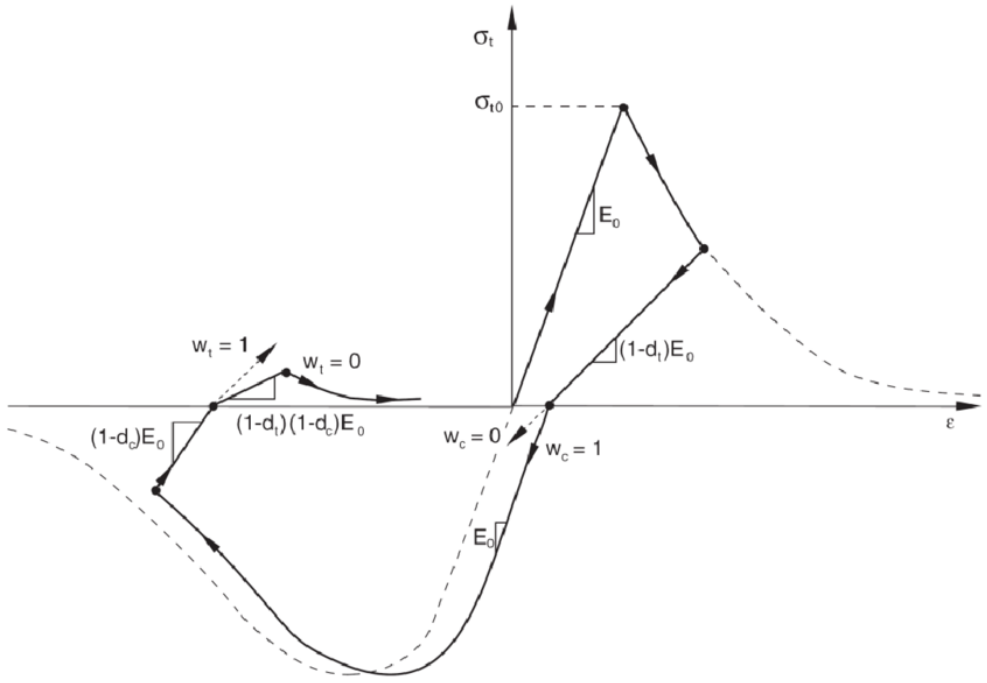

Figure C.1 Uniaxial Load Cycle (tension-compression-tension) **(Abaqus, 2011)**.

C.2.1.2 Plasticity Parameters

Lubliner et al. (1989) introduced the Drucker- Prager flow potential yield surface, which can be solved by identifying five parameters, with improvements suggested by Lee and Fenves (1998). Many tests would have to be done for the different materials utilized in the experimental model to establish the exact value of these parameters; the suggested numerical parameters investigations or default parameters in ABAQUS have been used. The following are the five parameters that must be defined:

• Ψ is the dilation angle which represents the ratio of the volume change to shear strain, determined in the plane p − q at high confining pressure where p = − 1/ 3 ($2\sigma_1 + \sigma_3$) and q = $\sqrt{3/2\,(\bar{s} : s)}$ are the hydrostatic pressure stress and Misses

equivalent effective stress respectively and σ_1 σ_3 are maximum and minimum principal stresses in a triaxial test. The majority of published studies place the dilation angle for concrete between 120° and 37° (**(Enochsson et al., 2007), (Abaqus, 2011)**).

• ϵ is a parameter referred to as flow potential eccentricity that defines as the eccentricity tends to zero the flow potential G tends to a straight line, see Figure C.2 (0.1 the default value of eccentricity is used).

• $\epsilon_{bo}/\epsilon_{co}$ is the ratio of initial equibiaxial compressive strength to initial uni-axial compressive strength (the default value is used in analysis 1.16) as shown in Figure C.3.

• μ is the viscosity parameter which represents the relaxation time of the viscoplastic system and usually helps improve the rate of convergence of the beam model in the softening region, the viscosity parameter is assumed to be zero because the beam model did not cause the severe convergence difficulty. Thus, no viscoplastic regularization is performed in the current analysis.

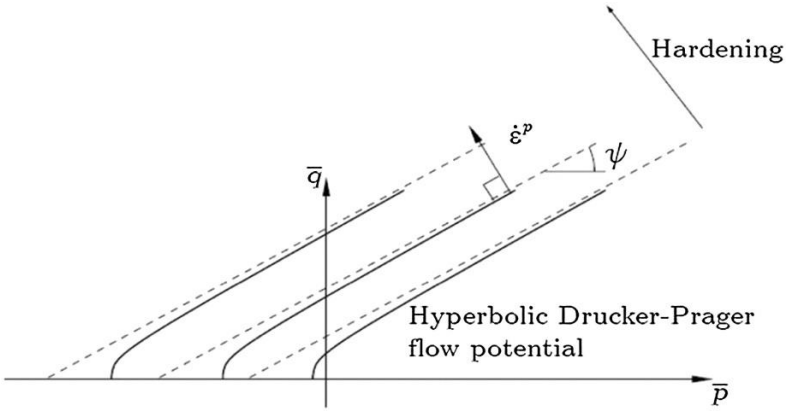

Figure C.2 Flow Potentials in p-q Plane **(Abaqus, 2011)**.

• K_c is the ratio of the second stress invariant on the tensile meridian (T.M.) to that on the compressive meridian (C.M.) and it represents the yield surface in

deviatoric plane, as shown in Figure C.4 and it should satisfy the condition 0.5 < Kc ≤ 1.0

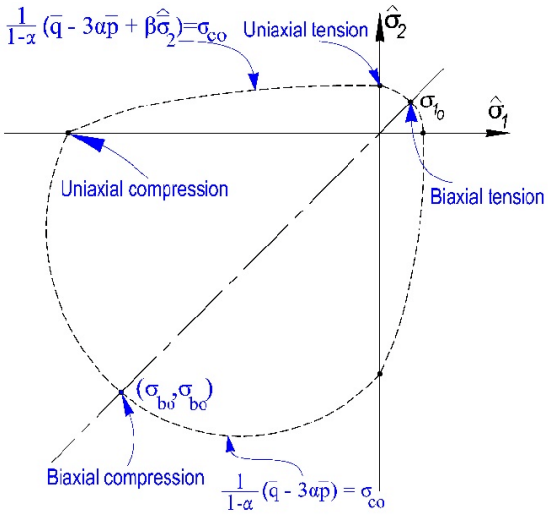

Figure C.3 Yield Surface in Plane Stress **(Carstensen et al., 2011)**

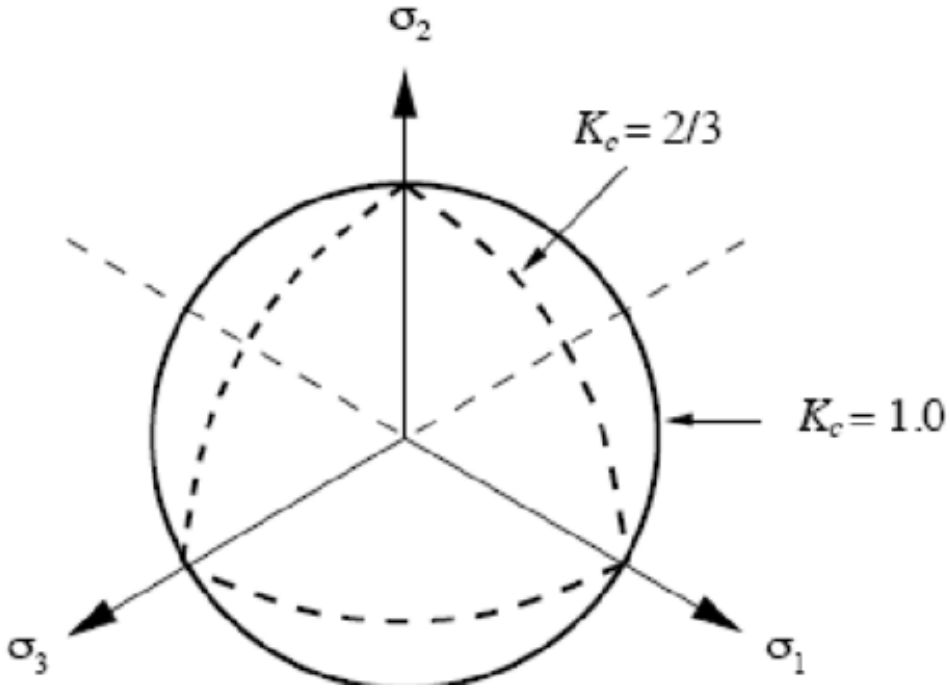

Figure C.4 Yield Surfaces in the Deviatoric Plane, Corresponding to Different Values of k_c **(Abaqus, 2011)**

C.2.1.3 Uniaxial Compressive behavior

Normal Concreter

After the elastic regime, the uniaxial compressive stress-strain relationship for plain concrete must be defined. Both hardening and strain softening ranges, according to ABAQUS, are described in terms of compressive stress, σ_c, and elastic strain, $\epsilon_c^{\sim in}$, which is provided as follows:

$$\epsilon_c^{\sim in} = \epsilon_c - \epsilon_{0c}^{el} \quad \text{C.3}$$

where $\epsilon_{0c}^{el} = \sigma_c / E_{cm}$, E_{cm} is the initial modulus of elasticity,

and $\varepsilon_c =$ total compression strain.

The finite element analysis described in this study was performed using uniaxial compressive concrete model of BSI (2004) Euro code 2 Design of Concrete Structures, as describes by the expression below.

$$\frac{\sigma_c}{f_{cm}} = \frac{kn - n\,2}{1 + (k-2)\,n} \quad \text{C.4}$$

Where:

$$n = \frac{\epsilon_c}{\epsilon_{c1}} \quad \text{C.5}$$

$$k = 1.05\, E_{cm} \times \frac{|\epsilon_{c1}|}{f_{cm}} \quad \text{C.6}$$

It should be emphasized that Equation C.6 remains true for $0 < |\epsilon_{c1}| < |\epsilon_{cu1}|$, where ϵ_{cu1} is the nominal ultimate strain (0.0035), ϵ_{c1} is the strain at peak stress and f_{cm} is the mean compressive strength.

Reactive powder concrete

Mechanical characteristics of RPC are different from the normal concrete and high compressive strength concrete under loads due to very high strength in compressive load as well as tensile load of RPC. Many studies were carried out to predict the behavior of RPC, but very few researches described the uniaxial behavior of RPC. Considering that the RPC is a type of UHPC with fibers, the latter was approved to obtain a behavior close to RPC. UHPC that with fibers have a clear ductile property under compression and tension test compared to the UHPC without fibers **(Schmidt & Fehling, 2005).**

RPC under uniaxial compression was modeled in form of elastic–plastic model as illustrated in figure C.5. The input data includes: the concrete compressive strength; f_{cu}, modulus of elasticity; E_c, Poisson's ratio; v_c, stress-plastic strain relationship.

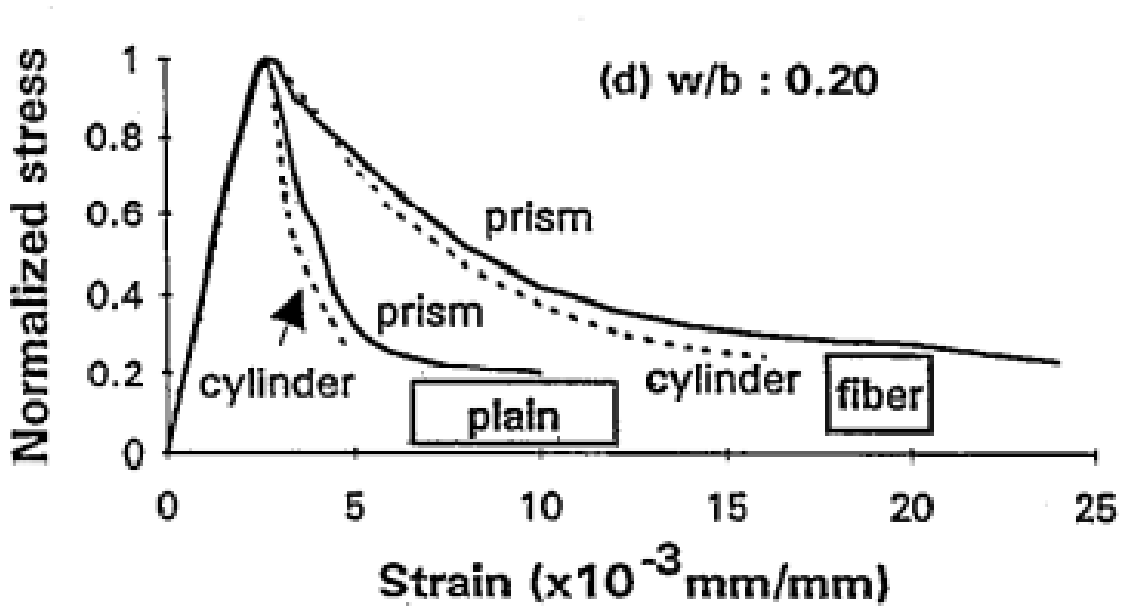

Figure C.5 Stress-Strain Curves for Both Horizontally and Vertically Cast Prisms with and without Fiber Under Uniaxial Compression **(Mansur et al., 1999)**

C.2.1.4 Uniaxial Tensile Behavior

Normal Concreter

In ABAQUS/standard, users may specify strain, crack opening (displacement), or fracture energy to represent the post-cracking tension softening curve, as illustrated in Figure C.5. In plain concrete, the tensile stress-strain softening relationship based on strength criteria may induce mesh sensitivity in the findings, the finite element predictions do not converge to a unique solution when the mesh is refined, according to **(Abdullah, 2011)**, since mesh refinement results in narrower crack bands rather than the development of new cracks. As a result, applying the strain method to structural elements with little or no reinforcement is not advised since failure occurs in isolated areas of the structure. The softening data are defined as tabular yield stress- cracking strain data. Where cracking strain equal the total strain minus the elastic strain corresponding to the undamaged material, $\epsilon_t^{\sim ck} = \epsilon_t - \epsilon_{0t}^{el}$ where $\epsilon_{0t}^{el} = \sigma_t / E_{cm}$, E_{cm} as shown in Figure C.6 (a) ,and tensile stress (σ_t) Fracture energy and stress-displacement, on the other hand, may be used interchangeably to characterize concrete tensile behavior since they are linked cracks. These two approaches based on a fracture energy cracking criterion, developed by **(Hillerborg et al., 1976)**, overcome the deficiencies of the previous way by reducing the mesh dependency problem. A tensile stress-displacement curve, rather than a stress-strain curve, was used to illustrate the brittle behavior of concrete, as shown in Figure C.6 (b).

The method relies on brittle fracture principles; the concrete fracture energy being defined as the energy necessary to open a unit area of crack. The area under the stress-displacement curve, which physically reflects the work done by the tensile stress and its corresponding opening displacement, can be used to depict fracture energy.

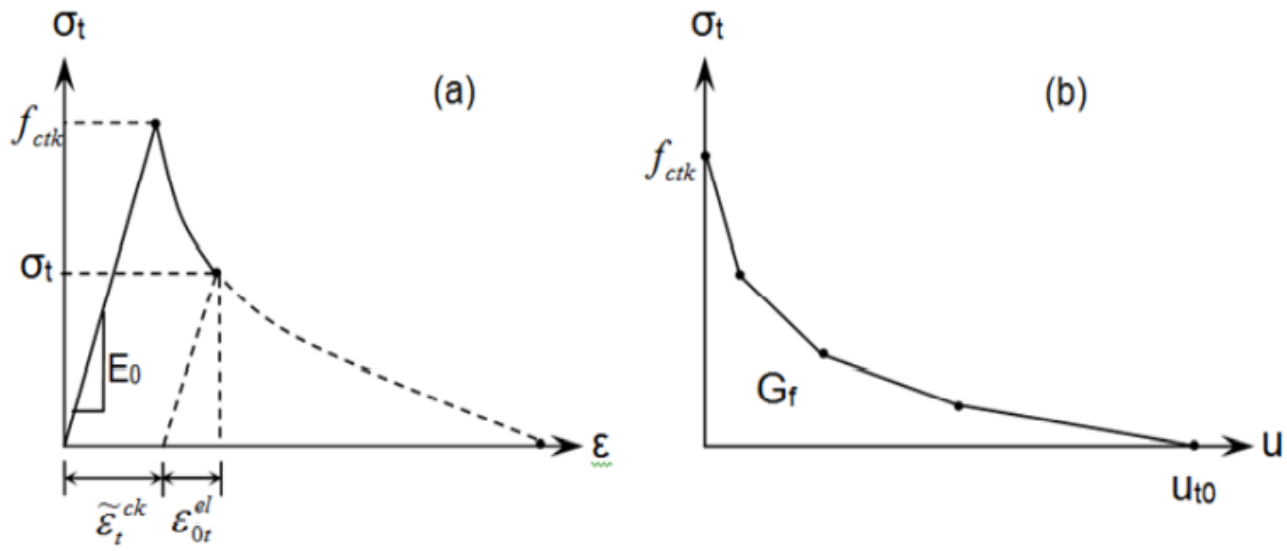

Figure C.6 Post-failure tensile behavior: (a) stress-strain approach; (b) fracture energy approach **(Daud, 2015)**

Reactive Powder Concrete

RPC in tension was modeled as linear elastic brittle material with strain softening. Tension stiffening is allowed by modifying the concrete softening behavior. Post-cracking stress–strain relationship was as suggested by **(Habel et al., 2008)** and is shown in Figure C.7. This relationship assumed that the strain softening after cracking reduces the stress to zero at a total strain of about 16 times the strain at first cracking. The input data includes: the concrete tensile strength; f_{ctmax}, the strain at first crack; ε_{cr} and the strain softening curve.

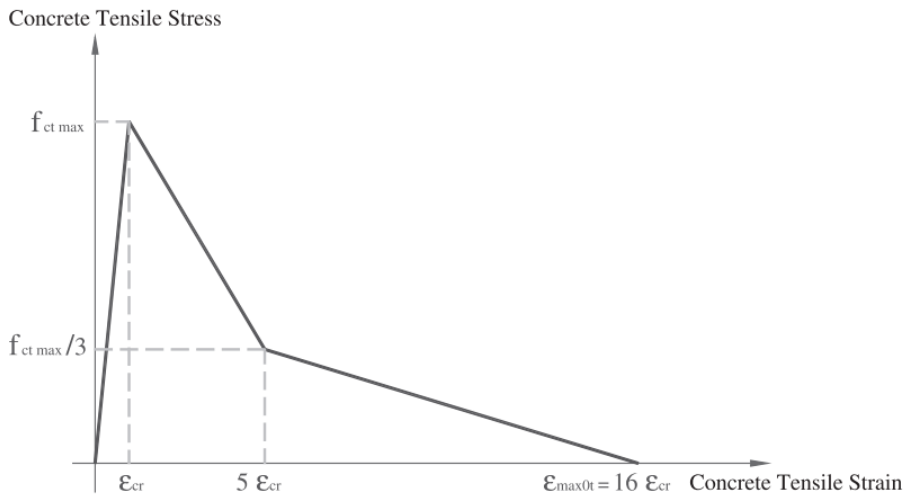

Figure C.7 Uniaxial tensile stress-strain behavior of Reactive Powder Concrete **(Habel et al., 2008)**

C.2.1.4.1 Tension Stiffening Model

The tension stiffening effect is taken into account since the cracked concrete will initially carry some tensile stresses in the direction normal to the crack as a result of the interaction between the concrete and the steel reinforcement. This may be done by assuming that the concrete stress component normal to the cracked plane gradually releases. In the analysis, tension stiffening models based on strength requirements were represented by three curves: linear, bilinear, and exponential curves. The exponential curve shown in Figure C.8 was obtained from **(Wang & Hsu, 2001)**. While, the bilinear curve was obtained by (**Peterson, 1996**).

$$\sigma_t = f_t \left(\frac{\epsilon_{cr}}{\epsilon_t} \right)^{0.4} \qquad \epsilon_t > \epsilon_{cr} \qquad \text{C.7}$$

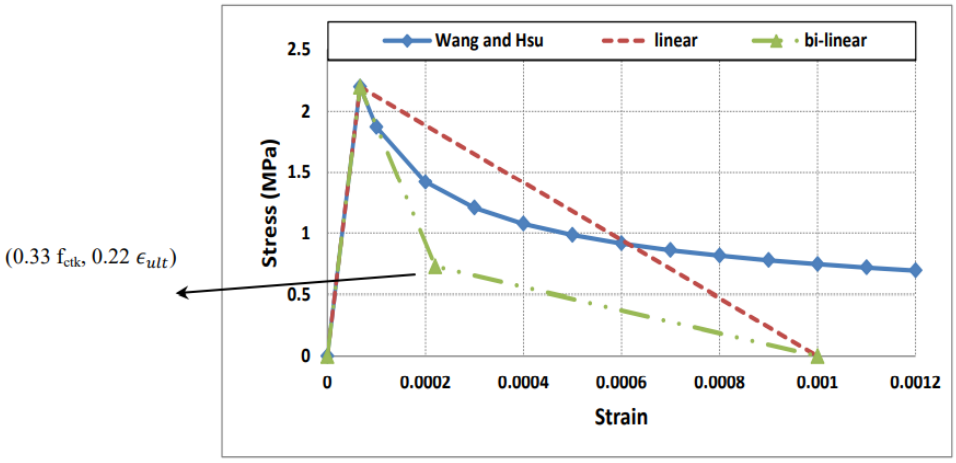

Figure C.8 Uniaxial tensile stress-strain behavior of concrete **(Daud, 2015)**

C.2.2 Steel Reinforcement

For steel reinforcement, the standard plasticity model for steel based on elasto-plastic hardening material is employed. The stress, strain, and elasticity module input values are obtained from the tensile test of these materials, as described in Chapter three.

C.2.3 CFRP

The CFRP composite sheet was modeled as an orthotropic material. It has linear behavior to the end of failure. The expression below represents the stress-strain of CFRP.

$$\begin{bmatrix} \sigma_1 \\ \sigma_2 \\ \sigma_3 \\ \tau_{12} \\ \tau_{13} \\ \tau_{23} \end{bmatrix} = \begin{bmatrix} D_{1111} & D_{1122} & D_{1133} & 0 & 0 & 0 \\ & D_{2222} & D_{1212} & 0 & 0 & 0 \\ & & D_{3333} & 0 & 0 & 0 \\ & & & D_{1212} & 0 & 0 \\ & & Sym. & & D_{1313} & 0 \\ & & & & & D_{2323} \end{bmatrix} \begin{bmatrix} \varepsilon_{11} \\ \varepsilon_{22} \\ \varepsilon_{33} \\ \gamma_{12} \\ \gamma_{13} \\ \gamma_{23} \end{bmatrix}$$

Equations below defined the nine independent elastic stiffness parameters (D_{ijkl}) **(J. Lubliner, 1989)**

$$D_{1111} = E_1(1 - \nu_{23}\nu_{32})\gamma,$$

$$D_{2222} = E_2(1 - \nu_{13}\nu_{31})\gamma,$$

$$D_{3333} = E_3(1 - \nu_{12}\nu_{21})\gamma,$$

$$D_{1122} = E_1(\nu_{21} - \nu_{31}\nu_{23})\gamma = E_2(\nu_{12} - \nu_{32}\nu_{13})\gamma,$$

$$D_{1133} = E_1(\nu_{31} - \nu_{21}\nu_{32})\gamma = E_3(\nu_{13} - \nu_{12}\nu_{23})\gamma,$$

$$D_{2233} = E_2(\nu_{32} - \nu_{12}\nu_{31})\gamma = E_3(\nu_{23} - \nu_{21}\nu_{13})\gamma,$$

$$D_{1212} = G_{12}, \quad D_{1313} = G_{13}, \quad D_{2323} = G_{23}$$

$$\gamma = \frac{1}{1-\nu_{12}\nu_{21}-\nu_{23}\nu_{32}-\nu_{31}\nu_{13}-2\nu_{21}\nu_{32}\nu_{13}}$$

C.2.4 Approaches to Model Delamination

Three approaches are available in ABAQUS for modeling the behavior of adhesive joints or interfaces in composite layers. In the current finite element analysis, the three approaches of cohesive elements, cohesive surfaces, and virtual crack closure technique (VCCT) will be explored, and then it will be chosen which approach is most appropriate.

C.2.4.1 Cohesive elements approach

The initial method for analyzing the bond interface behavior between a FRP composite plate and a concrete substrate is to use cohesive elements in

ABAQUS/standard. Using tie constraint, the top and bottom surfaces of the cohesive element must be tied to the concrete and CFRP plate. Debonding occurs along the layer of cohesive elements, with no deformation of surrounding parts. As a result, the cohesive element method can simulate bond behavior from initial loading until damage initiation and subsequently damage propagation. However, in a solution technique, this approach encounters convergence issues. Because the nodal coordinates of the cohesive elements are derived based on the starting thickness, constitutive thickness has a substantial influence on interface behavior in this technique. When the adhesive layer is thin and parameters like stiffness and strength of the adhesive material are accessible, it may be more acceptable to describe the interface with traditional cohesive parts. Furthermore, the material points define the cohesive restrictions of cohesive parts. As a result, the damage must be specified as a property of the material **(Daud, 2015)** .

C.2.4.2 Cohesive surfaces approach

In terms of constitutive reaction, ABAQUS/Standard provides an alternate method for defining adhesive junctions that is quite similar to that of cohesive parts. The surface interaction features that are assigned to a contact pair using the finite-sliding, node-to-surface formulation are represented by the surface-based cohesive method. It is preferable to begin the study with the surfaces just touching each other on a cohesive surface. Consequently, interface thickness has no effect on cohesive surfaces in ABAQUS (2011). So the surface-based cohesive approach is widely used in cases in which the adhesive thickness is negligibly small. Furthermore, each slave node enforces the cohesive restriction of cohesive surfaces. Therefore, the slave surface must be improved in comparison to the master surface in order to increase constraint satisfaction and provide more accurate results in cohesive surfaces. Finally, damage is always described in the interaction property in the surface-based cohesive approach **(Daud, 2015)**.

C.2.4.2.1 Linear elastic traction-separation behavior

A traction-separation model describes the constitutive reaction in both of the aforementioned ways. This model exhibits linear elastic behavior at first, followed by damage initiation and development. Before the injury, the elastic behavior. The concept of initiation is expressed in terms of an elastic constitutive matrix, which makes the process possible. The nominal stresses and nominal strains across the interface have a connection. In 3D FE analysis, the nominal traction stress vector, t, is made up of three components: t_n, t_s, and t_t, which represent the interface plane's normal and the two shear traction stresses along the local first and second directions, respectively.

$$t = \begin{Bmatrix} t_n \\ t_s \\ t_t \end{Bmatrix} = \begin{bmatrix} K_{nn} & K_{ns} & K_{nt} \\ K_{ns} & K_{ss} & K_{st} \\ K_{nt} & K_{st} & K_{tt} \end{bmatrix} \begin{Bmatrix} \epsilon_n \\ \epsilon_s \\ \epsilon_t \end{Bmatrix} = K\epsilon \qquad \text{C.8}$$

The nominal strains are the corresponding separations, represented by δ_n, δ_s, and δ_t, divided by the initial constitutive thickness, denoted by T_0. The initial constitutive thickness T_0 was assumed equal to unity. Therefore, the nominal strain components are equivalent to the relative displacement components.

$$\epsilon_n = \frac{\delta_n}{T_0}, \quad \epsilon_s = \frac{\delta_s}{T_0}, \quad \epsilon_t = \frac{\delta_t}{T_0}, \qquad \text{C.9}$$

C.2.4.2.2 Damage modelling

Modeling of the onset and progress of failure in cohesive elements or cohesive surfaces where the response is specified in terms of traction-separation is possible using ABAQUS/Standard. Damage is started according to a user-defined damage evolution law after the damage initiation criterion is met. If the damage initiation

criterion is specified without a corresponding damage evolution model, ABAQUS determines the criterion for output requirements only, and no damage will occur on cohesive surfaces or elements. When tensile and shear loads are applied to the cohesive surfaces and elements, the penalty stiffness of the surfaces and elements degrades, but not when pure compressive stress is applied **(Abaqus, 2011)**.

A. Damage initiation

Damage initiation occurs when the constitutive response at the bonding junction begins to degrade. When stresses and/or separations at contact locations meet specific damage beginning requirements, the degradation process begins. There are several damage initiation criteria available, including

1. Maximum nominal stress criterion: when the maximum nominal stress ratio (as explained in the function below) equals one, damage initiates. This criterion can be represented as

$$max\left\{\frac{\langle t_n \rangle}{t_n^0}, \quad \frac{t_s}{t_s^0}, \quad \frac{t_t}{t_t^0}\right\} = 1 \qquad \text{C.10}$$

2. Maximum nominal separation criterion: when the maximum nominal strain ratio (as explained in the function below) equals one, damage initiates. This criterion can be represented as

$$max\left\{\frac{\langle \epsilon_n \rangle}{\epsilon_n^0}, \quad \frac{\epsilon_s}{\epsilon_s^0}, \quad \frac{\epsilon_t}{\epsilon_t^0}\right\} = 1 \qquad \text{C.11}$$

B. Damage evolution

The damage evolution law begins once the start damage criterion is met. This indicates that the rate of cohesive stiffness degradation has begun. (D) is a scalar damage variable that indicates the total amount of damage to the contact surfaces.

It should have a number ranging from 0 if no harm has occurred to 1 if the element has entirely lost its power. The evolution response is estimated by the following criteria:

• Evolution based on effective displacement

This evolution is defined by specifying the difference in the effective displacement at complete failure δ_t^f, relative to the effective displacement at damage initiation δ_t^0. To illustrate the decline in penalty stiffness during the damage development, three methods might be employed.

Linear damage evolution: ABAQUS uses an evolution of the damage variable, D, that reduces to the equation presented by Camanho and Dávila (2002) for linear softening, Figure C.9.

$$D = \frac{\delta_t^f(\delta_t^m - \delta_t^0)}{\delta_t^m(\delta_t^f - \delta_t^0)} \qquad \text{C.12}$$

Where, δ_t^m is the maximum value of the effective slip attained during the loading history in the pull-out load direction.

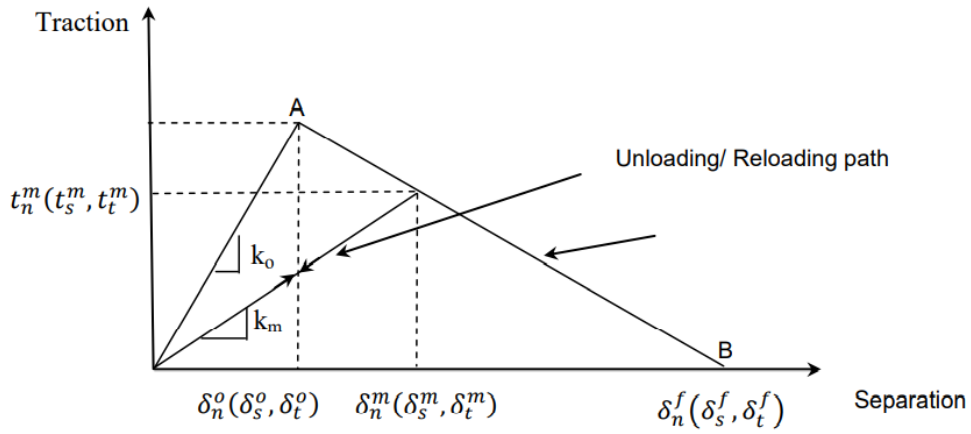

Figure C.9 Typical traction-separation response

Exponential damage evolution: For exponential softening (Figure C.10) ABAQUS uses an evolution of the damage variable, D, that reduces to

$$D = 1 - \left\{\frac{\delta_t^o}{\delta_t^m}\right\}\left\{1 - \frac{1-\exp\left(-\alpha\left(\frac{\delta_t^m-\delta_t^o}{\delta_t^f-\delta_t^o}\right)\right)}{1-\exp(-\alpha)}\right\} \qquad \text{C.13}$$

A non-dimensional material parameter specifies the rate of damage evolution in the formula above.

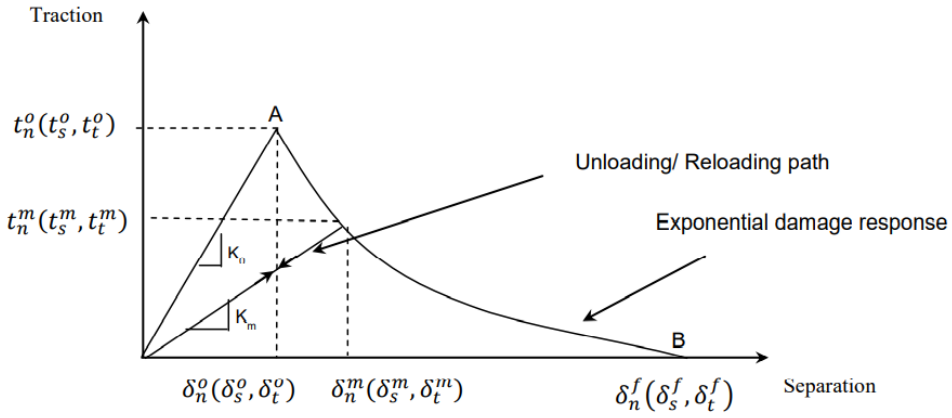

Figure C.10 Typical traction-separation response

Tabular damage evolution: is described directly in a tabular function, which depicts the difference between the effective displacement and the effective displacement at initiation. As illustrated in Figure C.11, the damage variable D is evaluated as follows:

$$D = \frac{T_{eff} - T_m}{T_{eff}} \qquad \text{C.14}$$

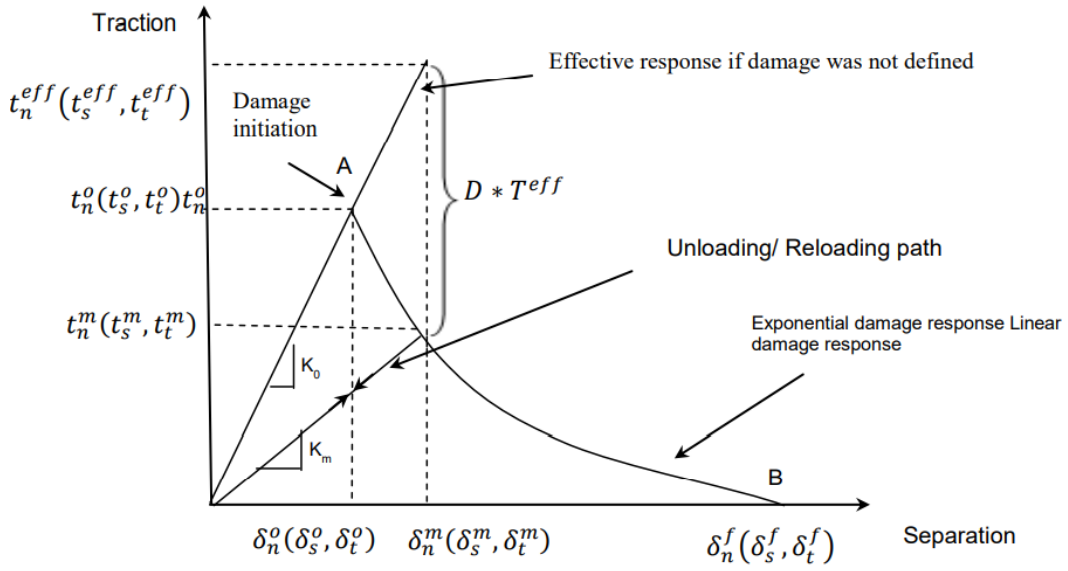

Figure C.11 Typical traction-separation response

• Evolution based on energy

The energy dissipated as a result of the damage process, also known as fracture energy, is used to define this evolution. The area under the traction-separation curve was used to estimate this. Depending on the mechanical material properties, it can be specified in ABAQUS as a linear or exponential softening behavior.

Linear damage evolution: for a linear softening, ABAQUS uses the damage evolution variable that is used in linear softening based on effective displacement Equation C.15. However, δ_t^f is determined by this expression

$$\delta_t^f = \frac{2G^C}{t_t^0} \qquad \text{C.15}$$

where, G^C is the mixed-mode fracture energy, $G^C = G_n + G_t + G_s$. G_n, G_t and G_s refers to the work done by traction in the normal, first, and second shear directions, as well as its conjugate relative displacement. $\delta_t^0$is the effective traction at damage initiation in the first direction.

Exponential damage evolution: ABAQUS utilizes an evolution of the damage variable based on the following formula for exponential softening.

$$D = \int_{\delta_t^0}^{\delta_t^f} \frac{T_{eff} d\delta}{G^C - G_0} \quad \text{C.16}$$

T_{eff} and G_0 are the effective traction and elastic energy at damage initiation, respectively, in the formula above. The unloading/reloading stiffness is determined as $K_m = (1\text{-}D)\, K_0$. According to the following functions, the damage affects the contact stress elements in the normal, first, and second directions between points A and B, Figure C.11.

$$t_n = \begin{cases} (1-D)\overline{t_n}, & \overline{t_n} > 0 \\ \overline{t_n}, & otherwise\ (no\ damage\ to\ compressive\ stiffness) \end{cases} \quad \text{C.17}$$

$$t_s = (1-D).\bar{t}_s \quad \text{C.18}$$

$$t_t = (1-D).\bar{t}_t \quad \text{C.19}$$

C.2.4.3 Virtual crack closure technique (VCCT)

The virtual crack closure technique (VCCT) is a new approach for simulating the delamination of two composite layers under static and fatigue loads. When applying the mixed-mode fracture criteria in three-dimensional finite element studies, the constitutive response of this technique is based on linear elastic fracture mechanics by estimating energy release rates to supply debonding required. The (VCCT) has the problem of being numerically difficult and requiring small time increments to solve crack propagation concerns. A small clearance is added to the previously un-bonded area by matched meshes between the slave and master surfaces of the debonding contact pair. Nonetheless, it may

result in an unnecessarily severe discontinuity in iterations as the crack progresses and causes a convergence difficulty while the program is running **(Daud, 2015)**.

References

Abaqus, G. (2011). Abaqus 6.11. *Dassault Systemes Simulia Corporation, Providence, RI, USA*.

Abdullah, A. M. (2011). *Analysis of repaired/strengthened RC structures using composite materials: punching shear*. The University of Manchester (United Kingdom).

Al-Zubaidy, H., Zhao, X.-L., & Al-Mahaidi, R. (2013). Mechanical characterisation of the dynamic tensile properties of CFRP sheet and adhesive at medium strain rates. *Composite Structures*, *96*, 153–164.

Carstensen, J. V., Pankaj, P., & Jomaas, G. (2011). *MATERIAL MODELLING OF THE POST-PEAK RESPONSE OF REINFORCED CONCRETE AT ELEVATED TEMPERATURES*. *10th International Symposium on Fire Safety Science*.

Chaudhari, S. V, & Chakrabarti, M. A. (2012). Modeling of concrete for nonlinear analysis using finite element code ABAQUS. *International Journal of Computer Applications*, *44*(7), 14–18.

Daud, R. A. (2015). *Behaviour of reinforced concrete slabs strengthened externally with two-way FRP sheets subjected to cyclic loads*. The University of Manchester (United Kingdom).

Enochsson, O., Lundqvist, J., Täljsten, B., Rusinowski, P., & Olofsson, T. (2007). CFRP strengthened openings in two-way concrete slabs–An experimental and numerical study. *Construction and Building Materials*, *21*(4), 810–826.

Habel, K., Charron, J.-P., Braike, S., Hooton, R. D., Gauvreau, P., & Massicotte,

B. (2008). Ultra-high performance fibre reinforced concrete mix design in central Canada. *Canadian Journal of Civil Engineering*, *35*(2), 217–224.

Hillerborg, A., Modéer, M., & Petersson, P.-E. (1976). Analysis of crack formation and crack growth in concrete by means of fracture mechanics and finite elements. *Cement and Concrete Research*, *6*(6), 773–781.

J. Lubliner, J. Oliver, S. Oller, and E. Oñate. A plastic-damage model for concrete. Int. J. Solids Struct., vol. 25, no. 3, pp. 299–326, 1989.

Lin, H. (2011). Secondary development functions and applications of Abaqus/CAE. *Computer Aided Engineering*, 4.

Mansur, M. A., Chin, M. S., & Wee, T. H. (1999). Stress-strain relationship of high-strength fiber concrete in compression. *Journal of Materials in Civil Engineering*, *11*(1), 21–29.

Naghipour, P., Schneider, J., Bartsch, M., Hausmann, J., & Voggenreiter, H. (2009). Fracture simulation of CFRP laminates in mixed mode bending. *Engineering Fracture Mechanics*, *76*(18), 2821–2833.

Rusinowski, P. (2005). *Two-way concrete slabs with openings: experiments, finite element analyses and design*.

Schmidt, M., & Fehling, E. (2005). Ultra-high-performance concrete: research, development and application in Europe. *ACI Spec. Publ*, *228*(4), 51–78.

Taplin, G. R., & Grundy, P. (1999). Steel-concrete composite beams under repeated loading. *Australasian Conference on the Mechanics of Structures and Materials 1999*, 315–320.

Wang, T., & Hsu, T. T. C. (2001). Nonlinear finite element analysis of concrete structures using new constitutive models. *Computers & Structures*, *79*(32), 2781–2791.

الخلاصة

تبحث هذه الدراسة في سلوك وأداء الاعتاب الصندوقية المقوسة أفقياً من الخرسانة المسلحة و الحاوية على فتحات رأسية أو عرضية غير مقواة او مقواة باستخدام خرسانة المساحيق الفعالةRPC أو المقواة خارجيا باستحدام بشرائح الكاربون EBR-CFRP حول الفتحات تحت تاثير الحمل باتجاه واحد أوالتكراري. تضمن العمل المختبري بالإضافة إلى العتب التجريبي ، تصنيع واختبار خمسة عشر عتبا صندوقيا مقوس افقيا من الخرسانة المسلحة مقسمة إلى ثلاث مجموعات. تضمت المجموعة الأولى ستة اعتاب (واحدة بدون فتحات وخمسة بفتحات رأسية) ، وتألفت المجموعة الثانية من خمسة اعتاب ذات فتحات عرضية ، بينما تضمنت المجموعة الثالثة أربع عينات (واحدة بدون فتحة وثلاث بفتحات عرضية) تحت تاثير الحمل التكراري. يأخذ البرنامج التجريبي في الاعتبار مجموعة من المتغيرات المستقلة: اتجاه محور الفتحات ، وموقع الفتحات خلال فضاء العتب، بالاضافة الى امكانية استعادة القوة بتقنية الخرسانة الهجينة (خرسانة المساحيق الفعالةRPC حول الفتحات) أو مقوى خارجيا بواسطة شرائح الكاربون EBR- CFRP حول الفتحات . تم اختبار جميع الاعتاب الصندوقية المستمرة ذات فضائين تحت تأثير الأحمال المركزة في الوجه العلوي عند منتصف كل فضاء.

أشارت النتائج التجريبية إلى أن وجود الفتحات في منطقة الالتواء و القص الاقصى (عند الزاوية 60 درجة) أدى إلى انخفاض كبير في الحمل النهائي بحوالي 11.5٪ للعتب الحاوي على فتحات رأسية و 46.4٪ للعتب الحاوي على فتحات عرضية بالمقارنة مع العتب بدون فتحات. أدى استخدام الخرسانة الهجينة (خرسانة المساحيق الفعالة RPC) إلى تعزيز قدرة الحمولة القصوى للعتب الحاوي على فتحات بزاوية 60 درجة بنسبة 4.8٪ و 25.9٪ للعتب بفتحات رأسية وعرضية على التوالي. أدى استخدام شرائح الكاربون EBR- CFRP كتقوية خارجية حول الفتحات إلى زيادة الحمل الاقصى للعتب الحاوي على فتحات رأسية ، في حين ان الحمل النهائي للعتب الحاوي على فتحات عرضية كان أقل من العتب بدون فتحات بنسبة 25.9٪. كان تصرف الاعتاب الصندوقية المقوسة المقواة وغير المقواة تحت الحمل التكراري مماثلة لتلك التي تعرضت للحمل باتجاه واحد مع انخفاض طفيف في الحمل الاقصى ويعزى ذلك الى تأثير الكلل و لكلا النوعين من التعزيز حول فتحات الخرسانة الهجينة (خرسانة المساحيق الفعالةRPC حول الفتحات) أو المقواة الخارجيا باستخدام رقائق الكاربون EBR- CFRP.

اعتمدت الدراسة العددية استخدام نموذج ثلاثي الأبعاد للعناصر المحددة ، باستخدام نموذج لدونة الخرسانة المشوه وخواص المواد التي تم الحصول عليها من الاختبارات العملية لمحاكاة جميع الاعتاب المختبرية الخمسة عشر ، بالإضافة إلى دراسة عددية للنظر في تاثير بعض المتغيرات التي لم يتم دراستها خلال

العمل المختبري ضمن برامج ABAQUS / standard 2017. تضمنت الدراسة العددية تأثيرات بعض المتغيرات على اداء الاعتاب الصندوقية من الخرسانة المسلحة المقوسة أفقيًا ؛ شكل الفتحات ونصف قطر الانحناء وقوة خرسانة المساحيق الفعالة RPC. تمت مقارنة النتائج العددية مع تلك التي تم الحصول عليها من العمل المختبري متمثلا بمنحنى الحمولة- هطول منتصف الفضاء للعتب وكيفية انتشار و تفاقم التشققات بمتوسط تباين حوالي 5٪ و 8٪ و 20٪ لحمل التشقق الاولي والحمل الاقصى والهطول عند حمل الخدمة ، على التوالي. نتيجة للدراسة العددية ، أدى وجود فتحات دائرية أو مستطيلة في الاتجاه الرأسي إلى نفس الحمل الاقصى تقريبًا بواسطة استخدام نموذج ثلاثي الأبعاد للعنصر المحددة للعتب الحاوي على فتحة مربعة الشكل عند الزاوية °60 ، بينما في الاتجاه العرضي ، تم زيادة الحمل الاقصى قليلاً للعتب الحاوي على فتحة دائرية وانخفاض طفيف للعتب الحاوي على فتحة المستطيلة الشكل ، عند مقارنتها بالحمل الاقصى للعتب الحاوي على فتحة مربعة. يُظهر الحمل الاقصى للاعتاب بدون فتحات زيادة في الحمل الاقصى مقابل تقليل التقوس(1 / R) لنفس طول الفضاء وكانت تقريبًا (10.5٪ و 19.41٪) للتقوس (0.67 و 0.0) على التوالي إذا ما قورنت بالعتب ذو تقوس 0.87 للعملي ، بالنسبة للاعتاب الحاوية على فتحات زاد الحمل الاقصى بنحو (14.7٪ و 59.4٪) للتقوس (0.67 و 0.0) على التوالي مقارنتا بالعتب ذو تقوس 0.87 للعملي. زيادة طفيفة في الحمل الاقصى للاعتاب الحاوية على فتحات عند الزاوية °60 وكانت الزيادة 6.4٪ و 3.8٪ للفتحات الرأسية والعرضية ، على التوالي عند استخدام خرسانة المساحيق الفعالةRPC حول الفتحات ذو مقاومة MPa 200 مقارنةً باستخدام خرسانة المساحيق الفعالة RPC ذو مقاومة MPa120 . باستخدام تحليل العناصر المحددة ، تمكنا من توقع سلوك الاعتاب الصندوقية المقوسة أفقيا ذات الفتحات بدجة مقبولة، وكذلك استجابة الاعتاب ذات المتغيرات المختلفة.

جمهورية العراق

وزارة التعليم العالي والبحث العلمي

جامعة بابل - كلية الهندسة

قسم الهندسة المدنية

سلوك الاعتاب الصندوقية المقوسة أفقياً من الخرسانة المسلحة و الحاوية على فتحات تحت حمل باتجاه واحد و تكراري

أطروحة

مقدمة إلى كلية الهندسة في جامعة بابل

كجزء من متطلبات نيل درجة الدكتوراه فلسفة في الهندسة/الهندسة المدنية/ الإنشاءات

من قبل

امير محسن هاشم

(بكالوريوس هندسة المدنية 2003)

(ماجستير هندسة الإنشاءات 2014)

إشراف

الأستاذ الدكتور عمار ياسر علي

2022م ***1443 هـ***